NEXT GENERATION PAN-EUROPEAN GROUND-MOTION PREDICTION
EQUATIONS FOR ENGINEERING PARAMETERS

A THESIS SUBMITTED TO
THE GRADUATE SCHOOL OF NATURAL AND APPLIED SCIENCES
OF
MIDDLE EAST TECHNICAL UNIVERSITY
AND
L'ÉCOLE DOCTORALE TERRE UNIVERS ENVIRONNEMENT
OF
UNIVERSITE DE GRENOBLE

BY

MUSTAFA ABDULLAH SANDIKKAYA

IN PARTIAL FULFILLMENT OF THE REQUIREMENTS
FOR
THE DEGREE OF DOCTOR OF PHILOSOPHY
IN
CIVIL ENGINEERING

APRIL 2014

Approval of the thesis:

**NEXT GENERATION PAN-EUROPEAN GROUND-MOTION
PREDICTION EQUATIONS FOR ENGINEERING PARAMETERS**

submitted by **MUSTAFA ABDULLAH SANDIKKAYA** in partial fulfillment of the requirements for the degree of **Doctor of Philosophy in Department of Civil Engineering, Middle East Technical University** and **Docteur de L'université de Grenoble, l'École Doctorale Terre Univers Environnement**, **Université de Grenoble** by,

Prof. Dr. Canan Özgen   _____
Dean, Graduate School of **Natural and Applied Sciences**

Prof. Dr. Jean Braun   _____
Head of Graduate School, **Terre, Universe and Environment**

Prof. Dr. Ahmet Cevdet Yalçıner   _____
Head of Department, **Civil Engineering**

Prof. Dr. Sinan Akkar   _____
Supervisor, **Civil Engineering Dept., METU**

Prof. Dr. Pierre-Yves Bard   _____
Supervisor, **ISTerre, UdG**

Examining Committee Members:

Prof. Dr. Bilge Siyahi   _____
Earthquake and Structural Dept., GIT

Prof. Dr. Sinan Akkar   _____
Civil Engineering Dept., METU

Prof. Dr. Pierre-Yves Bard   _____
ISTerre, UdG, France

Assist. Prof. Dr. M. Tolga Yılmaz   _____
Engineering Sciences Dept., METU

Prof. Dr. Fabrice Cotton   _____
ISTerre, UdG, France

Prof. Dr. Eser Çaktı   _____
Dept. of Earthquake Engineering, KOERI

Prof. Dr. Marco Mucciarelli   _____
University of Basilicata, Italy

Date: 11.04.2014

I hereby declare that all information in this document has been obtained and presented in accordance with academic rules and ethical conduct. I also declare that, as required by these rules and conduct, I have fully cited and referenced all material and results that are not original to this work.

Name, Last Name: Mustafa Abdullah Sandıkkaya

Signature:

ABSTRACT

**NEXT GENERATION PAN-EUROPEAN GROUND-MOTION
PREDICTION EQUATIONS FOR ENGINEERING PARAMETERS**

Sandıkkaya, Mustafa Abdullah

Ph.D., International Joint Programme in Department of Civil Engineering

Supervisor: Prof. Dr. Sinan Akkar

Supervisor: Prof. Dr. Pierre-Yves Bard

April 2014, 241 pages

This study firstly presents the recent pan-European strong-motion databank that is updated and extended version of previous pan-European databases. The pertaining metadata is carefully compiled and reappraised. The database meets high standards for being a resource for the pan-European earthquake engineering community. Then, an empirical nonlinear site amplification model, a function of the time-based average of uppermost 30m shear wave velocity profile and peak ground acceleration on rock, is developed. The primary aim of deriving such a model is to use it in ground motion prediction equations (GMPEs). Besides, the evaluation of site factors in the seismic design codes shows that it is also applicable in computing site factors. To this end, an alternative methodology that considers the results of probabilistic seismic hazard analysis and deterministic site models is proposed. Finally, this study generates GMPEs for horizontal and vertical elastic response spectral ordinates for different damping values between 1% to 50%. Rather than direct equations for vertical motion, to obtain consistent horizontal and vertical hazard spectrum, compatible vertical-to-horizontal ratio

GMPEs are preferred. Additional damping scaling models to modify horizontal and vertical spectra at other damping ratios are proposed.

Keywords: Seismic hazard, strong-motion database, nonlinear site amplification, ground-motion prediction equations for horizontal and vertical components, damping scaling factors

ÖZ

MÜHENDİSLİK PARAMETRELERİ İÇİN SON NESİL PAN-AVRUPA YER HAREKETİ TAHMİN DENKLEMLERİ

Sandıkkaya, Mustafa Abdullah

Doktora, Uluslararası Ortak Programı İnşaat Mühendisliği Bölümü

Tez Yöneticisi: Prof. Dr. Sinan Akkar

Tez Yöneticisi: Prof. Dr. Pierre-Yves Bard

Bu çalışmada ilk olarak en son pan-Avrupa kuvvetli yer hareketi veri tabanı sunulmuştur. Bu veri tabanı muadillerine göre hem muhteva ettiği ivme kayıt sayısı açısından genişletilmiş hem de bilgileri güncellenmiştir. Bu vesileyle pan-Avrupa deprem mühendisliği çevrelerinde kullanılmak üzere yüksek kalitede veri sunulmuştur. Sonrasında tamamen verilere dayanan doğrusal olmayan zemin büyütme modeli geliştirilmiştir. Bu model, 30 m lik üst katmandaki kayma dalga hız profilinin zaman ortalamasını ve kaya zemindeki pik yer ivmesini kullanmaktır. Bu model esas olarak yer hareketi tahmin denklemlerinde (YHTD) kullanılmak üzere üretilmiştir. Deprem şartnamelerindeki zemin katsayılarının incelenmesi sonucunda bu modelin bu katsayı hesaplamalarında da kullanılabileceği görülmüştür. Hem olasılıksal sismik tehlike analizi sonuçlarını hem de determinist zemin modellerini kullanan alternatif bir metot önerilmiştir. Son olarak bu çalışmada temel amacı yatay ve düşey bileşenler için % 5 sönümlemedeki elastik spektral ivme hesaplamalarında kullanmak üzere son nesil yer hareketi tahmin denklemlerini sunmaktır. Direk olarak düşey hareketi veren

denklemlerden ziyade, yatay ve düşey tehlike spektrumlarında tutarlı sonuçlar verecek olan dikey-yatay oran denkleminin verilmesi tercih edilmiştir. Ayrıca yatay ve düşey spektrumları diğer sönümleme oranlarında (%1 -%50) elde etmek üzere gerekli olan ek modellerde bu çalışmada sağlanmıştır.

Anahtar Kelimeler: Sismik tehlike, kuvvetli yer hareketi veri tabanı, doğrusal olmayan zemin büyütmesi, yatay ve dikey bileşenler için zemin hareketi tahmin denklemleri, sönümleme faktörleri

RÉSUMÉ

NOUVELLE GENERATION D'EQUATIONS DE PREDICTION DES MOUVEMENTS SISMIQUES POUR LA ZONE PAN-EUROPEENNE

Sandıkkaya, Mustafa Abdullah

Ph.D., Cotutelle Département de Génie Civil

Directeur de thèse: Prof. Dr. Sinan Akkar

Directeur de thèse: Prof. Dr. Pierre-Yves Bard

Avril 2014, 241 pages

Ce mémoire commence par présenter une nouvelle banque de données de mouvements forts pan-européennes constituée sur la base d'une extension et d'une mise à jour des bases de données antérieures: les métadonnées ont été soigneusement compilées et réévaluées selon les standards les plus récents pour servir de nouveau support aux travaux de la communauté paneuropéenne de génie parasismique. Il se poursuit par diverses études se fondant sur une analyse statistique de cette base de base de données. La première concerne l'élaboration d'un modèle simple traduisant les effets d'amplification non-linéaire en fonction du proxy classique "V_{S30}" (moyenne harmonique de la vitesse des ondes de cisaillement sur les 30 mètres les plus superficiels) et de l'accélération maximale au rocher. L'objectif principal est l'incorporation d'un tel modèle dans les équations de prédiction des mouvements du sol ("GMPEs"), mais ce même modèle est également utilisé pour proposer les facteurs de site dans les règlements de construction parasismique, sur la base d'une méthodologie combinant les résultats d'une analyse probabiliste de l'aléa sismique et un modèle déterministe de l'effet de site. Enfin, ce mémoire se termine par l'élaboration de GMPEs donnant

l'évolution des valeurs des spectres de réponse des mouvements horizontaux et verticaux, pour des amortissements de 1 à 50%, en fonction de divers paramètres physiques (magnitude, distance, conditions de site, notamment). Pour le mouvement vertical, il a été jugé préférable de proposer une GMPE donnant l'évolution du rapport spectral vertical/horizontal en fonction des mêmes paramètres physiques; quant à l'influence de l'amortissement spectral, elle est établie sur la base de facteurs d'échelle passant de l'amortissement "standard 5% à d'autres valeurs.

Mots-clés: risque sismique, base de données mouvements forts, amplification non-linéaire de site, équations de prédiction de mouvements sismiques, spectres de réponse horizontaux et verticaux, facteurs d'échelle en amortissement

To my beloved wife, Hilal

ACKNOWLEDGMENTS

SUMMARY OF THESIS IN FRENCH

L'objectif principal de cette thèse est de présenter une nouvelle génération d'équation de prédiction des mouvements sismiques pour la zone pan-européenne. Ces équations peuvent être utilisés pour prédire les valeurs des spectres de réponse des composantes horizontale et verticale pour différents niveaux d'amortissement dans une gamme comprise entre 1% et 30%. Ces équations intègrent un modèle purement empirique d'amplification non-linéaire en focntions de conditions de site et du niveau du mouvement au rocher. Ce modèle proposé est également utilisé pour proposer une méthodologie à combiner avec les résultats d'une analyse probabiliste de l'aléa sismique pour déterminer des facteurs de site du type NEHRP ou Eurocode 8 à utiliser dans la prochaine version des réglementations parasismiques.

Le présent mémoire, composé de sept chapitres, commence au chapitre 1 par une revue bibliographique des travaux récents sur cette thématique, et un exposé de l'articulation générale du mémoire.

Le chapitre 2 décrit la constitution d'une nouvelle banque de données sur les mouvements sismiques forts dans la zone pan-européenne, et des métadonnées correspondantes. Il expose la procédure de sélection des enregistrements adoptée en vue de la génération d'équations prédictives des mouvements sismiques pour la région paneuropéenne. La dernière section de ce chapitre présente les enregistrements supplémentaires d'origine non-européenne qui ont été sélectionnés pour élaborer un modèle purement empirique d'amplification non-linéaire.

Le chapitre 3 est justement consacré à l'''élaboration de ce modèle. Après une revue bibliographique des divers modèles de site utilisés dans les équations de prédiction de mouvements sismiques, les paramètres et les formes fonctionnelles du modèle non-linéaire empirique retenu sont exposés, ainsi que la procédure d'estimation de ses différents coefficients. Les résultats du modèle ainsi proposé sont comparés à ceux des modèles récents, et débouchent sur une première évaluation simple des facteurs de site à utiliser dans le règlements parasismiques est faite, avant une discussion plus approfondie de ces facteurs dans le chapitre 4.

Le chapitre 4 examine tout d'abord l'évolution des facteurs de site dans les codes de conception parasismique et élargit ensuite les propositions simplifiées du chapitre 3 en appliquant de multiples scénarios de tremblement de terre dérivés d'une approche probabiliste pour l'aléa au rocher. La méthodologie ainsi proposée pour calculer les facteurs de site conduit à des estimations légèrement différentes de celles obtenues avec l'approche simplifiée du chapitre 3.

Le chapitre 5 présente l'élaboration de nouvelles équations prédictives pour les spectres de réponse horizontaux fondés sur la nouvelle base de données pan-européennes du chapitre 2, et le modèle empirique d'amplification non-linéaire du chapitre 3. Après une vue d'ensemble des GMPE pan-européennes et une analyse critique de leurs limites, le modèle général pour la génération d'une nouvelle équation prédictive pan-européenne est introduit. Les équations ainsi obtenues sont applicables à diverses métriques de distance source-récepteur, pour des sources tant étendues que ponctuelles. Ce chapitre se termine par une analyse des limites de ces nouvelles équations de prédiction, et leur comparaison avec un ensemble de GMPEs mondiales, régionales et locales.

Le chapitre 6 complète le chapitre 5 en s'attachant à l'estimation de la composante verticale des mouvements sismiques, et l'extension à d'autres valeurs

d'amortissement spectral. Après un bref aperçu des approches et relations prédictives disponibles pour ces deux aspects différents, un choix est fait de partir des GMPE "spectres de réponse horizontaux à 5% d'amortissement" du chapitre 5 et de leur appliquer une GMPE complémentaire donnant le rapport V/H (Vertical/Horizontal) en fonction des mêmes variables explicatives, et des facteurs d'échelle permettant de passer à d'autres valeurs d'amortissement.

Le dernier chapitre [7] conclut la thèse par une série de remarques et de réflexions sur l'ensemble des travaux de ce mémoire, et notamment une discussion de leurs limitations, ainsi que quelques considérations sur les perspectives de recherche pour permettre des améliorations significatives palliant ces limitations.

Les chapitres 2 à 6 de cette thèse reprennent cinq articles récemment publiés ou en revue dans différentes revues scientifiques internationales. Sandıkkaya et al. (2013, publié) décrit l'élaboration du modèle de site non linéaire (chapitre 3). Les travaux des chapitres 5 et 6 décrivant les modèles prédictifs paneuropéens pour les mouvements horizontal et vertical ont également fait l'objet de deux publications : Akkar et al (2014b, publié) et Akkar et al. (2014c, en revue). La base de données utilisée dans ces études, présentée au chapitre 2, a également fait l'objet d'une publication spécifique (Akkar et al., 2014a, publié). Enfin, la méthodologie proposée pour obtenir les valeurs des coefficients de sites réglementaires (chapitre 4) a été soumise et est actuellement en revue (Sandikkaya et al., 2014).

TABLE OF CONTENTS

LIST OF TABLES

TABLES

xxiii

CHAPTER 1

INTRODUCTION

1.1 General

Research projects that aim at improving the definition of seismic hazard in the broader Europe have been accelerated significantly in the first decade of the 21st century. Among these projects, the **S**eismic **H**azard HA**R**monization in **E**urope (SHARE[1]) project with an objective of providing reliable assessment of seismic hazard in Europe and surrounding regions can be considered as one of the most remarkable efforts in this respect. The SHARE project triggered the multi-purpose SIGMA[2] (**SeI**smic **G**round **M**otion **A**ssessment) project. One of the primary objectives of SIGMA is to assemble a reliable European strong-motion databank that expands and improves its predecessors for developing consistent ground-motion prediction equations (GMPEs) that better address the epistemic uncertainty and aleatory variability of hazard estimates in Europe. Both the SHARE and SIGMA projects closely interact with the other similar multi-national projects. For example, SHARE has conveyed its experience to the EMME[3] (Earthquake Model of the Middle East) project that assumes a similar mission as of SHARE for the hazard assessment of the Middle East, Caucuses, Iran, Pakistan and Afghanistan. The SIGMA project joins efforts with NERA[4] (Network of European Research Infrastructures for Earthquake Risk Assessment and

---

[1] SHARE project was funded by the EC-Research Framework Programme FP7, under contract number 226967 (Giardini et al., 2013).
[2] SIGMA project is being funded and supported by EDF, AREVA, CEA and ENEL
[3] EMME project has been funded by Japan Tobacco International
[4] NERA project has been funded by the EC-Research Framework Programme FP7, under contract number 262330

Mitigation) as one of the aims of the latter project in providing a robust infrastructure to archive and integrate European strong-motion data.

The topics covered by this dissertation are closely related to some of the objectives put forward by the SHARE and SIGMA projects. One of the main goals of the dissertation is to propose a set of ground-motion predictive models for the pan-European region by addressing the weaknesses of previous European GMPEs. This target is in line with the SHARE objectives as the emphasis in SHARE is reliable measurement of hazard via robust pan-European GMPEs. The proposed pan-European GMPEs not only consider the estimation of horizontal ground motions but can be used for estimating the vertical ground-motions via vertical-to-horizontal spectral ordinate ratios. Horizontal and vertical damping-scaling GMPEs that are derived as part of the predictive models enable one to estimate the horizontal and vertical spectral ordinates for damping ratios varying between 1% and 50%. The aforementioned ground-motion equations are developed from a subset of the recent pan-European strong-motion databank that is collected as a collaborative work within the SIGMA project. Thus, the pan-European strong-motion databank that is presented as part of this thesis is believed to comply with the current needs of the SIGMA project. As the proposed GMPEs are derived from the same ground-motion database, they would yield consistent horizontal and vertical spectral ordinates for a given ground-motion scenario. The compiled pan-European strong-motion databank enabled this study to model the linear as well as nonlinear soil behavior as a continuous function of V_{S30} (time-based average of shear-wave velocity in the upper 30 m of the soil) because many of the strong-motion stations in the databank have known shear-wave velocity profiles. The nonlinear site model with the consideration of continuous V_{S30} is realized for the first time in pan-European GMPEs. This novel feature of the proposed GMPEs led this dissertation to evaluate the site factors of NEHRP (BSSC, 2009) and Eurocode 8 (CEN, 2004) that essentially prompted the proposition of a new methodology to compute hazard-consistent site factors by making use of probabilistic seismic hazard assessment results. These findings are

2

believed to be useful for the future evaluation of site factors in Eurocode 8 (CEN, 2004). The following sections summarize the main contributions of this dissertation and describe the essential structuring in each chapter.

1.2 Areas of the Contribution and Relevant Literature

Each subsection describes a particular topic that is studied in detail within the context of this thesis. The discussions held in these subsections first summarize the most relevant literature in each topic and then describe the major contributions of this dissertation to those fields.

1.2.1 Pan-European Strong-Motion Database (RESORCE)

The compilation of the strong-motion data from Europe and the Middle East has gradually developed since the 1970s (Ambraseys, 1978; Ambraseys, 1990; Ambraseys and Bommer, 1991; Bommer and Ambraseys, 1992; Ambraseys et al., 2000; Bommer and Douglas, 2004; Ambraseys et al., 2004a; Ambraseys et al., 2004b). The major focus point in these studies is the consistent evaluation of earthquake and strong-motion station metadata information. The uniform processing of strong-motion records with physically justifiable methods, on the other hand, was only applied to a limited number of accelerograms. The above studies collectively resulted in the Internet Site for European Strong-Motion Data web page (ISESD; http://www.isesd.hi.is; Ambraseys et al., 2004a) and its refined subset, European Strong-Motion Database (ESMD, Ambraseys et al., 2004b). For about a decade the main accelerometric data of the broader Europe is disseminated to the engineering and seismological community through these archives.

The recent national strong-motion projects in Europe (e.g., Hellenic Arc Database, HEAD, http://www.itsak.gr/en/db/data; Theodulidis et al., 2004, ITalian ACcelerometric Archive; ITACA; http://itaca.mi.ingv.it; Luzi et al., 2008, Turkish

National Strong-Motion Project; T-NSMP; http://kyh.deprem.gov.tr/; Akkar et al., 2010; Swiss accelerometric archives, arclink.sed.ch) compiled the national accelerometric data using state-of-the-art techniques and especially performed in-situ site measurements for characterizing the soil conditions of the strong-motion recordings stations. However, these projects implemented their own methods while compiling their databases.

A world-wide strong-motion databank was collected (Yenier et al., 2010) under the SHARE project with a major focus on the shallow active crustal earthquakes. The SHARE strong-motion databank considers the accelerometric data from ISESD, ESMD, ITACA and T-NSMP projects as well as those of Japan and the United States. During the compilation of the SHARE strong-motion databank, however, no attempt was made to homogenize or improve the metadata or process the accelerograms. The SHARE strong-motion databank contains a significant number of accelerograms from the pan-European region, including data of the recent national projects. This fact motivated establishing the Reference Database for Seismic Ground-Motion in Europe (RESORCE), one of the products of the SIGMA (SeIsmic Ground Motion Assessment) project. The relevant studies in this dissertation form the major backbone of RESORCE.

The compilation of RESORCE contains three main parts: event, station and record information. Event information includes major source characteristics of the earthquakes (location, focal depth, magnitude in various scales, faulting mechanism, etc.). This set of information is obtained from the local, regional and global seismological agencies as well as earthquake-specific studies. The location, site class and housing information of the recording instrument are all provided under the umbrella of station information. Site characterization is determined from in-situ site measurements (geophysical explorations). Geological and geotechnical information are also used to classify the soil category. Event-related station parameters are source-to-site distance metrics. The most important recording

information is the type of recording device and data processing parameters of the accelerograms as well as the usable period ranges of the recordings.

RESORCE gives upmost importance to the reliability and uniformity of each one of the above metadata parameters and can be of use for developing robust GMPEs for the pan-European region as well as provide valuable information for other seismology and engineering related studies in and around Europe.

1.2.2 Site Amplification Model and Its Engineering Application

Site response is one of the essential components of earthquake engineering design. It has been of interest to many researchers since the early works of Borcherdt (1970) who defined the site amplification as the ratio of a ground-motion intensity measure at a soil site to its counterpart measured at a nearby rock site. Each site has its own characteristics (degradation modulus, stiffness, plasticity index, etc.) that affect (modify) the seismic waves from source to the ground surface. Thus, it is impossible to have a unique site amplification model that can be validated for each site. However, the pragmatic engineering approach seeks for the simplest and the most robust parameter(s) to simulate the physical conditions of a site to make the best estimate of soil response. Although it is debatable, currently V_{S30}, the time-based average of the shear-wave velocity of the uppermost 30 m soil profile, seems to be the most appropriate physical parameter for describing the site amplification for most engineering work. This proxy has been extensively used in site classification schemes (Borcherdt, 1994; Dobry et al., 2000; Rey et al., 2002). The NEHRP provisions and Eurocode 8 (EC8) used the major outcomes of these studies (or other similar ones) to shape their in-practice site classification and corresponding site factors.

The integration of soil effects in GMPEs has evolved progressively. Site effects were initially addressed by defining two broad site classifications: soil and rock (e.g., Sadigh et al., 1997). Some ground-motion models (e.g., Akkar and Bommer,

2010) account for the site influence by considering more detailed generic soil categories that are based on certain V_{S30} intervals. Ground-motion models that classify soils into different generic categories assume linear site response. Boore et al. (1997) also propose a linear site model but their site function is in terms of continuous V_{S30}. The site model by Abrahamson and Silva (1997) is the first one that considers nonlinear soil behavior in soil sites. The studies by Boore et al. (1997) and Abrahamson and Silva (1997) have shaped the recent site modeling trend in GMPEs. That is representing the soil effects by a site amplification model as a function of V_{S30} and reference rock motion that sets thresholds for nonlinear soil behavior (Choi and Stewart, 2005; Abrahamson and Silva, 2008; Boore and Atkinson, 2008; Campbell and Bozorgnia, 2008; Chiou and Youngs, 2008; Walling et al., 2008). The functional forms of these site models were developed using either empirical data or stochastic simulations.

An empirical nonlinear site model is also developed in this dissertation by using a global database that consists of European strong-motion recordings with known V_{S30} (from RESORCE) as well as accelerometric data obtained from NGA (Chiou et al., 2008) and Japanese (Pousse et al., 2005) databases. The proposed site model has a functional form similar to that of Walling et al (2008) that is developed from simulated ground motions. The comparable site amplification estimates from the proposed model and Walling et al. (2008) validate the physics behind the functional form of Walling et al. (2008) that is entirely based on simulated ground motions.

The proposed nonlinear site model is used in the ground-motion predictive models that are also developed within this dissertation. Moreover, it is used in the evaluation of the site factors proposed by the NEHRP and Eurocode8 provisions. The proposed site model is also used to develop a method for the computation of site factors that is capable of using the outcomes of the probabilistic seismic hazard assessment. This novel method is believed to be the alternative to the

traditional record-based site factor computation scheme (e.g., Borcherdt, 2002a; Rey et al., 2002).

1.2.3 Pan-European GMPEs

GMPEs estimate ground-motion intensity measures by a suite of seismological variables that model the source characteristics of the earthquakes, attenuation of seismic waves along the path and site response in the soil media. The main estimators of source, path and site effects in GMPEs are moment magnitude (M_w), style-of-faulting, geometric spreading, anelastic attenuation and V_{S30} dependent site term. These variables constitute the basis of the simplest functional forms used in modern GMPEs.

The first 5%-damped horizontal GMPE for spectral acceleration for the pan-European region is developed by Ambraseys et al. (1996). Later, it has been improved by Bommer et al. (2003) for different fault mechanisms. Ambraseys et al. (2005a), Akkar and Bommer (2007a; 2007b), Bommer et al. (2007), Akkar and Bommer (2010) and Bommer et al. (2012) improved the pan-European ground-motion predictive model by using more complicated functional forms as well as by improvements in the ground-motion databases. These equations were derived using the maximum-likelihood regression approach of Joyner and Boore (1993). Generic site classes (rock, stiff soil and soft soil) that are based on predetermined V_{S30} intervals are preferred in addressing the site response. The source-to-site distance common to all of these GMPEs is the Joyner and Boore (1981) distance measure. The Ambraseys et al. (1996) equations use a simple functional form: a linear dependence on surface-wave magnitude, M_s, and geometric spreading as a function of R_{JB}. As indicted, Bommer et al. (2003) added the style-of-faulting term to the Ambraseys et al. (1996) GMPE to include the effect of reverse, normal or strike-slip faulting on ground-motion estimates. Ambraseys et al. (2005a) replaced M_s by M_w and included the magnitude-dependency to the geometrical

spreading term. Akkar and Bommer (2007a; 2007b) added quadratic magnitude scaling to the pan-European GMPEs by using almost the same ground-motion dataset of Ambraseys et al. (2005a) with the reconsideration of data processing of the whole database. Moreover the horizontal component definition of Akkar and Bommer (2007a; 2007b) GMPEs is the geometric mean of two horizontal components. Ambraseys et al. (2005a) use maximum horizontal component for their ground-motion estimates. The functional form used in Akkar and Bommer (2007a; 2007b) are also used in Bommer et al. (2007) as well as Akkar and Bommer (2010) and Bommer et al. (2012). The Bommer et al. (2007) GMPE investigated the small-magnitude effect on ground-motion estimates. The Akkar and Bommer (2010) and Bommer et al. (2012) models are the updates of Akkar and Bommer (2007a; 2007b). The first GMPE (i.e., Akkar and Bommer, 2010) considers magnitude-independent standard deviation and fixes the unexpected trends observed in the spectral ordinates estimates of Akkar and Bommer (2007b). The second GMPE (i.e., Bommer et al., 2012) extends the spectral ordinates towards very short periods (i.e., $0.01s \leq T \leq 0.05s$).

The progressive evolution of vertical spectrum pan-European GMPEs start with the one proposed by Ambraseys and Simpson (1996). This GMPE is followed by Ambraseys et al. (2005b) and Bommer et al. (2011). Ambraseys et al. (2005b) propose a ground-motion model for the direct estimate of vertical spectral ordinates. On the other hand, Ambraseys and Simpson (1996) and Bommer et al. (2011) developed ground-motion models for estimating vertical-to-horizontal spectral ratios that modify horizontal spectrum for the corresponding vertical spectrum. The Ambraseys and Simpson (1996) vertical-to-horizontal spectral ratio model is almost consistent (some of the vertical components did not exist in the study) with the horizontal GMPE that is produced by the same authors in the same study. However, it is superseded by the Bommer et al. (2011) vertical-to-horizontal spectral ratio GMPE. Although the Bommer et al. (2011) vertical-to-horizontal spectral ratio GMPE was meant to be compatible with the Akkar and Bommer (2010) horizontal predictive model, the magnitude and distance ranges as

well as the ground-motion database of the former model is significantly different than those of the latter GMPE. Therefore, the vertical spectral ordinates produced with the convolution of these two GMPEs may not be fully compatible with the horizontal spectral ordinate estimates of the Akkar and Bommer (2010) ground-motion model.

The estimation of spectral ordinates for damping levels other than 5% of critical can be obtained by either deriving different sets of GMPEs for each damping ratio or by computing damping scaling factors. For damping scaling in the broader Europe, Akkar and Bommer (2007b) followed the first approach whereas Bommer et al. (1998), Tolis and Faccioli (1999) and Faccioli et al. (2004) preferred deriving damping-scaling-factors to modify 5% damped spectrum. It is believed that the damping scaling factor GMPEs is advantageous as they are easier to implement in practice. However, the aforementioned studies on this approach can be considered as outdated particularly after the recent updates of the pan-Europen strong-motion databases (i.e., RESORCE) as well as recent observations for the improved estimates of damping scaling factors (e.g., Rezaeian et al., 2012).

Based on the shortcomings of previous pan-European GMPEs as discussed above as well as the recent updates in the ground-motion databank of the broader Europe, this dissertation focuses on developing new ground-motion models for the prediction of horizontal and vertical pseudo-spectral accelerations, as well as corresponding peak ground accelerations and velocities. The ground-motion estimates are made for various damping levels via damping scaling GMPEs that are also developed as part of this thesis. The models were developed from a subset of RESORCE. The accelerometric data used in this dissertation almost triple the data of previous pan-European GMPEs. As it has already been indicated, the metadata quality of RESORCE is better than those of previous pan-European GMPEs, which is believed to result in more reliable ground-motion estimates for the broader Europe.

New GMPEs are capable of estimating the nonlinear site response with a function composed of V_{S30} and reference peak ground acceleration on rock. Both magnitude and distance ranges are increased in the proposed equations that are valid for spectral periods between 0.01s and 4s. Horizontal and vertical components are fully compatible for different damping levels between 1% and 50%. These consistent models are applicable for both point-source (epicentral; R_{epi}, and hypocentral distance; R_{hyp}) and finite-fault (distance to the surface projection of the rupture, R_{JB}) distance metrics.

1.3 Objective and Scope

The study presented here is composed of seven chapters and began with Chapter 1 that gave the basic literature review, major contributions and outline of the dissertation.

Chapter 2 describes the recently developed pan-European strong-motion databank (RESORCE) and its seismological features. It also includes a part that details the followed selection procedure to assemble the subset database used in the development of pan-European predictive models in this dissertation. The last section of this chapter presents the additional recordings from the United States and Japan that are used to develop the nonlinear site model.

Chapter 3 summarizes the literature survey on the site models used in ground-motion prediction equations. The development of the empirical nonlinear site model is the principal body of this chapter. The site factors estimated by the proposed model are compared with recent site models. A preliminary evaluation of the proposed site factors with those recommended by the seismic design codes is made here as well.

Chapter 4 firstly discusses the evolution of the site factors in seismic design codes then expands the previous discussion in Chapter 3 by applying multiple

earthquake scenarios obtained from probabilistic seismic hazard assessment. This chapter proposes a procedure to compute site factors by using the results of regional seismic hazard studies.

Chapter 5 starts with an overview of the pan-European GMPEs with emphasis on their limitations. Later, the new pan-European predictive equations for 5% damped horizontal component are introduced. These equations are applicable to both extended- and point-source distance metrics. This chapter ends by testing the limitations of the prediction equations and comparing them with the global, regional and local GMPEs.

Chapter 6 introduces a brief overview of the vertical GMPEs and damping scaling factors. Then the companion vertical-to-horizontal spectral ratio GMPE and the horizontal and vertical components damping scaling factors are presented.

The last Chapter terminates the dissertation by presenting the concluding remarks of the entire study with a proposal for a set of research interests that call for the shortcomings of the procedures followed here and improvements needed in the future versions of the pan-European predictive models.

CHAPTER 2

REFERENCE DATABASE FOR SEISMIC GROUND MOTION IN EUROPE (RESORCE) AND DATA SELECTION PROCEDURE

Adapted from Akkar S., M.A. Sandıkkaya, M. Şenyurt, A. Azari Sisi, B.Ö. Ay, P. Treversa, J. Douglas, F. Cotton, L. Luzi, B. Hernandez, S Godey (2014a). Reference Database for Seismic Ground-Motion in Europe (RESORCE).Bulletin of Earthquake Engineering, 12:311–339.

This chapter presents the overall procedure followed in order to assemble the most recent pan-European strong-motion databank: Reference Database for Seismic Ground-Motion in Europe (RESORCE). RESORCE is one of the products of the SIGMA (**Se**ismic **G**round **M**otion **A**ssessment; projet-sigma.com) project. RESORCE is intended to be a single integrated accelerometric databank for Europe and surrounding areas for use in the development and testing of ground-motion models and for other engineering seismology and earthquake engineering applications. RESORCE aims to contribute to the improvement of earthquake risk studies in Europe and surrounding areas. RESORCE principally updates and extends the previous pan-European strong-motion databank (Ambraseys et al., 2004a) with recently compiled Greek, Italian, Swiss and Turkish accelerometric archives. The updates also include earthquake-specific studies published in recent years. The current content of RESORCE includes 5882 multi-component and uniformly processed accelerograms from 1814 events and 1540 strong-motion stations. The moment magnitude range covered by RESORCE is $2.8 \le M_w \le 7.8$. The source-to-site distance interval extends to 587 km and distance information is

13

given by the common point- and extended-source distance measures. The paper presents the current features of RESORCE through simple statistics that also quantify the differences in metadata and strong-motion processing with respect to the previous version of the pan-European strong-motion databank.

This chapter also describes the selection procedure from RESORCE to form the database that is used in developing of the next generation predictive equations for Europe and surroundings. Besides, to enhance the capability of the derived nonlinear site model, a set of accelerogram is extracted from the global dataset compiled by Yenier et al. (2010).

2.1 Evolution of Strong-Motion Data Collection in Europe

The attempts to collect and compile strong-motion data from Europe and the Middle East started in the first half of 1970s at Imperial College, London after the 1967 Debar and 1969 Portugal earthquakes (Ambraseys, 1978). The volunteer work undertaken at Imperial College was later funded through various grants provided by the governmental agencies of the UK and the European Commission (Bommer and Douglas, 2004); the latter being collaborative projects with different European research centers (Ambraseys, 1990; Ambraseys and Bommer, 1991; Bommer and Ambraseys, 1992). The major focus point in these projects was the consistent evaluation of earthquake and strong-motion station metadata information as well as uniform processing of strong-motion records, leading to a reliable strong-motion databank for earthquake-induced hazard and risk studies in Europe.

The efforts which grew out from these studies resulted in a CD-ROM of 1068 tri-axial accelerograph data (Ambraseys et al., 2000) which was expanded later by additional recordings from the broader Europe (pan-European) region. The expanded strong-motion databank (2213 accelerograms from 856 earthquakes

recorded at 691 strong-motion stations) is disseminated through the Internet Site for European Strong-Motion Data web page (ISESD; http://www.isesd.hi.is; Ambraseys et al., 2004a). The ISESD strong-motion databank considers special studies on earthquakes (released as either institutional reports or articles published in peer-reviewed journals) as the primary sources for the earthquake and strong-motion station metadata. In the absence of such earthquake-specific studies, the earthquake metadata (e.g., epicentral location, focal depth as well as magnitude estimations other than local magnitude, M_L) were mostly taken from the Bulletin of the International Seismological Center (www.isc.ac.uk). The local magnitude information was gathered from local and national networks. The preferred source of information for earthquake location is the local or national networks whenever they were assessed as more reliable with respect to the international seismic agencies. The network owners are rated as the most reliable information source for strong-motion station metadata information (e.g., site conditions, station coordinates, shelter type) when strong-motion sites lack specific monograms. The soil conditions of strong-motion stations are classified using the Boore et al. (1993) scheme that is based on V_{S30} intervals (V_{S30} < 180 m/s; 180 m/s ≤ V_{S30} < 360 m/s; 360 m/s ≤ V_{S30} < 750 m/s; V_{S30} ≥ 750 m/s) where V_{S30} is the average shear-wave velocity in the top 30 m soil profile. However, the unavailable shear-wave velocity profiles at almost all strong-motion stations constituted the major difficulty in the soil classification of strong-motion sites. Almost all the processed strong-motion records in ISESD were band-pass filtered using an elliptical filter with constant high-pass and low-pass cut-off frequencies (0.25 Hz and 25 Hz, respectively). A subset of ISESD was re-processed using the bi-directional (acausal) Butterworth filter with cut-off frequencies adjusted individually for each accelerogram. The individual filter cut-off frequencies were determined from the signal-to-noise ratio of each accelerogram. This subset, later, was released as another CD-ROM (ESMD; European Strong-Motion Data; Ambraseys et al., 2004b) after the inauguration of the ISESD web site.

The efforts for the compilation of ISESD strong-motion databank were followed by important national and international strong-motion and seismic hazard projects in Europe and the surrounding regions. Of these projects the **IT**alian **AC**celerometric **A**rchive Project (ITACA; http://itaca.mi.ingv.it; Luzi et al., 2008) and the **T**urkish **N**ational **S**trong-**M**otion **P**roject (T-NSMP; http://kyh.deprem.gov.tr/; Akkar et al., 2010) are national initiatives to compile, process and archive local (national) accelerometric data using state-of-art techniques. The ITACA project compiled a total of 2182 accelerograms from 1004 events (Luzi et al., 2008) whereas T-NSMP studied 4607 strong-motion records from 2996 earthquakes recorded at 209 stations (Akkar et al., 2010). Both ITACA and T-NSMP also improved the site characterization of strong-motion stations either by reassessing the existing shear-wave velocity profiles and soil column lithology information or by utilizing invasive or noninvasive site exploration techniques to compute the unknown V_{S30} and other relevant site parameters (e.g., Sandıkkaya et al., 2010). A similar effort has also been started in Greece after 2000 to archive the uniformly processed Greek records of strong-motion stations operated by ITSAK (http://www.itsak.gr/; Theodulidis et al., 2004) under the HEAD (**HE**llenic **A**ccelerogram **D**atabase) databank. The **S**eismic **H**azard H**AR**monization in **E**urope project (SHARE; www.share.eu.org), a grant provided by the European Commission, compiled a strong-motion databank (Yenier et al., 2010) by collecting shallow crustal accelerometric data from the worldwide strong-motion databanks (ISESD, ESMD, ITACA and T-NSMP are among these databanks) to test the performance of candidate ground-motion prediction equations (GMPEs) for hazard calculations in Europe. This databank (13500 records from 2268 events recorded at 3708 stations) neither updates the metadata information nor develops a uniformly processed accelerometric data archive from the existing events of the selected strong-motion databanks. However, the developers of the SHARE strong-motion databank gave careful consideration to the removal of duplicated entries in the event, station and waveform information through a hierarchical approach.

2.2 Motivation behind the Development of RESORCE

Despite the significant efforts put forward in the development of ISESD, it suffers from poor strong-motion site characterization and the use of constant filter cut-offs in data processing. This latter feature has been proven to be inappropriate as it may result in misrepresentation of actual ground-motion frequency content of the recorded events (e.g., Akkar and Bommer, 2006). Recent national strong-motion projects (major ones have already been discussed in the previous section) tried to prevent these drawbacks but they evolved as individual attempts. These projects implemented their own procedures while assembling the databases that may result in lack of uniformity in metadata compilation and record processing during their integration under a single strong-motion databank. The SHARE project gathered strong-motion data from recent strong-motion databanks but no attempt was made to homogenize the data processing of accelerograms. Improvements of earthquake and station metadata from recent studies in the literature were also out of the scope of the SHARE strong-motion databank. The recordings from recent earthquakes of engineering significance in the broader European region (e.g., 2009 L'Aquila Earthquake M_w 6.3; 2011 Van Earthquake M_w 7.1; 2011 Van-Edremit Earthquake M_w 5.6; 2011 Kütahya-Simav Earthquake M_w 5.9; 2010 Elazığ-Kovancılar Earthquake M_w 6.1) are either entirely or mostly disregarded in the SHARE strong-motion databank.

The primary motivation behind RESORCE is to be a single integrated accelerometric databank for the broader European area. The basic ingredient of RESORCE is the pan-European subset of the SHARE strong-motion databank (Yenier et al., 2010). It updates and expands the ISESD accelerometric archive using information gathered from recently carried out strong-motion database projects as well as from other relevant earthquake-specific studies in the literature. The uniform data processing of accelerograms as well as improved magnitude and source-to-site distance distributions constitute other important steps in RESORCE. RESORCE is one of the products of the SIGMA (**Se**ismic **G**round

Motion **A**ssessment) project whose main goal is to improve seismic hazard assessment methods in France and neighboring regions, with realistic characterization of aleatory and epistemic uncertainties. RESORCE, which is built using a consistent approach, is one of the building blocks for achieving these objectives. The development of RESORCE is realized as a collaborative work under SIGMA-Work Package 2 that consists of researchers from Électricité de France (EDF), Institut des Sciences de la Terre (ISTerre), Bureau de Recherches Géologiques et Minères (BRGM), European Mediterranean Seismological Centre (EMSC), Istituto Nazionale di Geofisica e Vulcanologia (INGV), Laboratoire de detection et de Géophysique (LDG) and Middle East Technical University (METU). The last institute is responsible for the compilation and processing of RESORCE whereas the first five institutions are heavily involved in its scientific revision, coordination and dissemination. RESORCE went through a peer review process during its evolution to provide verified accelerometric data together with reliable metadata that can be used in engineering seismology and earthquake engineering studies. The steps followed in assembling RESORCE are described in the following sections with emphasis on the differences between ISESD and RESORCE so as to display the level of improvements in the current pan-European accelerometric data archive.

2.3 Strategy Followed in the Compilation and Strong-Motion Data Processing

The accelerometric data and corresponding metadata information gathered in RESORCE are a collection of recordings from local accelerometric data providers, previously established regional and global databanks, seismological agencies and recent studies in the literature. Table 2.1 lists the six major sources (designated under the "Accelerogram" column) used for collecting the raw accelerograms in RESORCE. The timespan of these accelerometric data is given in Table 2.2. The reference sources also contain earthquake and strong-motion station metadata information as presented in Table 2.1.

Table 2.1 Major reference sources used in the compilation of RESORCE

Source	Accelerogram	Station Metadata	Earthquake Metadata
Internet site for European strong-motion data (ISESD; Ambraseys et al., 2004a)	√	√	√
Italian accelerometric archive (ITACA, Luzi et al., 2008)	√	√	√
The Next Generation Attenuation Models Project (NGA, Power et al., 2008)	√	√	√
Turkish national strong-motion project (T-NSMP, Akkar et al., 2010 and Sandıkkaya et al., 2010)	√	√	√
The Swiss Seismological Service (SED, www.seismo.ethz.ch)	√	√	√
Hellenic Accelerogram Database (HEAD, http://www.itsak.gr/en/db/data; Theodulidis et al., 2004)	√	√	√
European strong-motion database (ESMD, Ambraseys et al. 2004b)		√	√
European-Mediterranean Regional Centroid Moment Tensor catalog (RCMT; http://www.bo.ingv.it/RCMT/)			√
Global Centroid Moment Tensor Catalog Search (GCMT, www.globalcmt.org)			√
International Seismological Centre (ISC; http://www.isc.ac.uk/)			√
U.S. Geological Survey (USGS; http://earthquake.usgs.gov/)			√
Cauzzi and Faccioli (2008)		√	

Table 2. 2 Timespan of the accelerometric data

Source	Timespan	Exceptions
Internet site for European strong-motion data (ISESD; Ambraseys et al., 2004a)	1967-2003	2004 Kojur-Firoozabad (Iran), 2004 Leskoviku (Albania), 2005 Dahooeiyeh-Zarand (Iran) and 2008 Olfus (Iceland) earthquakes
Italian accelerometric archive (ITACA, Luzi et al., 2008)	1976-2004	2008 App. Parmense, 2009 L'Aqulia, its major aftershocks and 2009 Gran Sasso and its afterschock
The Next Generation Attenuation Models Project (NGA, Power et al., 2008)		1984 Pelekanada (Greece), 1992 Roermond (Netherlands), 1995 Kozani Aftershock (Greece) earthquakes
Turkish national strong-motion project (T-NSMP, Akkar et al., 2010 and Sandıkkaya et al., 2010)	1976-2007	2010 Kovancılar and its aftershock, 2011 Simav, 2011 Van and 2011 Edremit earthquakes
The Swiss Seismological Service (SED, www.seismo.ethz.ch)	1994-2012	
Hellenic Accelerogram Database (HEAD, http://www.itsak.gr/en/db/data; Theodulidis et al., 2004)	1973-1999	2003 Lefkada and 2006 Kythera earthquakes

The existing earthquake and strong-motion station metadata from these sources as well as other reliable references were studied individually while assembling RESORCE. The waveforms of raw accelerometric data were visually inspected one by one in terms of waveform quality and frequency content to implement a

well-established data processing technique into the entire strong-motion databank. The steps followed in this entire process are summarized below.

The major structure of RESORCE consists of two principal blocks: (1) earthquake and station metadata information, and (2) accelerometric data. Inherently, these two blocks are related to each other and are assembled from almost the same reference sources (see Table 2.1). Figure 2.1 summarizes the overall structure of RESORCE in this perspective. ISESD and its subset ESMD are considered as the primary sources of earthquake (M_w, epicentral coordinate, depth, style-of-faulting, fault geometry etc.) and strong-motion station (soil conditions, station coordinate, different source-to-site distance measures, recoding type – analog vs. digital – etc.) metadata for pre-2004 events. This preference is waived for the earthquakes that occurred in Italy as well as the Italian strong-motion stations as ITACA contains the most up-to-date station and event information for Italy. Notwithstanding, for Italian events that lack of M_w, the Castello et al. (2007) M_L-M_w empirical magnitude conversion relationship was used. This is the only modification made to ITACA within the context of these studies. A similar magnitude conversion process was also implemented in HEAD and T-NSMP during their compilation (Theodulidis et al., 2004; Akkar et al., 2010). For Greek events, Papazachos et al. (2002) was used for M_L- M_w conversion. The empirical relationships of Akkar et al. (2010) were used for M_w conversion of Turkish earthquakes if they are reported in other magnitudes. The resulting moment magnitude estimations are taken into account in RESORCE for Greek events, post-2004 Turkish earthquakes as well as for those that occurred before 2004 whenever they are not included in ISESD or ESMD. The preeminence of ISESD and ESMD for pre-2004 earthquake metadata of Turkish events is not overruled because T-NSMP provides earthquake information from a set of seismological references for each entry in its archive and both ISESD and ESMD are among these seismological sources. Thus, the decision on preferring ISESD and ESMD for pre-2004 Turkish earthquake metadata is in line with the database compilation policy of T-NSMP.

21
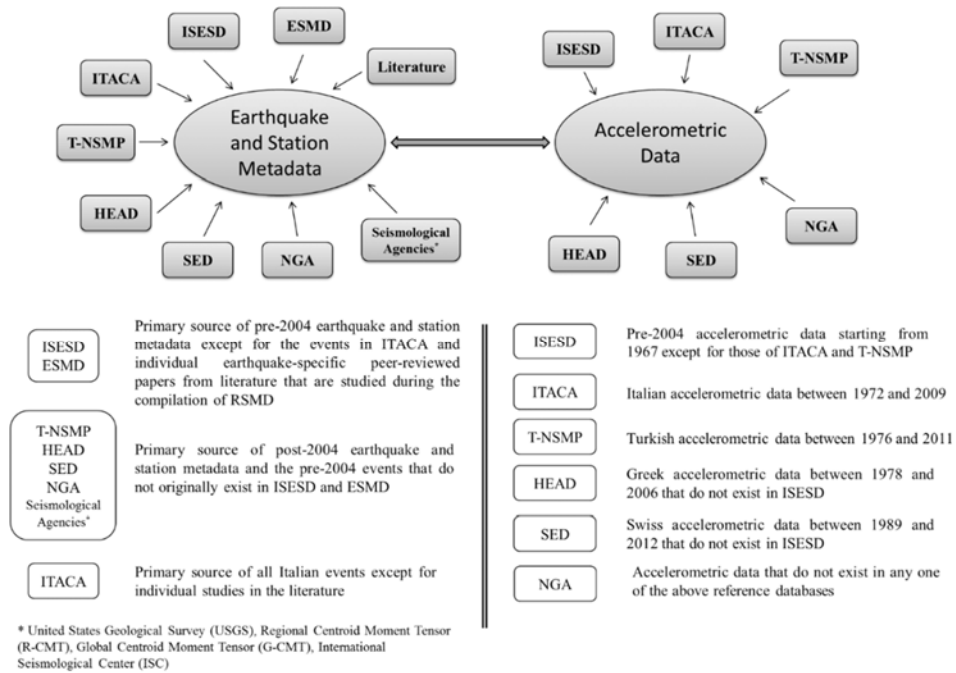
Figure 2. 1. Basic structure of RESORCE and reference sources that build the metadata information as well as the accelerometric data in RESORCE.

The earthquake and station information of additional references, other than ISESD and ESMD, (see Figure 2.1 as well as Tables 2.1 and 2.3) is primarily taken into account for post-2004 earthquake and station metadata in RESORCE. These references are also used for the pre-2004 RESORCE inventory to complete some of the missing earthquake metadata components of individual events or for including additional earthquakes that are not covered by the ISESD or ESMD archives. The event- and station-based information collected from earthquake-specific literature studies are always ranked as the primary reference for earthquake and station metadata in RESORCE regardless of the corresponding information in the other studied sources. Table 2.3 presents the peer-reviewed literature studies used from this standpoint. This table also lists the earthquake-specific literature survey compiled and used by ISESD that is inherently

considered during the compilation of RESORCE. The reported M_w values of seismic agencies are based on global or regional moment tensor solutions. These M_w values are accepted as they are and no quality assurance is made by tracing back the number of stations used in their computation. In a similar fashion while converting the body-wave magnitude (m_b) scale into M_w, the possibility of positive biases in m_b for small-to-moderate size events was not considered. Such additional quality assurance checks should be made in the upcoming versions of RESORCE to improve the reliability of information released by this strong-motion databank.

An important detail about the RESORCE station metadata is the site characterization of the Turkish and Greek strong-motion recording stations. The T-NSMP strong-motion inventory is preferred for the site information of the national-network stations of Turkey because it contains the most updated site characterization of these stations. Similarly, the recent site information of 19 Greek stations from the HEAD archive is used to update the site classification of corresponding Greek recordings in RESORCE. The site information of 7 Turkish strong-motion stations other than those pertaining to the national-network is compiled from the literature survey (Rosenblad et al., 2002; see Table 2.3). Site information of three Greek strong-motion stations not covered by HEAD is obtained via personal communication with Prof. Kyriazis Pitilakis and Ms. Evi Riga (AUTH, Greece). The primary parameter used for strong-motion site characterization in RESORCE is V_{S30} as ITACA, T-NSMP, HEAD as well as recent literature studies that are accounted for while compiling the RESORCE station metadata use in-situ shear-wave velocity profiles measured by invasive and noninvasive site exploration techniques. Table 2.4 presents the geophysical site exploration techniques whose shear-wave velocity measurements are evaluated by the above reference sources for site characterization of strong-motion stations in their archive.

Table 2. 3 Earthquake-specific literature used in earthquake and strong-motion station metadata in RSMD

Reference	Main Focus
Abercrombie et al. (1995) [b]	Source information on the 1981 Alkion earthquakes (Greece)
Amorese et al. (1995) [b]	Source information on the 1976 Gazli earthquake (Uzbekistan)
Arvidsson and Ekström (1998) and Chouliaras and Stavrakakis (1997) [c]	Magnitude information on three earthquakes occurred in 1995 (Greece)
Anderson et al. (2001) [b]	Source information on the 1995 Dinar earthquake (Turkey)
Anderson and Jackson (1987) [b]	Source information on the 1978 Basso Tirreno earhquake
Bajc et al. (2001) [b]	Source information on the 1998 Bovec earthquake (Slovenia)
Benetatos and Kiratzi (2006) [c]	Source information on the 1979 Montenegro earthquake (the M_w 6.2 aftershock)
Benetatos et al. (2007) [c]	Source information on the 2003 Lefkada earthquake (Greece)
Berberian et al. (1992) [b]	Source information on the 1990 Manjil earthquake (Iran)
Bernard et al. (1997) [b]	Source information on the 1992 Erzincan earthquake (Turkey)
Boore et al. (2009) [c]	Source information on the 2003 Kythira earthquake (Greece)
Decriem et al. (2010) [c]	Source information on the 2008 Olfus earthquake (Iceland)
Delouis et al. (2002) [c]	Source information on the 1999 Kocaeli earthquake (Turkey)
Erdik (1984) [b]	Source information on the 1983 Pasinler earthquake (Turkey)
Haessler et al. (1988) [b]	Source information on the 1984 Umbria earthquake (Italy)
Hatzfeld et al. (1997) [b]	Source information on the 1995 Kozani earthquake (Greece)
Jackson et al. (2006) [c]	Source information on the 2003 Bam earthquake (Iran)
Louvari et al. (2004) [b]	Source information on the 1983 Kefallinia Island earthquake (Greece)
Lyon-Caen et al. (1988) [b]	Source information on the 1986 Kalamata earthquake (Greece)

Table 2.3 Cont'd

Reference	Main Focus
Makaris et al. (2000) [b]	Source information on the 1997 Strofades earthquake (Greece)
Oncescu and Bonjer (1997) [b]	Source information on the 1977 Bucharest earthquake (Romania)
Pace et al. (2002) [b]	Source information on the 1984 Lazio Abruzzo earthquakes (Italy)
Pedersen et al. (2003) [c]	Source information on the two June 2000 Iceland earthquakes
Perniola et al. (2004) [c]	Source information on the 1976 Friuli earthquake and its major aftershocks (Italy)
Roumelioti and Kiratzi (2002) [b]	Source information on the 1979 Montenegro earthquake (Montenegro)
Salvi et al. (2000) [b]	Source information on the 1997 Umbria-Marche earthquakes (Italy)
Soufleris et al. (1982) [b]	Source information on the 1978 Volvi earthquake (Greece)
Talebian et al. (2006) [c]	Source information on the 2005 Dahooeiyeh-Zarand (Kerman) earthquake (Iran)
Tan et al. (2011) [c]	Source information on the 2008 Kovancılar earthquake (Turkey)
Tatar et al. (2007) [c]	Source information on the 2004 Kojur-Firoozabad earthquake (Iran)
Triep et al. (1995) [b]	Source information on the 1991 Racha earthquake (Georgia)
Tselentis and Zahradnik (2000) [b]	Source information on the 1999 Ano Liosia (Athens) earthquake (Greece)
Tselentis et al. (1996) [b]	Source information on the 1995 Aigion earthquake (Greece)
Umutlu et al. (2004) [c]	Source information on the 1999 Düzce earthquake (Turkey)
Walker et al. (2003) [b]	Source information on the 1978 Tabas earthquake (Iran)
Walker et al. (2005) [c]	Source information of the 2002 Avaj earthquake (Iran)
Kyriazis Pitilakis and Evi Riga (AUTH) [d]	Updated V_{S30} information of some of the Greek sites that are not considered in HEAD
Rosenblad et al. (2002) [c]	Updated V_{S30} information of some of the Turkish sites operated by KOERI[a]

[a] KOERI: Kandilli Observatory and Earthquake Research Institute
[b] Literature survey from ISESD (Ambraseys et al., 2004a).
[c] Additional literature survey
[d] Personal communication

Table 2. 4 In-situ site measurements of the RESORCE strong-motion recording stations

Measurement description	Reference source
Seismic cross-hole	HEAD and ITACA
Seismic down-hole	HEAD and ITACA
Extended spatial autocorrelation method from microtremor array measurements (ESAC)	ITACA
Frequency wavenumber spectrum method from microtremor array measurements (ESAC-FK)	ITACA
Multi-channel analysis of the surface waves (MASW)	ITACA and T-NSMP
Spectral analysis of surface waves (SASW)	Rosenblad et al., 2002

The unification of earthquake and station metadata for RESORCE as described in the previous paragraphs is finalized by homogenizing the classification of style-of-faulting (SoF). The homogenization of the SoF classification was a necessary step as the existing double-couple fault-plane solutions are evaluated differently by each reference source to identify the SoF of each event in their inventory. The procedure proposed in Boore and Atkinson (2007) is used to remove the differences in SoF classification of the considered reference sources. This procedure, which is modified from Frolich and Apperson (1992) and Zoback (1992), uses the plunge angles of the T- and P-axes of the double-couple fault-plane solutions. The procedure does not require the actual fault plane solution, which makes it appealing in the determination of SoF for earthquakes that occur on faults without a rupture trace on the surface. It determines a unique SoF, which is not the case for SoF classifications based on the rake angle. The rake angles of actual and auxiliary planes from double-couple fault-plane solutions can sometimes result in two different SoF classifications for the same earthquake. The missing plunges of the T- and P-axes for certain events in RESORCE does not constitute a drawback in the implementation of the Boore and Atkinson (2007) procedure as they can be computed from the strike, dip and rake angles of the

26

fault-plane solutions (Snoke, 2003). Table 2.5 lists the intervals of the plunges of the T- and P-axes for SoF classification in RESORCE.

Table 2. 5 Criteria of style-of-faulting classification using plunge angles

Style of Faulting	P-axis plunge angle	T-axis plunge angle
Normal	P-pl>40	T-pl<40
Reverse	P-pl<40	T-pl>40
Strike-slip	P-pl<40	T-pl<40

The completed earthquake and station metadata of RESORCE enabled the computation of missing source-to-site distance measures (epicentral distance, $R_{epi;}$ hypocentral distance, R_{hyp}; closest distance to the surface projection of ruptured fault, R_{JB}; closest distance to ruptured fault, R_{rup} as well as the evaluation (and, if necessary, re-calculation) of existing ones that are collected from the considered reference sources. The strategy outlined in gathering the RESORCE earthquake and station metadata guided this phase of the work: the existing source-to-site distance information in ISESD and ESMD for the pre-2004 accelerograms is kept as it is except for (a) the source-to-site distances originated from ITACA, (b) the distance modifications based on the revised earthquake metadata resulting from literature survey, and (c) the new distance calculations upon the completion of missing parameters from other reference sources. The distance measures of the post-2004 accelerograms as well as the additional pre-2004 recordings that are not considered by ISESD are also obtained from the other reference sources. In the absence of extended-source distance measures (R_{JB} and R_{rup}) by the reference source databases their computation is based on the double-couple fault-plane solutions extracted from international or local seismic agencies. For such cases, upon the existence of double-couple fault-plane solutions, the nucleation point is assumed to be at the center of the fault surface and the rupture dimensions of the fault (length and width) are estimated from Wells and Coppersmith (1994).

Leonard (2010) recently proposed a set of scaling relationships that relate M_w with rupture length, rupture width and rupture area. These relationships are self-consistent as they enable to estimate any one of these parameters from the others. Thus, the empirical relationships proposed by Leonard (2010) supersede Wells and Coppersmith (1994). The impact of these alternative approaches on the estimated extended-source distance measures is examined by running a set of analyses that consists of 1582 strong-motion records. The computed R_{JB} values from Leonard (2010) and Wells and Coppersmith (1994) did not show significant deviations from each other. Thus, the extended-source distance computations are completed by using the rupture length and width formulations provided by Wells and Coppersmith (1994).

The extended source metrics are calculated as pairs (i.e., $R_{JB_1} - R_{JB_2}$ and $R_{rup_1} - R_{rup_2}$) for each plane using the procedure described in Kaklamanos et al. (2011). RESORCE source-to-site distance inventory contains these distance pairs as well as their arithmetic averages ($\overline{R_{JB}}$ and $\overline{R_{rup}}$) as alternatives for the end user. The averaging approach that is mostly implemented for events falling into $3.0 \leq M_w \leq 6.8$ certainly involves uncertainties in the computed extended-source distances. The observations on the computed $R_{JB_1} - R_{JB_2}$ and $R_{rup_1} - R_{rup_2}$ pairs indicate that the differences between the components of each pair are small for far-source accelerograms and small-to-moderate size earthquakes (i.e., $3.0 \leq M_w \leq 5.5$). The difference between the components of extended-source distance pairs becomes significant for some large-magnitude ($5.5 < M_w \leq 6.8$) recordings that are close to the source. Figure 2.2 documents these cases for $R_{JB_1} - R_{JB_2}$ pairs. The far-source recording trends in Figure 2.2 indicate that unless there is a compelling reason for preferring one of the components of extended-source distance pairs, the choice of their average for distant accelerograms would not result in significant errors. The near-source scatters on this figure suggest that the averaging approach, rather than the random choice of one of the distance components, is a rational

28

compromise for extended-source distance metrics that show significant component-wise differences within this distance range. If a double-couple fault-plane solution does not exist for a given event, no attempt is made to calculate the extended-source distance metrics by using one of the suggested methods in the literature (e.g., Scherbaum et al., 2004; EPRI, 2004).
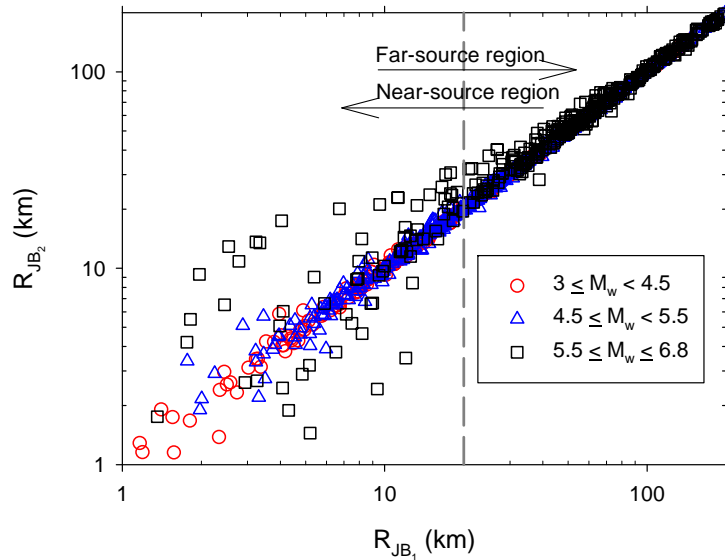
Figure 2. 2 Differences between $R_{JB,1} - R_{JB,2}$ pairs computed from the two planes given by the double-couple fault-plane solutions in the absence of extended-source distance measures (R_{JB} and R_{rup}) by the reference source databases.

The strong-motion data processing of RESORCE is based on both pre- and post-processing schemes (Boore et al., 2012). The non-standard errors are cleared by visual inspection of time series (Douglas, 2003a) and band-pass filtering is applied to remove both low- and high-frequency noise in the Fourier acceleration spectrum (e.g., Boore and Bommer, 2005; Akkar and Bommer, 2006; Douglas and Boore, 2011; Akkar et al., 2011). The entire RESORCE data processing scheme is given and discussed in Akkar et al. (2014a).

2.4 Modifications Made to ISESD during the Compilation of RESORCE

The major emphasis of the previous section is the use of ISESD as the primary reference source while structuring RESORCE. The content of ISESD is either updated (if necessary) or expanded from the other reference sources by following a hierarchical approach. This section describes the modifications to ISESD in metadata information. The summary of the improvements brought over ISESD in terms of data processing is elaborately discussed in Akkar et al. (2014a).

Figure 2.3 presents the magnitude, depth and source-to-site distance differences between the original ISESD strong-motion databank and the version integrated in RESORCE. The upper left panel of this figure indicates that the modifications in moment magnitude are noticeable in the small magnitude range ($M_w < 5$). Almost all events that show a difference of 0.1 magnitude units come from the updates using the recent ITACA information. The upper right panel of the same figure shows the changes in the ISESD depth information after the modifications. The differences are noticeable as depth computation involves significant uncertainties. The modifications in depth stem from the information retrieved from the literature survey and the ITACA project. The lower panel of Figure 2.3 addresses the source-to-site distance differences. The discrepancies in distance are emphasized by using the R_{JB} distance measure as its computation would also reflect the overall modifications made in ISESD in terms of depth, epicentral location as well as the geometry of ruptured fault plane. The major differences in R_{JB} between the original and modified versions of ISESD appear at short distances because extended-source metrics are sensitive to the above source parameters within this distance range. As in the case of changes in magnitude and depth, the major sources of distance modifications are recent literature studies and updated Italian event and station information by ITACA.
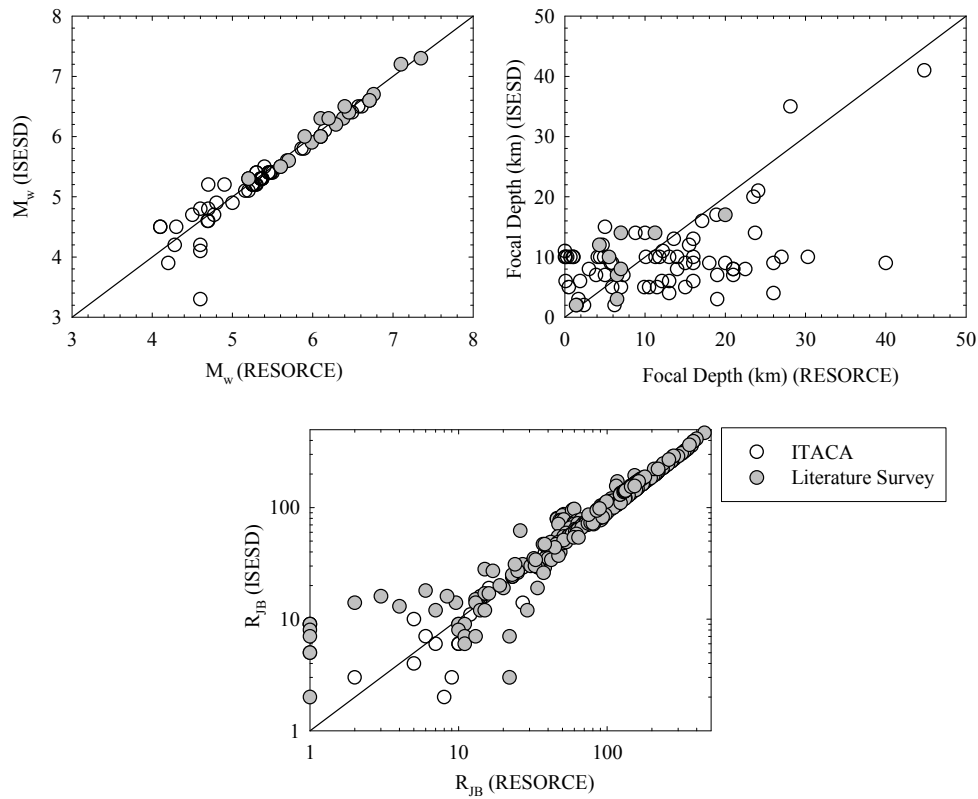
Figure 2. 3 Differences in moment magnitude (M_w), focal depth and source-to-site distance (R_{JB}) information before and after updating the ISESD strong-motion databank by following the strategy outlined in the previous section. (Grey circles show the modifications based on recent literature survey).

Table 2.6 shows the changes in strong-motion station site classification of ISESD after evaluating the updates made by the HEAD, ITACA, T-NSMP as well as other sources from the literature. The modifications are listed as Eurocode 8 (CEN, 2004) site classes (site class A: $V_{S30} \geq 800$ m/s; site class B: 360 m/s $\leq V_{S30} < 800$ m/s; site class C: 180 m/s $\leq V_{S30} < 360$ m/s and site class D: $V_{S30} < 180$ m/s). The information given in Table 2.6 indicates that the strong-motion site class updates are significant. A considerable amount of strong-motion sites that are previously categorized as site class B is identified as site class C in

RESORCE. Similarly, strong-motion stations falling under rock sites are modified as site class B in RESORCE after the recent information released by the above reference sources. Although not listed in Table 2.6, a total of 362 strong-motion stations that lack site information in ISESD are classified into one of the site categories of Eurocode 8 (via measured V_{S30} values) after the compilation of RESORCE. Of these strong-motion stations 195 sites are identified as site class C whereas 148 stations are defined as site class B. The rest of the strong-motion stations are site class A (7) and D (12). The reliability of new site classification in RESORCE is high with respect to the previous information given by ISESD as it is mainly based on measured V_{S30} values that are determined from the geophysical site exploration techniques (Table 2.4).

Table 2. 6. Changes in site classes between RESORCE and ISESD

		RESORCE			
		A	B	C	D
ISESD	A		36	2	-
	B	1		58	1
	C	-	3		19
	D	-	-	-	

2.5 Overall Seismological Features of RSMD

The compilation strategy of RESORCE and the summary of updates with respect to ISESD are given in the previous sections. This section presents a general picture about the major characteristics of RESORCE in order to understand the extents as well as the limitations of the most recent pan-European strong-motion databank. The databank consists of 5882 accelerograms from 1540 strong-motion stations and 1814 earthquakes. A total of 5810 accelerograms are tri-axial recordings whereas the rest misses either one of the horizontal components or the vertical component. The total number of singly-recorded events is 1021 in

RESORCE. Events with two and three recordings constitute 14% and 9% of RESORCE, respectively. This percentage decreases to 3.3% for earthquakes having five recordings. There are only 245 events in the RESORCE inventory that have six or above strong-motion accelerograms. Figure 2.4 demonstrates the yearly distribution of the earthquakes and accelerograms in the databank. The strong motions archived by the databank date back to the 1970s; the 1967 Debar Earthquake record occurred in Debar, Macedonia. More than half of the events and approximately 65% of accelerograms in the databank are compiled from the earthquakes that occurred in the last 15 years (1998-2012). Consequently, the current compilation efforts summarized in this paper resulted in an increase of ~30% in data size over ISESD. The higher concentration of events and records within the last 15-year time span can be attributed to the increased number of strong-motion stations all around the pan-European region. Most of the accelerograms collected in the last 15 years are recordings of digital sensors. As a matter of fact the analog and digital waveform percentages in RESORCE are 27% and 68%, respectively and almost the entire digital data (98% of the digital accelerograms) are recordings from the last two decades.
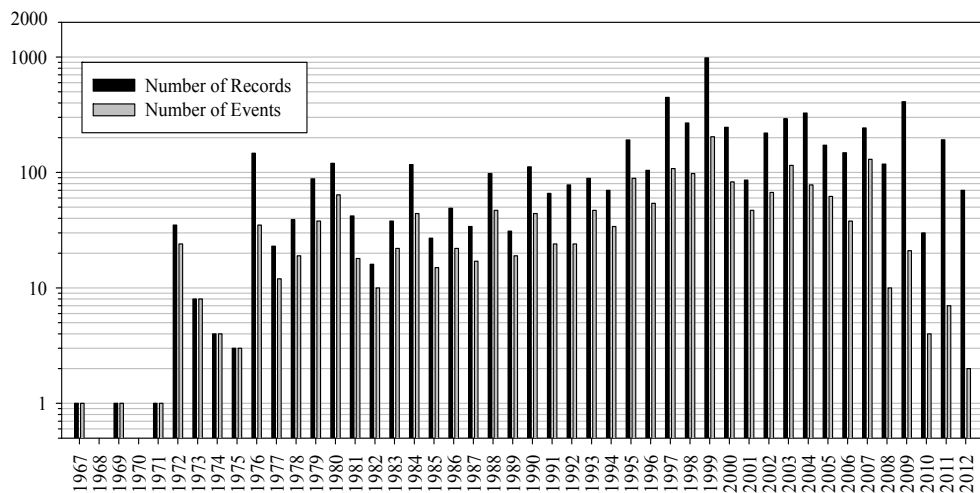
Figure 2. 4. Annual distribution of accelerograms and earthquakes in RSMD

The geographical distribution and the country-based breakdown of earthquakes and strong-motion stations in RESORCE are displayed in Figure 2.5 and Table 2.7, respectively. Table 2.7 also shows the limitations of RESORCE in terms of M_w, source-to-site distance and depth ranges. The separate sources of information,
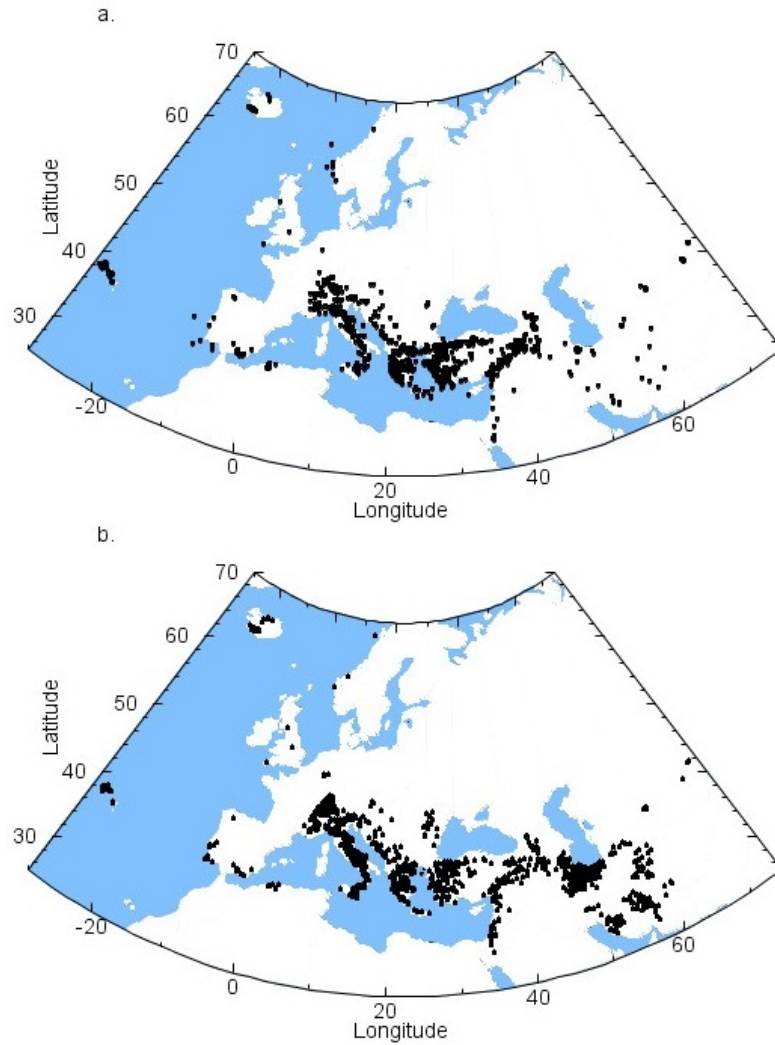
Figure 2. 5. Geographic distribution of (a) earthquakes and (b) strong-motion recording stations in the RSMD

Table 2. 7 Country-based contributions to the RESORCE

Country Name	Number of Events	Number of Records	Number of Stations	Focal Depth Range (km)	M_w Range	R_{epi} Range (km)
Albania	4	5	3	5-25	5.4-5.9	7-35
Algeria	22	28	5	2-12	5.2-5.9	3-50
Armenia	13	38	12	3-28	5.5-6.7	3-77
Austria	5	20	7	7-8	3.3-3.6	12-247
Bosnia and Herzegovina	7	13	11	10-33	5.7	7-44
Bulgaria	3	3	2	3-10	-	6-12
Croatia	10	15	9	0-39	5.5	4-132
Cyprus	1	1	-	19	6.8	435
Egypt	3	9	-	12-24	4.5-7.1	32-93
France	19	84	20	0-18	3.4-4.9	5-302
Georgia	13	46	10	4-19.7	4.8-6.8	9-115
Germany	12	74	19	4-22	3.1-5.2	4-260
Greece	386	772	130	0-127	3-6.91	1-238
Hungary	1	1	2	6	-	17
Iceland	47	205	31	1.4-17	4.3-6.6	4-64
Iran	44	396	325	0-44	4.6-7.4	1-375
Israel	3	6	15	9-18	5.1-5.3	22-46
Italy	315	1577	361	0-255.3	3.3-6.9	1-427
Kyrgyzstan	2	5	3	0-18	-	28-29
Lebanon	1	1	-	5	5.1	75
Liechtenstein	1	4	1	11	3.7	4
Macedonia	3	9	12	12-20	6.1	21-80
Montenegro	22	59	13	4-40	5.4-6.9	3-91
Netherlands	1	3	-	14.6	5.3	83

Table 2.7 Cont'd

Country Name	Number of Events	Number of Records	Number of Stations	Focal Depth Range (km)	M_w Range	R_{epi} Range (km)
Norway	7	10	3	0-21	3.6-5.5	26-309
Portugal	60	125	32	0-77	4.7-7.8	5-332
Romania	4	32	14	86-137	6.3-7.5	7-484
Serbia	8	8	3	3-10	5.5	8-237
Slovenia	14	32	16	4-16	4.3-5.7	1-88
Spain	12	23	16	5-28	3.9-5.3	1-486
Switzerland	30	208	110	1-31	3-3.9	2-119
Syria	1	10	10	29	5.5	303
Turkey	724	2027	330	0-98	2.8-7.6	2-399
United Kingdom	3	3	3	8-19	-	35-135
Uzbekistan	13	30	12	0-45	6.76	1-53

when interpreted together, indicate that almost all recorded events are shallow active crustal earthquakes and most of the accelerograms are from Turkey, Italy and Greece on the Mediterranean coast as well as from Switzerland in central Europe. This information emphasizes the importance of updates and expansion of metadata as well as accelerometric waveform content from above stated countries in RESORCE. The upcoming versions of RESORCE will include French accelerometric data for a wider coverage of low-to-moderate size events in Europe.

Figure 2.6 shows the earthquake (left column) and accelerometric (right column) data distributions in RESORCE for moment magnitude, depth and SoF. A total of 838 events have the reported moment magnitude information from international
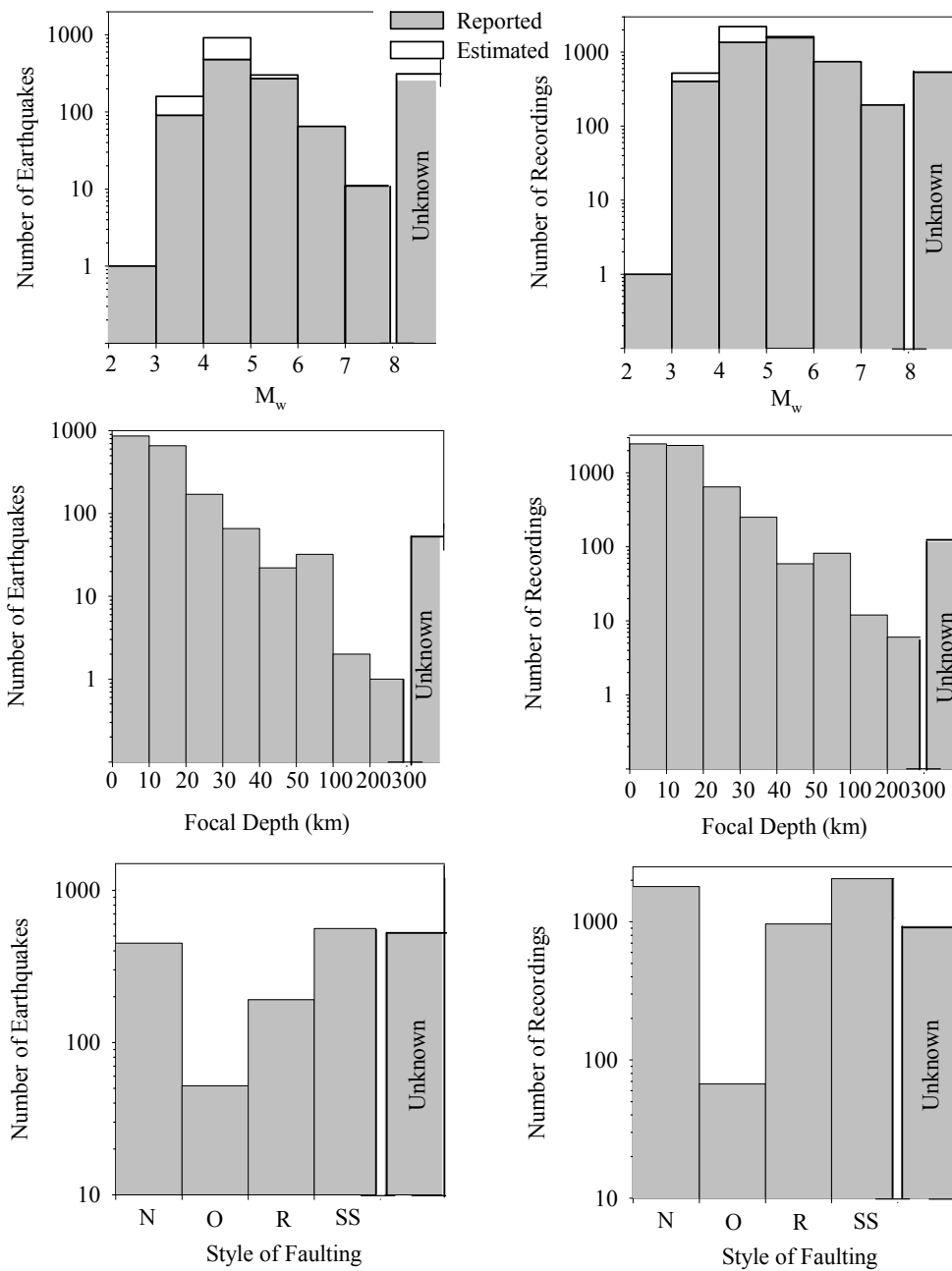
Figure 2. 6 Distributions of events (first column) and accelerograms (second column) in RSMD in terms of moment magnitude (first row), depth (second row) and style-of-faulting (third row).

and local seismological agencies as well as earthquake-specific literature studies (first row plots). When moment magnitudes that are estimated from empirical magnitude conversion relations are included, the number of events with M_w information raises to 1460. The moment magnitude estimations are concentrated between $3.5 \leq M_w \leq 5.5$. These relatively small events come from T-NSMP, HEAD and ITACA. They are originally reported as duration magnitude (M_d), local magnitude (M_L) and body-wave magnitude (m_b) for Turkish events; whereas M_L is the original magnitude scale in Italian and Greek earthquakes. The total number of accelerograms having M_w information is 5285 (4269 reported and 1016 estimated) out of 5882. The event and record based distributions of moment magnitude suggest the dominancy of moderate-size events ($4 \leq M_w \leq 6$) in RESORCE (41% of earthquakes and 50% of accelerograms). The fraction of events that can be considered as large earthquakes (i.e., $M_w \geq 6.5$) is only 2% in the entire population. The corresponding number of accelerograms constitutes 8% of the accelerometric data in RESORCE. The total number of events without moment magnitude information is 354 (20% of RESORCE). These events (labeled as "Unknown" on the histograms) are reported in different magnitude scales but their corresponding M_w values cannot be estimated due to the lack of proper empirical magnitude conversion relationships. The second row histograms display depth distribution in RESORCE. The depth range is less than 30km for about 94% of the events in RESORCE. The corresponding percentage in terms of strong-motion recordings is also 94% indicating that RESORCE is dominated by shallow crustal events. The events of depths ranging between 50 km and 140 km are mainly from the Hellenic and Cyprus Arc subduction zone, Vrancea region, Portugal and southern Turkey. The distribution of event and accelerometric data in terms of SoF is given in the last row of Figure 2.6. The majority of events and accelerograms are from the strike-slip, SS, (31% of events and 35% of records) and normal, N, (25% of events and 31% of records) faults. The data size of reverse, R, events and accelerograms are small when compared to the other SoF classes but they still constitute 11% of the events and 16% of the strong-motion records. The depth and SoF distributions also indicate that the corresponding

38

information is still missing (designated as "Unknown" on each histogram) for some earthquakes in RESORCE that mainly fall into the small magnitude range ($M_w \leq 5$). Earthquakes and accelerograms falling into this category are more prominent in the SoF statistics. The major reason behind this deficiency is the lack of double-couple fault-plane solutions for small magnitude earthquakes that provide direct information for the identification of SoF and depth parameters. Inherently, the literature survey (i.e., earthquake-specific publications) rarely focuses on the solutions of such small events unless they are associated with a major destructive earthquake. There are pragmatic solutions grossly determining the style-of-faulting of such small-size events. One alternative methodology is to overlay them on the seismotectonic maps to judge their SoF from their proximity to the fault zones. The complexity of source kinematics as well as insufficient resolution of seismotectonic maps in Europe and surrounding countries would increase the associated uncertainty in such classification. Thus, such an approach should be discouraged in SoF classification and is not implemented in the current version of RESORCE.

Figure 2.7 presents similar histograms as of Figure 2.6 to describe the distributions of strong-motion stations (left panel) and accelerograms (right panel) in terms of Eurocode 8 (CEN, 2004) site classification. The statistics are based on measured V_{S30} values and inferred site classes from local site geology. The site information of RESORCE contains a total of 423 strong-motion stations with known V_{S30} values due to the site characterization studies in Greece, Italy and Turkey (details are given in Table 2.4). The corresponding number of accelerograms recorded at these stations is 2936. The number of strong-motion sites and accelerograms with site classes inferred from the local geological conditions is 627 and 1876, respectively. Of the entire accelerometric data 1070 records (18% of strong-motion records in RESORCE) do not have any site characterization. The majority of accelerometric data (38%) is recorded at site class B strong-motion stations. Only 3% of the accelerograms in RESORCE fall

into site class D. The accelerograms in site class A and C constitute 17% and 24% of the databank, respectively.
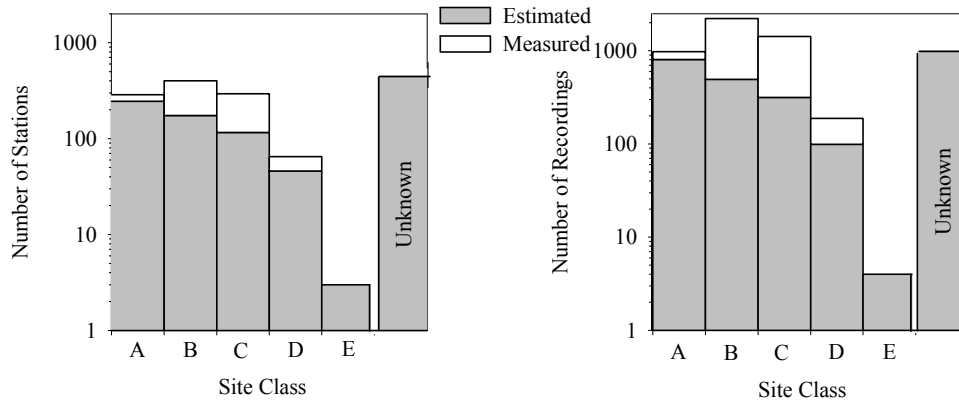
Figure 2. 7. Distributions of strong-motion stations (left panel) and accelerograms (right panel) in RSMD in terms of Eurocode 8 (CEN, 2004) site classes.

Figure 2.8 shows a general picture for M_w vs. distance distributions in RESORCE. The red and black circles refer to analog and digital recordings, respectively. This figure depicts relatively large volumes of analog recordings in RESORCE. Inherently, the recording quality of digital accelerograms is better than those of analog recordings except for the first-generation digital recorders having 12 bit resolution. In most cases the dynamic range of analog accelerographs varies between 45-55 dB (Trifunac and Todorovska, 2001) indicating high noise contamination that particularly dominates the recording quality of small-amplitude and distant events. The sampling intervals of accelerograms is RESORCE are mostly 0.01s and 0.005s regardless of the recorder type. The record quality of accelerograms in RESORCE is further emphasized while discussing the filter cut-off frequencies in the subsequent paragraphs.
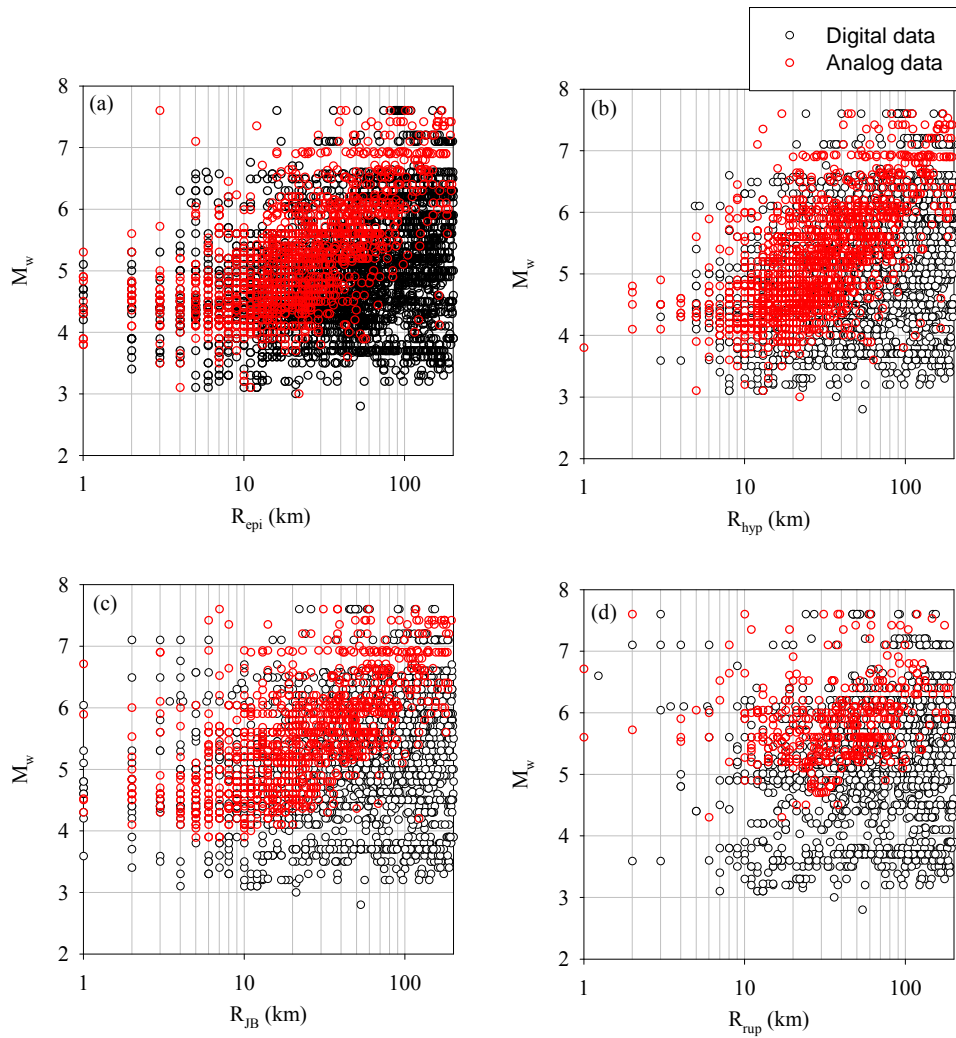
Figure 2. 8. Distribution of M_w versus a) R_{epi}, b) R_{hyp}, c) R_{JB} and d) R_{rup}. Scatter points in red color indicate analog records whereas black circles designate digital records. Moment magnitude information given on each plot is either directly extracted from the original reference source or estimated from an empirical relationship as explained under the "Compilation of Earthquake and Strong-Motion Station Metadata" subsection

The distance metrics (R_{epi}, R_{hyp}, R_{JB} and R_{rup}) are plotted up to 200 km to have a better perception in the M_w vs. distance distributions. The calculations of R_{epi} and R_{hyp} distance metrics are easier than R_{JB} and R_{rup} as the latter two distance measures require additional information about the ruptured fault geometry. The entire accelerometric data in RESORCE (5882 records) contain the R_{epi} information. The number of accelerograms having R_{hyp} information is 5751 as 131 recordings lack depth information. A total of 3906 records in RESORCE have R_{JB} values. This number reduces to 2490 recordings for R_{rup} as the calculation of this distance measure involves the largest number of seismic parameters, which is difficult to acquire with the current content of the reference sources used during the compilation process. The information on ruptured fault geometry as well as double-couple fault-plane solutions becomes poor towards smaller magnitude events in RESORCE (see discussions in the previous paragraphs) and these adverse features primarily affect the R_{rup} computations in the small magnitude range. The scatters in Figure 2.8 depict that the M_w vs. distance distribution is fairly uniform for distances greater than 10 km and moment magnitudes approximately greater than 4. For shorter distances and smaller magnitudes, the homogeneity in M_w vs. distance distributions diminishes and this is more visible in R_{hyp} and R_{rup}.

2.6 Selection of the Accelerometric Data for Derivation of the Next Generation pan-European Predictive Equations

The database compiled for derivation of the next generation pan-European predictive equations is a subset of RESORCE developed for the SeIsmic Ground Motion Assessment (SIGMA) project. The RESORCE is the extended and updated version of the pan-European strong-motion databases compiled under the Seismic HArmonization in Europe (SHARE) project (Yenier et al., 2010).

The selected database consists only of records from those stations with measured V_{S30}. The majority of stations have V_{S30} values that classify them as Eurocode 8

(CEN, 2004) classes B and C sites, i.e. $V_{S30} \leq 800$m/s. There are few rock stations ($V_{S30} > 800$m/s) classified based on measured V_{S30} values in the database. This is similar to the NGA database compiled by Chiou et al. (2008) and the majority of strong-motion databases worldwide. The only structure related free-field accelerograms are taken into account in order to remove the possible soil-structure interaction effects.

The vast majority of data that are the basis of this study were obtained from strong-motion instruments triggered by accelerations higher than a pre-defined threshold. Consequently ground motions below this threshold are not recorded. This leads to preferential recording of only larger-than-average motions from small earthquakes and/or at large distances. If these data were included within the regression analysis then the derived GMPEs would be biased upwards for weak motions. Based on a preliminary investigation using the PGAs predicted by the GMPE of Bommer et al. (2007) and various instrument resolutions, it was concluded that the available data are roughly unbiased for $M_w > 4$ at distances up to 200km (John Douglas, personal communication, 2011). Singly recorded earthquakes from 163 events were removed from the ground-motion database in order not to inflate the estimate of between-event variability in the proposed GMPEs. We considered 3-component accelerograms (two horizontal and one vertical) in our final database to develop a vertical-to-horizontal spectral acceleration ratio model that replaces the model of Bommer et al. (2011) is consistent with the GMPEs proposed here.

When deriving the NGA GMPEs the developer teams accounted for possible differences in ground motions from main shocks and aftershocks by either excluding data from aftershocks or by including terms to model these differences, which for short-period motions were found to be up to 40%. Douglas and Halldórsson (2010) investigated differences between spectral accelerations from main shocks and aftershocks using the same data as Ambraseys et al. (2005a) but did not find any significant differences. Various damaging earthquakes in Europe

that have been well recorded by strong-motion networks occurred as a series of events of similar magnitudes occurring on adjacent faults (e.g., Friuli 1976, Umbria-Marche 1997-1998, Molise 2002), which complicates the classification of earthquakes into main shocks and aftershocks. Due to these reasons, and the fact that up to half of the records available for this study come from earthquakes that could be classified as aftershocks, we have decided to retain all available strong-motion data for the derivation of the GMPEs. Any possible difference between aftershock and main shock motions is accommodated by the sigma value.

The distribution of the database in terms of magnitude, source-to-site distance, style-of-faulting and Eurocode 8 site class is presented in Table 2.8 and Figure 2.9. The distance measure is chosen as R_{JB} in the scatter plots as the use of R_{epi} or R_{hyp} does not significantly change the general picture displayed in this figure. From these scatter plots it can be seen that magnitudes up to roughly M_w 7 are well represented, particularly for normal and strike-slip faulting. For larger magnitudes there are almost no records from normal and reverse-faulting events and the available data are mainly from three large strike-slip earthquakes (Manjil, Kocaeli and Düzce). Reverse-faulting earthquakes are quite poorly represented whereas most data come from normal events: this is in contrast to the NGA models for which reverse earthquakes contribute a large proportion of the database and normal events relatively little. This prompts us to suggest that these new pan-European models should perhaps be considered in seismic hazard studies in the Basin and Range Province of the US where normal-faulting earthquakes dominate, in the same way that Spudich et al. (1999) developed a model based on global data for application in that region. The distribution with respect to style-of-faulting of the database for the current study is in part the consequence of using only records from sites with directly measured V_{S30} values, which excludes, for example, recordings from several large-magnitude earthquakes in Iran. The vast majority of earthquakes with $M_w>6$ have focal depths less than 20km whereas the depth distribution of events smaller than M_w 6 is roughly uniform between 0 and 30km (Figure 2.10). All earthquakes are shallower than 30km; as with earlier

European GMPEs, records from deeper events have been excluded from the database.

Table 2. 8 Data statistics for pan-European region

Magnitude (M_w) Range	Number of Events	Number of Records
$M_w < 5.0$	82	298
$5.0 \leq M_w < 6.0$	109	544
$6.0 \leq M_w < 7.0$	25	145
$7.0 \leq M_w < 8.0$	5	54
Depth (D) range (km)	Number of Events	Number of Records
$0 \leq D \leq 10$	120	611
$10 < D \leq 20$	78	452
$20 < D \leq 30$	23	78
Style-of-Faulting	Number of Events	Number of Records
Normal	104	532
Reverse	32	135
Strike-Slip	85	374
Country	Number of Events	Number of Records
Greece	32	106
Italy	69	319
Turkey	110	568
Others	10	48
V_{S30} range (m/s)	Number of Stations	Number of Records
$V_{S30} \leq 180$	14	50
$180 < V_{S30} \leq 360$	112	381
$360 < V_{S30} \leq 550$	107	361
$550 < V_{S30} \leq 800$	61	200
$V_{S30} > 800$	28	49
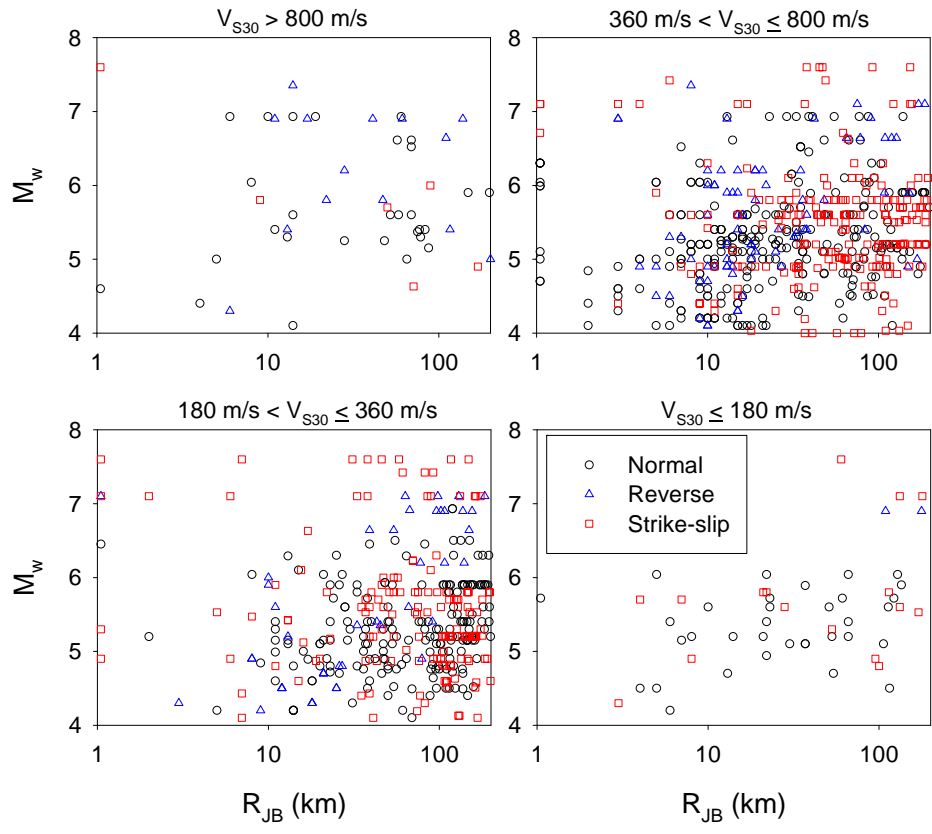
Figure 2. 9 Distribution of the data used in terms of magnitude, distance (R$_{JB}$), style-of-faulting and Eurocode 8 site class.
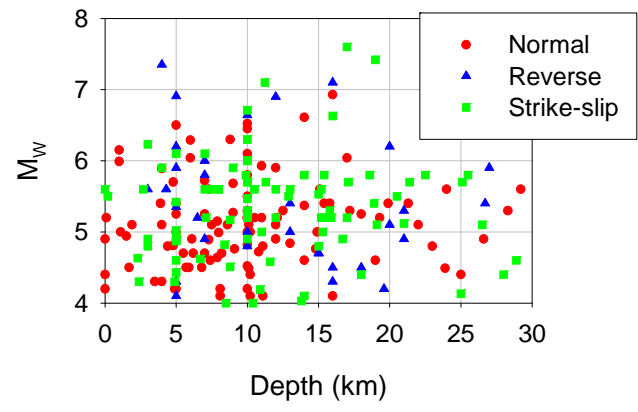
Figure 2. 10. Depth distribution of the earthquakes with respect to magnitude and mechanism

The individual filtering of each record means that the number of spectral accelerations available for regression at each period varies (Figure 2.11). The high-pass filtering effect on long-period spectral ordinates is minimized by applying the criteria given in Akkar and Bommer (2006). The number of records starts reducing for T>1s as the effect of the chosen high-pass filter values becomes more and more apparent. By 4s about 60% of the records in the database are still available for regression analysis. The data decays rapidly after T=4s, which prevented going beyond this spectral period in the regressions. This rapid drop-off is due to a large proportion of records from analogue instruments within the databank used despite the conversion of most European strong-motion networks to digital accelerometers in the past decade. The Akkar et al. (2011) criteria to account for low-pass filtering effects on the short period spectral ordinates (T<0.05s) were not followed as its application did not result in significant changes in the total number of data in this period range.
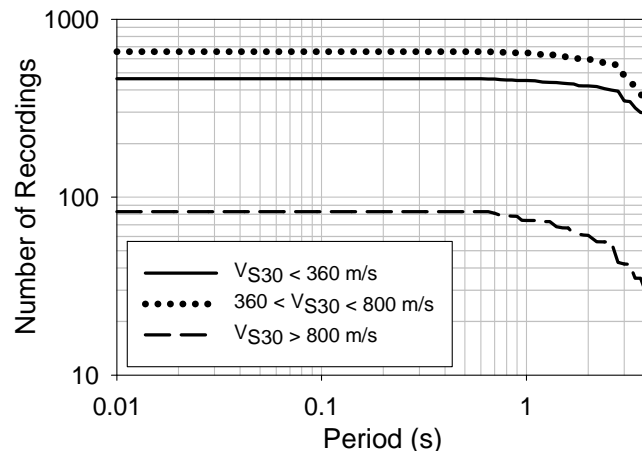
Figure 2. 11. Usable period range for pan-European region

The horizontal and vertical pseudo-acceleration spectral ordinates at 16 different damping levels (i.e., 1%, 2%, 3%, 4%, 5%, 6%, 7%, 8%, 9%, 10%, 15%, 20%, 25%, 30%, 40% and 50%) are computed from the compiled strong-motion

database for developing the ground-motion prediction models for horizontal, V/H spectral and damping scaling ratios. The geometric mean values of the horizontal spectrum components are calculated for PGA, PGV and 62 periods (0.01s-4.0s) and used as horizontal ground-motion demand throughout this study. The vertical demand is fulfilled by the same spectral ordinates those used in horizontal component. This way full compatibility is provided between the models developed in the context of this study.

2.7 Strong-Motion Database for the Nonlinear Site Model

In addition to the pan-European strong-motion database that is described above, a global dataset is also considered in the development of the nonlinear site model. This additional recordings are extracted from a comprehensive ground-motion databank that has been compiled within the framework of the SHARE project. Details about the compilation of SHARE strong-motion databank can be found in Yenier et al. (2010). Similar criteria described in the previous section are applied to increase the size of the database. This decision led to a database of 5530 3-component accelerograms from 414 events recorded at 1616 sites. Table 2.9 lists the magnitude, depth, SoF, V_{S30} and country based variation of the dataset in terms of number of events, records and stations.

Table 2.10 shows the types of in-situ measurement techniques applied for the computation of S-wave velocity (V_S) profiles at the strong-motion sites. The table also gives information about the exploration depth (maximum depth at which the final V_S measurement is computed) for the in-situ measurements. The in-situ measurement techniques of ~22% of the stations are not reported in the database. These stations are almost exclusively from the NGA database and their V_{S30} values reported by NGA project was considered as reliable in this study. The remaining stations that lack in-situ measurement information are from the ESMD and ISESD (Ambraseys et al., 2004a; 2004b) databases that are also known as well-documented strong-motion data sources. The V_{S30} values of sites whose V_S

48

Table 2. 9. Statistics about global dataset

Magnitude (M_w) Range	Number of Events	Number of Records
$M_w < 5.0$	160	1438
$5.0 \leq M_w < 6.0$	185	2089
$6.0 \leq M_w < 7.0$	55	1670
$7.0 \leq M_w < 8.0$	13	333
Depth (D) range (km)	Number of Events	Number of Records
$0 \leq D \leq 5$	94	1531
$5 < D \leq 10$	125	1556
$10 < D \leq 15$	109	1497
$15 < D \leq 20$	53	744
$20 < D \leq 25$	15	56
$25 < D \leq 30$	17	146
Style-of-Faulting	Number of Events	Number of Records
Normal	113	705
Reverse	125	2770
Strike-Slip	175	2055
Country	Number of Events	Number of Records
Greece	42	180
Italy	61	331
Japan	155	3288
Taiwan	7	689
Turkey	97	561
USA	42	434
Others	9	47
V_{S30} range (m/s)	Number of Stations	Number of Records
$V_{S30} \leq 180$	85	203
$180 < V_{S30} \leq 360$	639	1960
$360 < V_{S30} \leq 550$	570	2012
$550 < V_{S30} \leq 800$	230	995
$V_{S30} > 800$	112	360

profiles do not reach to 30m (i.e., profiles whose exploration depths are less than 30m) were computed by extending the S-wave velocity of the last layer to 30m. This method is proposed by Boore (2004) and it yields, though relatively safer, comparable V_{S30} values with those of soil columns that have a complete V_S profile up to 30m.

Table 2. 10. Types of measurements that applied to compute the S-wave velocity profiles of the sites used in this study. Exploration depth information is also included in the table.

In-situ measurement[*]	Exploration Depth <30 m	Exploration Depth >30 m	Unknown
Cross-hole	1	24	-
Down-hole	515	552	-
MASW	-	139	-
SASW	3	4	-
SLT	5	17	-
Others	1	13	-
Unknown	2	260	96

* MASW: Multi-channel analysis of surface waves, SASW: spectral analysis of surface waves analysis, SLT: Suspension logging test

Figure 2.12 shows various distribution plots about the strong-motion database for nonlinear site model. Figure 2.12a displays the M_w vs. R_{JB} scatters of the entire database whereas Figures 2.12b show the M_w vs. R_{JB} distribution of the subset of the database (records having $V_{S30} \geq 550$m/s) that is used in the derivation of reference rock ground-motion prediction equation (see details in the next chapter). The M_w vs. R_{JB} plots that are given for the entire database and its subset (Figures 2.12a and 2.12b, respectively) indicate a sparse data distribution for large-distance ($R_{JB} > 100$km) and small-magnitude records. The distance-dependent distribution of the entire database (Figure 2.12a) is fairly uniform for $5 \leq M_w \leq 7$ and it gradually diminishes towards larger magnitudes ($M_w > 7$).
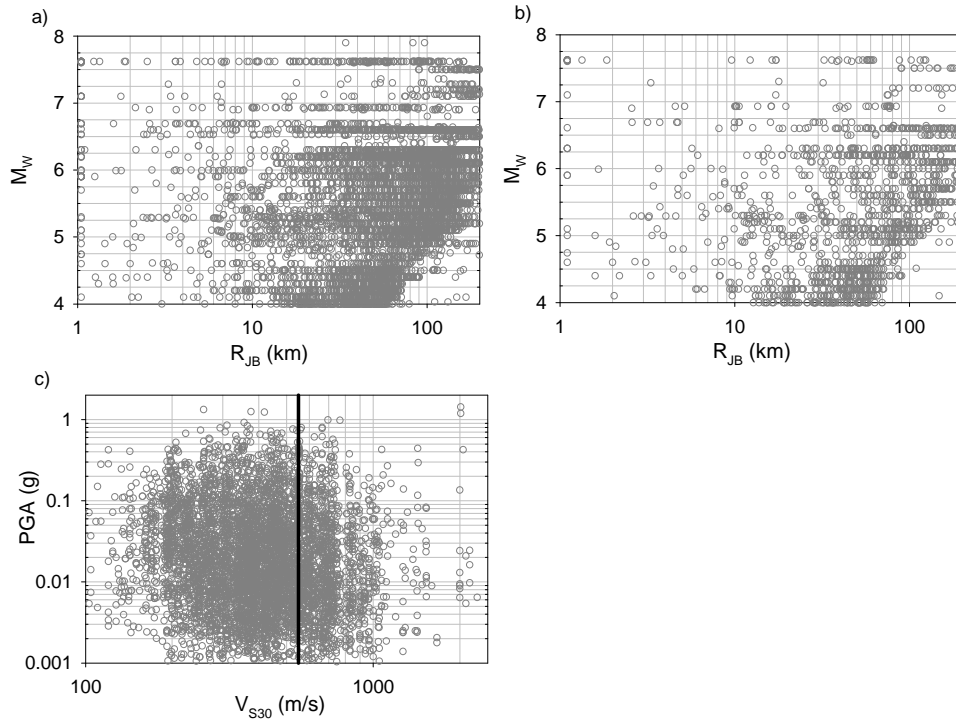
Figure 2. 12. (a) R_{JB} vs. M_w scatters of the entire database used in the derivation of site amplification model, (b) subset of (a) used in the derivation of PGA_{REF} GMPE, (c) PGA vs. V_{S30} scatters of the entire database. The solid black line in Figure 2.12c separates the data at $V_{S30} = 550$m/s.

The M_w vs. R_{JB} distribution of the subset is poorer with respect to the one given for the entire database as we constrained the data for records having soft-to-hard rock conditions (i.e., $V_{S30} \geq 550$m/s). Figure 2.12c shows V_{S30}-dependent PGA variation of the entire database. Records that are on the right hand side of the solid-black line (i.e., records having $V_{S30} \geq 550$m/s) are used in the derivation of reference rock ground-motion model. As one can infer from the distribution given in Figure 2.12c, the bulk of the data is in between 200m/s$\leq V_{S30} \leq 700$m/s. The records having 0.002g$\leq$PGA≤ 0.2g are uniformly distributed within this V_{S30} interval. Data outside of this V_{S30} range lose their homogeneity in particular for $V_{S30} > 1000$m/s and for large PGA values (PGA≥ 0.1g). Loose data distribution for

51

hard rock conditions is frequently observed in empirical strong-motion databases (e.g., NGA strong-motion database). Non-uniform data distribution of large PGA values is due to the sparse large-magnitude and short-distance recordings in our database at both ends of the V_{S30} limits considered in this study.

2.8 Conclusions

This chapter summarizes the general features of the most recent pan-European strong-motion databank that updates and expands its predecessor developed by Ambraseys et al. (2004a). The details of the topics discussed in this paper will be posted as a separate document on the official web site of RESORCE when the databank is made available for public use. The online documentation will use flags to describe the specific features of each entry (e.g., reference source of magnitude and V_{S30} information, specific literature on fault rupture information or data processing parameters etc.) in the metadata. The dissemination of RESORCE will be realized in the near future under the collaboration of multi-national European projects SIGMA, NERA (Network of European Research Infrastructures for Earthquake Risk Assessment and Mitigation) and EPOS (European Plate Observing System) together with non-profit European data centers (EMSC and ORFEUS – Observatories and Research Facilities for European Seismology –). As a matter of fact, a working group has already been established under ORFEUS and EPOS to coordinate these efforts for long-term sustainability of RESORCE. This new structure is entitled to shape the future policies among accelerometric networks in the broader European region to enhance integral approaches for the efficient use of strong-motion data in engineering seismology and earthquake engineering studies.

The current version of RESORCE increases the record and event size of its predecessor by approximately 2.5 times with improvements in magnitude and distance distributions through additional data from recent Turkish, Italian, Swiss and Greek events. The data size will be increased further in the upcoming versions

of RESORCE by including recordings of the French Accelerometric Network (RAP, http://www-rap.obs.ujf-grenoble.fr). The inclusion of French accelerograms in RESORCE will result in a larger coverage of moderate-to-low seismic events in Europe. The procedure followed in the compilation of RESORCE results in more reliable earthquake and station metadata. The strong-motion site characterization is primarily calibrated by measured V_{S30}. The extended- and point-source distance measures are computed from reliable literature studies or by following a systematic approach. The uniform strong-motion data processing, as part of these efforts, has increased the usable period range of the accelerograms in the inventory as the choice of filter cut-offs is guided by the frequency content of the accelerograms. This step, implemented efficiently in the evolution of RESORCE, supersedes the use of the constant filter cut-off approach in ISESD.

The current size of RESORCE consists of 5882 multi-component accelerograms from 1814 events recorded between 1967 and 2012. The number of strong-motion recording stations in the inventory is 1540 out of which one-third of stations have direct shear-wave velocity profiles. Almost 80% of the events have moment magnitude information. The earthquake magnitudes range between 2.8 and 7.8 in RESORCE. The entire databank has the R_{epi} source-to-site distance information. The corresponding numbers for R_{hyp}, R_{JB} and R_{rup} source-to-site distance metrics are 5751, 3906 and 2490, respectively.

The information summarized in this chapter comprises the entire accelerometric recordings that are evaluated in RESORCE. The public open version will not include the accelerograms suffering from extremely low quality waveforms in all three components. A set of source-to-site distance vs. event size criteria will also be established to remove small-amplitude and far distance accelerograms from the final version of RESORCE that are limited in use for engineering seismology and earthquake engineering. The total number of uniformly 563 processed accelerograms is approximately 86% of the entire RESORCE population.

The overall picture given in the above paragraphs makes RESORCE an important source of information for hazard and risk studies in and around Europe. The quality and content of RESORCE is comparable with similar databanks such as those from the NGA-West1 (Power et al., 2008) and NGA-West2 (Bozorgnia et al., 2012) projects. As summarized in the first paragraph the efforts put forward in the compilation of RESORCE should be supplemented by long-term research projects within the European context to complete the missing or (partially) unreliable metadata information. In particular, efficiently oriented financial funds for site characterization of strong-motion stations in terms of measured shear-wave velocity profiles or well-defined source characterization projects that seek double-couple solutions of small-to-moderate size events from regional seismotectonic and stress field studies as well as relocation of earthquakes for improvements in the spatial distribution of events will certainly minimize the metadata related uncertainties in RESORCE. Projects encouraging the inclusion of recordings from pan-European countries other than those contributing significantly to the accelerometric archive of RESORCE will also lead to a better reflection of seismic activity in the region covered by this strong-motion databank. Such grants will also create numerous research opportunities in the fields of earthquake engineering and engineering seismology in Europe. As a matter of fact the growth rate of accelerometric data in the broader Europe in the last two decades makes such Europe-wide projects indispensable.

More than a thousand 3-component recordings are selected from the RESORCE to generate next generation pan-European GMPEs. Besides, approximately 4500 global recordings from Yenier et al. (2010) are added to pan-European database to derive the nonlinear site model. The database used in this study is compiled from a considerably large SHARE strong-motion databank and RESORCE, their aforementioned limitations (due to imposed constraints as explained throughout this section) will certainly confine the findings of this study.

CHAPTER 3

THE NONLINEAR SITE AMPLIFICATION MODEL THAT IS DERIVED FOR THE NEXT GENERATION PREDICTIVE MODELS

Adapted from Sandıkkaya M.A., S. Akkar, P.-Y. Bard (2013). A nonlinear site amplification model for the next pan-European ground-motion prediction equations. Bulletin of Seismological Society of America, 103:19-32.

A site amplification model for shallow crustal regions that considers both linear and nonlinear soil effects is proposed in this chapter. The original functional form of the nonlinear site model is developed by Walling et al. (2008), [WAS08] using stochastic simulations and site response analysis. The major difference between the proposed model and WAS08 is that our site amplification expression is entirely based on empirical data. To comply with this objective, a database with the most recent V_{S30} information from pan-European region is compiled. This feature of the model encourages its use for the future ground-motion prediction equations that will be devised particularly for this region. World-wide accelerograms are also considered to have a better representation of the soil behavior under strong-motion excitations. As an auxiliary tool a ground-motion prediction equation (GMPE) for reference rock sites is also developed to calculate the site amplification factors. The coefficients of the site amplification model as well as the reference rock model are computed by applying random-effects regression technique proposed by Abrahamson and Youngs (1992). Then the possible usage of the proposed nonlinear site model for site specific hazard

analysis and the evaluation of the Eurocode and NEHRP site factors are investigated.

3.1 Site Amplification Terminology

The recent trend in ground-motion prediction equations (GMPEs) is to represent the soil effects by a site amplification model that mimics the soil behavior through functional forms that are either based on stochastic simulations or empirical data. The site conditions are generally described by V_{S30} but some models also consider complementary parameters to this proxy to fully capture the genuine soil behavior under various circumstances (e.g., Z1.0 and Z2.5 to describe the soil response of deep alluvium deposits). Although, the ongoing efforts to elaborate such additional complementary parameters are promising (e.g., Thompson et al., 2011), V_{S30} still preserves its significance as an estimator to describe the overall site effect on the ground-motion estimation.

The conventional method for implementing site effects in ground-motion prediction models is to use site amplification factors that are obtained by normalizing a chosen ground-motion intensity measure at a soil site with its counterpart measured at a nearby rock site (Borcherdt, 1970). The most important drawback of this approach is the lack of nearby rock sites while characterizing the site amplification for that specific event. One way of overcoming this drawback is to calibrate the ground motions at the site of interest by a geometrical spreading factor without modifying the particular site features to imitate their behavior at reference rock sites. This way the analyst can employ the conventional procedure by normalizing the amplitudes of calibrated ground motions with that of the reference rock site. Borcherdt (1994; 2002a; 2002b) and Dobry et al. (2000) utilized this approach for the Loma Prieta and Northridge earthquakes and obtained the site factors that formed the basis of the NEHRP (US National Earthquake Hazard Risk Reduction Program) site amplification factors (BSSC, 2009). Although this procedure increases the number of usable recordings for site

amplification studies, the likely regional dependency of geometrical spreading function may become critical for reliable modification of the recordings that are collected from various regions of different crustal features.

Another efficient way of estimating the site effects on ground-motion amplitudes is to use stochastic methods (e.g., Boore, 2005) for simulating different site conditions under different earthquake scenarios. Boore and Joyner (1997) presented the groundbreaking and pioneer study in this field that proposes site amplification factors at different spectral frequencies using the quarter-wave length theory and stochastic simulations representing generic site classes. More recent studies (e.g., Ni et al., 2000; Walling et al., 2008) generate stochastic reference rock motions and convolve the soil motion associated with different features via site response analysis to modify the simulated rock motion. This way they derive site models for different soil conditions by modeling the site amplification between rock and soil motion through regressions on various functional forms. Following a similar concept Sokolov (1997; 2000) first simulated the reference rock motions at specific sites and then normalized the actual ground motions recorded at these sites with the generated reference rock simulations to derive the site amplification factors. As in the case of recorded ground-motions the level of accuracy in stochastic simulations depends on the reliability of source information as well as the site features described by geophysical and geotechnical parameters. Nevertheless, they can contain very useful information for describing the functional form of the site model provided that they are based on the right physics for the background nonlinear model and the right order of magnitude for the corresponding soil nonlinear parameters.

An alternative to the above approaches is the utilization of existing empirical ground-motion predictive models for describing the reference rock conditions to compute site amplification factors by normalizing the observed ground motions with the estimated reference rock motions. Studies conducted by Steidl (2000), Field (2000), Lee and Anderson (2000), Stewart et al. (2003) and Choi and

Stewart (2005) consider this methodology either to observe the variation of site amplifications for different soil conditions or to derive site models for their use in GMPEs. Instead of employing the existing GMPEs to represent the reference rock motion, some studies derive specific predictive models to mimic different site conditions, including the reference rock, to compute the site factors through a similar normalization scheme as described above [e.g., Crouse and McGuire (1996); Rodriguez-Marek et al. (2001)].

The main objective of this chapter is to propose an empirical site amplification model to be used in GMPEs for shallow active crustal regions. The proposed model can capture the nonlinear soil effects as a function of V_{S30} for different input rock motion levels. The features of the strong-motion database of this chapter is described in the Section 2.7. The database is compiled from subset of an extensive strong-motion databank that has been compiled in the framework of the project entitled "Seismic Hazard HARmonization in Europe" (SHARE) and recent RESORCE databank. The selected database includes recordings from Europe and surrounding regions (Greek, Italian and Turkish strong-motion recordings) with measured shear-wave (S-wave) velocity information. The database also contains strong-motion data collected from Taiwan, Japan and California with measured V_{S30} values for a broader coverage of soil behavior. Relatively large amount of pan-European data can make the model useful for future pan-European GMPEs. The proposed site amplification function employs a reference rock model that is derived from a subset of the ground-motion database. This step is different in most of the similar studies because they either import the reference rock model from another research or use theoretical simulations to describe rock motion. The site amplifications computed by normalizing the observed data with the estimations obtained from the reference rock model are regressed by modifying the Walling et al. (2008) site function that is derived from the stochastic simulations.

This chapter firstly discusses the previous site models with special emphasis on recent GMPEs developed in the Next Generation Attenuation project (Power et al., 2008). Important observations from the NGA GMPEs constitute one of the major motivations of this study and are used in the development of the nonlinear soil model presented here. The comparisons of the proposed model with the existing ones is another important topic presented in this part of the study. A brief discussion on the NEHRP and Eurocode 8 site factors is also included under the findings of the proposed nonlinear site model.

3.2 Site Amplification Functions with Emphasis on the NGA Models

The integration of soil effects in GMPEs evolved progressively. In early GMPEs, the site effects were addressed by defining two broad site classifications (soil and rock). As an example, Sadigh et al. (1997) determined the site coefficients by employing separate regressions on rock and soil datasets. Other ground-motion models accounted for the site influence by considering more detailed soil categories that are based on certain V_{S30} intervals. In such GMPEs (e.g., Akkar and Bommer, 2010), the same source and path models were used and the differences arising from site effects are represented by different soil coefficients for each site category. Boore et al. (1997), [BJF97], proposed a more complicated site model that is a continuous function of V_{S30} [Eq. (3.1)]. In this model, the logarithm of the site amplification, (ln (Amp)) is proportional to the logarithm of V_{S30} normalized by a period-dependent reference velocity, $V_{LIN}(T)$). The period-dependent coefficients a(T) and $V_{LIN}(T)$ are computed from regression analysis.

$$ln(Amp) = a(T)ln(V_{S30} / V_{LIN}) \qquad (3.1)$$

The site-model proposed by BJF97 as well as the others described in the previous paragraph do not include the nonlinear soil behavior. To the best of our knowledge the Abrahamson and Silva (1997) site function [AS97] is the first model that considers nonlinear soil amplification. This model classifies sites as

rock and soil and applies a correction to the ground-motion amplitudes of soil sites to consider the nonlinear site effects as a function of input rock motion level (PGA_{rock}). The AS97 site function is given in Eq. (3.2) where the period-dependent coefficients, a(T) and b(T), are determined from regression analysis and the period-independent coefficient, c, is constrained to 0.03g for the entire period range.

$$ln(\,Amp\,) = a(\,T\,) + b(\,T\,)ln(\,PGA_{rock} + c\,)$$ (3.2)

Choi and Stewart (2005), [CS05], in a way, combined Eqs. (3.1) and (3.2) to obtain a site model that represents both linear and nonlinear site amplification. To this end, they proposed linear and nonlinear site terms that are functions of period and V_{S30} [Eq. (3.3)]. This functional form modifies the PGA_{rock} dependent logarithmic expression to account for the overall nonlinear soil response.

$$ln(\,Amp\,) = a(\,T\,)ln(\,V_{S30}\,/\,V_{LIN}\,) + b(\,V_{S30}, T\,)ln(\,PGA_{rock}\,/\,0.1\,)$$ (3.3)

The amplification factors in CS05 are computed by normalizing the observed acceleration spectrum ordinates with the corresponding estimations obtained from the reference rock model of AS97. CS05 assumes the reference rock V_{S30} as 760m/s although the reference rock definition of AS97 corresponds to an average V_{S30} value of 550m/s (Walling et al., 2008). CS05 accommodates this discrepancy by suggesting a modification in their site amplification.

Boore and Atkinson (2008), [BA08], one of the model developers in the NGA project, integrated the CS05 site model to their GMPE with some adjustments. The period-dependent V_{LIN} parameter in CS05 is a fixed reference V_{S30} value in BA08 that is called as V_{REF} (V_{REF}=760m/s). V_{REF} also describes the reference rock site in BA08. The overall contribution of soil nonlinearity in BA08 is formulated for 3 levels of input reference rock motion (i.e., $PGA_{rrock} \leq 0.03g$; $0.03g < PGA_{rock} \leq 0.09g$; $PGA_{rock} > 0.09g$). Furthermore, BA08 modified the

b(V_{S30},T) term with a piece-wise linear function (referred to as b_{nl} in their terminology). Figure 3.1a shows the PGA site amplifications of CS05 and BA08 at different PGA_{rock} levels. Figure 3.1b compares the behavior of b(V_{S30},T) with b_{nl} for T=0.0s. As it is inferred from Figure 3.1a the CS05 model results in a kink in site amplification in the vicinity of V_{S30}=520m/s due to the discontinuity in the b(V_{S30},T) term at this V_{S30} value (Figure 3.1b). The BA08 model removes this behavior by introducing a smooth transition in b_{nl} between 300m/s≤V_{S30}≤760m/s (Figure 3.1b). However, this smooth transition imposes lower nonlinear soil behavior with respect to CS05 for 300m/s≤V_{S30}≤520m/s. On the contrary, the linear trend in b_{nl} between 180m/s<V_{S30}<300m/s yields slightly higher soil nonlinearity with respect to CS05.
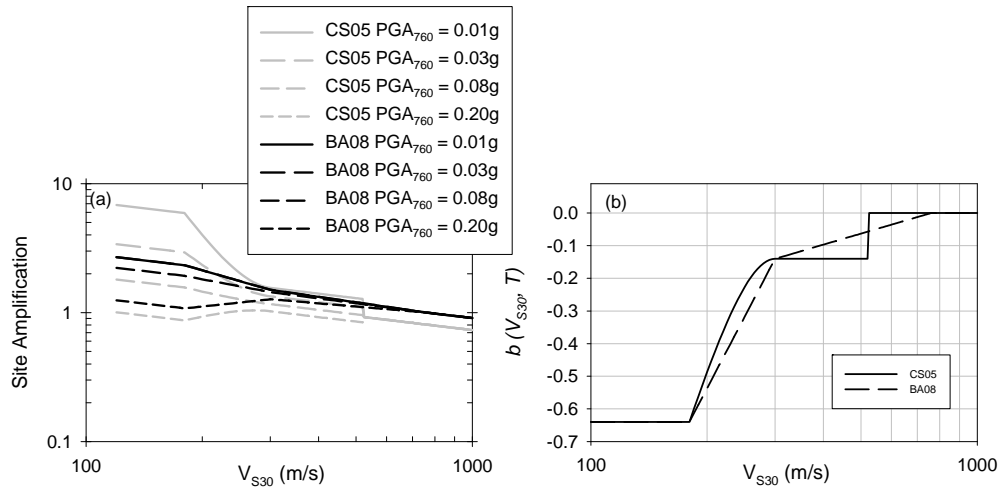
Figure 3. 1. (a) Comparisons between the amplification factors derived from Choi and Stewart (2005), [CS05] and Boore and Atkinson (2008), [BA08] for PGA. Each line represents different levels of input rock motion. (b) Comparison of the nonlinear coefficients for T = 0.0s proposed by CS05 and BA08.

Figure 3.1a also shows that BA08 results in higher amplification levels with respect to those of CS05 when V_{S30} attains larger values (i.e., V_{S30}>300m/s). This behavior can be attributed to the modifications to the V_{LIN} parameter by BA08 because linear site behavior generally governs for V_{S30}>300m/s as will be discussed in the following paragraphs. This observation suggests that the BA08 model would estimate larger site amplifications for linear soil behavior. In fact the use of period-independent V_{REF} in BA08 seems to shift the site amplifications towards higher values for the entire V_{S30} band at all rock PGA levels except for those of low V_{S30} sites subjected to low ground-motion amplitudes (mimicked by PGA_{rock}≤0.03g in Figure 3.1a). For very low ground-motion amplitudes the BA08 model prevents the increase in soil nonlinearity at softer sites by imposing a constant nonlinear amplification at the lowest range of input rock motion (i.e., PGA_{rock}≤0.03g). This fact is not accounted for CS05. The lower bound of V_{S30} for CS05 and BA08 is 180m/s. However the plots on Figure 3.1 extend V_{S30} towards much smaller values to show the behavior of these models if they are used for addressing soil amplification at low-velocity sites.

The site model proposed by Chiou and Youngs (2008), [CY08], was also developed within the framework of NGA project and it is similar to CS05. CY08 derived their functional form by interpreting the studies of BJF97 and AS97. The reference velocity that is considered as 760m/s in BA08 is 1130m/s in CY08 by assuming that no major soil nonlinearity can take place beyond this velocity level. The site amplification is set to unity for V_{S30} values greater than 1130m/s. Contrary to BA08 that uses the site coefficients of CS05, Chiou and Youngs (2008) determined the site coefficients by regressing on their own database that led to better representation of the data trend. Another important difference of CY08 with respect to other models is that the nonlinear site response term is expressed by reference rock spectral accelerations (instead of reference rock PGA) at the period of interest. This feature, according to our understanding, makes this model more complicated in terms of its implementation.

The Walling et al. (2008), [WAS08], site model that is also developed during the course of NGA project generated stochastic simulations for a single scenario event to obtain rock motions at V_{S30}=1100m/s. They performed site response analysis to obtain the soil motions at certain V_{S30} values. In site response analysis, four specific modulus and damping degradation curves were used to mimic different site conditions (i.e., Imperial Valley, Bay Mud, Peninsular range and EPRI models). The first and second degradation curves were used when V_{S30} attains values less than 270m/s. The third and fourth curves represent the cases for V_{S30}≥270m/s. The site amplification was calculated by dividing the convoluted soil motions by the simulated reference rock motions. These amplification factors were then utilized to derive the site model (Eq. 3.4) as two piece-wise functions. The Walling et al. (2008) model assumes linear site response (a) when PGA_{1100} goes to zero and (b) when V_{S30}≥V_{LIN}. WAS08 considers PGA_{1100} as the main controlling parameter in soil nonlinearity for all spectral periods. The coefficients a(T), b(T), c and n are the regression coefficients. The parameter d implicitly relates the linear transition between V_{LIN}(T) and the reference rock site shear-wave velocity that is taken as 1100m/s.

$$\ln(Amp) = \begin{cases} a(T)\ln(V_{S30}/V_{LIN}) + b(T)\ln(PGA_{1100}+c) \\ + b(T)\ln(PGA_{1100}+c(V_{S30}/V_{LIN})^n) + d & \text{for } V_{S30} < V_{LIN} \\ (a(T)+b(T)n)\ln(V_{S30}/V_{LIN}) + d & \text{for } V_{S30} \geq V_{LIN} \end{cases} \qquad (3.4)$$

The WAS08 nonlinear site model was implemented in the Campbell and Bozorgnia (2008), and Abrahamson and Silva (2008), [CB08 and AS08, respectively] GMPEs. In their site models, AS08 and CB08 used the nonlinear soil coefficients derived from the Peninsular range shear modulus and damping degradation curves. The major difference between the AS08 and CB08 models is the linear site term because they used different subsets of the NGA database. As these models have the same origin for site response, the results obtained from AS08 are presented in this study. The site amplification factors of AS08 are lower than unity at V_{S30}=1100m/s. The reason behind this behavior is that AS08 does

not consider the d term proposed in WAS08. As a matter of fact the d term is compensated by other regression coefficients (e.g., source and path coefficients) in the ground-motion prediction model of AS08. Since one of the aims of this study is the evaluation of different site models, this parameter is included in the original AS08 in order to observe an amplification ratio of unity at V_{S30}=1100m/s. AS08 also includes another period-dependent V_{S30} parameter, V_{CON}, above which the site term becomes constant. Consequently, for $V_{S30} \leq V_{LIN}$, the amplification is a function of PGA_{1100} and V_{S30}. For V_{S30} values between V_{LIN} and V_{CON}, the amplification depends only on V_{S30} (i.e., only linear amplification). For $V_{S30} > V_{CON}$ a constant amplification is imposed by this model whatever the PGA_{1100} and V_{S30} values.

Figure 3.2 shows the site-amplification factors computed from BA08. (The other site models discussed in this section show fairly similar trends to those of BA08 and are not shown on this figure.) The soil nonlinearity is dominant for sites with $V_{S30} < 300$m/s in BA08. The contribution of soil nonlinearity to site amplification decreases with increasing period when V_{S30} values are greater than 300m/s. The influence of soil nonlinearity seems to vanish completely beyond T=1.0s and no nonlinear site effect is considered for $V_{S30} > 760$m/s (V_{S30} for reference rock). For sites that are located on very soft soil deposits (i.e., $V_{S30} \leq 180$m/s) the amplification trend changes and starts to increase with increasing PGA_{rock}, which is due to the use of constant nonlinear coefficient in this range. The middle column panels in Figure 3.2 indicate that the amplification becomes independent of V_{S30} at a certain value of PGA_{rock}. This input rock motion level is called as hinging PGA in this article and it is a function of period. For PGA_{760} values that are lower than the hinging PGA, the linear site term dominates and softer sites show higher amplification. Beyond the hinging PGA the contribution of nonlinear term increases for soft sites with low V_{S30} values. As the stiffness of the site increases, the hinging PGA shifts to a larger value. This observation indicates that for stiffer sites the BA08 model does not expect nonlinear soil behavior except for very strong ground motions associated with high PGA_{rock}. The hinging PGA shifts
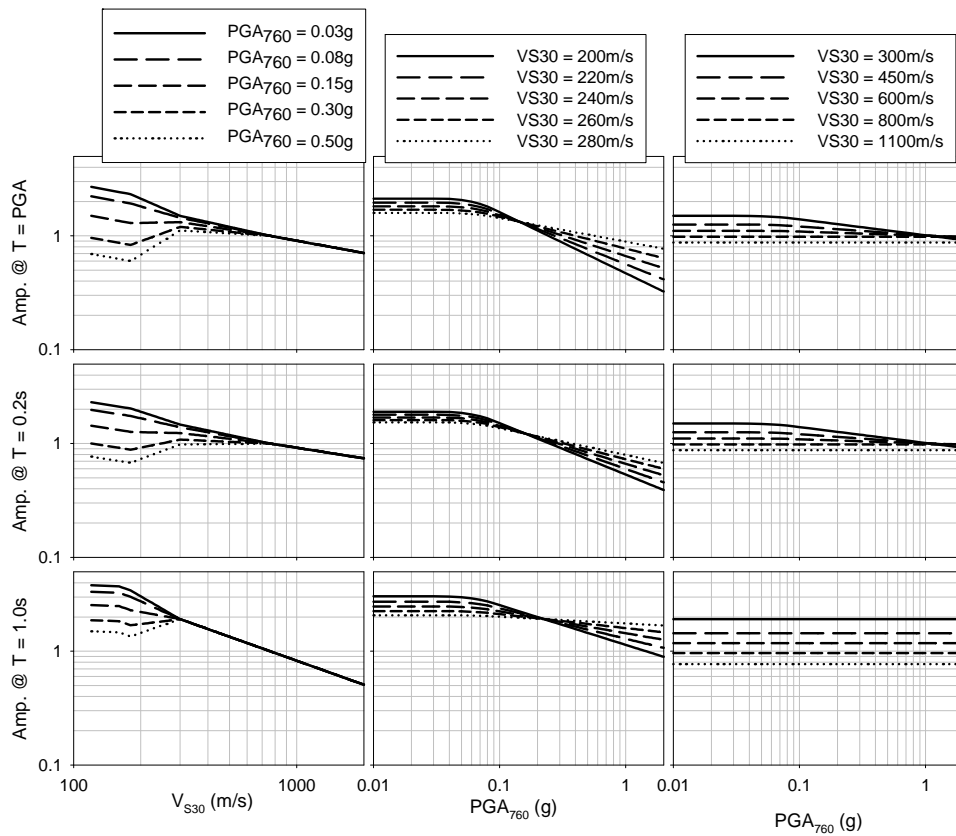
Figure 3. 2. Site amplifications proposed by Boore and Atkinson (2008) for T = 0.0s, 0.2s and 1.0s. The left column shows the variation of the site amplification with respect to V_{S30} for different levels of PGA_{rock}. (V_{S30} for reference rock is 760m/s in BA08. This is emphasized by designating PGA_{rock} as PGA_{760} in the legends). The middle and right columns show the variation of the site amplifications as a function of PGA_{rock} (PGA_{rock} is designated as PGA_{760} in x-axis labels) for different V_{S30} values. V_{S30} values range between 200m/s and 280m/s in the middle column plots whereas they change from 300m/s to 1100m/s in the right column plots).

65

towards larger values with increasing period for $V_{S30}<300$m/s. The same trend is also observed for 300m/s$\leq V_{S30}\leq 760$m/s at higher levels of input rock motion but in this case the amplitude of hinging PGA decreases with increasing period and vanishes after T>1.0s. This observation suggests that the BA08 model barely expects nonlinear soil behavior (i.e., PGA$_{rock}$ values larger than hinging PGA) for stiff sites.

We note that discrepancies in the reference velocity definitions of CS05 and BA08 with respect to AS97, which can be considered as the basis of these two site models as well as the verification of single-event based simulations used in the AS08 site function that may fail to describe the event uncertainty in soil behavior are among the major reasons behind the derivation of the site model presented here. The other driving factor of this study is the recently updated site information of the pan-European accelerograms. To this end, the proposed model can be considered as a good candidate for future pan-European GMPEs.

3.3 Proposed Site Model

The model presented here favors the functional form proposed by WAS08 because it is relatively simple with respect to other models. The WAS08 model is calibrated by considering (a) the limitations of our database, (b) the interpretations made on the observed amplification trends that are discussed previously (Figures 3.1 and 3.2) and (c) the residual trends of the regression analyses that will be discussed in this section. The following paragraphs describe the steps and the methodology implemented to finalize the functional form of the site model.

We made a modification in WAS08 before starting the regression analysis. Instead of using a period-dependent reference velocity (V_{LIN}) as proposed by WAS08, a period-independent reference velocity (V_{REF}) is preferred (e.g., BA08 and CY08 site models) to simplify the proposed expression. This choice is based on our preliminary investigations about site amplification models that use period-

dependent reference velocity. In such models period-dependent velocity attains significantly small values as spectral ordinates shift towards longer periods (e.g., AS08 assumes a reference velocity of 400m/s for T≥1.0s) that cannot be justified by our database. Site models that use period-independent velocity (such as the one proposed in this paper) would impose slightly higher nonlinearity with respect those that consider period-dependent reference velocity. However, this difference is not significant as it will be shown in the following paragraphs. The use of V_{REF} also eliminates the need for the d term in WAS08 thus making the regression analysis simpler. The PGA_{1100} parameter in WAS08 (PGA_{REF} in our model) that describes the input rock motion is also used in our model because changing it to reference rock spectral acceleration ordinates (as in the case of CY08) would complicate the model. In fact, our preliminary analyses did not show any improvements in the proposed site model by changing input rock PGA (PGA_{REF}) to input rock spectral acceleration.

In order to understand the capability of the strong-motion database in addressing the nonlinear site effects, a preliminary set of analyses was done by setting the nonlinear site terms to 0 (i.e., b(T)=0). These analyses showed that the increase in the level of input rock motion results in reduced site amplification factors indicating the existence of nonlinear behavior in soil sites. This exercise also ensured the adequacy of our database to capture the nonlinear soil behavior. The residuals of this preliminary study revealed relatively lower site amplification estimations at high V_{S30} values. Thus, the site amplification was held fixed for higher V_{S30} values. This behavior is also observed in AS08. The threshold limit for V_{S30} to fix the site amplification is referred to as V_{CON} in our model. Although the number of data is inadequate to determine the limiting shear-wave velocity, V_{CON} is constrained to 1000m/s. The final functional form of the proposed model is given in Eq. (3.5).

$$ln(\,Amp\,) = \begin{cases} a(\,T\,)ln(V_{S30}\,/\,V_{REF}\,) \\ +b(\,T\,)ln\left[\dfrac{PGA_{REF} + c(\,V_{S30}\,/\,V_{REF}\,)^n}{(\,PGA_{REF} + c\,)(\,V_{S30}\,/\,V_{REF}\,)^n}\right] & \text{for } V_{S30} < V_{REF} \\ a(\,T\,)ln(V_{S30}\,/\,V_{REF}\,) & \text{for } V_{REF} \leq V_{S30} < V_{CON} \\ a(\,T\,)ln(V_{CON}\,/\,V_{REF}\,) & \text{for } V_{S30} \geq V_{CON} \end{cases}$$

$$(3.5)$$

where a(T), b(T), c and n are regression coefficients. The parameter, V_{REF}, is the period independent reference V_{S30} (V_{REF}=750m/s as explained in the next paragraph). PGA_{REF} (in g; gravitational acceleration) is the level of input rock motion at V_{REF}. It is estimated from the reference rock ground-motion model (see below paragraph) that is developed from the dataset used in this study. The coefficient c provides the transition between higher and lower ground-motion amplitudes. The coefficient n mainly captures the soil nonlinearity at low V_{S30} sites.

The recordings from sites whose $V_{S30} \geq 550$m/s were selected as a subset of the entire database to derive the ground-motion model for estimating the reference rock motion, PGA_{REF}. Figure 2.12b shows M_w vs. R_{JB} scatter plot of this dataset. This subset consists of 1355 recordings collected from 283 events and 344 strong-motion stations. The magnitude and distance ranges of the subset are $4 \leq M_w \leq 7.6$ and $R_{JB} \leq 200$km, respectively. The average V_{S30} of the recordings in the subset is 750m/s that is considered as the period-independent reference velocity (V_{REF}) in our model. A functional form similar to Abrahamson and Silva (2008) that is discussed elaborately in the following chapter was used in the derivation of PGA_{REF} ground-motion model (Eq. 3.6). This functional form represents the overall trends in the subset fairly well. In Equation (3.6) the multiplier of the logarithmic distance term accounts for the magnitude-dependent ground-motion decay. It also controls the saturation of high-frequency ground motions at short distances (Abrahamson and Silva, 1997). The functional form includes quadratic magnitude term with a break in linear magnitude scaling. The parameters F_N and

F_R are dummy variables for the influence of style-of-faulting, taking values of 1 for normal and reverse faults, respectively, and zero otherwise. Our functional form for PGA$_{REF}$ estimations does not contain an independent parameter to account for the depth-to-rock effect on PGA$_{REF}$ amplitudes that is either defined as Z1.0 or Z2.5 in most of the NGA GMPEs. Such information is very limited in our subset for its inclusion as an estimator parameter. The reference rock model coefficients were obtained from the random effects regression analysis (Abrahamson and Youngs, 1992) for the geometric mean of two horizontal components.

$$
\begin{aligned}
\text{for } M_W \leq 6.75; \ \ln(\text{PGA}_{\text{REF}}) = \ & 3.17101 + 1.15371(M_w - 6.75) + 0.0803(8.5 - M_w)^2 \\
& + \left[-1.49513 + 0.13602(M_W - 6.75)\right]\ln(\sqrt{R_{JB}^2 + 13.39544^2}) \\
& - 0.35736 F_N + 0.06573 F_R \\
\text{for } M_W > 6.75; \ \ln(\text{PGA}_{\text{REF}}) = \ & 3.17101 - 0.31204(M_w - 6.75) + 0.0803(8.5 - M_w)^2 \\
& + \left[-1.49513 + 0.13602(M_W - 6.75)\right]\ln(\sqrt{R_{JB}^2 + 13.39544^2}) \\
& - 0.35736 F_N + 0.06573 F_R
\end{aligned}
$$

(3.6)

Figure 3.3 compares the derived reference rock ground-motion model with the 3 NGA GMPEs for V_{S30}=750m/s. The comparisons are done for a fictitious strike-slip fault with a dip angle of 90º and the site is placed on the footwall side. The differences in the distance measures among the compared GMPEs were taken into account based on the simple scenario described here. Default values proposed by the model developers were used for some particular estimator parameters (e.g., Z1.0) that are employed in the NGA GMPEs. Although the subset used for the reference rock model is limited due to sparsely distributed high-V_{S30} data (for example there are only 113 records for PGA≥0.1g for V_{S30}≥550m/s as given in Figure 2.12c), the reference rock estimations of our model are fairly comparable with the NGA GMPEs. This observation may suggest using one of the other NGA models for estimating PGA$_{REF}$. We did not prefer this option because NGA GMPEs consider some particular estimator parameters (e.g., Z1.0, Z2.5, R_X, depth
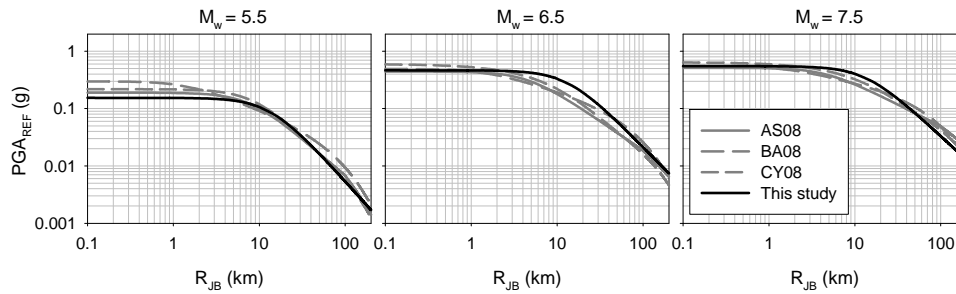
Figure 3. 3. Comparison of the proposed rock estimations with 3 NGA GMPEs (Abrahamson and Silva, 2008 [AS08], Boore and Atkinson, 2008 [BA08] and Chiou and Youngs, 2008 [CY08]) at V_{S30} = 750m/s. The left, middle, and right column illustrate variation in M_w = 5.5, M_w = 6.5, M_w = 7.5, respectively. The comparisons are done for a fictitious strike-slip fault with a dip angle of 90º and the site is placed on the footwall side. The differences in the distance measures among the compared GMPEs were taken into account based on the simple scenario described here. Default values proposed by the model developers were used for some particular estimator parameters (e.g., Z1.0) that are employed in the NGA GMPEs.

to top-of-rupture) that may be difficult to obtain in many cases unless particular assumptions are made for each earthquake scenario. (Some recent publications, such as Kaklamanos et al. (2011) suggest pragmatic approaches to compute the missing parameters in NGA GMPEs). Moreover these GMPEs are derived from the subsets of NGA strong-motion databank (Chiou et al., 2008) that may fail to reflect some of the specific features of the dataset used in the derivation of our PGA$_{REF}$ GMPE. We also wanted to have a complete set of tools while deriving our site model in order to verify one of the major objectives of this study: validity of WAS08 approach using observed data as well as to give a full perspective on the modeling uncertainties associated with every stage in our study. In brief, the rock ground-motion model derived in this study yields slightly lower estimations with respect to other GMPEs for small magnitude events (M_w=5.5). The reference

rock estimations by our GMPE tend to be larger in the short-to-intermediate distance range for moderate (M_w 6.5) and large (M_w 7.5) magnitude events. The last observation may result in slightly higher soil nonlinearity in our site amplification model.

Although it is not shown here, we also studied the distance-dependent behavior of within-event residuals of our reference rock GMPE against different regions existing in the dataset (pan-European region, Japan and Taiwan together with the US records). The residual analysis did not map any regional dependency in particular at distances beyond 50km where regional differences in geometric spreading may be dominant. Thus, we do not see any serious limitation to restrict the use of the reference rock GMPE for source-to-site distances greater than 50km. However, this observation should be considered with some reservation since the number of the reference rock data is limited at long distances (only 506 recordings for R_{JB}>70km). Subdividing the limited data into different regions essentially decreases the size of each bin and this, data-oriented, limitation may cast some doubts about our conclusive remark on the insignificance of regional effects. Upon the increase in rock data with reliable V_{S30} information, we can improve our reference rock GMPE by including additional estimator parameters to account for likely regional differences in the reference rock motion estimations.

The site amplification factors that are calculated by normalizing the observed spectral ordinates with the corresponding median estimations of the reference rock motions at V_{S30}=750m/s were used to obtain the site model coefficients by applying the random-effects regression analysis. The coefficients c and n were only computed at T=0.0s and held fixed for the entire period range because PGA_{REF} describes the input rock motion level for nonlinear soil behavior in the proposed model. The site model is derived for 62 spectral acceleration periods between 0.01s≤T≤4.0s, PGA and PGV. The regression coefficients and corresponding within- and between-event standard deviations (σ and τ, respectively) are given in Table 3.1.

71

Table 3. 1. Regression coefficients and corresponding standard deviations for the site amplification model. The period independent coefficients are V_{CON} = 1000m/s, V_{REF} = 750m/s, c = 2.5g and n = 3.2.

Period	a	b	σ	τ	σ_t
PGA	-0.41997	-0.28846	0.6448	0.4981	0.8148
PGV	-0.72057	-0.19688	0.6828	0.6823	0.9653
0.01	-0.41729	-0.28685	0.6452	0.4984	0.8153
0.02	-0.39998	-0.28241	0.6459	0.5042	0.8194
0.03	-0.34799	-0.26842	0.651	0.5146	0.8298
0.04	-0.27572	-0.24759	0.658	0.5305	0.8452
0.05	-0.21231	-0.22385	0.6658	0.5432	0.8593
0.075	-0.14427	-0.17525	0.6968	0.5672	0.8985
0.10	-0.27064	-0.29293	0.7177	0.5745	0.9193
0.11	-0.31025	-0.31837	0.7174	0.5728	0.918
0.12	-0.34796	-0.3386	0.7176	0.5659	0.9139
0.13	-0.39668	-0.36646	0.7177	0.5574	0.9087
0.14	-0.43996	-0.38417	0.7169	0.5436	0.8997
0.15	-0.48313	-0.39551	0.7158	0.5324	0.8921
0.16	-0.52431	-0.40869	0.714	0.5265	0.8871
0.17	-0.5568	-0.41528	0.7119	0.522	0.8828
0.18	-0.58922	-0.42717	0.7088	0.5166	0.8771
0.19	-0.62635	-0.4413	0.7069	0.5122	0.873
0.20	-0.65315	-0.44644	0.7048	0.5076	0.8686
0.22	-0.68711	-0.44872	0.7022	0.5073	0.8663
0.24	-0.72744	-0.46341	0.6985	0.5031	0.8608
0.26	-0.77335	-0.48705	0.697	0.5005	0.8581
0.28	-0.80508	-0.47334	0.6917	0.4982	0.8524
0.30	-0.82609	-0.4573	0.6874	0.4995	0.8497
0.32	-0.8408	-0.44267	0.6839	0.5029	0.8489
0.34	-0.86251	-0.43888	0.6817	0.5013	0.8462
0.36	-0.87479	-0.4382	0.6812	0.5023	0.8464
0.38	-0.88522	-0.43678	0.6817	0.5026	0.8469
0.40	-0.89517	-0.43008	0.6803	0.5017	0.8453
0.42	-0.90875	-0.4219	0.6767	0.499	0.8408

Table 3.1. Cont'd

Period	b_1	b_2	σ	τ	σ_t
0.44	-0.91922	-0.40903	0.6728	0.4961	0.8359
0.46	-0.9267	-0.39442	0.67	0.494	0.8324
0.48	-0.9372	-0.38462	0.6678	0.491	0.8289
0.50	-0.94614	-0.37408	0.665	0.4889	0.8254
0.55	-0.96564	-0.35582	0.6616	0.4851	0.8204
0.60	-0.98499	-0.34053	0.6586	0.4843	0.8175
0.65	-0.99733	-0.30949	0.6569	0.4844	0.8162
0.70	-1.00469	-0.28772	0.6547	0.4841	0.8142
0.75	-1.00786	-0.28957	0.6516	0.4749	0.8063
0.80	-1.00606	-0.28555	0.6506	0.4714	0.8034
0.85	-1.01093	-0.28364	0.6522	0.4712	0.8046
0.90	-1.01576	-0.28037	0.6545	0.4714	0.8066
0.95	-1.01353	-0.2839	0.6576	0.4679	0.8071
1.0	-1.01331	-0.28702	0.6574	0.4663	0.806
1.1	-1.0124	-0.27669	0.6577	0.468	0.8072
1.2	-1.00489	-0.27538	0.6593	0.4734	0.8117
1.3	-0.98876	-0.25008	0.6551	0.4775	0.8107
1.4	-0.9776	-0.23508	0.6539	0.4794	0.8108
1.5	-0.98071	-0.24695	0.6556	0.4778	0.8112
1.6	-0.96369	-0.2287	0.6549	0.4773	0.8104
1.7	-0.94634	-0.21655	0.6525	0.4728	0.8058
1.8	-0.93606	-0.20302	0.651	0.4717	0.8039
1.9	-0.91408	-0.18228	0.6471	0.4702	0.7999
2.0	-0.91007	-0.17336	0.6465	0.4712	0.8
2.2	-0.89376	-0.15463	0.6472	0.4745	0.8025
2.4	-0.87052	-0.13181	0.6381	0.4839	0.8008
2.6	-0.85889	-0.14066	0.6335	0.483	0.7966
2.8	-0.86106	-0.13882	0.6313	0.4669	0.7852
3.0	-0.85793	-0.13336	0.633	0.4614	0.7833
3.2	-0.82094	-0.1377	0.6204	0.4666	0.7763
3.4	-0.84449	-0.15337	0.619	0.4719	0.7784
3.6	-0.83216	-0.10884	0.6138	0.473	0.7749
3.8	-0.792156	-0.08884	0.6485	0.5178	0.8299
4.0	-0.75645	-0.07749	0.6407	0.495	0.8096

As it can be inferred from Table 3.1, the b(T) coefficient that controls the nonlinear soil behavior decreases with increasing period up to T=0.3s. This coefficient tends to increase towards longer periods (i.e., T>0.3s) that show the gradual decrease in soil nonlinearity. A similar behavior is also observed in WAS08, which indicates that the nonlinear site behavior derived from the empirical data of this study is consistent with the stochastic simulations of the WAS08 model.

Figure 3.4 show residual scatters (natural logarithm of observed values are subtracted from those of estimated ones, and throughout the text this definition is used to define residuals) of the proposed model. In the top row, the between-event residual scatters are shown as a function of magnitude. The middle and bottom rows on the same figure display the within-event residual distributions with respect to R_{JB} and V_{S30}, respectively. Each column in Figure 3.4 shows the variation of residuals for T=PGA, T=0.2s and T=1.0s. The residual trends in these particular spectral periods would give an overall idea about the success of the proposed model. They advocate that the site amplifications estimated by the model are unbiased as the variations in residuals are random in terms of selected seismological and geophysical parameters. Thus, its use would result in consistent site amplification estimations for 150m/s≤V_{S30}≤1200m/s.

3.4 Evaluation of the Proposed Site Model

Figure 3.5 compares the proposed model (black solid line) and the variation of the data for different PGA_{REF} intervals. The comparisons are done for T=0.0s (first row) and spectral ordinates at T=0.2s and T=1.0s (middle and bottom row, respectively). For the first two periods, the nonlinear soil behavior is dominant. The nonlinearity in soil behavior diminishes significantly for periods beyond T=1.0s, and almost vanishes for T>2.0s. The figure includes two of the NGA site models for comparison: AS08 (short dashed gray line) and BA08 (long dashed
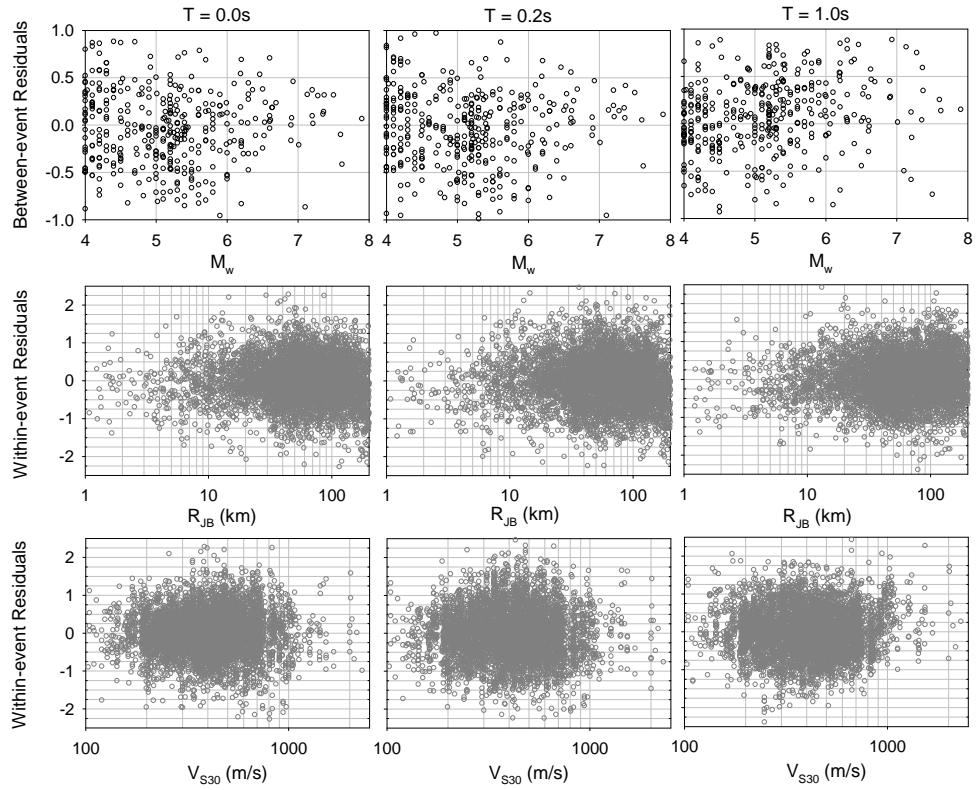
Figure 3. 4. Between-event (top row) and within-event (other two rows) residual distribution of the proposed site model. Left, middle and right columns show the distribution for T = 0.0s, T = 0.2s, and T = 1.0s, respectively.

gray line). AS08 was modified to obtain amplification factors consistent with 750m/s (i.e., V_{REF} in our model) because its reference PGA is defined at V_{S30}=1100m/s (PGA$_{1100}$ in their terminology). The modification to AS08 is an iterative process: (a) assign an arbitrary PGA$_{1100}$ value as an input for the AS08 site model, (b) compute site amplification, SF, from AS08 at V_{S30}=750m/s, (c) loop until the product of SF and PGA$_{1100}$ equals target PGA$_{REF}$ by modifying PGA$_{1100}$ in each iteration, (d) when (c) is satisfied, the last SF is the calibrated site amplification of AS08 for the chosen PGA$_{REF}$ and V_{REF} in the model.
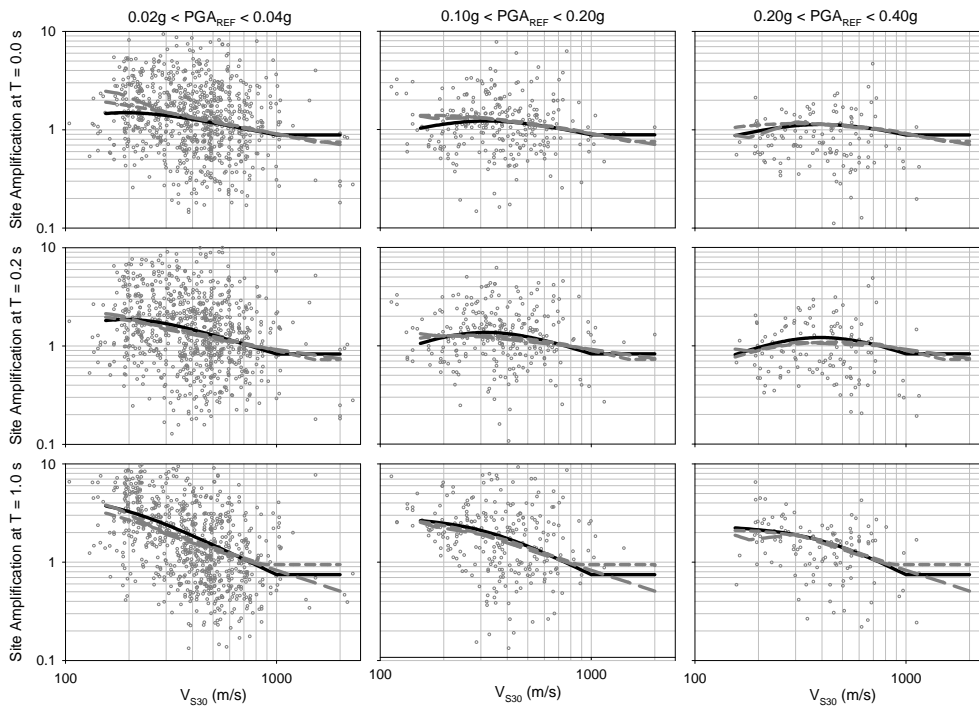
Figure 3. 5. Comparisons of the proposed site model (black solid line) with AS08 (short dashed gray curve) and BA08 (long dashed gray curve) together with the empirical data for T = 0.0s, T = 0.2s, and T = 1.0s (from top to bottom respectively). Each column represents different level of input rock motion, PGA$_{REF}$ indicated at the top of figure.

The immediate observation from Figure 3.5 is that the estimated site amplifications of the proposed model are comparable with AS08 and BA08. This is expected since all models explicitly impose nonlinear soil behavior. On the other hand, each site model plot in this figure shows its own characteristic features upon their careful examination. This is also not strange because the modeling approaches and the databases (including their metadata information) are different for each model, which results in such differences. These are discussed in the following paragraph.

76

When V_{S30} attains relatively large values ($V_{S30}{\geq}1000m/s$) the site model presented in this study as well as AS08 cap the site amplification to a constant value to prevent very small amplification factors. All models seem to follow the data trend closely for $300m/s{<}V_{S30}{\leq}1000m/s$. In other words, for increasing V_{S30} values, when soil behavior is presumably linear ($V_{S30}{>}300m/s$), all models yield similar amplification factors. In general, for low V_{S30} values ($V_{S30}{\leq}300m/s$), the site amplifications of the proposed model are slightly lower than those of AS08 and BA08. The observed differences between our model and other models indicate that the proposed site-amplification function imposes slightly higher nonlinearity for PGA_{REF}=0.2g for high-frequency ground motions (represented by T=0.0s and T=0.2s in Figure 3.5), which might be due to the conservative PGA_{REF} estimations. Other factors, such as the ground-motion databases and functional forms, can also play role in the observed differences. The proposed site model is derived using the data points given in these figures, so relatively better agreement between the data and the estimations of the model should be expected. Another source of discrepancy between the data and the two NGA models could be their lower V_{S30} limits. The lowest V_{S30} value for these models is approximately 180m/s that is slightly higher than the minimum V_{S30} value given in these plots.

The above discussions suggest that the soil nonlinearity is significant for high-frequency spectral ordinates (PGA or spectral acceleration at T=0.2s). This observation is particularly valid for the proposed model due to its specific features as discussed in the above paragraphs. This observation may contradict the site amplification factors in some of the well-known seismic design codes, such as Eurocode 8 that proposes period-independent site amplification factors for PGA and they are greater than unity even for high PGA values. These recommendations are significantly different than the soil amplification behavior presented in this article. To test the reliability of our site model for code implementation the results of a comparative case study are presented in a tabular format in Table 3.2. The case study compares our site amplification factors with those proposed in the updated NEHRP provisions that consider nonlinear soil behavior as a function of

Table 3. 2. Comparative table that lists the recommended NEHRP site amplifications (first numbers) and corresponding estimations (in bold) from the proposed site model.

Site Class	Site amplifications for spectral accelerations S_S at T = 0.2s				
	S_S=0.25g	S_S=0.50g	S_S=0.75g	S_S=1.00 g	S_S=1.25g
C	1.20 / **1.21**	1.20 / **1.17**	1.10 / **1.14**	1.00 / **1.12**	1.0 / **1.10**
D	1.60 / **1.37**	1.40 / **1.13**	1.20 / **1.01**	1.10 / **0.94**	1.0 / **0.89**
E	2.50 / **1.20**	1.70 / **0.94**	1.20 / **0.82**	0.90 / **0.75**	0.9 / **0.70**
Site Class	Site amplifications for spectral accelerations at T = 1.0s				
	S_1=0.10g	S_1=0.20g	S_1=0.30g	S_1=0.40 g	S_1=0.50g
C	1.70 / **1.39**	1.60 / **1.34**	1.50 / **1.32**	1.40 / **1.31**	1.3 / -
D	2.40 / **2.22**	2.00 / **1.88**	1.80 / **1.81**	1.60 / **1.74**	1.5 / -
E	3.50 / **2.48**	3.20 / **2.00**	2.80 / **1.92**	2.40 / **1.85**	2.4 / -

five different spectral acceleration levels at T=0.2s and T=1.0s. The reference rock is described by V_{S30}=760m/s in the NEHRP provisions that is slightly higher than the one in our model (i.e., V_{S30}=750m/s). This difference is neglected in this case study. The site amplification comparisons are done for three site classes: NEHRP C (360m/s<V_{S30}≤760m/s), NEHRP D (180m/s<V_{S30}≤360m/s) and NEHRP E (V_{S30}=180m/s). We assumed that the geometric means of the upper and lower bound V_{S30} values can represent the NEHRP C and D site classes (i.e., V_{S30}=525m/s and V_{S30}=255m/s, respectively) while estimating the site amplifications from our model. NEHRP E site class was represented by V_{S30}=180m/s. Since the NEHRP provisions consider period-dependent site amplifications (for discrete spectral accelerations at T=0.2s and T=1.0s as presented in Table 3.2), we first computed the corresponding PGA_{REF} value for each discrete spectral acceleration value for our site model. This is achieved by

computing the reference rock regression coefficients Eq. (3.6) for spectral acceleration ordinates at T=0.2s and T=1.0s. These particular equations were used to identify the most appropriate earthquake scenario that would give approximately the same spectral acceleration values indicated in the NEHRP provisions. The determined earthquake scenarios were then used in Eq. (3.6) to compute corresponding PGA_{REF}, which were, in turn, inserted into Eq. (3.5) to compute our site amplification estimations. For each specific case, our site amplifications and those of NEHRP provisions are given side by side in Table 3.2. In order to distinguish our site amplification estimations they are given in bold. Although we applied various intermediate steps to obtain the comparative site amplification values from our model, they are fairly in good agreement with those recommended by the NEHRP provisions. The good agreement presented in Table 3.2 advocates the consistency of our site model while addressing the nonlinear soil behavior. It also emphasizes the importance of period dependency in site amplification for different reference rock ground-motion intensity levels, as site factors are not the same for every case.

Figure 3.6 discusses the last remark in the above paragraph in a more detailed way. This figure shows period-dependent site amplifications of our model as well as AS08 and BA08 for three different V_{S30} values: V_{S30}=525m/s, V_{S30}=255m/s and V_{S30}=180m/s. These values grossly represent the NEHRP C, D and E site classes (as discussed in the above paragraph). They also characterize the Eurocode 8 B, C and D site classes fairly well as their V_{S30} intervals are almost identical to those of NEHRP C, D and E, respectively. The site amplifications were computed for two reference earthquake scenarios that represent Type-I and Type-II hazard levels in Eurocode 8. The top row plots in Figure 3.6 shows the amplifications calculated for a strike-slip earthquake scenario of M_w 7.5 (Type-I hazard level) whereas the bottom row panels give amplifications for an M_w 5 strike-slip event. For both cases the site is assumed to be located at a distance of R_{JB}=0.1km. The rock site condition used for computing site amplifications is mimicked by V_{S30}=800m/s that is consistent with the Eurocode 8 rock definition. The panels on

this figure also display the period-independent site factors of Eurocode 8 for Type-I (top row) and Type-II (bottom row) hazard levels.
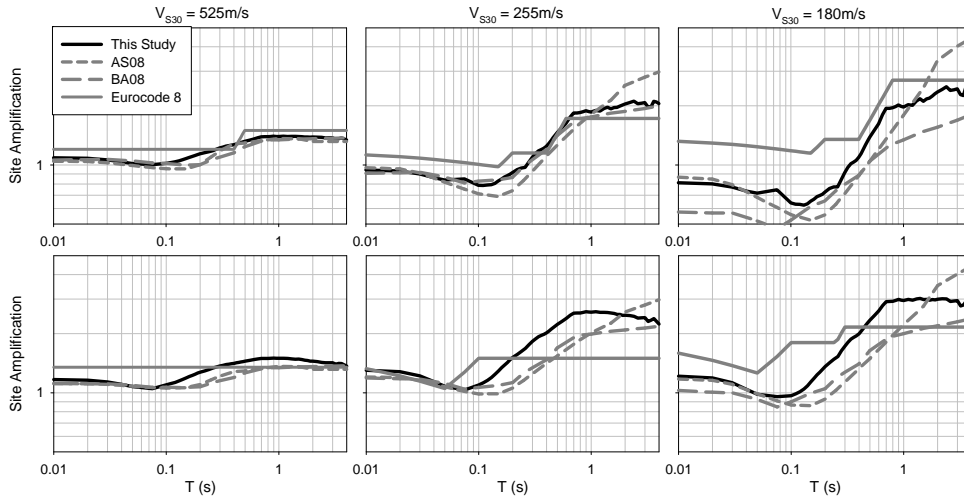
Figure 3. 6. Period-dependent variation of the site amplification of proposed site model (black solid curve) for different V_{S30} values and its comparison with AS08 (short-dashed gray curve) and BA08 (long-dashed gray curve).

The preliminary observation from these comparative plots is the fairly good match between the proposed model and the other two site models for V_{S30}=525m/s and V_{S30}=255m/s. The dispersive behavior of the 3 models becomes quite visible for soft soil (V_{S30}=180m/s) conditions, which may stem from the sparse low V_{S30} recordings in the ground-motion databases as well as the differences in the implemented modeling approach in each functional form. Nevertheless, even for soft soil conditions, the site amplification trends imposed by these models are similar. (The amplification estimations of our model as well as BA08 impose lower gradients for this site class as vibration period increases). The other important observation from Figure 3.6 is the incompatible variation of nonlinearity-independent site amplification factors of Eurocode 8 with respect to

other site models. The site amplifications suggested by Eurocode 8 are generally conservative in the short periods and they seem to fail following the trends of other site models towards longer periods. We note that this observation is limited to the selected earthquake scenario and it should be validated further by a comprehensive study.

3.5 Conclusions

The empirical site amplification model that can be used in GMPEs derived for shallow active crustal regions. The functional form is capable of addressing the linear and nonlinear soil behavior and it is based on a well-studied extensive dataset with the most recent updates of the Greek, Italian and Turkish site information. The database includes global recordings from Taiwan, the Western US, and Japan. Therefore, it can be of particular use for future pan-European GMPEs. A ground-motion predictive model is also derived to estimate the level of input rock motion (PGA_{REF}) that is used in the calculation of site amplification factors. The reference rock motion is defined for V_{S30}=750m/s in our study. Confined to the limitations of the strong-motion database, we recommend the use of our site model for 150m/s≤V_{S30}≤1200m/s.

The functional form of the proposed site model carries similar features with the one in Walling et al. (2008; WAS08) that is entirely based on stochastic simulations. The consistency of our site amplifications with those of the WAS08 model validates the theoretical aspects of WAS08 through the use of empirical data. The agreement between these comparisons also advocates the reliability and robustness of our site model. Notwithstanding the proposed model also draw consistent trends with other similar site amplification equations (e.g., Boore and Atkinson, 2008; Abrahamson and Silva, 2008). It imposes slightly higher soil nonlinearity for softer sites due to differences in modeling approach, strong ground-motion database, and PGA_{REF} GMPE. The observed trends in the proposed site model are also consistent with the NEHRP seismic provisions that

consider period-dependent nonlinear soil behavior. The preliminary cook-based discussions presented here can also be taken into account by Eurocode 8 committees for future modifications in site amplification factors that are currently independent of soil nonlinear behavior.

CHAPTER 4

A PROCEDURE TO COMPUTE SITE FACTORS IN SEISMIC DESIGN CODES

Adapted from Sandıkkaya M.A., S. Akkar, P.-Y. Bard (2014). A Proposal to Describe Site Amplification Factors for Seismic Design Codes. Submitted to Earthquake Spectra.

The nonlinear site model based on V_{S30} and PGA_{rock} as proxies to characterize site conditions and input ground motion level, respectively, is used to evaluate current site factors presently enforced in the Eurocode 8 (CEN, 2004) and NEHRP (BSSC, 2009) codes. The overall results obtained from a preliminary simplified analysis led to the investigation of various approaches based on the outputs of probabilistic seismic hazard analysis (PSHA) to improve the quality of the evaluation in view of proposing an alternative method to derive period-dependent site-specific and regional site amplification factors. Following Cramer (2003), a hybrid approach in probabilistic hazard studies that combines probabilistic results for rock hazard maps and deterministic approach is applied to compute site amplification. The current PSHA maps provided by the USGS Hazard Tool (Petersen et al., 2008) for the US territory were used as an example to investigate the effects of seismicity region, return period and different definitions of design spectra (uniform hazard spectrum, UHS, conditional mean spectrum, CMS, and scenario-based spectrum, SBS) on site amplification. A robust procedure to derive site factors is then proposed. The final aim of this study is to emphasize the need to define new site factors for the pan-European region – even if keeping the site

class definition unchanged –, by using the proposed procedure together with the PSHA results of the **S**eismic **H**azard H**AR**monization in **E**urope (SHARE) project that will be investigated later.

4.1 Background

Estimation of site effects is one of the essential components of earthquake engineering design. It has been one of the prime interests of the research and engineering community since the early work of Borcherdt (1970) who defined the site amplification as the ratio of ground-motion intensity measures at a soil site to its counterpart measured at a nearby rock site. The site amplification strongly depends on the site classification schemes that have gradually evolved during the last four decades. Seed et al. (1976) first showed the differences between four site conditions in terms of spectral shapes. Borcherdt (1994) and Dobry et al. (2000) studies led the formulation of site classification schemes that utilize either geophysical or geotechnical parameters. Site classification schemes have been further investigated in many other studies (e.g., Rodriguez-Marek et al., 2001; Stewart et al., 2003; Cadet et al., 2012a; Pitilakis et al., 2013). The NEHRP Provisions (BSSC, 2009) and Eurocode 8 (EC8; CEN, 2004) have used the major outcomes of these studies (or other similar ones) to shape their in-practice site classification as well as the corresponding design spectra and site factors.

Currently, the state-of-art practice in site amplification is to develop empirical (or theoretical) models that are continuous functions of V_{S30} (the time-based average of the uppermost 30-m shear-wave velocity profile) and PGA_{rock} (peak ground acceleration for rock site conditions) that is considered as a robust proxy to represent rock-motion intensity level for describing the linear and nonlinear soil behavior (e.g., Abrahamson and Silva, 1997; Choi and Stewart, 2005; Walling et al., 2008). Other supplementary parameters such as depth-to-bedrock and fundamental site frequency (or predominant site period) have been proposed and used in recent studies for both site characterization and site amplification

(Abrahamson and Silva, 2008; Campbell and Bozorgnia, 2008; Cadet et al., 2012b; Derras et al., 2012). However, V_{S30} still preserves its importance as a common proxy to site conditions, especially in presently enforced building codes.

There are minor differences in the existing site classification schemes of NEHRP and EC8 codes. These codes classify different soil conditions in terms of discrete V_{S30} intervals. However, the way they compute site factors (spectral amplifications) is different. Studies by Borcherdt (1994; 2002a; 2002b), Idriss (1990), and Dobry et al. (2000) determine the NEHRP site factors as functions of V_{S30} and rock pseudo-spectral accelerations (PSA_{rock}) at short- and long-periods (T = 0.2 s and T = 1 s, respectively). They modify design spectrum for different PSA_{rock} levels and for different site classes with respect to a reference rock site characterized by V_{S30} = 760 m/s. EC8 implements the Rey et al. (2002) study and provides two sets of site factors for low and high seismicity regions. The ground-motion intensity (PGA_{rock} that is defined for V_{S30} = 800 m/s) used by EC8 is implicitly considered in the low and high seismicity spectral shapes. This code prefers combining period-independent site factors together with site-class and seismic-region dependent spectral shapes (by means of corner periods; see Table 3.1). The EC8 site factors basically disregard nonlinear soil behavior (apart from the fact that site factors are lowered from moderate seismicity areas – EC8 type II – to active seismic areas – EC8 type I, see Table 3.1), whereas the NEHRP site factors consider soil nonlinearity with a decrease in soil stiffness at high levels of short-period spectral ordinates.

Pitilakis et al. (2012) have recently proposed a revision to the existing EC8 site factors by using an improved version of the Rey et al. (2002) procedure. They kept the existing normalized spectral shapes recommended in EC8 and used an improved strong-motion dataset (Yenier et al., 2010) to refine the period-independent site factors (designated as "S" in EC8) for each EC8 site class and seismicity level. The comparisons between the site factors recommended by Pitilakis et al. (2012) and EC8 are given in Table 3.1. Their findings are

systematically higher than the original EC8 site factors except for site class D. As discussed by Bommer and Pinho (2006) as well as Akkar and Bommer (2007b) the current EC8 spectral shapes and their fixed corner periods do not provide full information about the level of seismicity in different regions of Europe as they are only scaled with PGA and disregard the effect of magnitude scaling towards long spectral periods. Thus, establishing site amplification factors relying on spectral shapes that misrepresent seismic design demands may not yield consistent site factors. Moreover, the procedure used in Pitilakis et al. (2012) overlooks soil nonlinearity and its results depend on the size of the existing data sets in different site class bins, which proves to be particularly insufficient for very soft sites (i.e., soil class D according to EC8 site classification) in their dataset.

Table 4. 1 Corner periods of PGA normalized spectral shapes and corresponding site factors (S) of EC8 and site factors proposed by Pitilakis et al. (2012; Petal12)

	Site Class[*]	T_b	T_c	T_d	S (EC8)	S (Petal12)
Type I[**]	B	0.15	0.50	2.0	1.20	1.30
	C	0.20	0.60	2.0	1.15	1.70
	D	0.20	0.80	2.0	1.35	1.35[***]
Type II[**]	B	0.05	0.25	1.2	1.35	1.40
	C	0.10	0.25	1.2	1.50	2.10
	D	0.10	0.30	1.2	1.80	1.80[***]

[*] Site class B (360 m/s $\leq$ V_{S30} < 800 m/s), site class C (180 m/s $\leq$ V_{S30} < 360 m/s), site class D (V_{S30} < 180 m/s)

[**] Type I and Type II spectral shapes refer to high- and low-seismicity regions, respectively.

[***] Requires site specific analysis

Huang et al. (2011) developed a procedure to compute NGA site factors to compare with those from NEHRP. The NGA site factors are the average of site amplifications computed from three NGA GMPEs namely: Boore and Atkinson (2008), Campbell and Bozorgnia (2008) and Chiou and Youngs (2008); for a set of combinations. These combinations reflect style-of-faulting effects (strike-slip and reverse earthquakes), magnitude effects (M_w 5 to 8) and distance effects (0 km to 50 km). The site effect is considered via V_{S30} in the range of 150 m/s to 1500 m/s. Each estimate using these variables are normalized by the counterpart with the site condition of V_{S30} = 760 m/s. They observe that as sites get softer, the dependency of site amplification on period increases. This dependency reaches its maximum at very soft sites. Under strong excitations, period-dependent site amplifications become more visible. When compared to NEHRP site factors, they found higher soil nonlinearity at the short-period range, on the other hand the long-period site factors are lower.

Although the major objective of the proposed nonlinear site model that is developed in the context of the previous chapter is to implement it into GMPEs, the last section briefly evaluates the site factors provided by NEHRP and EC8. The low- and high-seismicity scenarios that were chosen for the evaluation of EC8 site factors advocated that disregarding nonlinear soil behavior can result in conservative short-period spectral accelerations. The site factors computed by the proposed nonlinear site model for short- and long-period (i.e., T = 0.2 s and T = 1 s, respectively) spectral accelerations showed similarities with those of NEHRP provisions, though imposing slightly higher nonlinearity compared to the NEHRP site factors.

The observed similarities between the NEHRP site factors and those computed from the limited case study in the previous chapter are the major motivations to use the proposed nonlinear site amplification model to propose a robust procedure to compute new site factors for seismic design codes; in particular for EC8 as this code should undergo a revision process by 2015. I started by improving and

increasing the number of earthquake scenarios used in previous study (as they were too few to capture all possible earthquake scenarios) to perform a comprehensive evaluation of the site factors that are currently provided in EC8 and NEHRP. The observed trends from this step refined our understanding about the behavior of site factors to propose an alternative site amplification procedure that is based on the main outcomes of PSHA. The proposed procedure follows Cramer (2003) that applies a hybrid approach to compute site amplification factors by combining the rock PSHA results with deterministic site models. The current PSHA maps provided by the USGS Hazard Tool (Petersen et al., 2008) for the US territory were used as an example to assess the practicality of the procedure for site factor calculations with emphasis on the effects of regional seismicity, return period and design spectrum definitions (i.e., Uniform Hazard Spectrum, UHS, Conditional Mean Spectrum, CMS, Scenario Based Spectrum, SBS). The essential objective is to emphasize the need for defining new site factors for the pan-European region – even if keeping the EC8 site class definitions as they are - and to present a relatively simple procedure to compute site factors for the future updates of EC8 by making use of PSHA results of the Seismic Hazard Harmonization in Europe (SHARE) project (Giardini et al., 2013).

4.2 Evaluation of Current Site Factors

As indicated in the previous section, the trends in EC8 and NEHRP site factors by using the proposed site model is investigated for a limited number of scenarios at different PGA levels. These limited studies did not consider the various aspects of the problem; for example, the influence of spectral shape that mainly depends on magnitude and is weakly related to distance except for very remote sites from the source. To this end, more comprehensive analyses by generating a significant number of magnitude-distance pairs together with a range of epsilon values (ε; number of standard deviation above or below the median ground-motion estimation) are performed to account for the aleatory variability in ground

motions. This effort yielded a large sample size for each PGA_{rock} level that led to more reliable results on the behavior of site amplification. The moment magnitudes (M_w) range of the selected scenarios is between 4 and 8 and recordings within R_{JB} = 200 km. The magnitude increments were chosen as 0.2 units whereas, given the power law dependence of distance, the distance increment was adapted to increase with logarithmic distance intervals. At short distances (i.e., R_{JB} < 50 km), the logarithmic distance interval was considered to have an increment of 0.2 ln-units (21 distance intervals between 1 and 50 km). The logarithmic distance increment was reduced to 0.1 log-units at longer distances (i.e., R_{JB} > 50 km) that results in 14 long-distance intervals between 50 km and 200 km for this exercise. The ε range was taken between -2 to 2 with 0.25 unit increments. For each magnitude-distance-epsilon ternary (triplet), the spectral ordinates were calculated by the recent pan-European GMPE that will discussed in the next chapter. The site amplifications were computed for V_{S30} values of 525 m/s, 255 m/s and 150 m/s using the corresponding PGA_{rock} values. The first two V_{S30} values represent the log-average V_{S30} of NEHRP C and D site classes, while the third V_{S30} value represents NEHRP E site class. The selected V_{S30} values describe EC8 B, C and D site classes, respectively. (Minor differences in reference rock site definitions between EC8, NEHRP and the proposed site model are disregarded in this study).

Three PGA_{rock} levels of 0.01 g, 0.1 g, and 0.5 g were selected to illustrate the nonlinear site effects. The triplets that yield PGA_{rock} values within ±10% of target PGA_{rock} levels (i.e., 0.01 g, 0.1 g, and 0.5 g) were grouped into three separate bins. The corresponding M_w-R_{JB} distributions are displayed in Figure 4.1 that also shows their variation for different epsilon intervals. The median site amplification for each group is computed with an equal weight on all triplets. Figure 4.2 shows these median site amplifications as a function of period. This figure also includes the site amplification factors of EC8 and Pitilakis et al. (2012) by considering the combined effects of site factor and site class dependent spectral shape. The immediate observation from these plots is the period-dependent behavior of site

amplifications that also vary with the changes in PGA$_{rock}$ level. The short-period (T < 0.5 s) and long-period (T > 1 s) amplifications are very different from one another and this difference becomes more prominent for soft sites. For large PGA$_{rock}$ levels, the short-period site amplifications at soft sites show strong nonlinearity. The long-period site amplifications of the approach are generally higher than those suggested by Pitilakis et al. (2012) and EC8 with decreasing PGA$_{rock}$ levels and soil stiffness (i.e., for stiff or soft sites). The site amplifications of the triplet approach yield fairly similar results with respect to Pitilakis et al. (2012) and EC8 for large V$_{S30}$ values (mimicked by V$_{S30}$ = 525 m/s in our study) when soil nonlinearity is almost immaterial. This observation indicates that neither Pitilakis et al. (2012) nor current EC8 provisions correctly consider nonlinear soil behavior in their site factor computation.
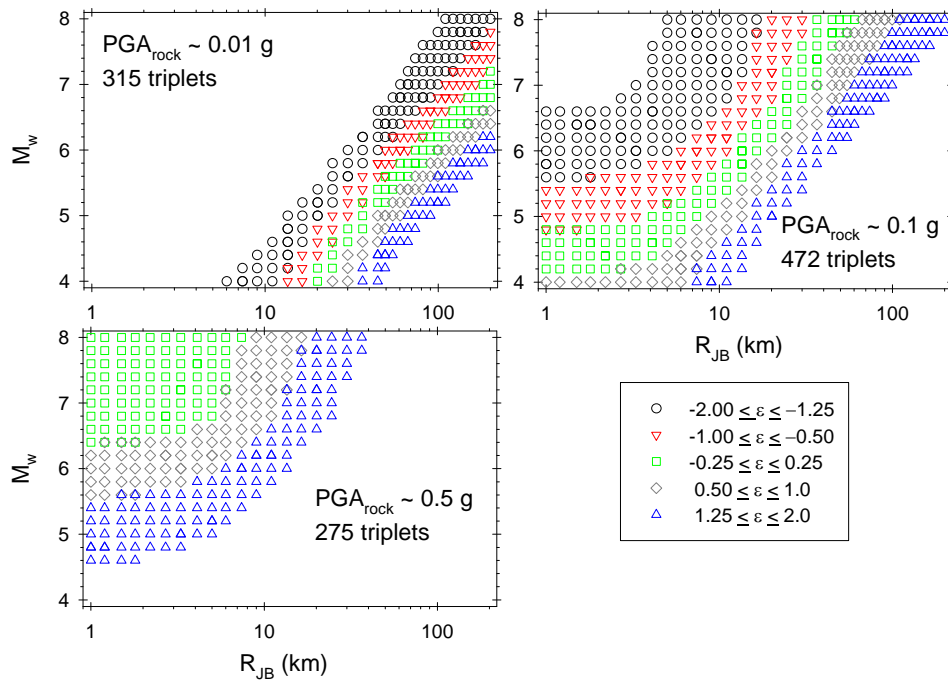
Figure 4. 1: M$_w$ - R$_{JB}$ - ε scatters for three PGA$_{rock}$ levels that are used in the triplet approach. The numbers of triplets for each PGA$_{rock}$ bin are indicated on the plots.
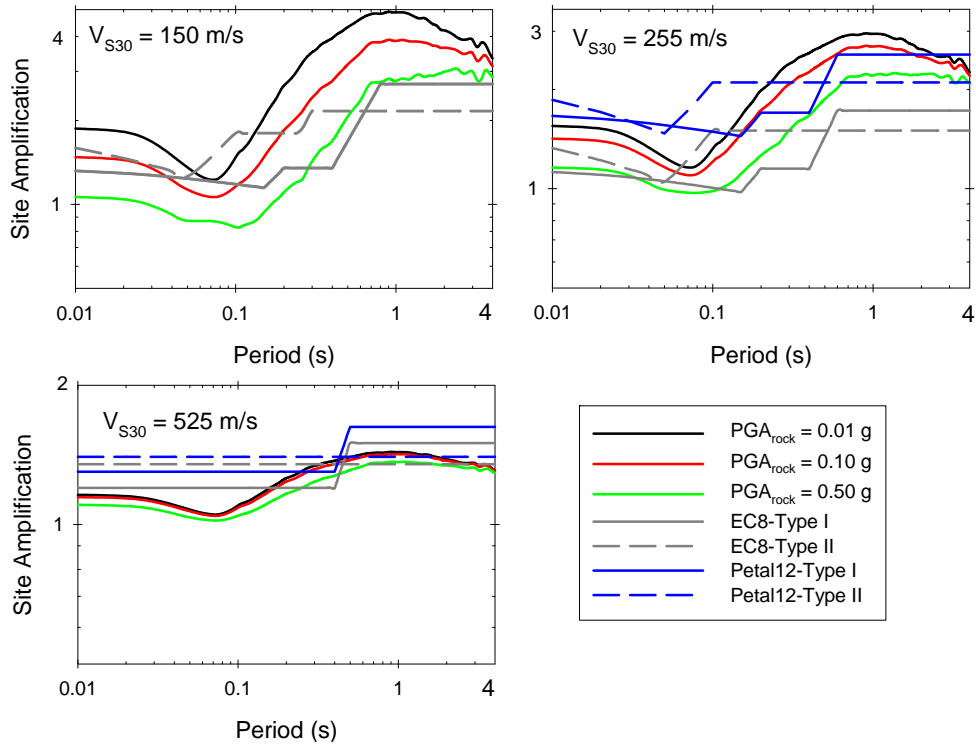
Figure 4. 2 Period-dependent median amplification factors for different V_{S30} values that are computed from the triplet approach. The median site amplifications were computed for each PGA_{rock} bin.

Similar type of comparisons are repeated for NEHRP site factors. The comparisons were done for short-period (T = 0.2 s) and long-period (T = 1 s) spectral ordinates as they are used by NEHRP to describe design spectrum for different site conditions. It is noted that site amplification at T = 1 s is a good proxy to describe average behavior of spectrum at long periods because the site amplification becomes maximum at about this period and follows a fairly stable trend (Figure 4.2) that leads to the proposition of robust site factors for code approach. The choice of spectral ordinate at T = 0.2 s for representing site amplification at short periods is questionable; yet we still used it in our study to follow the current NEHRP practice. A more rational course of action for the

computation of site factors might be to follow Borcherdt (1994) who suggested using the average site amplifications over 0.1 s ≤ T ≤ 0.5 s and 0.5 s < T < 1.5 s to define short- and long-period site behavior, respectively. However, we did not make any attempt to investigate this suggestion.

As NEHRP provisions account for site factors by using PSA_{rock} at T = 0.2 s and T = 1 s for a reference rock site of V_{S30} = 760m/s, we had to make some adjustments to use the proposed site model because it is based on PGA_{rock} to define soil amplification. All triplets that fall within ±10% of the target NEHRP PSA_{rock} values at T = 0.2 s and T = 1 s were grouped into separate bins. These bins were assembled such that the logarithmic median of PSA_{rock} values at T = 0.2 s and T = 1 s correspond to the pre-defined NEHRP values. Similar to the EC8 case study, the PGA_{rock} value of each triplet was then used to compute the site amplification for V_{S30} = 525 m/s (NEHRP C), 225 m/s (NEHRP D) and 150 m/s (NEHRP E). The median site amplifications computed from each bin for the representative site conditions are compared with the NEHRP site factors in Table 4.2. The comparisons between the triplet approach and NEHRP site factors yield fairly similar values except for a few cases in very soft soil conditions (NEHRP E site class) at short periods, where higher non-linear effects are predicted by the NEHRP site factors. These are highlighted by bold figures in Table 4.2. This comprehensive case study indicates that the site model can consistently capture the soil amplification at different ground motion levels for common site classes.

4.3 Integration of Earthquake Probability and Design Spectrum Concept in the Computation of Site Factors

The case study in the previous section gives insightful information about the differences in EC8 and NEHRP for site amplification factors. It also demonstrates the efficiency of the nonlinear site model for capturing the soil behavior at different ground-motion intensity levels. The triplet approach used in these analyses can be a practical tool to propose site factors for design codes; however,

Table 4. 2 Comparison of the NEHRP site factors (first numbers) with computed site factors within this study (second numbers).

Site amplifications for spectral accelerations S_S at T = 0.2 s				
Site Class	S_S=0.25g	S_S=0.50g	S_S=0.75g	S_S=1.00g	S_S=1.25g
C	1.2 / 1.2	1.2 / 1.2	1.1 / 1.2	1.0 / 1.2	1.0 / 1.2
D	1.6 / 1.7	1.4 / 1.5	1.2 / 1.4	1.1 / 1.3	1.0 / 1.2
E	2.5 / 1.7	1.7 / 1.4	1.2 / 1.2	0.9 / 1.1	0.9 / 1.1
Site amplifications for spectral accelerations S_l at T = 1 s				
Site Class	S_1=0.10g	S_1=0.20g	S_1=0.30g	S_1=0.40g	S_1=0.50g
C	1.7 / 1.4	1.6 / 1.4	1.5 / 1.4	1.4 / 1.4	1.3 / 1.3
D	2.4 / 2.6	2.0 / 2.4	1.8 / 2.3	1.6 / 2.1	1.5 / 2.1
E	3.5 / 3.5	3.2 / 3.1	2.8 / 2.9	2.4 / 2.7	2.4 / 2.5

it may not be entirely convenient in probabilistic seismic hazard view point because the earthquake scenarios generated by triplets are assumed to have equal chances of occurrence. This is not the case in PSHA as it primarily considers different annual exceedance rates of earthquakes as well as ground-motion intensities. In other words, although some of the important aspects of PSHA are considered implicitly in triplets (via different PGA_{rock} levels with equal likelihoods of occurrence), the major outcomes of PSHA should be taken into account while suggesting consistent site amplifications for seismic design codes that are compatible with modern seismic hazard analysis.

To this end, the role of return period (T_R), the seismicity level and different formats of design spectrum (description of seismic demand) are used to propose a robust procedure for computing site factors that are compatible with regional or site-specific PSHA results and can be efficiently implemented in design codes. The return period and regional seismicity can be basically mapped by the PGA_{rock}

value – which is the main parameter in assessing the period-dependent site behavior by the site model – and rock spectral shape whereas different definitions of design spectrum (i.e., UHS, CMS and SBS) may have different implications on seismic demand as well as site factors.

The UHS that provides spectral ordinates with equal exceedance probabilities pools all likely events contributing to the hazard and may yield conservative spectral accelerations when considering simultaneously different periods of interest. Depending on the chosen return period, the conservative UHS spectral ordinates may result in misleading site amplification factors.

The SBS that is computed after the deaggregation (Bazzuro and Cornell, 1999) of PSHA at a specific period disregards the correlation between the target hazard level and the other spectral ordinates. Thus, depending on how large the difference between median SBS and target hazard level, SBS may yield unconservative seismic demand results that in turn can affect the reliability of site factors as in the case of UHS. The construction of SBS also depends on the definition of the most contributing earthquake scenario at the particular period of interest. Deaggregation analysis yields either the mode or mean earthquake scenario (designated by M_{mode}-R_{mode}-ε_{mode} or M_{mean}-R_{mean}-ε_{mean}, respectively). Harmsen (2001) indicated that the mean earthquake scenario may yield misrepresentative seismic demands as it is the weighted average of all contributing events derived from deaggregation.

The recently proposed CMS (Baker, 2011) overcomes the aforementioned impracticalities of both UHS and SBS. CMS considers an earthquake scenario of M_{mean} and R_{mean} that is derived from the PSHA deaggregation at a particular period of interest (T_0). This spectrum considers the normalized difference between the target hazard level and median spectral ordinate corresponding to M_{mean} and R_{mean} at T_0. The normalization is done with the standard deviation of GMPE used in PSHA and the resulting expression is called ε_0. For a pre-determined range of

spectral periods, T_i, CMS estimates the corresponding epsilon values, ε_i, by considering the correlation between ε_0 and ε_i. CMS provides the expected response spectrum conditioned on the occurrence of a given target spectral acceleration at the period of interest, T_0. It is considered to overcome much of the conservatism imposed by UHS. It is originally linked to one single GMPE and Lin et al. (2013) introduced the conditional spectrum (CS) approach that adapts multiple GMPEs in CMS. CS eliminates the differences between the mean and modal earthquake scenarios. This spectrum type is now routinely provided by the USGS hazard tool (http://earthquake.usgs.gov/hazards/apps; Petersen et al., 2008).

The major outcomes of PSHA, as described above, have already been considered in the computation of site factors. Tsai (2000), Cramer (2003), Bazzuro and Cornell (2004a; b), Goulet and Stewart (2009), and Papaspiliou et al. (2012a,b) are some of the benchmark studies that investigated the possible effects of PSHA results on soil amplification. These studies use either fully probabilistic or hybrid methods for site factor computation and particularly focused on soil nonlinearity. Thus, procedures presented in some of these studies can be implemented into the concepts discussed here. The findings of Goulet and Stewart (2009) indicated that the hybrid approach under predicts the actual soil response. However, we preferred this method in our study as the fully probabilistic approach is rather a time consuming procedure as it requires additional computational effort. In essence, we deterministically modified the generic rock PSHA spectrum by a soil response function (Cramer, 2003) for the computation of site factors. Firstly, we investigate the effects of return period and seismicity level on site amplification. We compare the results for three return periods for two sites located at low- and high-seismic regions. Secondly, the possible influence of design spectrum formats is searched. With the observations retrieved from these preliminary analyses, we will compute the factors for a region for a number of site conditions and compare them with current site factors given in seismic design codes. The following subsection clarifies our procedure through a detailed case study.

4.3.1 Example Case Study

To illustrate the PSHA based site factor methodology, two specific regions are considered in Western US. These regions are located in southern California and western Arizona. The reason for choosing this case study from the US territory is the availability of well-studied hazard inventory for the entire country for different return periods through the USGS hazard tool that can return the deaggregation results at specific spectral periods (Petersen et al., 2008). The considered regions represent different levels of seismic activity and seismic sources: the location in southern California is dominated by moderate-to-large earthquakes that mainly occur on well-known faults whereas the region in western Arizona has a low-to-moderate seismic activity, which is attributed to background events (earthquakes that cannot be associated with known faults). Three return periods: T_R = 72 years, 475 years and 2475 years are selected to mimic seismic demands of frequent, less frequent and rare events, respectively. The exceedance probabilities of the chosen return periods, under the Poisson process assumption, are 50% (T_R = 72 years), 10% (T_R = 475 years) and 2% (T_R = 2475 years) for an exposure time of 50 years. The central coordinates of the selected regions are 35.0°N - 120.0°W (southern California) and 35.0°N - 113.0°W (western Arizona). 25 sites for each region that are distributed regularly over a 0.2 degrees mesh are considered and shown in Figure 4.3.

The analysis is first focused on the central site of each region to compare the NEHRP site factors with those derived from the nonlinear site model. This model is implemented for UHS, SBS and CMS design spectra to see the effects of different spectrum formats on the computed site factors. This analysis was then repeated for all sites in each region (2 × 25 = 50) to present the proposed procedure and compare its results with those of NEHRP and EC8. The subsequent sections first discuss the observations for the central site of each selected region and then discuss the performance of our procedure for the computation of regional site factors.
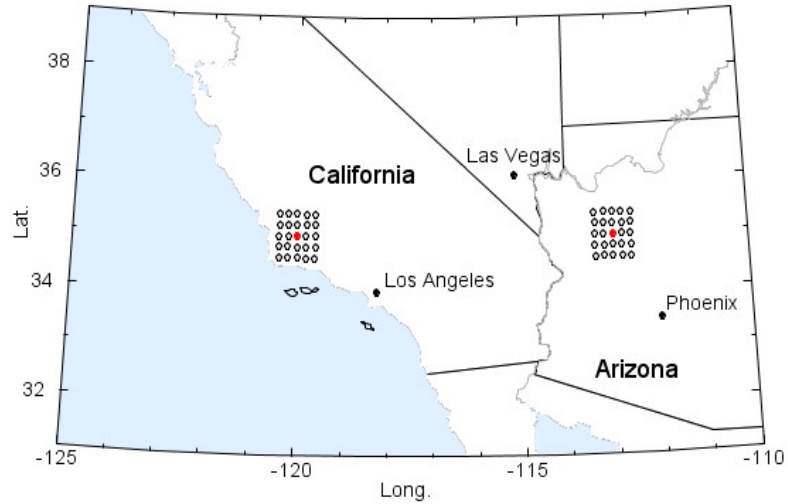
Figure 4. 3 Overall view of the selected regions in the southern California and western Arizona. Dots in each region are the sites distributed over a mesh with 0.2 degrees. The central site of each region is given in red color.

4.3.2 Discussions on the Site-Specific Soil Factors

Figure 4.4 displays the deaggregation results for the central site of each region for reference rock spectral acceleration ordinates at T = 0.2 s and T = 1 s for all three return periods considered in the case study. As expected, the hazard is dominated by a single earthquake scenario for the central site in southern California due to the existing San Andreas Fault segment. There are multiple earthquake scenarios dominating the hazard in the central site of western Arizona region due to the dominance of background seismicity. This simple observation advocates that the response spectrum of these two sites will show variations due to the level of seismicity as well as the distribution of dominant earthquake scenarios in each region. It is noteworthy that a proper site factor procedure should be considered for such variations.
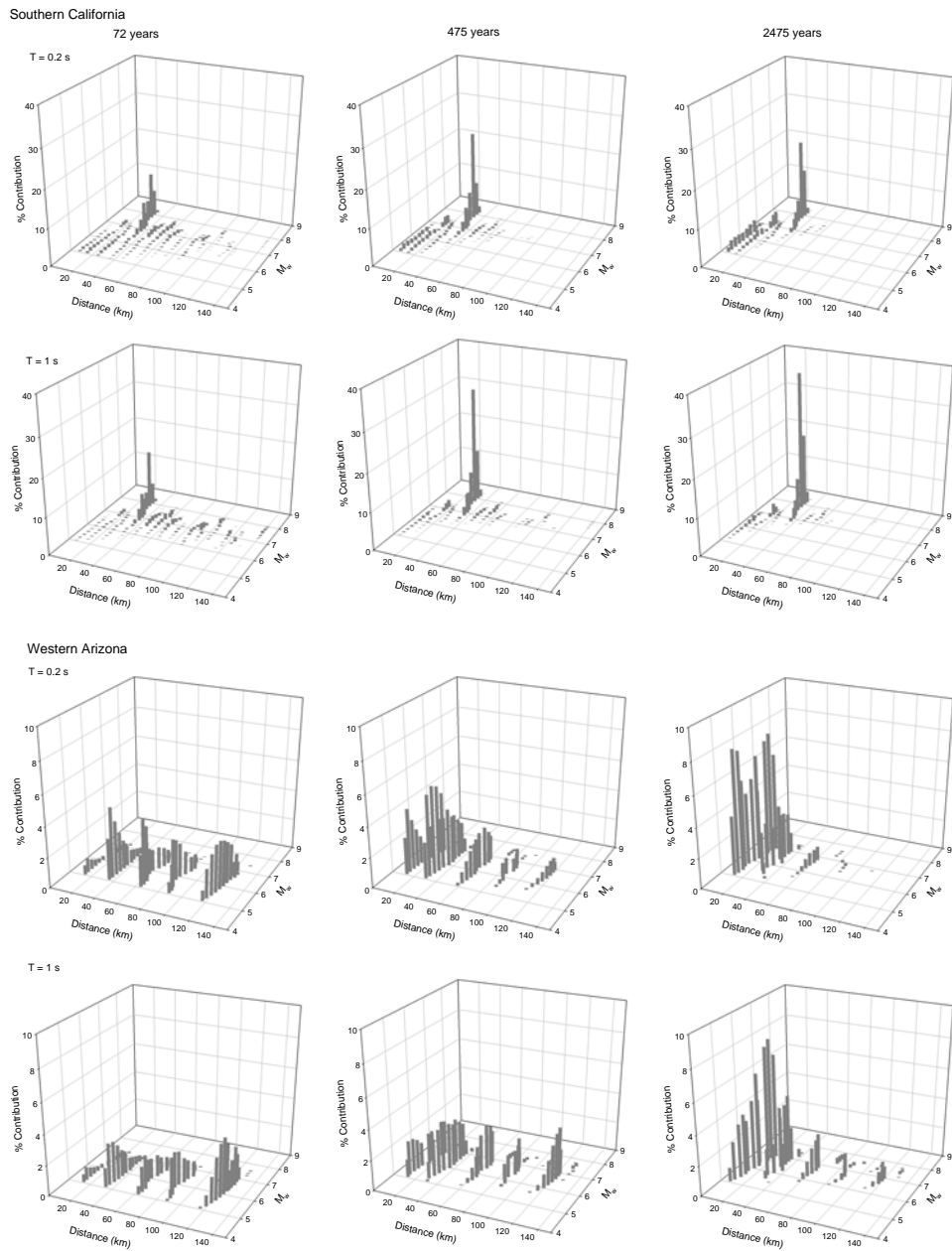
Figure 4. 4 Deaggregation results at T = 0.2 s and T = 1 s for the central sites of the regions selected from southern California (top two rows) and western Arizona (bottom two rows) for T_R = 72 years (left column), 475 years (middle column) and (right column) 2475 years.

Figure 4.5 shows the reference rock UHS, CS and SBS spectral shapes computed after the deaggregation analyses of spectral ordinates at T = 0.2 s and T = 1 s. They show variations among each other due to different seismic activity and configuration of seismic sources (southern California vs. western Arizona) as well as different hazard levels (i.e., T_R = 72 years, 475 years and 2475 years). In essence, the site factors computed for each one of these cases would be different. Thus, site factors for design codes should consider these variations carefully for a full consistency with PSHA results on a regional or single-site scale. The state-of-art procedures generally use spectral acceleration ordinates at T = 0.2 s and T = 1 s (e.g., NEHRP) in the computation of design spectrum envelope. Thus, if an hybrid approach is used, the site factor procedure should consider the amplitudes of these spectral ordinates and their exceedance likelihoods to properly map the site influence on reference rock design spectrum. Table 4.3 lists the reference rock PGA, T = 0.2 s and T = 1 s spectral values for each design spectrum format for the central sites of these two regions.
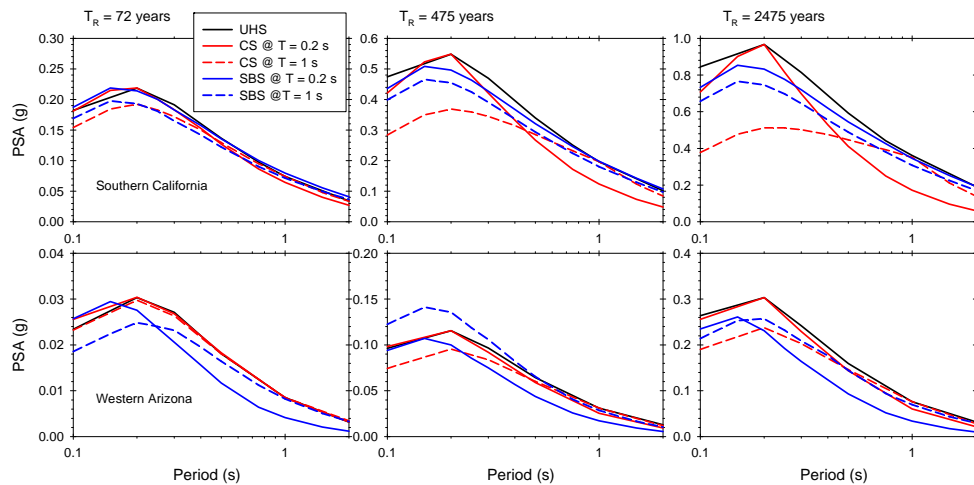
Figure 4. 5 UHS, SBS and CS spectral shapes for the central sites of the regions selected from southern California (top row) and western Arizona (bottom row) for T_R = 72 years, 475 years and 2475 years.

Table 4. 3 Reference rock PGA values of the center sites for the regions selected in southern California and western Arizona: (a) southern California and (b) western Arizona. (UHS rock PGA only varies for different return periods whereas CS and SBS rock PGA values depend on the deaggregation results at distinct spectral ordinates and return periods).

a)		Southern California region - center site		
		T_R = 72 years	T_R = 475 years	T_R = 2475 years
Deaggregation (T = 0 s; PGA)	PGA_{UHS} (g)	0.0965	0.2404	0.4150
	PGA_{CS} (g)	0.0965	0.2404	0.4150
	PGA_{SBS} (g)	0.0944	0.2127	0.3410
	$M_{mean} - R_{mean} - \varepsilon_{mean}$	6.97/40.3/-0.05	7.17/28.5/0.77	7.08/23.7/1.31
	$M_{mode} - R_{mode} - \varepsilon_{mode}$	7.79/31.9/-0.83	7.81/31.9/0.67	7.81/31.9/1.55
Deaggregation (T = 0.2 s)	PGA_{UHS} (g)	0.0965	0.2404	0.4150
	PGA_{CS} (g)	0.0990	0.2255	0.3701
	PGA_{SBS} (g)	0.1073	0.2304	0.3677
	$M_{mean} - R_{mean} - \varepsilon_{mean}$	6.91/41.6/0.12	7.09/28.9/0.89	7.01/23.4/1.41
	$M_{mode} - R_{mode} - \varepsilon_{mode}$	7.79/31.9/-0.61	7.81/31.9/0.80	7.80/31.9/1.68
Deaggregation (T = 1 s)	PGA_{UHS} (g)	0.0965	0.2404	0.4150
	PGA_{CS} (g)	0.0898	0.1767	0.2495
	PGA_{SBS} (g)	0.0979	0.2126	0.3335
	$M_{mean} - R_{mean} - \varepsilon_{mean}$	7.18/53.9/0.14	7.46/35.2/0.91	7.56/30.2/1.52
	$M_{mode} - R_{mode} - \varepsilon_{mode}$	7.80/31.9/-0.79	7.81/31.9/0.65	7.81/31.9/1.49
b)		Western Arizona region - center site		
		T_R = 72 years	T_R = 475 years	T_R = 2475 years
Deaggregation (T = 0 s; PGA)	PGA_{UHS} (g)	0.0130	0.0481	0.1239
	PGA_{CS} (g)	0.0130	0.0481	0.1239
	PGA_{SBS} (g)	0.0123	0.0435	0.0967
	$M_{mean} - R_{mean} - \varepsilon_{mean}$	5.83/90.5/-0.61	6.00/42.8/-0.13	6.12/21.1/0.18
	$M_{mode} - R_{mode} - \varepsilon_{mode}$	5.20/36.4/-1.10	5.40/32.1/0.45	5.20/12.5/0.37
Deaggregation (T = 0.2 s)	PGA_{UHS} (g)	0.0130	0.0481	0.1239
	PGA_{CS} (g)	0.0139	0.0500	0.1254
	PGA_{SBS} (g)	0.0134	0.0450	0.1051
	$M_{mean} - R_{mean} - \varepsilon_{mean}$	5.83/91.8/-0.49	6.00/44.9/-0.01	6.14/22.3/0.28
	$M_{mode} - R_{mode} - \varepsilon_{mode}$	5.20/36.3/-0.98	5.40/32.4/0.50	5.20/13.0/0.56
Deaggregation (T = 1 s)	PGA_{UHS} (g)	0.0130	0.0481	0.1239
	PGA_{CS} (g)	0.0131	0.0417	0.1028
	PGA_{SBS} (g)	0.0111	0.0599	0.113927
	$M_{mean} - R_{mean} - \varepsilon_{mean}$	6.03/132.8/-0.33	6.33/77.4/0.22	6.45/39.5/0.44
	$M_{mode} - R_{mode} - \varepsilon_{mode}$	6.00/124.2/0.12	5.80/33.6/0.48	6.78/18.1/-0.57

The hazard results summarized in Table 4.3 were used to compute the median site factors for site-specific UHS, CS and SBS from the nonlinear site model. The site factors were computed for 150 m/s $\leq$ V_{S30} $\leq$ 1200 m/s and they are given in Figure 4.6 for all three return periods. The first two rows on Figure 4.6 show the V_{S30} dependent variation of site factors in the central site of southern California. The last two rows of this figure display the same information for the central site chosen in western Arizona. The left, middle and right columns on Figure 4.6 show the site factors for T_R = 72 years, T_R = 475 years and T_R = 2475 years, respectively. We used the modal earthquake scenario in SBS for the derivation of SBS-based site factors. Although Goulet and Stewart (2009) recommended using only the M_{mode}-R_{mode} pair for SBS, we also considered ε_{mode} in our SBS computations to fully describe the modal earthquake scenario. The PGA_{rock} values of scenario-based spectra that were separately computed from the deaggregation analysis of T = 0.2 s and T = 1 s (see Table 3) were used in the site model to compute the SBS-based site factors for T = 0.2 s and T = 1 s, respectively. The PGA_{rock} values that were used in the computation of CS-based site factors for T = 0.2 s or T = 1 s were identified in the same way: it is only replaced the scenario-based spectra by the conditional spectra for this case. The panels on Figure 4.6 also show the site factors provided by NEHRP. The NEHRP site factors were computed from the site amplification values listed in Table 4.2. We used the spectral ordinates of UHS to describe NEHRP site amplifications. Linear interpolation was done for cases when the spectral accelerations at T = 0.2 s or T = 1 s fall into any one of the two consecutive spectral ordinates given in Table 4.2. The site factors of UHS are directly tied to the PGA_{rock} value of this design spectrum format for different return periods (see Table 4.3). The observed variations of UHS-based site factors are due to the period-dependent site amplifications of the nonlinear site model.

The comparisons in Figure 4.6 indicate that the site amplifications computed from different approaches are most often very close to each other. As far as the site amplifications computed from alternative design spectrum formats are of concern,
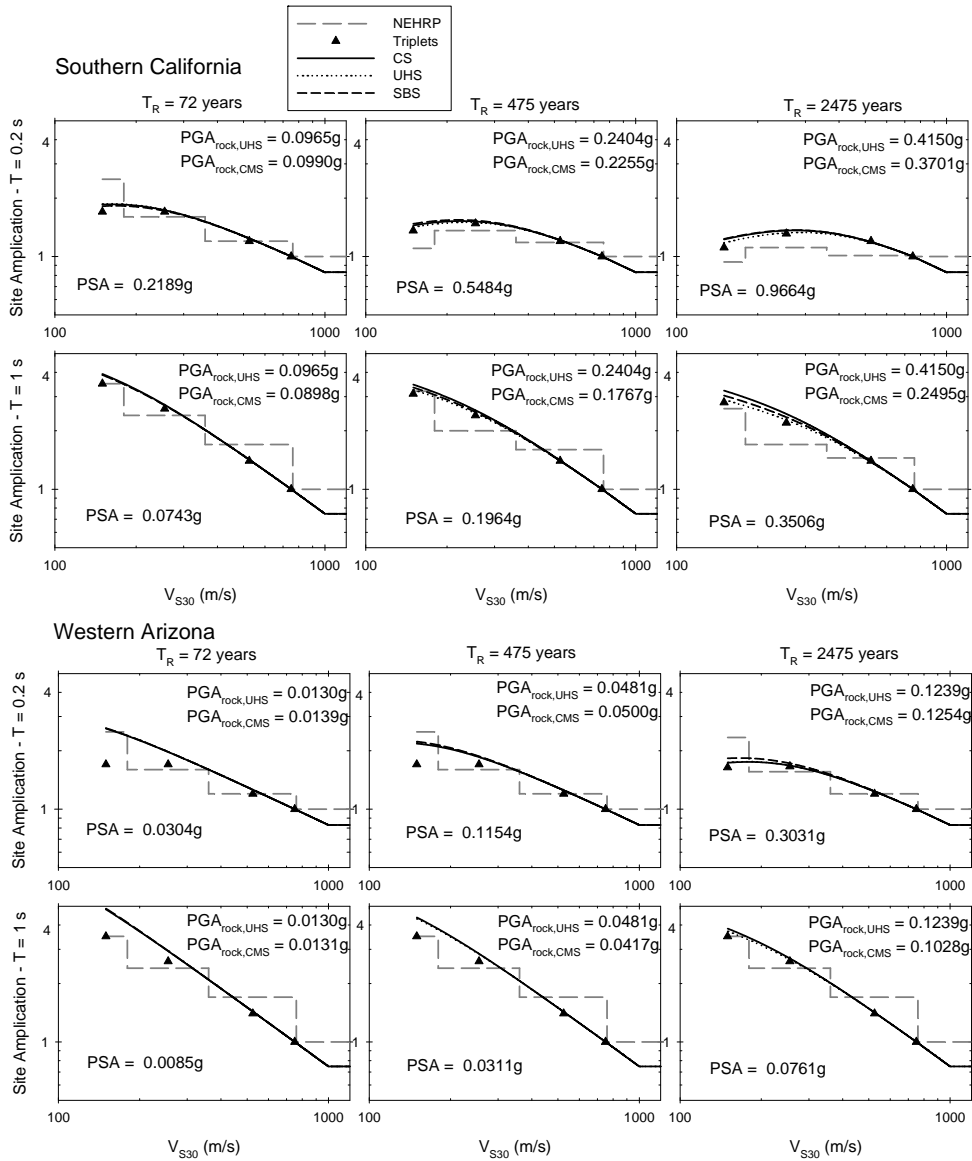
Figure 4. 6: Top two rows: short-period (T = 0.2 s) and long-period (T = 1 s) site amplifications for the central site in southern California. Bottom two rows: same type of plots for the central site of the region in western Arizona. Each column shows the site amplifications for a different return period: T_R = 72 years (first column), T_R = 475 years (second column), T_R = 2475 years (third column).

it is clear that the site model is not very sensitive to the variations in PGA_{rock} levels resulting from these design spectrum formats. The exceptions are those of the NEHRP site factors. The discrete NEHRP site factors provided for different V_{S30} intervals result in a stepwise behavior as given in Figure 4.6. The observed discrepancies in NEHRP are not surprising as the site factors of all spectral formats but the NEHRP bear on the site amplifications computed from the nonlinear site model.

Figure 4.7 demonstrates the design spectrum envelopes computed from the site factors of each alternative method given in Figure 4.6. Two V_{S30} values ($V_{S30}=$ 200 m/s and $V_{S30} = 400$ m/s) are used to describe the trends in design spectrum envelopes at soft and stiff soils, respectively. The soft site that is described by $V_{S30} = 200$ m/s implies high soil nonlinearity in site response. The design spectrum envelope of each alternative method was plotted by using the corresponding reference rock short- and long-period acceleration spectral ordinates at $T = 0.2$ s and $T = 1$ s, respectively. These spectral ordinates were modified by the period-dependent site factors given in Figure 4.6 to obtain the short-period ($PSA_{mod,S}$) and long-period ($PSA_{mod,L}$) spectral accelerations for V_{S30} $= 200$ m/s and $V_{S30} = 400$ m/s. The constant-acceleration plateau attains the value of $PSA_{mod,S}$ and it is between $0.2 \cdot (PSA_{mod,L}/PSA_{mod,S}) \leq T \leq (PSA_{mod,L}/PSA_{mod,S})$. The spectral ordinates of the decaying branch are computed from $PSA_{mod,L}/T$. The spectral ordinate at $T = 0$ s (PGA) is taken as 40% of $PSA_{mod,S}$ in this procedure. This procedure has been in use for the last decade and is suggested by the NEHRP provisions. The first two row plots on Figure 4.7 show the soft and stiff soil design spectrum envelopes of the central site in southern California for $T_R = 72$ years (left panel), $T_R = 475$ years (middle panel) and $T_R = 2475$ years (right panel). The last two rows show the same comparisons for the central site in western Arizona. The design spectrum envelopes computed from the NEHRP and SBS-based site factors are generally different than those computed from the UHS- and CS-based site factors. The discrepancies between the latter two design spectrum envelopes and the SBS-based design spectrum originate from different

spectral shapes (thus, different spectral ordinates) as shown in Figure 4.5. The NEHRP spectrum is different from the other three design spectrum envelopes as its site factors follow different patterns with respect to those computed from UHS, CS and SBS formats (see Figure 4.6). The CS- and UHS-based design spectrum envelopes almost overlap each other because their spectral ordinates are almost the same at T = 0.2 s and T = 1 s; this is a theoretically expected result for many cases unless ε_0 is negative (Burks and Baker, 2012). Minor differences in the CS- and UHS-based site factors lead to the observed discrepancies in their design envelopes. It is preferred using CS-based factors in the proposed methodology. The reference PGA$_{rock}$ values constitute the key input in our site-factor approach and CS can properly describe them for the spectral ordinates at T = 0.2 s and T = 1 s, which define the pattern of the design spectrum envelope. The next section discusses the implementation of CS in our method for the computation of regional site factors.

4.3.3 Discussions on Regional Site Factors

The above discussions on a site-specific case study emphasize the role of seismicity level and return period in the computation of site-specific soil amplifications. Both of these parameters are also important for the derivation of site factors for a region. However, their consideration in the regional site factors for a continent or even for a country featuring complicated seismic activity schemes may not be practical. To this end, the influence of seismicity and return period can be merged into a single proxy that can efficiently represent the individual effects of these parameters. In the case of the proposed site model, this proxy is the reference PGA$_{rock}$. Although this simplification requires further studies to justify its appropriateness, for derivation of regional site factors it is used without discussing its limitations. The site factors computed from the 50 sites that are located in the regions selected from southern California and western Arizona (see their patterns on Figure 4.3) are combined. The reference rock short-
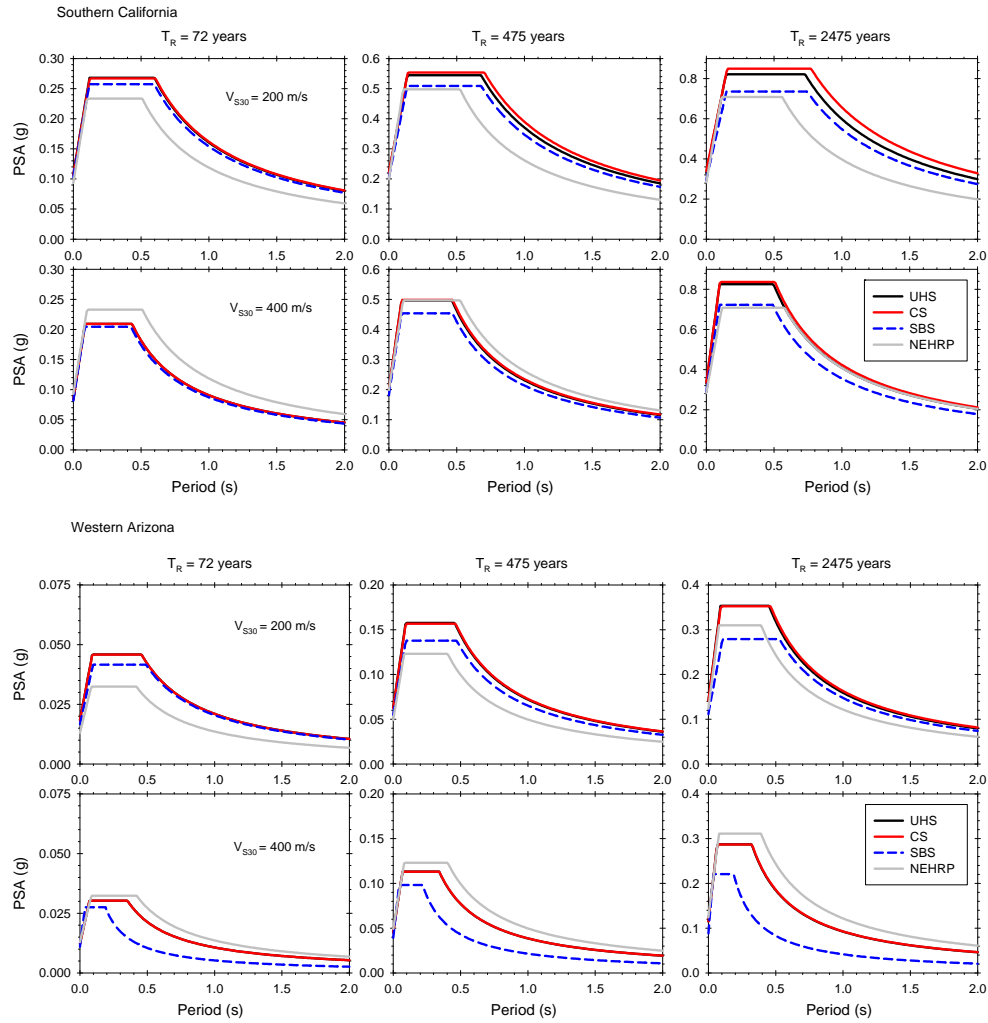
Figure 4. 7: Design spectrum envelopes at different return periods computed from the site factors of alternative approaches for soft (V_{S30} = 200 m/s) and stiff (V_{S30} = 400 m/s) sites for the central site in southern California (top two rows) and western Arizona (bottom two rows).

period (T = 0.2 s) and long-period (T = 1 s) spectral acceleration ordinates computed at each site for the return periods of T_R = 72 years, 475 years and 2475 years were used to compute the corresponding reference PGA$_{rock}$ levels via CS design spectrum format. The reference rock spectral acceleration ordinates for

each one of these periods were divided into 8 bins for different acceleration intervals. These groups are listed in Tables 4.4-5 that also shows the median of each group assuming that their distribution is log-normal. The sample sizes of these groups are displayed in the tables as well. Note that some of the bins contain very large spectral acceleration values and they pertain to the sites located in the vicinity of the San Andreas that crosses the region selected from southern California. These spectral acceleration values have return periods of $T_R = 2475$ years and were accepted as they are without questioning their applicability in engineering design. The large spectral accelerations would essentially show the margins of the site factors in the proposed methodology.

Table 4. 4 Distribution of PSA$_{rock}$ values at short and long-periods for the case study demonstrating the proposed methodology for regional site factors

	Short-period (T = 0.2 s) spectral amplitude			
Group No	PSA$_{rock}$ interval	PGA$_{rock}$ interval	NS*	μ** (g)
G01	(0.02, 0.10]	[0.011, 0.118]	34	0.03
G02	(0.10, 0.25]	[0.045, 0.115]	35	0.16
G03	(0.25, 0.50]	[0.109, 0.207]	34	0.31
G04	(0.50, 0.75]	[0.213, 0.314]	12	0.59
G05	(0.75, 1.00]	[0.307, 0.395]	12	0.9
G06	(1.00, 1.25]	[0.383, 0.460]	8	1.08
G07	(1.25, 1.75]	[0.474, 0.636]	8	1.5
G08	(1.75, 3.10]	[0.664, 1.048]	7	2.17

* NS: Number of samples in each group

** μ: Median PSA$_{rock}$ value of each group

Table 4. 5 Distribution of PSA$_{rock}$ values at short and long-periods for the case study demonstrating the proposed methodology for regional site factors

Long period (T = 1 s) spectral amplitude				
Group No	PSA$_{rock}$ interval	PGA$_{rock}$ interval	NS*	μ** (g)
G09	(0.005, 0.05]	[0.004, 0.049]	50	0.02
G10	(0.05, 0.10]	[0.073, 0.172]	50	0.08
G11	(0.10, 0.20]	[0.150, 0.210]	10	0.18
G12	(0.20, 0.30]	[0.176, 0.320]	11	0.25
G13	(0.30, 0.40]	[0.229, 0.405]	12	0.34
G14	(0.40, 0.50]	[0.293, 0.411]	5	0.43
G15	(0.50, 0.60]	[0.452, 0.615]	6	0.55
G16	(0.60, 1.20]	[0.468, 0.739]	6	0.83

* NS: Number of samples in each group

** μ: Median PSA$_{rock}$ value of each group

The reference PGA$_{rock}$ values computed from each group via CS were used in the site model for 120 m/s ≤ V$_{S30}$ ≤ 1200 m/s with increments of 10 m/s. For each group, the median site factors were computed from the data falling into the V$_{S30}$ intervals defined by NEHRP (site classes C: 360 m/s ≤ V$_{S30}$ < 760 m/s, site class D: 180 m/s ≤ V$_{S30}$ < 360 m/s and site class E: 120 m/s ≤ V$_{S30}$ < 180 m/s). Although the NEHRP site classification scheme is used in this case study, the observations made here are practically valid for site classifications suggested by EC8 as NEHRP C, D and E site classes coincide with the EC8 B, C and D sites.

Figure 4.8 shows the median site amplifications computed from the above described procedure. The median site factors are plotted against the median reference rock short- and long-period spectral acceleration values of the corresponding group. The top row in Figure 4.8 shows the short-period median

site factors for NEHRP site classes E (left panel), D (middle panel) and C (right panel) together with the site factors proposed by EC8 and NEHRP. The panels also display ± standard deviation band over the median site factors computed from the proposed procedure. The bottom panels show the same information for long-period site factors.
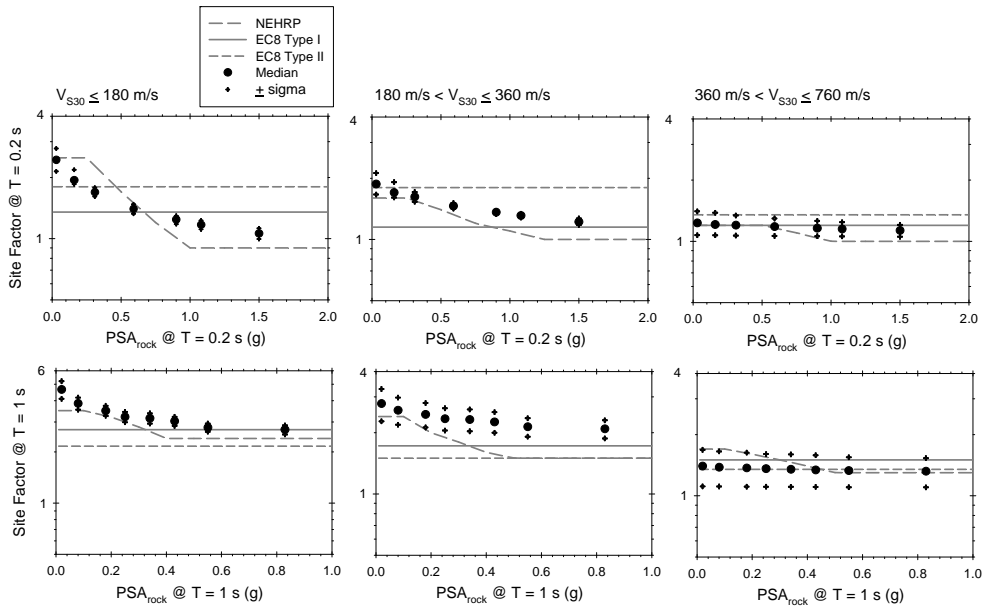
Figure 4. 8 Comparisons of short- and long-period site amplifications for NEHRP, EC8 and the proposed regional site factor method.

The comparative plots on Figure 4.8 indicate that the short-period EC8 site factors suggest conservative site amplifications for very soft sites when reference rock short-period spectral accelerations reach large values. This observation is reversed for very small short-period PSA_{rock} values. The site factor trends in EC8, as discussed from these plots, are expected as they disregard nonlinear soil behavior that becomes prominent at high levels of short-period reference PSA_{rock}. Given a spectral period, the insensitivity of EC8 factors to the changes in rock spectral

ordinates seems to misrepresent the soil amplifications for cases where soil nonlinearity is less significant (e.g., short- and long-period site factors of NEHRP D soil conditions). The observed discrepancies between EC8 site factors and those obtained from the other two schemes for NEHRP D soil conditions (middle panels on Figure 4.8) justify this assertion. The comparative plots in the rightmost panels of Figure 4.8 advocate that EC8 site factors are compatible with those obtained from NEHRP and the proposed method for stiff soils where one expects only very weak non-linearity whatever the reference PSA_{rock} value is. In general, the site amplification trends derived from the proposed procedure and those of NEHRP follow each other. The model seems to draw an upper bound with respect to the site factors of NEHRP for very soft (NEHRP E) and soft (NEHRP D) soil conditions. The differences between our method and NEHRP site factors practically vanish for stiff soil conditions (NEHRP C).

4.4 Conclusions

This study compares the current site factors of EC8 and NEHRP through an alternative procedure that can be designed for the estimation of site- and region-specific soil amplification. The first part of the paper discusses the results of a comprehensive analysis that generated earthquake scenarios with magnitudes ranging from $4 \leq M_w \leq 8$ and source-to-site distances of $R_{JB} < 200$ km to fully understand the behavior of site factors for different soil conditions. The analysis made use of the recent pan-European GMPE to estimate the reference rock ground-motion intensities that were implemented together with the nonlinear soil amplification model to estimate site factors. The aleatory variability in the generated earthquake scenarios were taken into account by the fractions of the standard deviation of the predictive model. The results of this method (called as triplet approach) indicated the significance of soil nonlinearity and period dependency in site amplification calculations. The statistics from these analyses also emphasized the differences between EC8 site factors and those computed from the triplet approach. We believe that the underlying philosophy of EC8 that

disregards soil nonlinearity in the computation of site factors is the major source of difference with the triplet approach as the median soil amplification trends of triplets and NEHRP site factors follow each other very closely. The fairly good comparisons between the triplet statistics and the NEHRP site factors is the primary motivation to develop the new procedure.

The proposed procedure uses probabilistic rock hazard together with a deterministic site amplification model. It accounts for the level of seismicity and influence of mean annual exceedance rate (i.e., return period) of rock ground-motion intensities that dominate the shape of design spectrum envelope and amplitude of site factors for different soil conditions. The main input to this model is the reference PGA_{rock} and the use of CS (derivative of CMS for multiple GMPEs used in probabilistic hazard analysis) is proposed to describe reference PGA_{rock} from the pseudo-acceleration spectral ordinates at T = 0.2 s and T = 1 s. The consideration of spectral accelerations at T = 0.2 s and T = 1 s not only results in realistic site amplifications but also defines proper shapes of design spectrum envelopes. In essence, CS (apart from other alternative design spectrum formats such as UHS and SBS that were also verified in this study) can consistently describe the reference PGA_{rock} values that correlate with the spectral accelerations at T = 0.2 s and T = 1 s. The proposed methodology directly accounts for the level of seismicity and return period for the computation of site-specific soil amplifications. These factors are merged into a single parameter, the reference PGA_{rock}, for the estimation of regional site factors in order to keep the method as simple as possible. The case studies presented for the description of proposed procedure yields justifiable site factors that one would expect from the genuine behavior of soil under seismic excitation.

The discussions on the presented site- and region-specific case studies as well as comparisons with the NEHRP and EC8 site factors advocate the necessity of reassessing the EC8 design spectrum shape and site factors. It is believed that the next update to EC8 should consider the state-of-art procedures to define the

design spectrum envelope and site factors. This chapter has emphasized that the EC8 site factors should be period and PGA$_{rock}$ dependent to satisfactorily account for linear and nonlinear soil behavior. Both updated design spectrum envelope and new site factors should rely on regional PSHA results, such as those published in SHARE. The shape of design spectrum should not only depend on PGA but also consider representative spectral ordinates at short- and long-periods such as those implemented in NEHRP (i.e., $T = 0.2$ s and $T = 1$ s). The site factors should be described in terms of soil-dependent amplification at these specific spectral ordinates, and nonlinear site models should be used for a consistent correlation between the soil behavior and spectral periods at the short- and long-period spectral range. To this end the procedure proposed in this study can be a serious candidate for the compilation of new site factors for EC8 by making use of SHARE PSHA results. We note that the model uncertainty in site factor estimations can be taken into account by focusing on a few models similar to the one used here. The proposed model can easily be fine-tuned for such modifications.

CHAPTER 5

THE NEXT GENERATION PAN-EUROPEAN PREDICTIVE EQUATIONS FOR HORIZONTAL COMPONENTS

Adapted from Akkar S., M.A. Sandıkkaya, and J.J. Bommer (2014b). Empirical ground-motion models for point- and extended-source crustal earthquake scenarios in Europe and the Middle East, Bulletin of Earthquake Engineering, 12:359–387.

This chapter presents the latest generation of horizontal ground-motion models for the prediction of elastic response (pseudo-) spectral accelerations, as well as peak ground acceleration and velocity, derived using pan-European databases. The models present a number of novelties with respect to previous generations of models (Ambraseys et al., 1996, 2005a; Bommer et al., 2003; Akkar and Bommer, 2007a; 2007b; Akkar and Bommer, 2010; Bommer et al., 2012), namely: inclusion of a nonlinear site amplification function that is a function of V_{S30} and reference peak ground acceleration on rock; extension of the magnitude range of applicability of the model down to M_w 4; extension of the distance range of applicability out to 200km; extension to shorter and longer periods (down to 0.01s and up to 4s); and consistent models for both point-source (epicentral, R_{epi}, and hypocentral distance, R_{hyp}) and finite-fault (distance to the surface projection of the rupture, R_{JB}) distance metrics. A predictive model that is based on the closest distance to fault rupture, R_{rup}, is not developed because the current pan-European strong-motion database lack sufficiently detailed information about most

causative fault ruptures to allow determination of this distance metric for most events. In addition, data from more than 1.5 times as many earthquakes, compared to previous pan-European models, have been used, leading to regressions based on approximately twice as many records in total. The metadata of these records have been carefully compiled and reappraised in recent European projects. These improvements lead to more robust ground-motion prediction equations than have previously been published for shallow (focal depths less than 30km) crustal earthquakes in Europe and the Middle East.

5.1 Overview of the pan-European GMPEs

The evolution of strong ground-motion recording and modeling in Europe has always been some way behind that in the western United States. The first accelerogram recorded in Europe was obtained more than 30 years after the first strong-motion recordings from the 1933 Long Beach earthquake in California, and the first set of ground-motion prediction equations (GMPEs) for response spectral ordinates in Europe was derived about 20 years after the first models in the United States. With time, however, the gap has been gradually closing and in this article we present a set of new GMPEs derived from European and Middle Eastern strong-motion data for crustal earthquakes that are comparable with the equations produced by the PEER Center Next Generation of Attenuation (NGA) project (Power *et al.*, 2008). The continuous development in the field of ground-motion modeling means that just as this study brings pan-European GMPEs in line with the NGA models—now referred to as the NGA-West models to distinguish that endeavor from the on-going NGA-East project to develop new GMPEs for the Central and Eastern United States—the NGA-West2 models are being presented (Bozorgnia *et al.*, 2012). As discussed later, the question arises as to whether efforts will continue to close the gap or whether the move will now be towards global GMPEs for regions of shallow crustal earthquakes.

114

This Chapter begins with a brief overview of the evolution of ground-motion models in Europe and the Middle East, highlighting the new features of the models presented herein. The strong-motion database is then described, followed by a description of the selection of the functional form for the models, including the selection and definition of explanatory variables. Then the regressions to obtain the coefficients of the equations and the associated sigma values are presented, after which the new predictions are explored for a number of scenarios, and also compared with previous models.

5.2 A New Generation of European Ground-Motion Models

The historical development of ground-motion recording and prediction for the pan-European region is recounted by Bommer *et al*. (2010a). Globally, there are more GMPEs for peak ground acceleration (PGA) than for elastic response spectral accelerations (Douglas, 2003b, 2011), although GMPEs are now generally derived for spectral ordinates and PGA simultaneously. The first equations for response spectral ordinates using strong-motion records from across Europe and the Middle East were those of Ambraseys *et al.* (1996), and these have undergone a number of revisions and improvements, as summarized in Table 5.1. In parallel, recent GMPEs have been produced for individual European countries such as Greece, Italy and Turkey (e.g., Danciu and Tselentis, 2007; Bindi *et al*., 2010; Akkar and Çağnan, 2010), but the focus herein is exclusively on models derived for all seismically-active regions bordering the Mediterranean Sea and extending to the Middle East. This excludes those models derived for this region using indigenous datasets supplemented by recordings from other regions such as California and Japan (e.g., Berge-Thierry et al., 2003; Fukushima *et al*., 2003). Table 5.1 summarizes the evolution of GMPEs for the prediction of spectral ordinates in Europe and the Middle East, and Table 5.2 lists key characteristics of the same equations.

Table 5. 5 Evolution of GMPEs for spectral ordinates for Europe and the Middle East. Dark grey cells indicate effect in final model. Light grey cells indicate effect investigated but not retained in the final model either because not statistically significant or coefficients non-physical.

GMPE Feature	ASB96	BDS03	Aetal05	Betal07	AB10	This study
Three site classes	■	■	■	■	■	■
Style-of-faulting		■	■	■	■	■
Within- and between-event variability		■	■	■	■	■
Magnitude-dependent attenuation			■	■	■	■
Nonlinear magnitude scaling			▨	■	■	■
Parallel model for PGV					■	■
Explicit inclusion of V_{S30}						■
Nonlinear site response						■
Consistent models for point and extended sources						■
Anelastic attenuation*	▨		▨			▨

* It should be noted that the expression 'anelastic attenuation' is only strictly valid for GMPEs for Fourier amplitudes and not response spectral ordinates.

The models included are the following, together with the codes used to identify them in the tables: ASB96 – Ambraseys *et al*. (1996); BDS03 – Bommer e*t al*. (2003); Aetal05 – Ambraseys *et al.* (2005a); Betal07 – Bommer *et al.* (2007); AB10 – Akkar and Bommer (2010). The equations for spectral displacement ordinates by Akkar and Bommer (2007a) are not included because these were superseded by Akkar and Bommer (2010) but would have identical entries to the latter in Table 5.1 and 5.2.

Table 5. 6 Characteristics of GMPEs for spectral ordinates for Europe and the Middle East; each model also includes an equation for PGA. Number of earthquakes and records reported for spectral acceleration at 0.1 s.

GMPE Feature	ASB96	BDS03	Aetal05	Betal07	AB10	This study
Number of Earthquakes	157	157	135	289	131	397
Number of Records	422	422	595	997	532	1203
Horizontal Component	Larger	Larger	Larger	GM*	GM*	GM*
Minimum Response Period (s)	0.1	0.1	0.05	0.05	0.05	0.01
Maximum Response Period (s)	2	2	2.5	0.5	3	4
Magnitude Scale	M_s	M_s	M_w	M_w	M_w	M_w
Minimum Magnitude	4	4	5	3	5	4
Maximum Magnitude	7.9	7.9	7.6	7.6	7.6	7.6
Maximum Distance (km)	260	260	99	100	99	200
Number of free coefficients	6	8	10	10	10	11

* GM: Geometric mean of the two horizontal components. Table1.2 does not include a row for the distance metric because all of these models have been based on Joyner-Boore distance, R_{JB}, which is the horizontal distance to the closest point on the surface projection of the fault rupture (Joyner and Boore, 1981).

Table 5.2 does not include a row for the distance metric because all of these models have been based on Joyner-Boore distance, R_{JB}, which is the horizontal distance to the closest point on the surface projection of the fault rupture (Joyner and Boore, 1981). A predictive model that is based on the closest distance to fault rupture, R_{rup}, is not developed because the current pan-European strong-motion databases lack sufficiently detailed information about most causative fault ruptures to allow determination of this distance metric for most events.

Following the suggestion of Bommer and Akkar (2012) that GMPEs should be derived in pairs, one based on a point-source measure for use with area sources (at least for area sources other than the host zone containing the site, for which the simulation of virtual faults is an unnecessary computational effort) and another using an extended-source metric for fault sources, in this study additional models based on hypocentral distance, R_{hyp}, and on epicentral distance, R_{epi}, are also presented. The reason for providing equations in terms of both point-source distance metrics is that hypocentral distance is considered to be a better metric, not least because studies have shown that the hypocenter is often located close to regions of large slip (Mai *et al*., 2005; Manighetti *et al*., 2005). Additionally, in performing inversions to obtain equivalent stochastic parameters for empirical GMPEs, Scherbaum *et al*. (2006) found that regardless of the distance metric used in the GMPE, hypocentral distance frequently yielded the best results (in terms of minimized misfit) for the stochastic parameters. However, the use of GMPEs based on R_{hyp} for PSHA requires integration over the depth distributions—which should not be achieved through the addition of logic-tree branches with alternative depths (Bommer and Scherbaum, 2008), although it is legitimate to have branches with alternative depth distributions—with the attendant onus to determine depth distributions and the consequent computational penalty. The use of an R_{epi}-based model can bypass these issues. Additionally, the model based on epicentral distance allows direct comparison with the R_{JB} model, which may offer some advantages, including assurance about the behavior of the point-source distance-based equations.

From Table 5.1, the evolution of the complexity of the models is immediately apparent. The Ambraseys *et al.* (1996) equations were of a rather simple functional form and in addition to linear dependence on surface-wave magnitude, M_s, and geometric spreading as a function of R_{JB}, the only other explanatory variable were two dummy variables representing the variations in ground motions amongst three site classes. These classes (rock, stiff soil and soft soil) were nominally defined in terms of ranges of 30m shear-wave velocities, V_{S30}, but at

the time the equations were derived shear-wave velocity measurements were available for very few European strong-motion accelerograph sites (*e.g*., Rey *et al*., 2002).

The equations derived by Bommer *et al*. (2003) used the same database, explanatory variables and functional form as Ambraseys *et al*. (1996), but added two additional terms as functions of dummy variables to include the influence of reverse, normal or strike-slip faulting. This model also presented separately the within-event and between-event components of the aleatory variability (Al Atik *et al*., 2010); although Ambraseys *et al.* (1996) used the two-stage regression approach of Joyner and Boore (1981), they only reported total sigma values.

The model of Ambraseys *et al.* (2005a) represented a major advance in European ground-motion modeling, adopting a more complex functional form for the equation that included the magnitude-dependence of the geometric spreading. Table 5.2 also records other notable advances embodied in this GMPE, including the move to moment magnitude, M_w, (the preferred choice for state-of-the-art hazard assessments) instead of M_s, and, through careful processing of the accelerograms, an extension of the range of response periods for which predictive equations were derived. Another important advance, which may not be immediately apparent from the information in Table 5.2, is that the database used for this study was considerably improved with respect to that of Ambraseys *et al*. (1996), including having a much larger average number of records per event and more complete metadata (*e.g*., centroid moment tensors). Although the total number of records is not much larger, it must be noted that the minimum magnitude was larger: M_w 5, which corresponds to roughly M_s 4.8 using the M_s-M_w relation of Scordilis (2006), rather than M_s 4. Moreover, although the maximum magnitude and distance ranges covered by Ambraseys *et al.* (1996) appear impressive, they actually correspond to a single recording from a large earthquake; the maximum event covered by the remainder of the database was M_s

119

7.3. All but one of the records were obtained at distances of less than 200km, and below M_s 6.5, only four accelerograms were recorded at distances beyond 100km.

The Bommer *et al*. (2007) equations were derived only to explore the influence of the magnitude range in the database and were not intended for use in seismic hazard assessments (for which they would be hampered by the very limited period range that they cover). The GMPE of Akkar and Bommer (2010) was based on the same database as used by Ambraseys *et al*. (2005a), but the individual re-processing of all the records – 63 records used by Ambraseys et al. (2005) were not available in unprocessed form so they were not used by Akkar and Bommer (2010) – to determine the maximum usable period (Akkar and Bommer, 2006), enabled the maximum response period to be extended to 3s; this is still much shorter than would be desirable but is a consequence of the large proportion of the database obtained on analogue accelerographs. The functional form adopted for this equation was similar to that adopted by Ambraseys *et al*. (2005a) but additionally included a quadratic term in magnitude. This model also included a model for peak ground velocity, PGV, which had previously been derived separately (Akkar and Bommer, 2007b); this is noteworthy since although most engineering design applications make use of response spectra, there are a number of uses for PGV (Bommer and Alarcón, 2006). As noted in Table 5.2, this study also adopted the more widely-used convention of the geometric mean of the horizontal components rather than the larger of the two.

The new models presented in this article constitute a new generation of predictive equations rather than an incremental development. As discussed in Chapter 2, the database has continued to expand in size, but more importantly there have been very significant improvements regarding the metadata associated with the accelerograms. One particular benefit of this is that for the first time the pan-European models include V_{S30} explicitly as an explanatory variable rather than generic site classes. The new models also include the influence of nonlinear soil response; in deriving a predictive equation for PGV, Akkar and Bommer (2007b)

searched without success for empirical evidence for soil nonlinearity in European strong-motion data. In this respect the new equations represent a departure from purely empirical fitting, with the use of externally developed models to constrain the influence of non-linear soil response.

Another development envisaged regarding the functional form is the inclusion of an anelastic attenuation term to accommodate extrapolation of the equations beyond the 200 km limit of the dataset, which is almost inevitable in probabilistic seismic hazard analysis (PSHA). In passing we note that the use of the term 'anelastic attenuation' is not strictly correct since it applies to Fourier amplitude spectra (FAS) rather than response spectra, but the terms in GMPEs involving ln(R) and R are modeled after the geometric spreading and apparent attenuation (scattering plus anelastic) of FAS. However, it is noted that in almost all cases the coefficients on this term were found to be positive, so none of the final equations includes this effect. As noted in Table 5.1, two previous European GMPEs explored the inclusion of such terms but their authors also omitted them from the final models, suggesting that the European dataset is not currently sufficient to constrain both contributions to the decay of amplitude with distance, at least with a constant geometrical spreading model and not accounting for the Moho bounce effect. It may be the case that data recorded over a much wider range of distances would be needed to constrain such terms in the predictive models.

The derivation of these new equations also addresses a problem identified by Bommer *et al*. (2007), namely that empirical GMPEs, even if their functional form includes non-linear magnitude scaling, tend to over-estimate ground-motion amplitudes at the lower limit of their magnitude range. This observation has been subsequently confirmed for the NGA models by Atkinson and Morrison (2009) and Chiou *et al*. (2010). Douglas and Jousset (2011) discuss the reasons for this over-estimation using stochastic models. The new models address this issue by extending the lower magnitude limit of the dataset to M_w 4. This means that when the models are applied at M_w 5 (often the lower end of integration within PSHA)

they should not over-predict ground motions, unlike GMPEs that only use data down to M_w 5. We emphasize that the original motivation was not to provide models that can be used with confidence at M_w 4, but rather to remove the bias in the models at the commonly used lower limit of M_w 5 in PSHA, following the recommendation by Bommer *et al.* (2007) to include data to one magnitude unit lower than the minimum threshold in PSHA integrations. However, we conclude that the new models can be used for magnitudes as small as M_w 4.0.

Another innovation in these new equations is the extension of the range of periods at the shorter end, following new insights into the relatively low sensitivity of short-period ordinates to the high-frequency filtering of accelerograms (Douglas and Boore, 2011; Akkar *et al.*, 2011). Bommer *et al.* (2012) provided coefficients at short periods as an extension of the model of Akkar and Bommer (2010), as well as exploring the options for interpolating missing coefficients at short periods.

Akkar and Bommer (2007a) provide coefficients up to 4s but later Akkar and Bommer (2010) highlighted the unreliability of this model beyond 3s because of a sharp reduction in the number of records used; the new models presented in this article include 62 spectral ordinates starting from the period of 0.01s. The models presented here are reliable for structural periods up to 4s, a longer period than previous generations of GMPEs for this part of the world (Table 5.2).

5.3 Functional Form of Predictive Equations and Regressions

To find an appropriate functional form that models the observed scaling in terms of magnitude, distance and style-of-faulting, we undertook many trial regressions, using the random-effects procedure of Abrahamson and Youngs (1992). These regressions were performed on the observed spectral accelerations at a handful of periods, adjusted to a constant V_{S30} of 750m/s using the nonlinear site amplification model developed in Chapter 3, which is the first site amplification

model developed explicitly for pan-European sites. We also undertook some regressions using simple site classes to check the impact of adopting the nonlinear site response model and similar scaling in terms of magnitude, distance and style-of-faulting was obtained. The following paragraphs first discuss the development of reference ground-motion model that addresses the magnitude, distance and style-of-faulting scaling of ground-motion amplitudes anchored at V_{S30}=750m/s (reference rock). The rest of the section introduces the complete model that modifies the reference rock motion estimations for different site conditions.

The optimum magnitude scaling expression for the proposed GMPE was obtained by analyzing the behavior of three main functional forms. The simplest model among these alternatives is the continuous quadratic magnitude scaling (designated as "Quadratic" herein) that is used in the Akkar and Bommer (2010) GMPE. This functional form is modified by adding a cubic magnitude term (abbreviated herein as "Cubic") because Douglas and Jousset (2011) suggest that cubic magnitude scaling better represents the magnitude-dependent variation of ground motions for both small and large events (Figures 2 and 3 in their paper). As for the third alternative, we adopted the magnitude scaling proposed by Abrahamson and Silva (2008) and also by Boore and Atkinson (2008). This quadratic functional form (Q-hinged) introduces a hinging magnitude to the magnitude scaling to simulate magnitude saturation for events larger than this magnitude level. The efficiency of these alternative models is assessed by visual comparisons with the actual data trend (physical argument) and studying the reduction in between-event sigma. Our observations indicated that the impact of different functional forms on the between-event sigmas was minimal. Thus, we used the physical argument to decide on the final functional form in terms of magnitude scaling.

Figure 5.1 shows the comparisons of three magnitude scaling functions for PGA as well as spectral ordinates at T = 0.2s, T = 1.0s and T = 4.0s. The observed data used in the comparisons are adjusted to a strike-slip rupture mechanism,

R_{JB}=10km and reference rock site of V_{S30}=750m/s. The adjustment, or normalization, of the empirical data was done by developing individual GMPEs for each magnitude scaling function for the above spectral quantities. The nonlinear site response model is used to scale the ground motions to reference rock conditions. The resulting reference rock empirical data trends from each one of these specific GMPEs do not show significant differences; the empirical data given in Figure 5.1 are those obtained from the ground-motion model that uses Q-hinged magnitude scaling. As inferred from this figure, all three functional forms exhibit similar scaling for magnitudes up to M_w 6 for all considered spectral ordinates. The negligible differences in these alternative functional forms for smaller magnitudes become significant after M_w 7. The quadratic magnitude scaling yields larger estimations with respect to the other two functional forms for $M_w \geq 7.0$. The functional form that includes a cubic magnitude term shows over-saturation (a decrease in ground-motion amplitudes with increasing magnitude) for $M_w \geq 7.25$. Although a cubic magnitude term is supported by predictions from stochastic models (Douglas and Jousset, 2011), the empirical data do not reveal the existence of such over-saturation. The superior consistency between the Q-hinged functional form and the empirical data at large magnitudes led to prefer Q-hinged magnitude scaling in the final ground-motion model. However, we note that this might be somewhat unconservative and clearly there is greater epistemic uncertainty regarding the amplitudes at these larger magnitudes. Since the data do not reject any of the three models, a defensible course of action when applying the new equations proposed herein would be to add logic-tree branches with alternative higher and lower amplitudes for magnitudes of M_w 7.5 and larger, following a scheme such as that used by the USGS for the 2008 national hazard maps in the United States (Petersen *et al.*, 2008).
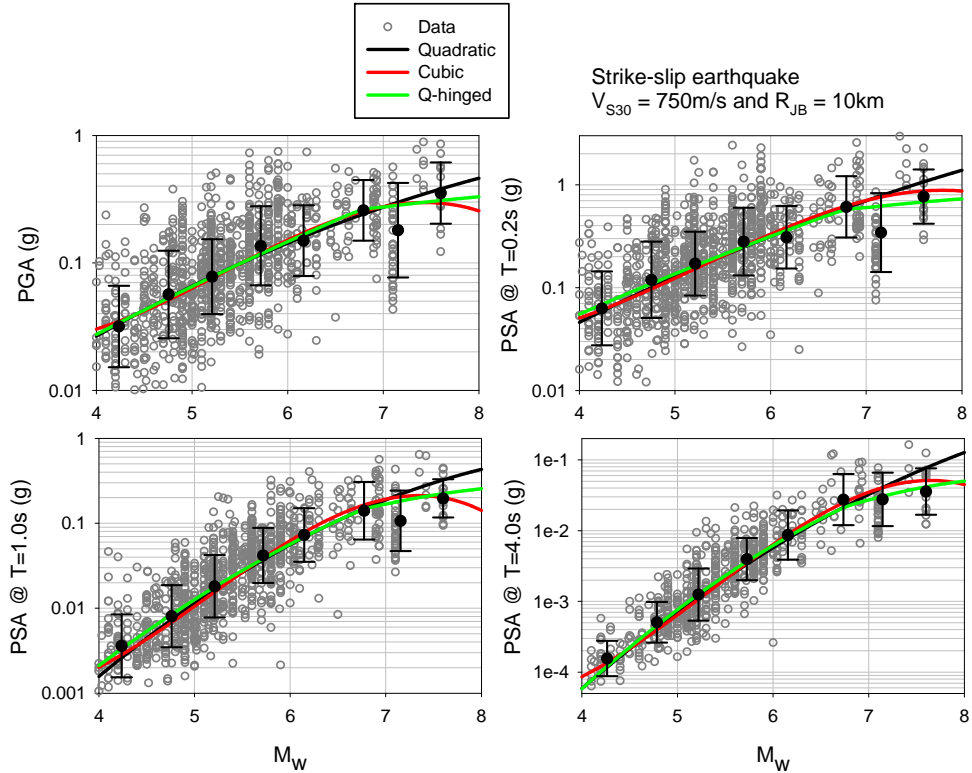
Figure 5. 1. Comparisons of magnitude-scaling trial functions with the empirical data for four spectral ordinates (PGA, PSA at T = 0.2s, 1.0s and 4.0s). The empirical data is calibrated for R_{JB}=10km, strike-slip rupture mechanism and V_{S30}=750m/s.

The distance scaling of ground-motion amplitudes is studied separately for anelastic attenuation and the influence of magnitude-dependent distance saturation. Inclusion of the anelastic attenuation term yielded a positive regression coefficient, which is not justifiable as it implies an increase in ground-motion amplitudes with increasing distance. Two previous pan-European GMPEs (Ambraseys *et al.*, 1996; 2005a) that are listed in Table 5.1 also explored the possibility of including the anelastic attenuation term in their functional forms. Their analyses also did not converge to a physically meaningful result in terms of anelastic attenuation, as in our case. Thus, the anelastic attenuation term is

removed from the final model. The magnitude-dependent distance saturation is accounted for by modifying the fictitious depth term with a multiplicative exponential term that is a function of magnitude. Figure 5.2 shows the distance scaling with and without magnitude-dependent distance saturation term.
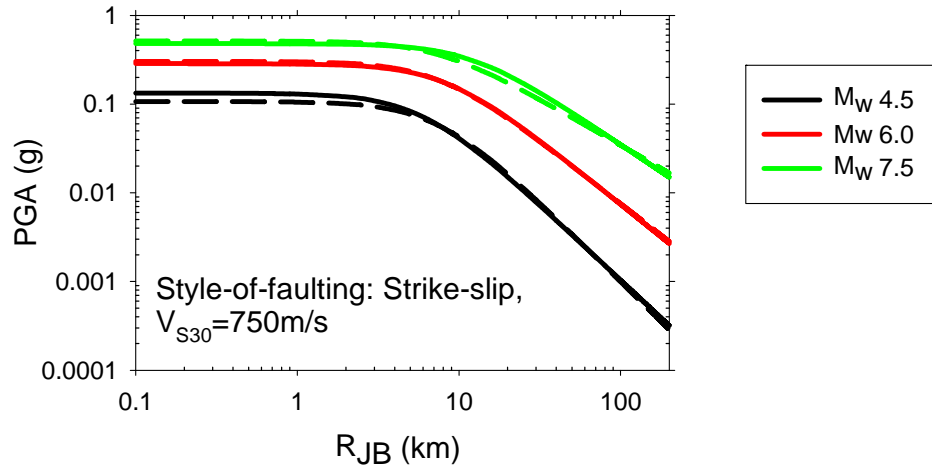
Figure 5. 2. Comparisons of magnitude-dependent and -independent distance saturation at different magnitudes for strike-slip style-of-faulting and a rock site of $V_{S30} = 750$ m/s. Solid and dashed lines represent with and without magnitude-dependent distance saturation, respectively.

The regression analysis resulted in very similar ground-motion estimations. The magnitude-dependent distance saturation slightly changes the median ground-motion estimations at short distances and towards intermediate distances for high magnitude events (M_w 7.5). Inclusion of magnitude-dependent distance saturation term also did not show a significant impact on the reduction of standard deviation. Therefore, we disregarded this term in the final ground-motion model to preserve the optimum number of estimator parameters in the prediction of ground motions. The observations on distance-scaling suggest that pan-European strong-motion

databases still need supplementary recordings from wider distance ranges to allow simultaneous derivation of 'geometric' and 'anelastic' decay coefficients (these adjectives, as noted earlier, strictly only apply for Fourier amplitudes).

The style-of-faulting effect is addressed through multiplicative coefficients on dummy variables (additive in log space) in the reference model. We did not incorporate the depth effect while modeling different styles-of-faulting in our predictive model as the availability of depth-to-top-of-rupture information is very limited in the compiled strong-motion database. This metadata information might have been estimated through empirical relationships (e.g., Wells and Coppersmith, 1994) but we avoided this option in order not to inflate the aleatory variability in ground-motion estimations. The style-of-faulting (SoF) is not uniformly distributed within the magnitude and distance range covered by the strong-motion database. For this reason, we trimmed the database by removing small magnitude events (M_w<5) having less than three recordings to obtain more accurate normal-to-strike-slip and reverse-to-strike-slip spectral amplitude ratios in order to prevent unexpected SoF scaling factors dominated by low-magnitude recordings. Style-of-faulting coefficients computed for three models using different distance metrics did not show significant differences along the period band of interest. This observation is counter to the findings of Bommer and Akkar (2012) for reverse-to-strike-slip (R:SS) ratios as their R:SS estimations from an R_{epi}-based model are higher than those predicted by a R_{JB}-based GMPE, although both ground-motion models were derived from the same database. This observation is attributed to the specific database features by Bommer and Akkar (2012) that are also discussed in the following section while we compare our style-of-faulting ratios with the estimations of other GMPEs. In essence, the proposed GMPEs of this study use the same style-of-faulting coefficients for all three models after smoothing those found for the three individual models based on different distance metrics, as suggested by Bommer and Akkar (2012).

The final functional form of our ground-motion predictive model is given in Eqs. (5.1)-(5.3):

$$\ln(Y) = \ln\left[Y_{REF}(M_w, R, SoF)\right] + \ln\left[S(V_{s30}, PGA_{REF})\right] + \varepsilon\sigma \qquad (5.1)$$

where

$$\ln(Y_{REF}) = \begin{cases} a_1 + a_2(M_w - c_1) + a_3(8.5 - M_w)^2 + \left[a_4 + a_5(M_W - c_1)\right]\ln(\sqrt{R^2 + a_6{}^2}) + \\ a_8 F_N + a_9 F_R \qquad\qquad \text{for } M_w \leq c_1 \\ a_1 + a_7(M_w - c_1) + a_3(8.5 - M_w)^2 + \left[a_4 + a_5(M_W - c_1)\right]\ln(\sqrt{R^2 + a_6{}^2}) + \\ a_8 F_N + a_9 F_R \qquad\qquad \text{for } M_w > c_1 \end{cases}$$

$$(5.2)$$

and

$$\ln(S) = \begin{cases} b_1 \ln(V_{S30}/V_{REF}) + b_2 \ln\left[\dfrac{PGA_{REF} + c(V_{S30}/V_{REF})^n}{(PGA_{REF} + c)(V_{S30}/V_{REF})^n}\right] & \text{for } V_{S30} \leq V_{REF} \\ b_1 \ln\left[\dfrac{\min(V_{S30}, V_{CON})}{V_{REF}}\right] & \text{for } V_{S30} > V_{REF} \end{cases} \qquad (5.3)$$

Equations (5.1)-(5.3) indicate that the median spectral acceleration *ln(Y)* is computed by modifying the reference ground-motion model *ln(Y_{REF})* through the nonlinear site amplification function *ln(S)*. The estimator parameters of the reference ground-motion model are as follows: moment magnitude, M_w; source-to-site distance measure, R, for which R_{JB}, R_{epi}, R_{hyp} are used for different models; and the style-of-faulting dummy variables, F_N and F_R that are unity for normal and reverse faults, respectively, and zero otherwise. The parameter c_1 in the reference ground-motion model is the hinging magnitude and it is not obtained as part of regression analysis. It is taken as M_w 6.75 (which happens to be the same value used in Boore and Atkinson, 2008) and is imposed in the regression analysis after making several observations in the empirical data trend for different magnitude and distance interval. The total aleatory variability of the model is given by σ that is composed of within-event (ϕ) and between-event (τ) standard deviations (SDs). The period-dependent estimators parameters of the nonlinear site function (*i.e.*,

128

b_1(T) and b_2(T)) as well as the period-independent c and n coefficients are directly adopted from the nonlinear site model developed in Chapter 3. The reference V_{S30} (V_{REF}) is 750m/s in the nonlinear site model and V_{CON}=1000m/s that stands for the limiting V_{S30} after which the site amplification is constant. The reference rock site PGA (PGA_{REF}) is calculated from the reference ground-motion model in Eq. (2). It is the updated version of PGA_{REF} model given Eq. (3.6) by considering the particular magnitude, distance and style-of-faulting distributions of the strong-motion database used in this chapter. Regressions were performed by first scaling observed spectral ordinates to reference rock conditions.

No smoothing or truncation is done on the regression coefficients due to the unexpected jagged variation of response spectrum estimations observed in the Akkar and Bommer (2007) predictive model. This problem is discussed in detail by Akkar and Bommer (2010) and it was one of the motivations behind the development of the new GMPE in that paper, which superseded the former Akkar and Bommer (2007b) model. The fictitious depth coefficient (a_6) was decided to be kept with one decimal as trials in regressions showed that the increase in its precision neither improves the ground-motion predictions nor decreases the standard deviation of the model. The period independence of this coefficient stems from the observations made from many trials in regression analysis as variations in a_6 were found to be minimal in the spectral period band of interest in our model. A similar observation on the behavior of this coefficient was also observed in Bommer *et al.* (2011) that describe the recent pan-European vertical-to-horizontal spectral ratio model. A similar reasoning also applies to the linear magnitude coefficients (*i.e.*, a_2, a_5 and a_7) as they do not show significant fluctuations across the spectral period band of interest: we constrained them to the regression coefficients computed for PGA for the models using R_{JB}, R_{epi} and R_{hyp}. Keeping these coefficients as constants also resulted in a smooth variation of period-dependent spectral ordinate estimations for the entire ranges of period, magnitude and distance covered by the proposed models. Table 5.3 lists the period-independent coefficients of the proposed models. Tables 5.4 – 5.7 give the

period-dependent coefficients, and between- and within-event standard deviations for the models with different distance metrics.

Table 5. 7 Period-independent regression coefficients

a_2	a_5	a_6	a_7	a_7	V_{REF}	V_{CON}
0.0029	0.2529	7.5	-0.5096	-0.5096	750	1000

Table 5 8 Distance-metric independent regression coefficients

Period	a_8	a_9	b_1	b_2
PGA	-0.1091	0.0937	-0.41997	-0.28846
PGV	-0.0616	0.063	-0.72057	-0.19688
0.01	-0.1115	0.0953	-0.41729	-0.28685
0.02	-0.104	0.1029	-0.39998	-0.28241
0.03	-0.0973	0.1148	-0.34799	-0.26842
0.04	-0.0884	0.1073	-0.27572	-0.24759
0.05	-0.0853	0.1052	-0.21231	-0.22385
0.075	-0.0779	0.0837	-0.14427	-0.17525
0.10	-0.0749	0.0761	-0.27064	-0.29293
0.11	-0.0704	0.0707	-0.31025	-0.31837
0.12	-0.0604	0.0653	-0.34796	-0.3386
0.13	-0.049	0.0617	-0.39668	-0.36646
0.14	-0.0377	0.0581	-0.43996	-0.38417
0.15	-0.0265	0.0545	-0.48313	-0.39551
0.16	-0.0194	0.0509	-0.52431	-0.40869
0.17	-0.0125	0.0507	-0.5568	-0.41528
0.18	-0.0056	0.0502	-0.58922	-0.42717
0.19	0	0.0497	-0.62635	-0.4413
0.20	0	0.0493	-0.65315	-0.44644
0.22	0	0.0488	-0.68711	-0.44872
0.24	0	0.0483	-0.72744	-0.46341
0.26	0	0.0478	-0.77335	-0.48705
0.28	0	0.0474	-0.80508	-0.47334
0.30	0	0.0469	-0.82609	-0.4573
0.32	0	0.0464	-0.8408	-0.44267

Table 5.8. Cont'd

Period	a_8	a_9	b_1	b_2
0.34	0	0.0459	-0.86251	-0.43888
0.36	0	0.0459	-0.87479	-0.4382
0.38	0	0.0429	-0.88522	-0.43678
0.40	0	0.04	-0.89517	-0.43008
0.42	0	0.0374	-0.90875	-0.4219
0.44	0	0.0349	-0.91922	-0.40903
0.46	0	0.0323	-0.9267	-0.39442
0.48	0	0.0297	-0.9372	-0.38462
0.50	0	0.0271	-0.94614	-0.37408
0.55	0	0.0245	-0.96564	-0.35582
0.60	0	0.0219	-0.98499	-0.34053
0.65	0	0.0193	-0.99733	-0.30949
0.70	0	0.0167	-1.00469	-0.28772
0.75	0	0.0141	-1.00786	-0.28957
0.80	0	0.0115	-1.00606	-0.28555
0.85	0	0.0089	-1.01093	-0.28364
0.90	0	0.0062	-1.01576	-0.28037
0.95	0	0.0016	-1.01353	-0.2839
1.0	0	0	-1.01331	-0.28702
1.1	0	0	-1.0124	-0.27669
1.2	0	0	-1.00489	-0.27538
1.3	0	0	-0.98876	-0.25008
1.4	0	0	-0.9776	-0.23508
1.5	0	0	-0.98071	-0.24695
1.6	0	0	-0.96369	-0.2287
1.7	0	0	-0.94634	-0.21655
1.8	0	-0.003	-0.93606	-0.20302
1.9	0	-0.006	-0.91408	-0.18228
2.0	0	-0.009	-0.91007	-0.17336
2.2	0	-0.0141	-0.89376	-0.15463
2.4	0	-0.0284	-0.87052	-0.13181
2.6	0	-0.0408	-0.85889	-0.14066
2.8	0	-0.0534	-0.86106	-0.13882
3.0	0	-0.0683	-0.85793	-0.13336
3.2	0	-0.078	-0.82094	-0.1377
3.4	0	-0.0943	-0.84449	-0.15337
3.6	0	-0.1278	-0.83216	-0.10884
3.8	0	-0.1744	-0.792156	-0.08884
4.0	0	-0.2231	-0.75645	-0.07749

Table 5. 9 Period-dependent regression coefficients of the R_{JB} model

Period	a_1	a_3	a_4	ϕ	τ	σ
PGA	1.85329	-0.02807	-1.23452	0.6201	0.3501	0.7121
PGV	5.61201	-0.0998	-0.98388	0.6014	0.3311	0.6865
0.01	1.87032	-0.0274	-1.23698	0.6215	0.3526	0.7146
0.02	1.95279	-0.02715	-1.25363	0.6266	0.3555	0.7204
0.03	2.07006	-0.02403	-1.27525	0.641	0.3565	0.7335
0.04	2.20452	-0.01797	-1.30123	0.6534	0.3484	0.7405
0.05	2.35413	-0.01248	-1.32632	0.6622	0.3551	0.7514
0.075	2.63078	-0.00532	-1.35722	0.6626	0.3759	0.7618
0.10	2.85412	-0.00925	-1.38182	0.667	0.4067	0.7812
0.11	2.89772	-0.01062	-1.38345	0.6712	0.4059	0.7844
0.12	2.92748	-0.01291	-1.37997	0.6768	0.4022	0.7873
0.13	2.95162	-0.01592	-1.37627	0.6789	0.4017	0.7888
0.14	2.96299	-0.01866	-1.37155	0.6822	0.3945	0.7881
0.15	2.96622	-0.02193	-1.3646	0.6796	0.3893	0.7832
0.16	2.93166	-0.02429	-1.35074	0.6762	0.3928	0.782
0.17	2.88988	-0.02712	-1.33454	0.6723	0.396	0.7803
0.18	2.84627	-0.03003	-1.31959	0.6694	0.396	0.7778
0.19	2.79778	-0.033	-1.3045	0.6647	0.3932	0.7723
0.20	2.73872	-0.03462	-1.28877	0.6645	0.3842	0.7676
0.22	2.63479	-0.03789	-1.26125	0.66	0.3887	0.766
0.24	2.53886	-0.04173	-1.236	0.6651	0.3792	0.7656
0.26	2.48747	-0.04768	-1.21882	0.665	0.3754	0.7636
0.28	2.38739	-0.05178	-1.19543	0.659	0.3757	0.7586
0.30	2.3015	-0.05672	-1.17072	0.6599	0.3816	0.7623
0.32	2.17298	-0.06015	-1.13847	0.6654	0.3866	0.7696
0.34	2.07474	-0.06508	-1.11131	0.6651	0.3881	0.7701
0.36	2.01953	-0.06974	-1.09484	0.6662	0.3924	0.7732
0.38	1.95078	-0.07346	-1.07812	0.6698	0.3945	0.7773
0.40	1.89372	-0.07684	-1.0653	0.6697	0.3962	0.7781
0.42	1.83717	-0.0801	-1.05451	0.6696	0.389	0.7744
0.44	1.77528	-0.08296	-1.04332	0.6641	0.3929	0.7716
0.46	1.73155	-0.08623	-1.03572	0.6575	0.4009	0.7701
0.48	1.70132	-0.0907	-1.02724	0.654	0.4022	0.7678
0.50	1.67127	-0.0949	-1.01909	0.6512	0.4021	0.7653
0.55	1.53838	-0.10275	-0.99351	0.657	0.4057	0.7722
0.60	1.37505	-0.10747	-0.96429	0.663	0.406	0.7774
0.65	1.21156	-0.11262	-0.93347	0.6652	0.4124	0.7827
0.70	1.09262	-0.11835	-0.91162	0.6696	0.4135	0.787

Table 5.9. Cont'd

Period	a_1	a_3	a_4	ϕ	τ	σ
0.75	0.95211	-0.12347	-0.88393	0.6744	0.4043	0.7863
0.80	0.85227	-0.12678	-0.86884	0.6716	0.3974	0.7804
0.85	0.76564	-0.13133	-0.85442	0.6713	0.3971	0.78
0.90	0.66856	-0.13551	-0.83929	0.6738	0.3986	0.7829
0.95	0.58739	-0.13957	-0.82668	0.6767	0.3949	0.7835
1.0	0.52349	-0.14345	-0.81838	0.6787	0.3943	0.7849
1.1	0.3768	-0.15051	-0.79691	0.6912	0.3806	0.7891
1.2	0.23251	-0.15527	-0.77813	0.7015	0.3802	0.7979
1.3	0.10481	-0.16106	-0.75888	0.7017	0.3803	0.7981
1.4	0.00887	-0.16654	-0.74871	0.7141	0.3766	0.8073
1.5	-0.01867	-0.17187	-0.75751	0.7164	0.3799	0.8109
1.6	-0.0996	-0.17728	-0.74823	0.7198	0.3817	0.8147
1.7	-0.21166	-0.17908	-0.73766	0.7226	0.3724	0.8129
1.8	-0.273	-0.18438	-0.72996	0.7241	0.371	0.8136
1.9	-0.35366	-0.18741	-0.72279	0.7266	0.3745	0.8174
2.0	-0.42891	-0.19029	-0.72033	0.7254	0.3717	0.8151
2.2	-0.55307	-0.19683	-0.71662	0.7207	0.3758	0.8128
2.4	-0.67806	-0.20339	-0.70452	0.7144	0.3973	0.8174
2.6	-0.80494	-0.20703	-0.69691	0.7122	0.4001	0.8169
2.8	-0.91278	-0.21074	-0.6956	0.7129	0.4025	0.8187
3.0	-1.05642	-0.21392	-0.69085	0.6997	0.4046	0.8083
3.2	-1.17715	-0.21361	-0.67711	0.682	0.4194	0.8006
3.4	-1.22091	-0.21951	-0.68177	0.6682	0.3971	0.7773
3.6	-1.34547	-0.22724	-0.65918	0.6508	0.4211	0.7752
3.8	-1.3979	-0.2318	-0.65298	0.6389	0.415	0.7619
4.0	-1.37536	-0.23848	-0.66482	0.6196	0.3566	0.7149

Table 5. 10 Period-dependent regression coefficients of the R_{epi} model

Period	a_1	a_3	a_4	ϕ	τ	σ
PGA	2.52977	-0.05496	-1.31001	0.6375	0.3581	0.7312
PGV	6.13498	-0.12091	-1.04013	0.6143	0.3485	0.7063
0.01	2.54832	-0.05434	-1.31268	0.6389	0.3607	0.7337
0.02	2.6442	-0.05452	-1.33135	0.6434	0.3615	0.738
0.03	2.77723	-0.05196	-1.35509	0.6569	0.3617	0.7499
0.04	2.92666	-0.04657	-1.38259	0.6693	0.353	0.7567

Table 5.10. Cont'd

Period	a$_1$	a$_3$	a$_4$	ϕ	τ	σ
0.05	3.09355	-0.04168	-1.41008	0.6773	0.3612	0.7676
0.075	3.38462	-0.03506	-1.44268	0.6791	0.3853	0.7808
0.10	3.61906	-0.03936	-1.4687	0.6851	0.416	0.8015
0.11	3.66537	-0.04081	-1.47079	0.6884	0.4163	0.8045
0.12	3.68544	-0.04295	-1.4652	0.696	0.4118	0.8087
0.13	3.70155	-0.04581	-1.45986	0.6997	0.4102	0.8111
0.14	3.70871	-0.04848	-1.45433	0.7032	0.4028	0.8104
0.15	3.70477	-0.05156	-1.44613	0.7011	0.3978	0.8061
0.16	3.65565	-0.0535	-1.42989	0.6997	0.3989	0.8054
0.17	3.59764	-0.05583	-1.4111	0.697	0.403	0.8051
0.18	3.53732	-0.0583	-1.39329	0.6956	0.4041	0.8045
0.19	3.47722	-0.0609	-1.37648	0.6915	0.4017	0.7997
0.20	3.40112	-0.0621	-1.3577	0.6922	0.3965	0.7977
0.22	3.27214	-0.06461	-1.32624	0.6893	0.4005	0.7972
0.24	3.15842	-0.06791	-1.29833	0.6942	0.3919	0.7972
0.26	3.09498	-0.07344	-1.27945	0.6938	0.3898	0.7958
0.28	2.9809	-0.07698	-1.25442	0.6877	0.3883	0.7898
0.30	2.87449	-0.08126	-1.22665	0.6897	0.3894	0.792
0.32	2.72364	-0.08387	-1.19143	0.6947	0.3941	0.7987
0.34	2.60904	-0.08816	-1.16231	0.6939	0.3937	0.7978
0.36	2.54266	-0.09239	-1.14444	0.6945	0.3997	0.8013
0.38	2.46615	-0.09576	-1.127	0.6971	0.4012	0.8043
0.40	2.40119	-0.09885	-1.11318	0.6971	0.4012	0.8043
0.42	2.3454	-0.10198	-1.10318	0.6955	0.3946	0.7996
0.44	2.28213	-0.10464	-1.09241	0.6891	0.3985	0.796
0.46	2.2344	-0.10771	-1.08445	0.6825	0.4056	0.7939
0.48	2.20123	-0.11199	-1.07592	0.6785	0.4068	0.7911
0.50	2.16953	-0.11604	-1.06795	0.6751	0.4065	0.788
0.55	2.03012	-0.12344	-1.04242	0.6788	0.4087	0.7923
0.60	1.84644	-0.12745	-1.01046	0.6845	0.4085	0.7971
0.65	1.6676	-0.13195	-0.97801	0.6857	0.4128	0.8004
0.70	1.53432	-0.13715	-0.95428	0.6902	0.4101	0.8028
0.75	1.38296	-0.14169	-0.92585	0.6937	0.4011	0.8013
0.80	1.28662	-0.14485	-0.91241	0.6884	0.3962	0.7943
0.85	1.20114	-0.14922	-0.89909	0.6866	0.3951	0.7922
0.95	1.01256	-0.157	-0.8705	0.6904	0.3955	0.7957
1.0	0.94162	-0.16069	-0.86109	0.6922	0.3965	0.7977
1.1	0.78017	-0.16727	-0.83743	0.7047	0.3819	0.8015
1.2	0.63219	-0.17174	-0.81877	0.7138	0.3807	0.809
1.3	0.48905	-0.17712	-0.79698	0.7137	0.3827	0.8098
1.4	0.38492	-0.18237	-0.78548	0.7263	0.3787	0.8191

Table 5.10. Cont'd

Period	a_1	a_3	a_4	ϕ	τ	σ
1.5	0.36315	-0.1879	-0.79498	0.7287	0.3821	0.8228
1.6	0.28812	-0.19363	-0.78665	0.7307	0.3854	0.8261
1.7	0.18172	-0.19545	-0.77778	0.7322	0.3751	0.8227
1.8	0.13021	-0.20069	-0.77282	0.7316	0.3749	0.8221
1.9	0.05074	-0.20386	-0.76574	0.7341	0.3761	0.8248
2.0	-0.02806	-0.20666	-0.7626	0.7333	0.3734	0.8229
2.2	-0.15016	-0.21319	-0.75952	0.7277	0.3794	0.8207
2.4	-0.26608	-0.2196	-0.75011	0.7199	0.4025	0.8248
2.6	-0.39025	-0.2233	-0.74326	0.7171	0.4049	0.8235
2.8	-0.49742	-0.22716	-0.74185	0.7175	0.409	0.8259
3.0	-0.64241	-0.23038	-0.73634	0.7051	0.4115	0.8164
3.2	-0.7667	-0.23049	-0.72149	0.6876	0.428	0.8099
3.4	-0.80566	-0.23726	-0.72539	0.675	0.4029	0.7861
3.6	-0.945	-0.24437	-0.70115	0.6571	0.4252	0.7827
3.8	-0.98457	-0.2493	-0.69696	0.6438	0.4243	0.771
4.0	-0.93329	-0.25756	-0.7121	0.6241	0.3659	0.7235

Table 5. 11 Period-dependent regression coefficients of the R_{hyp} model

Period	a_1	a_3	a_4	ϕ	τ	σ
PGA	3.26685	-0.04846	-1.47905	0.6475	0.3472	0.7347
PGV	6.72743	-0.11474	-1.17694	0.628	0.3312	0.71
0.01	3.28656	-0.04784	-1.48197	0.6492	0.3481	0.7366
0.02	3.38936	-0.04796	-1.50214	0.6543	0.3508	0.7424
0.03	3.53155	-0.04537	-1.52781	0.6685	0.3526	0.7558
0.04	3.68895	-0.03991	-1.55693	0.6816	0.3513	0.7668
0.05	3.86581	-0.0349	-1.58672	0.6899	0.3659	0.7809
0.075	4.18224	-0.02826	-1.62527	0.6881	0.3942	0.793
0.10	4.4375	-0.03256	-1.65601	0.6936	0.4122	0.8068
0.11	4.48828	-0.03407	-1.65903	0.6965	0.4065	0.8064
0.12	4.51414	-0.03635	-1.6547	0.7022	0.3964	0.8064
0.13	4.5329	-0.03929	-1.64994	0.7043	0.3937	0.8069
0.14	4.53834	-0.042	-1.64398	0.7071	0.3853	0.8053
0.15	4.52949	-0.04509	-1.63467	0.7048	0.3779	0.7997
0.16	4.47016	-0.04701	-1.61626	0.7032	0.3851	0.8017
0.17	4.40011	-0.04932	-1.59485	0.7011	0.39	0.8023
0.18	4.33238	-0.05181	-1.57545	0.6992	0.3889	0.8001
0.19	4.26395	-0.05442	-1.55685	0.6947	0.3903	0.7968
0.20	4.1775	-0.05565	-1.53574	0.6954	0.3848	0.7948

Table 5.11. Cont'd

Period	a_1	a_3	a_4	ϕ	τ	σ
0.22	4.03111	-0.05817	-1.50045	0.6925	0.3891	0.7943
0.24	3.90131	-0.06152	-1.46889	0.6973	0.3839	0.796
0.26	3.82611	-0.06706	-1.44738	0.6973	0.3839	0.796
0.28	3.6978	-0.0706	-1.41925	0.6914	0.3865	0.7921
0.30	3.57698	-0.0749	-1.38832	0.6934	0.3896	0.7954
0.32	3.40759	-0.07756	-1.34898	0.6992	0.3908	0.801
0.34	3.2758	-0.08183	-1.31609	0.699	0.3888	0.7999
0.36	3.19725	-0.08602	-1.29558	0.7006	0.3916	0.8026
0.38	3.11035	-0.08937	-1.27591	0.7036	0.3913	0.8051
0.40	3.03752	-0.09243	-1.26045	0.7037	0.3894	0.8043
0.42	2.97485	-0.09556	-1.24891	0.7023	0.3847	0.8008
0.44	2.90617	-0.09822	-1.237	0.6956	0.3908	0.7979
0.46	2.85484	-0.10132	-1.22822	0.6893	0.3986	0.7963
0.48	2.8172	-0.1056	-1.21874	0.6852	0.4017	0.7943
0.50	2.77997	-0.10964	-1.20953	0.6821	0.4017	0.7916
0.55	2.62299	-0.11701	-1.1801	0.6866	0.4044	0.7968
0.60	2.42234	-0.12106	-1.14424	0.6926	0.4005	0.8001
0.65	2.2277	-0.12555	-1.10853	0.6949	0.3981	0.8009
0.70	2.08102	-0.13074	-1.08192	0.6993	0.3967	0.804
0.75	1.91625	-0.13547	-1.05027	0.7028	0.389	0.8033
0.80	1.81167	-0.13856	-1.03514	0.6981	0.3824	0.796
0.85	1.71853	-0.14294	-1.0201	0.6959	0.3831	0.7944
0.90	1.60822	-0.14669	-1.00315	0.6983	0.3825	0.7962
0.95	1.51532	-0.15056	-0.98859	0.7006	0.3797	0.7969
1.0	1.43982	-0.15427	-0.97812	0.7022	0.3826	0.7997
1.1	1.26728	-0.16107	-0.95163	0.7137	0.3721	0.8049
1.2	1.11475	-0.1663	-0.93048	0.7224	0.3723	0.8127
1.3	0.95965	-0.1717	-0.90604	0.7226	0.3746	0.8139
1.4	0.85203	-0.17699	-0.89379	0.7349	0.3697	0.8227
1.5	0.83007	-0.18248	-0.90319	0.7378	0.3758	0.828
1.6	0.74487	-0.18787	-0.89323	0.7406	0.3794	0.8321
1.7	0.63568	-0.18961	-0.88392	0.7418	0.3686	0.8283
1.8	0.56996	-0.19551	-0.87459	0.7431	0.3692	0.8298
1.9	0.485	-0.19853	-0.86659	0.7457	0.3705	0.8327
2.0	0.40614	-0.20136	-0.86343	0.7446	0.3676	0.8304
2.2	0.28608	-0.20791	-0.86086	0.7391	0.3718	0.8273
2.4	0.15432	-0.2148	-0.84778	0.7311	0.3941	0.8306
2.6	0.0225	-0.21843	-0.83937	0.7281	0.3967	0.8292
2.8	-0.07822	-0.22224	-0.83964	0.7279	0.3987	0.8299
3.0	-0.22534	-0.22564	-0.83314	0.7154	0.4019	0.8206
3.2	-0.36165	-0.22496	-0.81702	0.6984	0.4113	0.8105
3.4	-0.39423	-0.23237	-0.82109	0.6867	0.38	0.7848

Table 5.11. Cont'd

Period	a_1	a_3	a_4	ϕ	τ	σ
3.6	-0.54126	-0.24003	-0.79431	0.6687	0.4009	0.7797
3.8	-0.59607	-0.24448	-0.78785	0.6565	0.3952	0.7663
4.0	-0.51893	-0.25256	-0.80922	0.6364	0.3318	0.7177

As a check on the statistical behavior of the developed models, Figure 5.3 presents residual plots for spectral ordinates at three response periods with respect to M_w, R and V_{S30} for the model using R_{JB} (residual plots for the other models are similar). The residuals are grouped into several magnitude, distance and V_{S30} bins to show the average residual variation (solid circles on each plot) for each independent variable. The error bars given on the same plots indicate the ±1 standard deviation about the bin averages. The within-event residuals as a function of distance do not show any apparent trends. The proposed model slightly overestimates motion at very soft soil sites (V_{S30}<180m/s) and underestimates motions for rock sites (V_{S30}>800 m/s) at relatively short periods (T=0.2s). This observation, however, may not reflect the actual performance of the ground-motion model as the data in these V_{S30} ranges are sparse and poorly distributed. The magnitude-dependent variation of between-event residuals also suggests some level of bias towards large magnitudes at all periods. The between-event residuals appear to show a narrowing at all periods with increasing magnitude up to M_w 7, which could suggest a reduction of aleatory variability at large magnitudes. However, the sampling of data at large magnitudes is sparse and this could be the cause of the apparently smaller variability and the observed bias (particularly at T=1.0s). In two previous sets of GMPEs for Europe and the Middle East (Ambraseys *et al.*, 2005a; Akkar and Bommer, 2007a) such behavior led to the characterization of sigma as linearly dependent on magnitude. Later on it was argued (Akkar and Bommer, 2010) that the appearance of a magnitude-dependent sigma could be because data are only available from a handful of large-

magnitude earthquakes leading to an underestimation of the true variability at $M_w>6.5$, and because of poorly constrained metadata (particularly seismic moments) for smaller events, which despite the improvements in the current database is a problem that is likely to still persist to some degree. We think that these arguments still hold and we do not model the standard deviation as a function of magnitude in the current set of GMPEs.
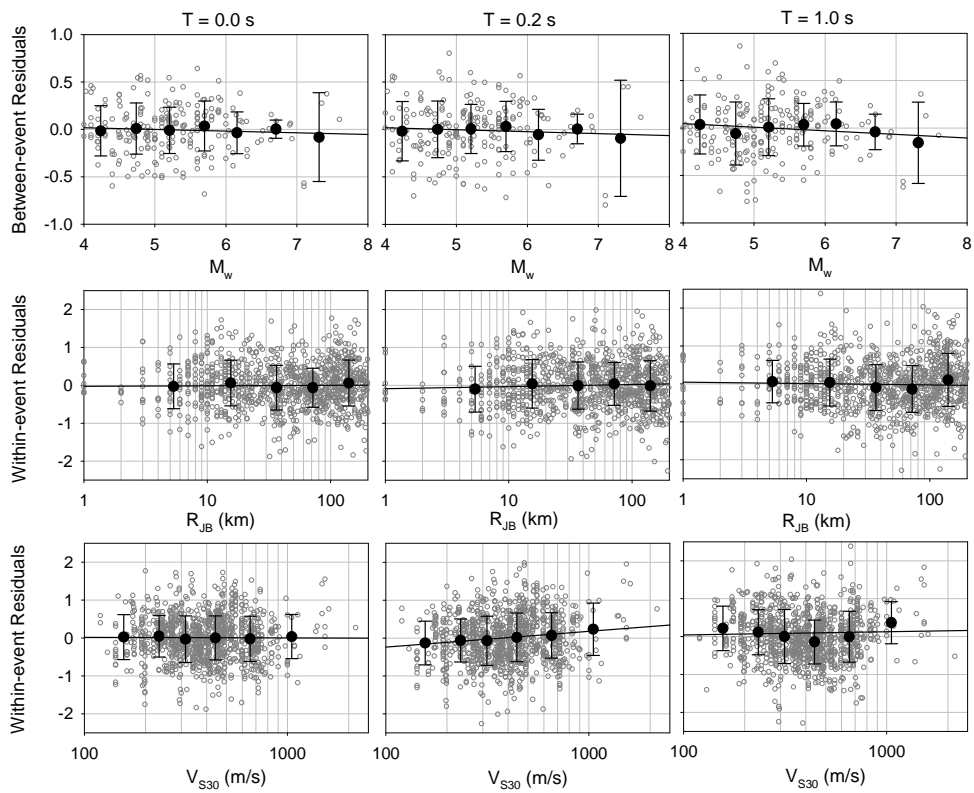
Figure 5. 3. Residual plots for R_{JB} model.

Figure 5.4 shows the period-dependent variation of the between-event, within-event and total sigmas for the GMPEs derived in this study. As is universally observed, within-event sigmas are much larger than the between-event component

(*e.g.*, Strasser *et al*., 2009). The between-event variability is almost model-independent but the within-event variability of the R_{JB} model is slightly lower than the other two GMPEs, as would be expected. The standard deviations obtained are almost independent of period and the total sigmas are similar to those of the NGA models and those of the previous pan-European model by Akkar and Bommer (2010).
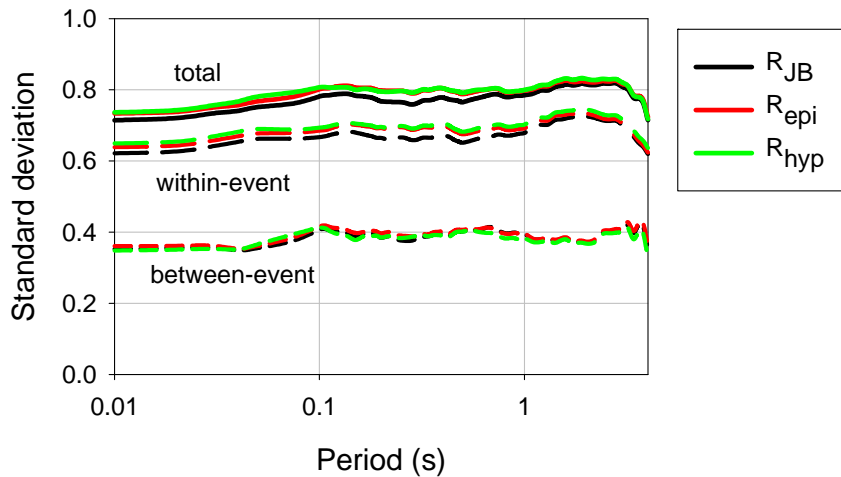
Figure 5. 4. Components of the standard deviation of the models.

As with the study of Bommer and Akkar (2012), it is perhaps surprising that the sigma values for the point-source based models are not larger compared to that for the extended-source based model. The reason probably lies in the relative lack of data from earthquakes of $M_w>6$ recorded at short distances (less than 10-15 km). An estimate of the true variability in the R_{epi} model could be obtained by generating ground-motion fields at dense grid points around various hypothetical ruptures (with dimensions appropriate to the earthquake magnitude), predicting the motions (at various exceedance levels) using the R_{JB} model. The epicentral distances could then be calculated (making appropriate assumptions about the

distribution of unilateral and bilateral ruptures) and regressions performed in R_{epi} to obtain sigma values that may better reflect the added variability from using point-source distance metrics. The sigma model developed in this way may need to be magnitude- and/or distance-dependent, and the values would then likely differ from those presented herein only for larger magnitudes and relatively short epicentral distances.

5.4 Predictions and Comparison with other Models

Figure 5.5 compares the magnitude-scaling of the proposed model with the magnitude scaling of Akkar and Bommer (2010), which used data from M_w 5 upwards, and Bommer *et al.* (2007), which used data from M_w 3 upwards. The comparisons are made for a generic rock site (V_{S30}=750m/s) located R_{JB}=10km from a strike-slip fault. We considered PGA (PSA at T=0s) as well as PSA at T=0.2s and T=1.0s in comparisons as they are widely used spectral ordinates to construct smoothed spectrum in several seismic design codes. Only the proposed model and Akkar and Bommer (2010) are compared for PSA at T=1.0s as the Bommer *et al.* (2007) GMPE predicts spectral ordinates up to 0.5s. The proposed model and Bommer *et al.* (2007) follow very similar trends for $M_w \geq 5$ although the lower magnitude limit of our strong-motion database is one magnitude unit above that used for the derivation of the Bommer *et al.* (2007) model. Our new model appears to overestimate the spectral ordinates for $M_w < 5$ if compared to Bommer *et al.* (2007), possibly due to the differences in the lower magnitude bounds of these models. This interpretation would suggest that the phenomenon of empirical models over-estimating ground-motion amplitudes at the lower magnitude limit of the dataset persists to smaller magnitudes. However, this is almost entirely predicated on the comparison with Bommer *et al.* (2007), which may give excessive credence to that earlier model. It may equally be the case that by extending the lower magnitude limit of the database to M_w 4, we have better constrained the (more) linear part of the magnitude scaling and therefore the new model may perform satisfactorily at this lower limit. The Akkar and Bommer

(2010) GMPE overestimates the ground-motion amplitudes in the magnitude range of 4≤M_w≤6.5 with respect to the other two models. This model constitutes the lower bound of the three sets of predictions at higher magnitude levels (*i.e.*, M_w>6.5). Similar to above explanations, the higher ground-motion estimations of Akkar and Bommer (2010) are directly related to the lower magnitude limit of this model (*i.e.*, M_w 5). The quadratic-magnitude functional form of the Akkar and Bommer (2010) model predicts over-saturation at large magnitudes, which was a characteristic of the database used at the time (similar patterns were observed in the early versions of the NGA equations, which the model developers addressed by forcing the models not to pass into over-saturation).
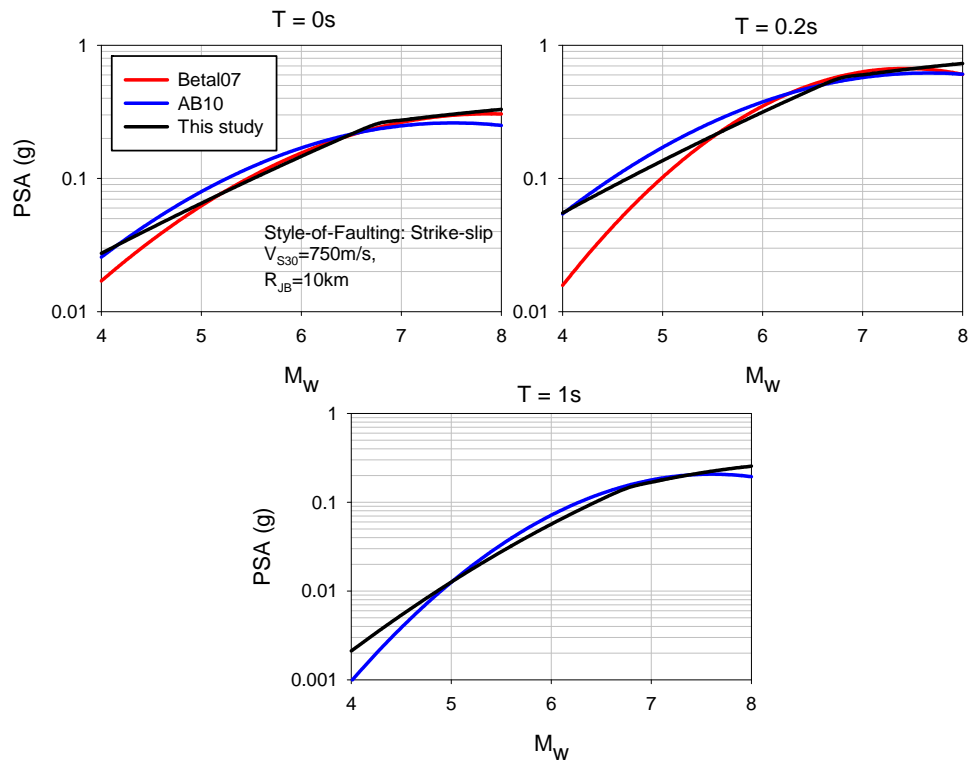
Figure 5. 5 Magnitude-scaling comparisons between two previous pan-European GMPEs (Bommer et al., 2007 – Betal07 and Akkar and Bommer, 2010 –AB10) and the proposed model. Comparisons are made for a rock site (V_{S30}=750m/s) located R_{JB}=10km from a strike-slip fault.

Figure 5.6 compares the normal-to-strike-slip (N:SS) and reverse-to-strike-slip (R:SS) amplitude ratios of our ground-motion model with those of previously published GMPEs (Akkar and Bommer (2010) – AB10, with its extension for T<0.05s (Bommer *et al.*, 2012) – BAD12, Abrahamson and Silva (2008) – AS08, Boore and Atkinson (2008) – BA08, Campbell and Bozorgnia (2008) – CB08, and Chiou and Youngs (2008) – CY08). The fault rupture is assumed to reach the surface (Z_{TOR}=0.0) while computing the spectral amplitude ratios of AS08, CB08 and CY08. The N:SS of our models yield a pattern that is fairly consistent with the predictions of AS08, CB08 and AB10. This is not the case for the N:SS ratios predicted by BA08 and CY08 as they show large differences in terms of N:SS ratios. Moreover, the N:SS ratios predicted by BA08 and CY08 diverge from each other and follow completely different trends after T=0.75s. The reverse-to-strike-slip (R:SS) ratio estimations of the considered GMPEs show significant discrepancies over the period range given in Figure 5.6. Although the reverse-to-strike-slip spectral (R:SS) ratios of AS08 and BA08 are similar for T ≤ 1.0s, they diverge from each towards longer periods. The proposed model and the former pan-European GMPE, AB10, only show similar R:SS ratios for 1.5s ≤ T ≤ 3.0s. The period-dependent R:SS estimations of CB08 and CY08 have similar shapes but their amplitudes differ significantly from each other.
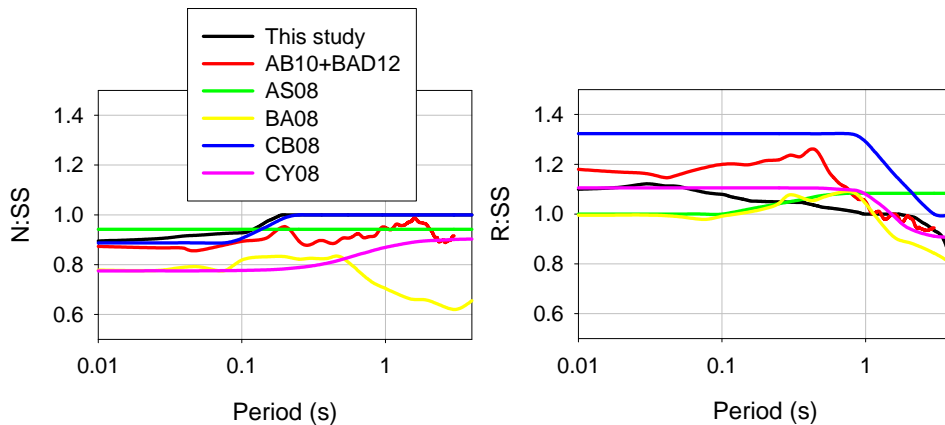
Figure 5. 6. N:SS and R:SS spectral ordinate ratios of different GMPEs.

The observed model differences in the spectral amplitude ratio predictions of different styles-of-faulting warrant some discussion here. Several factors may be contributing to these observations, and we do not believe that we can currently identify the definitive reason(s) behind these observations but rather offer a number of remarks for consideration by the reader. Although most previous equations have predicted larger motions from strike-slip than from normal earthquakes, the differences have generally been small. Westaway and Smith (1989) concluded that there were no systematic differences between the two styles-of-faulting, and Spudich *et al*. (1999) reached the same conclusion for earthquakes in extensional regimes, although they noted that these were systematically lower than motions from compressional regions. Therefore, style-of-faulting effects may represent or be concealed by regional differences in ground motions. Similarly, the style-of-faulting effect can trade-off with effects such as the fact that buried ruptures tend to produce higher amplitudes of motion than ruptures that break the surface (Kagawa *et al*., 2004), reflected in the NGA models by the inclusion of a parameter reflecting the depth-to-the-top-of-rupture (Z_{TOR}). This trade-off is related to the fact that deeper events are likely to be associated with higher stress drop, which may have a more pronounced effect than the increased separation of source and site. Another factor that must be considered is the limitations of strong-motion databases in terms of different rupture mechanisms. For example, normal-faulting earthquakes are poorly represented in the datasets used for the NGA models, which is not the case for this pan-European database. On the other hand, in the current database, nearly all records from events with $M_w > 7$ are from strike-slip earthquakes with none from normal events and only two from reverse events. Thus, it may also be the case that such non-uniform distribution of rupture mechanisms in the databases contributes to the observed discrepancies in style-of-faulting ratios. The variation in style-of-faulting ratios under the influence of strong-motion database features is discussed in Sandıkkaya and Akkar (2012) by using alternative subsets of the strong-motion database used in this study.

Figure 5.7 shows the distance scaling of the proposed GMPEs for two magnitude levels (M_w 4.5 and M_w 7.5) at T=0s (PGA). The reference site condition (V_{S30}= 750m/s) and strike-slip rupture mechanism are considered in the comparative plots. As expected the models using R_{epi} and R_{JB} overlap each other for M_w 4.5 as R_{epi} and R_{JB} are practically the same when the seismic energy radiation is concentrated at a relatively small rupture area (point-source). The discrepancy between the R_{epi} and R_{JB} models increases for the M_w 7.5 scenario as the rupture dimensions lead to very large differences between average values of the R_{epi} and R_{JB} distance metrics. At short distances from the source the R_{epi} model results in higher predicted ground motions because R_{JB} would be equal to or less than R_{epi}, thus reducing the ground-motion amplitudes for a given distance. As the source-to-site distance increases the rupture size losses its significance even for large magnitudes, thus the difference between R_{epi} and R_{JB} diminishes and the predicted ground motions become almost equal for these models. On such a plot, where each GMPE is plotted against its own distance metric, the proposed GMPE using R_{hyp} predicts apparently larger ground motions regardless of magnitude for distances closer to the site because at comparable horizontal distances, the other models are implicitly accounting for the attenuation over the focal depth. As the source-to-site distance increases the difference between R_{hyp} and the other distance measures becomes insignificant.

The distance scaling of the predictive model using R_{JB} is presented in more detail in Figure 5.8. The plots on this figure show the median estimations of PGA and spectral ordinates at T = 0.2s, T = 1.0s and T = 4.0s for M_w > 6. As in all other comparative plots, the distance-dependent median estimations are for a rock site of V_{S30} = 750 m/s and strike-slip fault. The plots do not show decreasing amplitudes at very short distances. For magnitudes M_w 7.5 and above, the short- and intermediate-period spectral ordinates (*i.e.*, PGA, PSA at T = 0.2s and 1.0s) tend to converge and overlap each other. This phenomenon is the so-called magnitude saturation but our model gives no indication of magnitude oversaturation that results in a decreasing trend in spectral ordinates at large M_w
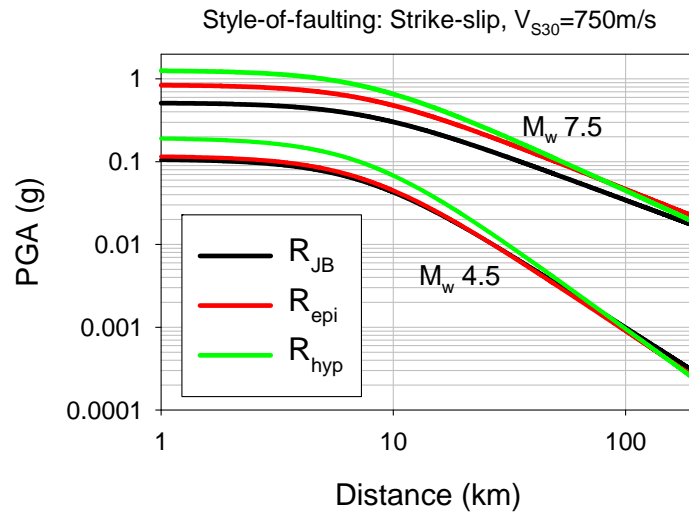
Figure 5. 7. Distance scaling of the proposed ground-motion models.
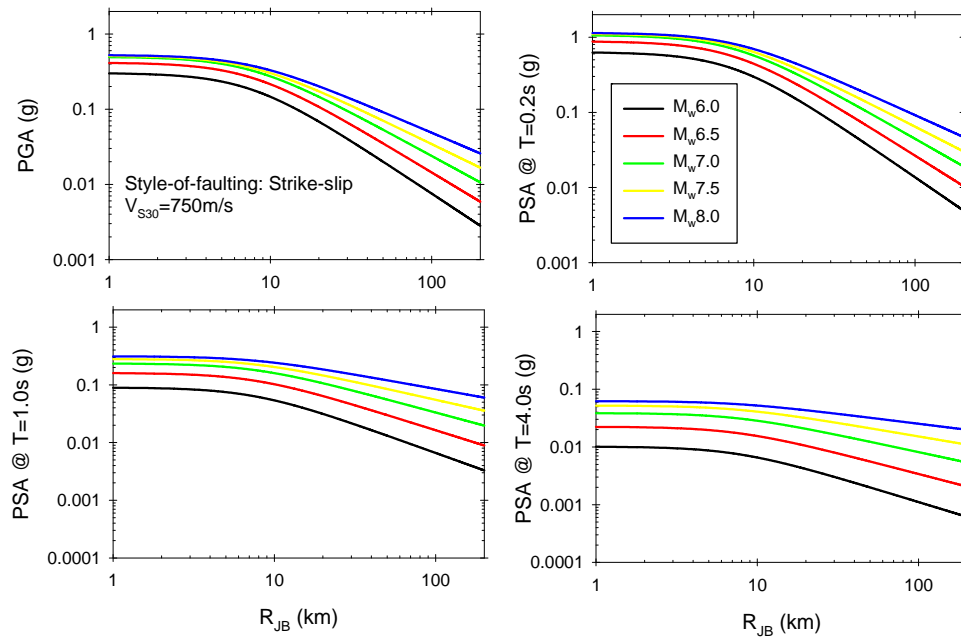
Figure 5. 8: Distance scaling of R_{JB} model at different spectral ordinates (PGA, PSA at $T = 0.2s$, 1.0s and 4.0s) for magnitudes above 6.

and short distances. Predictive models that use a reference distance term in their distance scaling function can impose magnitude oversaturation in ground-motion estimations (Dr. David M Boore, *personal communication*, 2013). Thus, our functional form is not tailored for capturing magnitude oversaturation effects.

When presenting new GMPEs it is common to compare predictions in terms of median spectra to those from previous well-known GMPEs. The median estimations of the R_{JB} model are compared with the NGA GMPEs and the previous pan-European GMPE of Akkar and Bommer (2010) with its extension for T<0.05s (Bommer *et al.*, 2012) in Figure 5.9. Two magnitude levels (M_w 5 and M_w 7) are chosen in the comparisons that can encompass small-to-large size events in Europe and surrounding regions. The site is assumed to be located R_{JB}=30km from a 90° dipping strike-slip fault and all common Eurocode 8 site classes (A as V_{S30}=800m/s, B as V_{S30}=525m/s, C as V_{S30}=255m/s and D as V_{S30}=180m/s) are taken into account to observe the behavior of R_{JB} model together with the other GMPEs. For the rupture geometry of the chosen scenario, R_{JB} and R_{rup} are equivalent hence no adjustments are needed to compare predictions from the NGA models. Surface rupture is assumed and other estimator parameters used by NGA models are estimated from Kaklamanos *et al.* (2011). The plots indicate that the median estimations of the R_{JB} model are comparable with the other GMPEs for all magnitude and site classes considered in the case study. The new model tends to estimate relatively small spectral amplitudes, particularly at short periods, for small magnitudes (M_w 5).

As a variant on the previous figure, Figure 5.10 compares predicted spectra from all three proposed models to those estimated by the GMPEs in Figure 5.9 as well as those that use either R_{epi} or R_{hyp}. The selected earthquake scenarios generically represent the moderate seismicity (median+0.5σ for an M_w 6 event) and high seismicity (median+1.0σ for an M_w 7 event) regions in Europe and are used in the comparisons to give a more complete picture of the influence of adopting these new R_{JB}, R_{epi} and R_{hyp} models over those already in the literature. The spectra

predicted by these new models are generally comparable to those from previous GMPEs but are often higher (particularly for M_w 6 and at short periods).
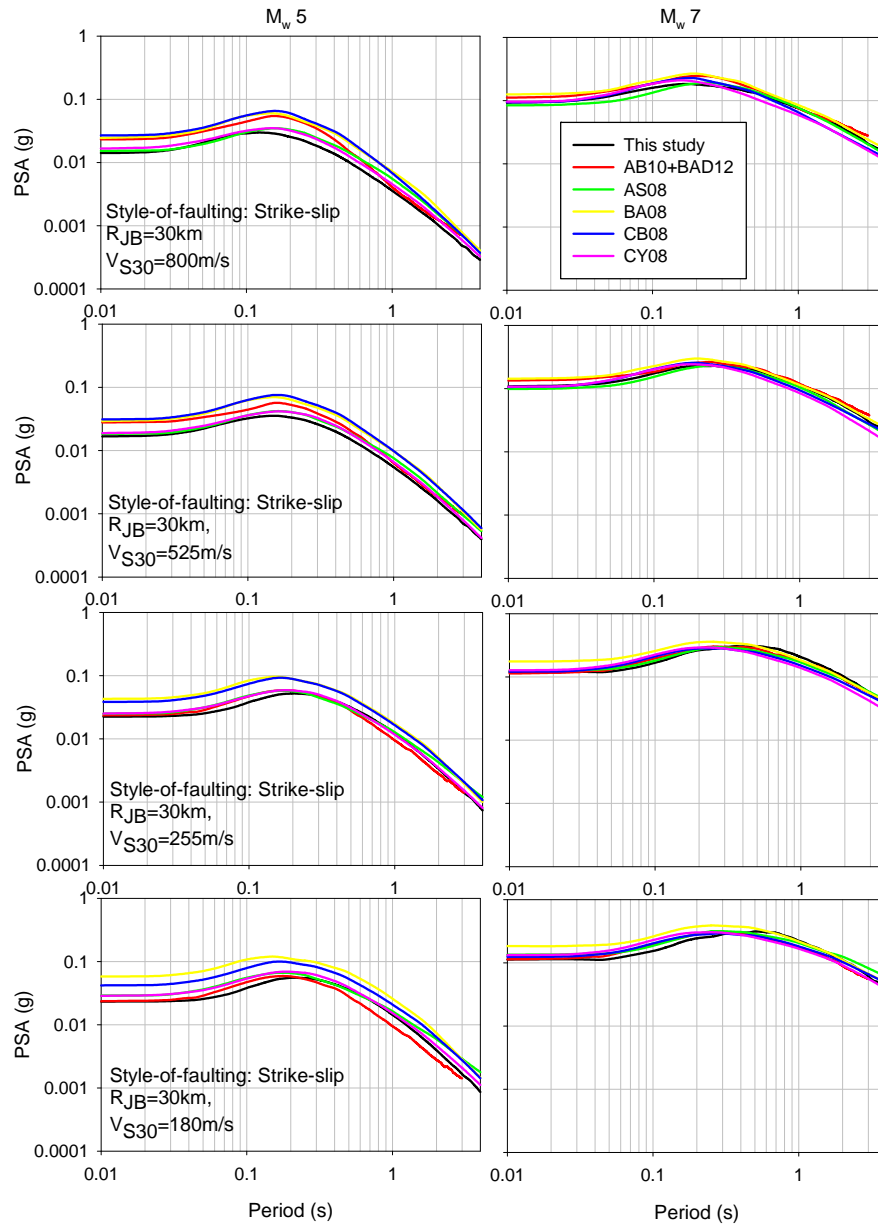
Figure 5. 9. Median estimation comparisons of R_{JB} model with other GMPEs.
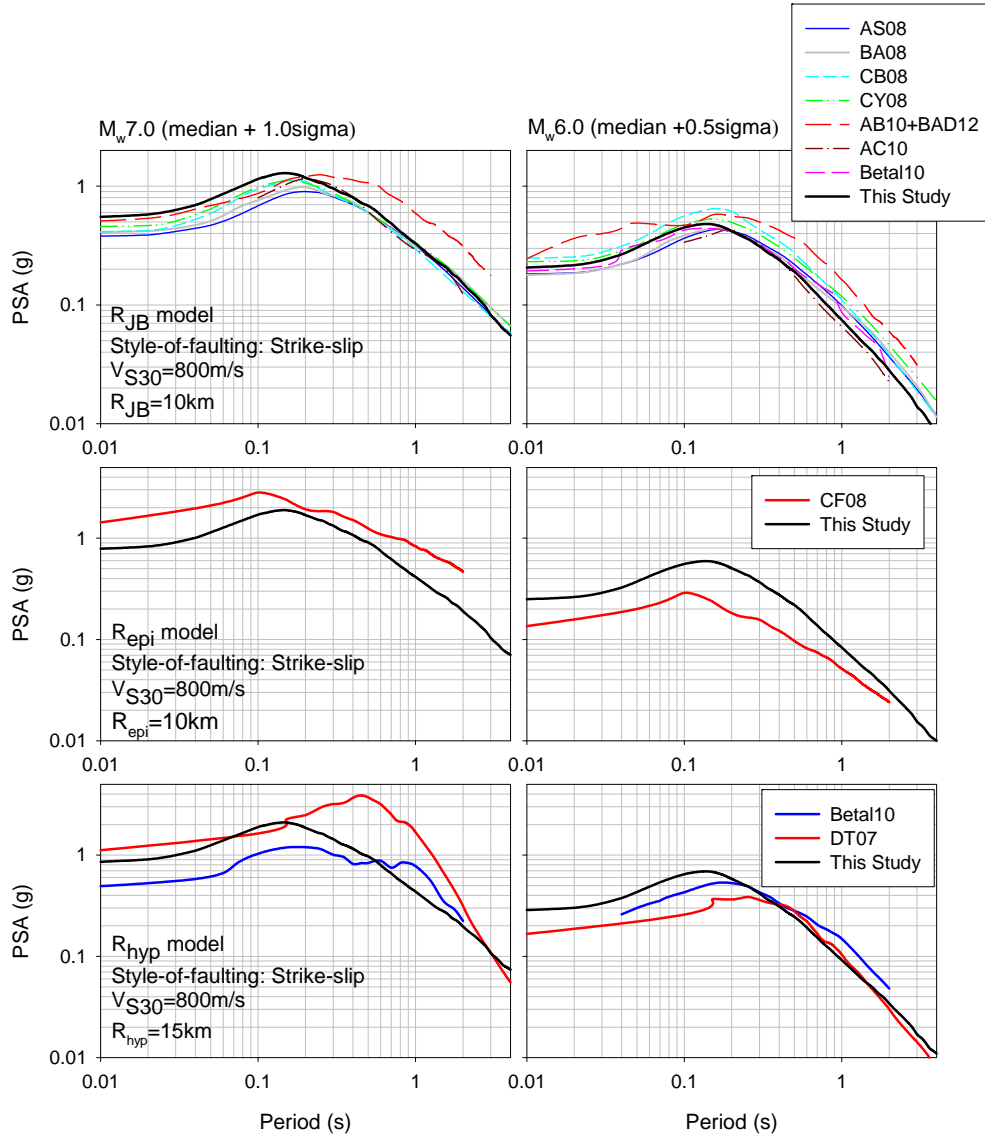
Figure 5. 10. Comparison of predicted spectra from the new models and some global, regional and local models. This comparison is for a surface-rupturing vertically-dipping strike-slip fault with a focal depth of 11km and an epicentre in the centre of the fault ($R_{JB}=R_{epi}=R_{rup}=10km$ and $R_{hyp}=15km$). The site is a generic rock site with $V_{S30}=800m/s$. The abbreviations AC10, Betal10, CF08 and DT07 stand for Akkar and Çağnan (2010), Bindi et al. (2010), Cauzzi and Faccioli (2008) and Danciu and Tselentis (2007) GMPEs, respectively.

As a test of our model outside the 'comfort zone' (Akkar and Bommer, 2010) Figure 5.11 presents predicted 84th percentile spectra for M_w 8.0 at R_{JB}=5km and R_{JB}=200km for a rock site (V_{S30}=800m/s). The predicted spectra are compared with the global GMPEs considered in this study. The comparisons for R_{JB}=5km indicate good agreement between the proposed model and the other GMPEs although our spectral ordinates are slightly higher in the short-period range. The trend in the predicted spectrum at R_{JB}=200km is roughly similar to the compared NGA models. However, the NGA models also show great variations with respect to one another at this distance, which may suggest that the data on which they are based, and the way the models are derived, means that the decay at such distances has not been well constrained in all cases. Our model is generally on the high side for M_w 8.0, and envelopes the other spectra at longer periods, probably due to its larger standard deviations with respect to the other compared GMPEs. Most of the NGA GMPEs (except for BA08) impose smaller sigma at large magnitudes due to their magnitude-dependent standard deviation modeling.
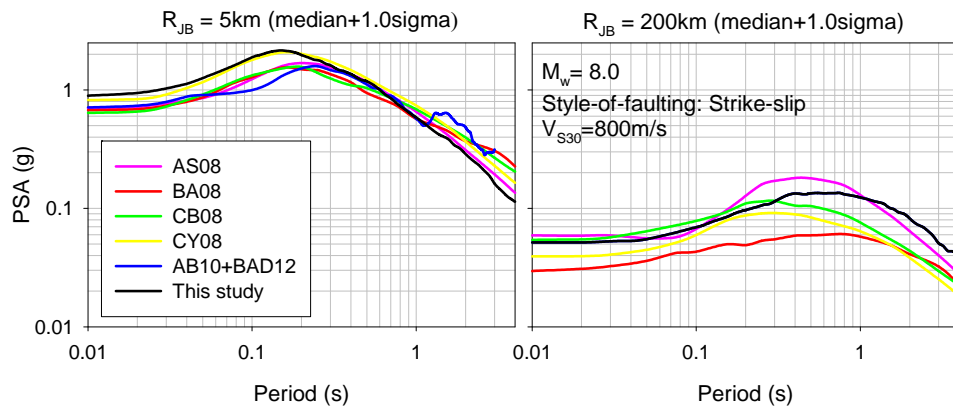
Figure 5. 11 Comparisons of proposed model with global GMPEs for an earthquake of M_w 8.0 showing 84-percentile values on rock site (V_{S30} = 800 m/s) at 5 km (left) and 200 km (right).

5.5 Detailed Evaluation of the Proposed Model for Future Versions

This section starts with investigation of M_w dependence on SoF and continues with a brief information on depth dependence for the horizontal ground-motion estimates. Besides the reasons for producing higher sigma with respect to new NGA-West2 GMPEs are searched. Figure 5.12 shows the variation of between-event residuals on M_w for different SoF for T = 0 s, T = 0.2 s and T = 1 s. The insignificant M_w-dependent between-event residual trends for normal and strike-slip estimates indicate better performance of the proposed model for these faulting mechanisms. However, the same performance is not observed for reverse earthquakes.
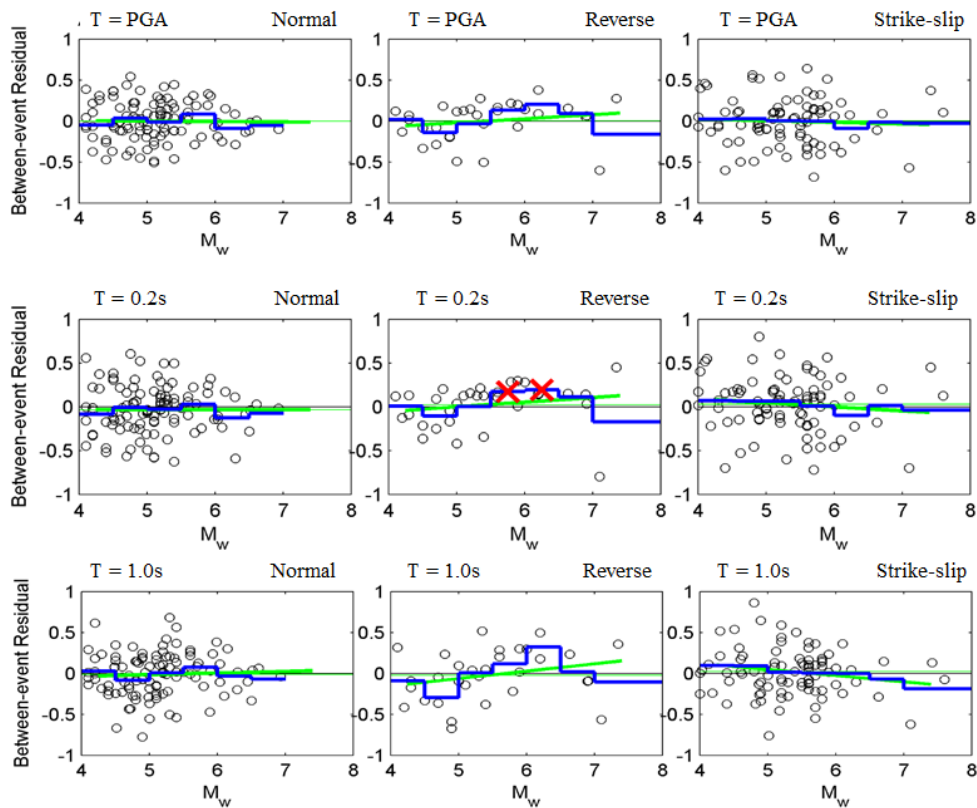
Figure 5. 12 Residual distribution of the proposed model for magnitude for different style-of-faulting

The event residuals are elaborately investigated to identify depth effect for style of faulting in Figures 5.13 and 5.14. Left, middle and right columns in these figures show normal, reverse and strike-slip earthquakes, respectively. Figure 5.13 displays the scatters for T = 0 s (top row), T =0.2 s (middle row) and T= 1 s (bottom row). Those for 2 s, 3 s and 4 s are presented in Figure 5.14. The variation of between-event residuals in terms of depth indicate that the bias in normal and strike-slip ground-motion estimations is insignificant. Normal earthquakes are not biased for the entire period and depth range. Estimates of strike-slip ground motions are conservative towards deeper events for the longest period (T = 4 s). Whereas, reverse ground-motion estimates are always biased (overestimated with increasing depth) in terms of depth for the entire spectral period range. These figures also advocates that the estimates of reverse earthquakes are limited when compared with normal and strike-slip events.
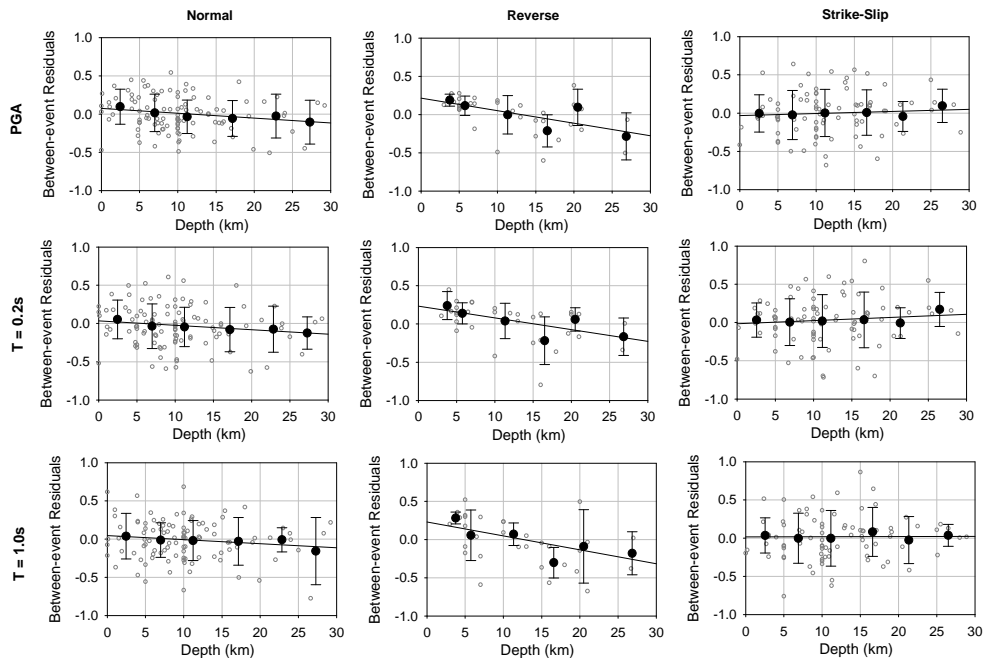
Figure 5. 13 Residual distribution of the proposed model for depth for different style-of-faulting for periods of 0 s, 0.2s and 1s.
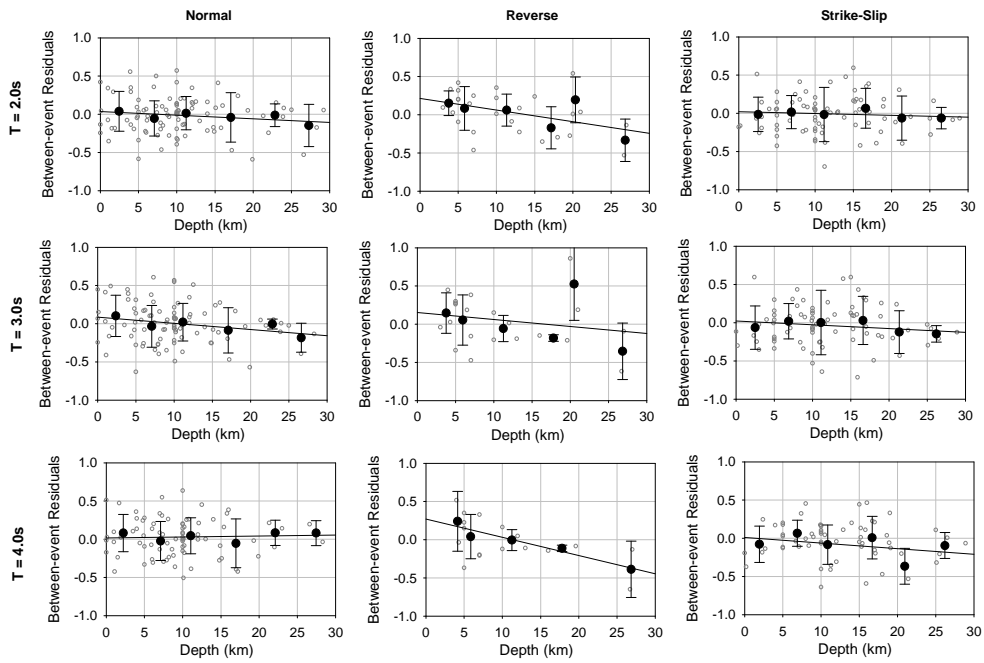
Figure 5. 14 Residual distribution of the proposed model for depth for different style-of-faulting for periods of 2 s, 3 s and 4s.

The magnitude variation of depth effect discussed in Figures 5.15 and 5.16. These plots are grouped for small (M_w 4 – 5) earthquakes (in upper panel) and moderate (M_w 5 – 6) earthquakes (in lower panel). The strong earthquakes (M_w > 6) are not included in these figures to avoid correlations between magnitude and depth (Chiou and Youngs, 2013). The first figure shows the residual distributions for periods 0 s, 0.2 s and 1 s (left middle and right columns); the second figure displays the scatters for long periods (i.e., T = 2 s, T = 3 s and T = 4 s in left middle and right columns, respectively). Depth seems to increase its effect on ground-motion estimates for moderate magnitudes towards longer periods (T ≥ 2 s). A similar conclusion is also observed for low magnitudes (M_w 4-5). However, it is not as visible as moderate magnitude events.

152
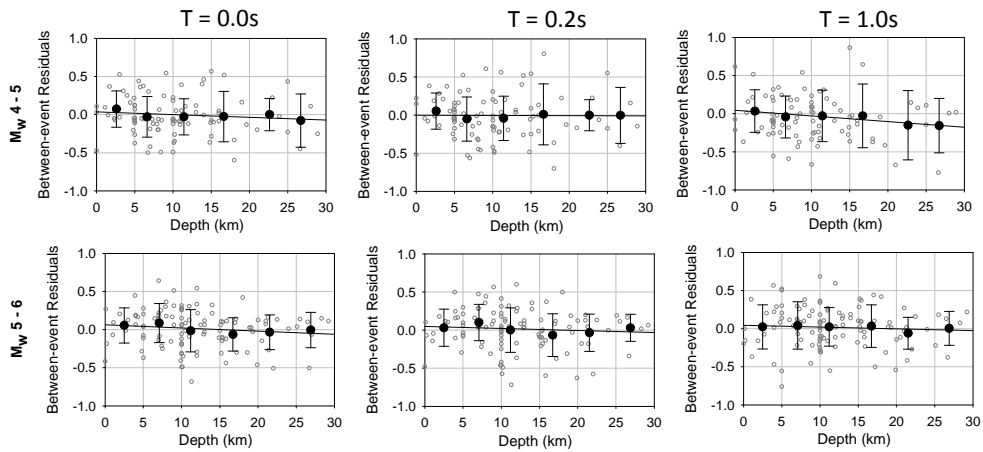
Figure 5. 15 Residual distribution of the proposed model for depth for different magnitude bins for periods of 0 s, 0.2s and 1s.
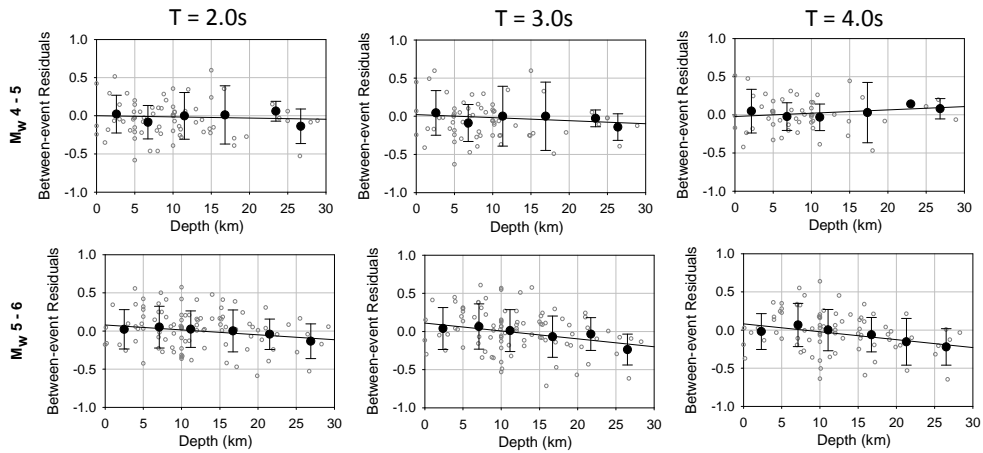
Figure 5. 16 Residual distribution of the proposed model for depth for different magnitude bins for periods of 2 s, 3 s and 4s.

Figure 5.17 shows the variation of tau (between-event standard deviation) and phi (within-event standard deviation) for small to large magnitude and short to long

distance ranges. Database contains few large magnitude events above M_w 7. Thus, the distribution of data does not allow establishing a magnitude-dependent sigma. However, it seems that small magnitude ($M_w < 5.5$) events increase tau towards longer periods. For short periods there is no major influence of distance on phi. A large bump in phi at longer periods is observed due to the existence of long-distance ($R_{JB} > 70$ km) recordings.
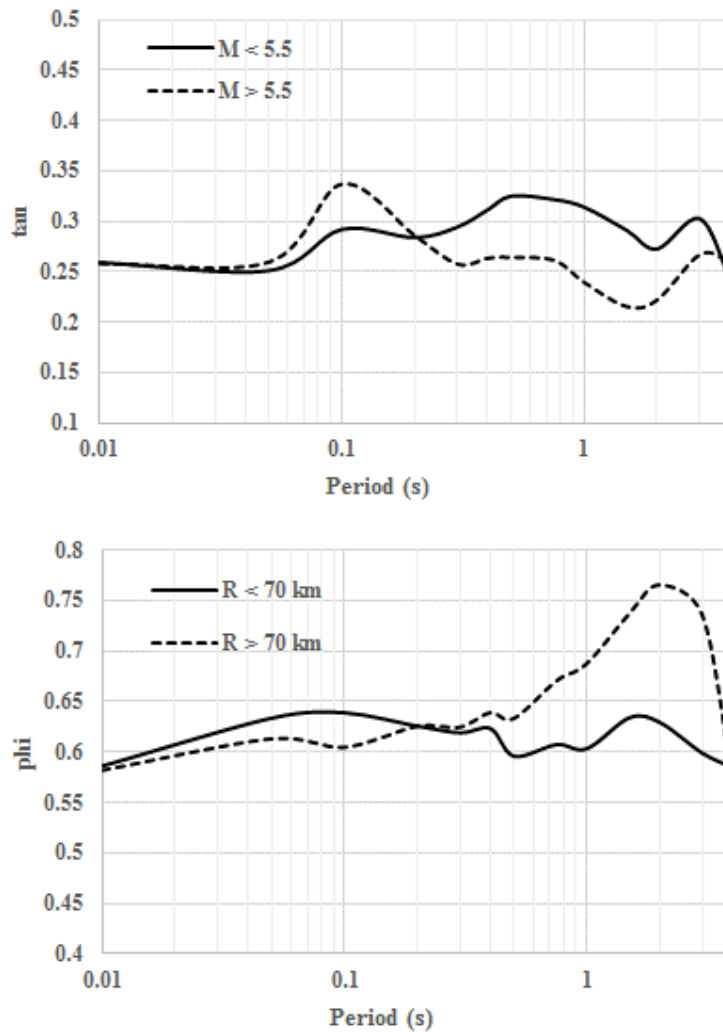
Figure 5. 17 Variation of tau (top plot) and phi (bottom plot) for magnitude and distance bins, respectively.

5.6 Conclusions

In this chapter, the new empirical GMPEs are presented for the prediction of PGA, PGV and ordinates of horizontal spectral acceleration at oscillator periods from 0.01 to 4.0 seconds derived from strong-motion recordings obtained in the Mediterranean region and the Middle East. It is believed that the models can be applied to earthquakes (of focal depth not greater than 30 km) with moment magnitudes in the range from 4 to 8, although we acknowledge that there is a possibility of over-estimating motions at the lower limit, and there is some uncertainty at the upper end, which is poorly constrained by the data (which only extends to M_w 7.6). The models include the influence of the style-of-faulting and are well constrained for normal, strike-slip and reverse ruptures. To facilitate hazard analyses using both fault and area sources, three models are presented using the R_{epi}, R_{hyp} and R_{JB} distance metrics; the models are applicable up to at least 200 km, and may be extrapolated beyond this limit with some caution. The models include nonlinear site response effects and can be applied for sites with V_{s30} values from 150 to 1200 m/s.

A topic of considerable debate in the recent literature is the nature of the sigma model to be used with GMPEs (Strasser *et al*., 2009; Al Atik *et al*., 2010). One pressing question is whether aleatory variability of ground motions from small earthquakes is inherently larger than that of ground motions from large events. For the development of this model we chose to assume a homoscedastic (magnitude-independent) sigma even though residual plots suggested that sigma could be lower for larger events. This decision was made since we do not feel that there are sufficient data from large earthquakes to obtain a robust estimate of the coefficients of a more sophisticated sigma model. In addition, although much effort has been made in improving the metadata of our strong-motion database we feel that some of the apparent scatter in the residual plots for small earthquakes is coming from uncertainties in the independent parameters (*e.g*., Figure 4.13 of Moss, 2009). There are, however, possible mechanisms for magnitude-dependent

sigma. Figures 2 and 3 of Douglas and Jousset (2011) suggest that variations in kappa, κ, (Anderson and Hough, 1984) between sites could be partly responsible for short-period ground-motion variability increasing with decreasing magnitude.

Although these new GMPEs are relatively complex compared to previous generations of pan-European ground-motion models, they are still simple representations of very complex processes. The source characteristics of earthquakes are represented only by magnitude and style-of-faulting, and the predictions may well be biased if the dataset from which the equations have been derived has not sampled, for example, the full range of stress drops from earthquakes of a given magnitude and rupture mechanism in the region. Such considerations lead to recognition of epistemic uncertainty in the median ground-motion predictions, which necessitates the combination of several GMPEs within a logic-tree framework (Bommer *et al*., 2005). The question that then immediately arises is: which other models should be combined with these GMPEs for PSHA in Europe and the Middle East?

These new equations supersede previous GMPEs derived for Europe and the Middle East, and address shortcomings identified in those models. Moreover, the formulation of the new equations covering broader ranges of response period, earthquake magnitude and distance, means that the former equations are not compatible with the new models. For PSHA studies in Europe and the Middle East, one option would be to construct logic-trees by combining these new GMPEs with the Next Generation of Attenuation (NGA) models of Abrahamson and Silva (2008), Boore and Atkinson (2008), Campbell and Bozorgnia (2008), and Chiou and Youngs (2008). These NGA models are broadly consistent with the new model in terms of parameterization, and it has been demonstrated that the NGA models are broadly applicable in Europe (Stafford *et al*., 2008a), although Scasserra *et al*. (2009) and Akkar and Çağnan (2010) found some systematic differences between the NGA predictions and strong-motion data from Italy and Turkey, respectively. In addition to recommending the use of the NGA models,

Bommer *et al.* (2010b) identified the GMPEs of Zhao *et al.* (2006), derived predominantly from Japanese data, as another candidate for selection within PSHA for shallow crustal seismicity. Additional logic-tree branches could be populated using local GMPEs, provided these were compatible in terms of parameter definitions.

CHAPTER 6

CONSISTENT EQUATIONS TO PREDICT VERTICAL-TO-HORIZONTAL SPECTRAL AMPLITUDE RATIOS AT MULTIPLE DAMPING LEVELS

Adapted from S. Akkar, M.A. Sandıkkaya, and B.Ö. Ay (2014c). Ground-motion prediction equations on damping scaling factors and vertical-to-horizontal spectral amplitude ratios for their implementation in the broader Europe region. Bulletin of Earthquake Engineering, 12:517–547.

Previous chapter present a new ground-motion prediction equation (GMPE) for estimating 5%-damped horizontal pseudo-acceleration spectral (PSA) ordinates for shallow active crustal regions in Europe and the Middle East. This study provides a supplementary viscous damping model to modify 5%-damped horizontal spectral ordinates of the horizontal GMPE, generated in the previous chapter, for damping ratios ranging from 1% to 50%. This chapter also presents another damping model for scaling 5%-damped vertical spectral ordinates that can be estimated from the vertical-to-horizontal (V/H) spectral ratio GMPE that is also developed within the context of this study. For consistency in engineering applications, the horizontal and vertical damping models cover the same damping ratios as noted above. The applicability range of the presented models is the same as of the horizontal GMPE: as for spectral periods $0.01s \leq T \leq 4s$ as well as PGA and PGV for V/H model; and in terms of seismological estimator parameters $4 \leq M_w \leq 8$, $R \leq 200$ km, 150 m/s $\leq V_{S30} \leq 1200$ m/s, for reverse, normal and strike-

slip faults. The source-to-site distance measures that can be used in the computations are epicentral (R_{epi}), hypocentral (R_{hyp}) and Joyner-Boore (R_{JB}) distances. The implementation of the proposed GMPEs will facilitate site-specific adjustments of the spectral amplitudes predicted from probabilistic seismic hazard assessment (PSHA) in Europe and the Middle East region. They can also help expressing the site-specific design ground motion in several formats. The consistency of the proposed models together with the horizontal GMPE may be advantageous for future modifications in the ground-motion definition in Eurocode 8 (CEN, 2004).

6.1 Introduction

Base isolated structures, tall buildings and buildings with supplementary damping devices as well as the simplified equivalent linear procedures that mimic the nonlinear response of structures require scaling of commonly provided 5%-damped response spectrum to different damping levels. In addition, the vertical seismic hazard becomes crucial especially for short-period critical structural facilities (e.g., nuclear power plants and dams) that are prone to structural damage upon the exceedance of a certain level of vertical displacement (Campbell and Bozorgnia, 2003; Gülerce and Abrahamson, 2011; Bommer et al., 2011). The vertical ground motions have also been identified as important for the design of lifeline systems and ordinary short-period structures in the vicinity of the fault (Elnashai and Papazoglu, 1997; Kunnath et al., 2008; Gülerce and Abrahamson, 2011). Thus, proper predictive models for describing vertical ground-motion demands and elastic spectral ordinates at different damping levels are always needed in the engineering community.

A detailed review on viscous damping scaling models for estimating spectral ordinates other than 5% of critical is given in Rezaeian et al. (2012) and Applied Technology Council (ATC, 2010). Currently, modern seismic design codes and guidelines suggest multiplicative factors to scale the 5%-damped elastic spectral

160

ordinates into ordinates for other damping ratios by period-independent tabulated values (e.g., NEHRP, 2009) or simple period-dependent expressions (e.g., Eurocode 8; CEN, 2004). These simplified factors or expressions aggregate the likely influence of seismological parameters from a broad perspective. Consequently, their implementation to site-specific (or project-specific) PSHA may not always describe the accurate period-dependent variation of spectral ordinates for different damping levels.

The evolutionary progress in vertical design spectrum is summarized by Bommer et al. (2011) and Bozorgnia and Campbell (2004). Although it was common to use the ratio of 2/3 between vertical and horizontal design spectra in the past codes (based on the findings of Newmark and Hall [1982]), the recent seismic codes (e.g., NEHRP and Eurocode 8) acknowledge the period-dependent differences in the spectral shapes of horizontal and vertical design spectra because the frequency content, magnitude- and distance-dependent scaling of horizontal and vertical ground motions differ. The aforementioned codes define simplified vertical-to-horizontal (V/H) spectral ratios that are conditioned on PGA (Eurocode 8) and PSA at $T = 0.2s$ (NEHRP). Though conceptually different, the period-dependent V/H spectral ratios defined by these codes consider magnitude and source-to-site distance effects on vertical design spectrum. The NEHRP provisions also consider the influence of site class on the V/H ratios whereas differences in site class are assumed to be insignificant in Eurocode 8. For practical reasons, the above described generic V/H ratios can be of use for defining vertical code-based spectrum. However, such oversimplified expressions are not appropriate for site-specific probabilistic hazard studies. PSHA requires consistent and compatible earthquake scenarios for horizontal and vertical ground motions that are determined through scenario spectrum (computed from deaggregation of hazard at a specific period) or conditional mean spectrum, CMS (Baker, 2011). (The reader is referred to Gülerce and Abrahamson [2011] for extended discussions on the implementation of V/H GMPEs to scenario spectrum and CMS). This point is even more important if vertical and horizontal acceleration time series have to be

selected and scaled for the target hazard levels. For such cases, empirical V/H spectral ratio models are required for a proper mapping of source, path and site effects on to V/H ratios. Moreover, such complete V/H GMPEs would be beneficial for further improvements in code-based generic V/H spectral ratio expressions.

This chapter describes a set of ground-motion predictive models for scaling 5%-damped horizontal and vertical spectral ordinates for viscous damping ratios varying between 1% and 50%. The chosen damping range can sufficiently address the needs of most seismic design and performance assessment projects. This study also describes a model for predicting the ratios of vertical-to-horizontal 5%-damped PSA ordinates. These predictive models are derived from the ground-motion database to develop the horizontal GMPE for its use in the seismic hazard assessment of shallow active crustal regions in Europe and the Middle East. Having been developed from the same pan-European ground-motion database with the same spectral period interval and capable of addressing different distance metrics, the predictive models presented in this paper are the first fully compatible GMPEs for producing consistent scenario-based horizontal and vertical design spectra at different damping levels that can be of use in many engineering applications in the broader Europe region. The applicability range of the proposed models in this paper is similar to the horizontal GMPE. This property can be useful in future studies to update the definitions of horizontal and vertical ground-motion demands in Eurocode 8. The epsilon-based correlation coefficients that are used for developing horizontal and vertical conditional mean spectra (CMS); a concept proposed by Baker (2011) that accounts for the period-dependent variability of ground motion for scenario spectrum is discussed in detail by Akkar et al. (2014c).

6.2 Predictive Equations for Damping Scaling Factors

Bommer and Mendis (2005), Lin et al. (2005) and Rezaeian et al. (2012) give a detailed literature review on the predictive models for damping scaling factor (DSF). As shown in Eq. (6.1), DSF is the normalized PSA of different damping levels (β) with PSA at 5% damping.

$$DSF = \frac{\text{PSA at } \beta\% \text{ damping}}{\text{PSA at } 5\% \text{ damping}}$$

(6.1)

Most of the previous DSF models are either built on β (e.g., Ashour, 1987; Tolis and Faccioli, 1999; Priestly, 2003) or β together with spectral period, T, (e.g., Newmark and Hall, 1982; Wu and Hanson, 1989; Idriss, 1993; Naeim and Kircher, 2001; Ramirez et al., 2000; 2002; Lin and Chang, 2003; Atkinson and Pierre, 2004; Malhotra, 2006; Eurocode 8, NEHRP). Few models discussed the effects of other independent parameters on DSF. Stafford et al. (2008b) emphasized the significance of duration whereas Abrahamson and Silva (1996) included M_w as an additional predictor variable in their model. Lin and Chang (2004) and Hartzigeorgiou (2010) indicated the role of site class on DSF and considered this parameter in their functional forms. Cameron and Green (2007) modeled the influence of tectonic regime in their damping scaling relationship together with other important estimator parameters such as M_w, site class and source-to-site distance. The most recent study conducted by Rezaeian et al. (2012) showed that magnitude, source-to-site distance and spectral period are sufficient for unbiased DSF estimates.

In this study, the natural logarithm of DSF is regressed against M_w, R_{JB}, SoF (style-of-faulting) and V_{S30} for each damping level and period. Other estimator parameters (e.g., duration) are not included to keep the model as simple as possible for lesser complexity in hazard studies. The same functional form with the horizontal model is chosen as the backbone expression for the DSF model.

The magnitude scaling in the model is quadratic with a break in the linear term whereas a magnitude-dependent geometrical spreading is considered to account for path effects. The site term is composed of linear and nonlinear terms for a realistic modeling of soil behavior. The functional form addresses the SoF effects on ground-motion amplitudes by dummy variables for normal and reverse events over strike-slip earthquakes. The preliminary regression results showed that the bilinear magnitude scaling function or consideration of higher order magnitude terms in the backbone functional form do not increase the accuracy of DSF estimates. The magnitude-dependent slope term in geometrical spreading also did not play an efficient role on the distance scaling of median DSF trends. None of these complicated functions in magnitude and distance scaling decreased the standard deviation (aleatory variability) of the model. The style-of-faulting effect is also disregarded in the final model as DSF is insensitive to different faulting mechanisms. The averages of residual distributions for each SoF are almost zero that also justifies the decision to disregard the SoF terms in the final DSF model. It should be noted that the non-uniform SoF distribution in the strong-motion database may mask the actual effect of this parameter on DSF. Thus, overlooking the SoF effect in the DSF predictive model can increase the epistemic uncertainty in DSF estimates. The fictitious depth term in distance scaling is also kept constant for all spectral periods to have a smooth variation in the spectral shape. Consideration of fictitious depth as a period-dependent parameter did not change the model estimates, which advocates its marginal effect on DSF estimations. The nonlinear site amplification term is dropped after the first round of regression analyses as the variation of DSF is independent of nonlinear soil behavior. Thus, the modification of DSF amplitudes due to different soil conditions is described by the linear site term. The linear site term is constrained to a constant value for $V_{S30} > 1000$ m/s. The V_{S30} for reference rock condition is defined as $V_{REF} = 750$ m/s in the site term. The final functional form of the DSF ground-motion model is given in Eq. 6.2.

$$\ln(DSF) = c_1 + c_2(M_w - 6.75) + c_3 \ln(\sqrt{{R_{JB}}^2 + c_5^2}) + c_4 \ln\left[\frac{\min(V_{S30}, 1000)}{V_{REF}}\right]$$

(6.2)

In the above expression, c_i (i = 1 to 4) denotes period-dependent regression coefficients computed by mixed-effects regression procedure (Abrahamson and Youngs, 1992). They are smoothened by moving average technique to prevent jagged DSF trends. The regression coefficient c_5 is the fictitious depth term and it is taken as constant ($c_5 = 5$) for the entire period range for horizontal and vertical DSF models. The previous models for DSF (e.g., Trifunac and Lee, 1989; Boore et al., 1993; Bommer et al., 1998; Berge-Thierry et al., 2003; Faccioli et al., 2004; Akkar and Boomer, 2007b) provide different sets of regression coefficients for each damping level. This approach is not followed in this study. Each regression coefficient c_i (i = 1 to 4) is represented by a quadratic function in terms of natural logarithm of β (in percent) as given in Eq. (6.3).

$$c_i = b_{i1} + b_{i2} \ln(\beta/5) + b_{i3}\left[\ln(\beta/5)\right]^2$$

(6.3)

The primary aim of this approach is to increase the applicability of the model. Newmark and Hall (1982) are the first proponents of such polynomial functions. In their paper, Newmark and Hall (1982) proposed a linear function. Polynomial functions with different orders are tried and the observations from these trials indicated that the quadratic function [Eq. (6.3)] is sufficient to explain the data trend. Rezaeian et al. (2012) also use a quadratic expression in their damping model. Figure 6.1 compares the performance of Eq. (6.3) with the discrete DSF estimates that are directly obtained from regressions on Eq. (6.2). The comparisons are done for different damping levels and for a strike-slip earthquake scenario of M_w 7.5. The rock site ($V_{S30} = 750$ m/s) is located at a distance of $R_{JB} = 10$ km from the causative fault. The left and right panels show the comparisons for horizontal and vertical spectral components, respectively. The patterns between the comparative plots overlap with each other that certify the success of Eq. (3) in

representing the regression coefficients c_i ($i = 1 - 4$) to estimate DSFs for different damping values. The rational functional form of Bommer et al. (1998) that is used in Eurocode 8 was also evaluated as an alternative to Eq. (6.3) while developing the proposed DSF model. However, it was discarded in the later stages of the study because the resultant DSF estimates were unrealistic.
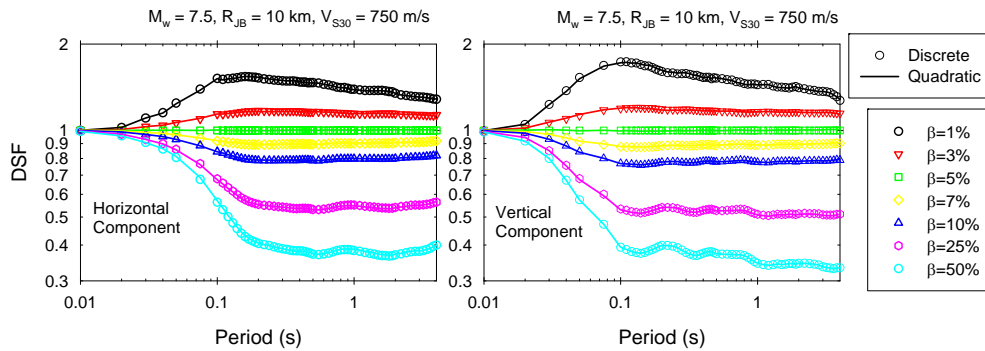
Figure 6. 1 Discrete damping scaling factors obtained from direct regressions on Eq. (2) for each damping level and their comparisons with those computed from Eq. (3) that describes each regression coefficient in Eq. (2) as a quadratic function

The within-event (ϕ) and between-event (τ) standard deviations are computed by using quadratic expressions that are given in Eqs. (6.4). The total standard deviation (σ) is the square root of the sum of the squares of within-event and between-event standard deviation terms.

Table 6.1 presents the horizontal spectral ordinate DSF regression coefficients b_{ij} for each c_i for a set of selected spectral periods. The index i varies from 1 to 3 whereas j takes values between 1 and 3. In a similar way, Table 6.2 lists the regression coefficients for the horizontal DSF model for index that varies from 4 to 6. In a similar way, the regression coefficients of vertical DSF model are given in Tables 6.3 and 6.4, respectively.

Table 6. 1. DSF regression coefficients for horizontal spectral ordinates (index i 1:3)

Per (s)	$c_{1,1}$	$c_{1,2}$	$c_{1,3}$	$c_{2,1}$	$c_{2,2}$	$c_{2,3}$	$c_{3,1}$	$c_{3,2}$	$c_{3,3}$
0.01	0.001198	-0.003583	-0.001243	0.00004	0.000045	0.000595	-0.000322	0.000585	0.00005
0.02	0.001663	-0.03478	-0.001645	-0.000418	0.000684	0.000079	-0.000319	0.007236	0.00023
0.03	0.005268	-0.106694	0.006535	-0.000405	0.002418	0.001401	-0.000927	0.021327	-0.001283
0.04	0.003168	-0.166434	0.005757	-0.000677	0.014843	0.00156	-0.000151	0.032546	-0.000589
0.05	0.001719	-0.233627	0.00509	-0.000174	0.019448	0.005037	0.000518	0.043221	0.000537
0.075	-0.002456	-0.332039	-0.009791	-0.000252	0.031044	0.008748	0.001643	0.051293	0.005062
0.1	0.001867	-0.371168	-0.031011	0.000455	0.028815	0.011975	0.000706	0.040656	0.010132
0.11	-0.000364	-0.373675	-0.040558	-0.000596	0.031434	0.011244	0.000925	0.037661	0.011263
0.12	-0.001186	-0.377048	-0.047884	-0.000626	0.028644	0.011762	0.000806	0.034583	0.01211
0.13	-0.00178	-0.379787	-0.05452	-0.001148	0.027479	0.011693	0.000832	0.031782	0.012883
0.14	-0.001594	-0.381415	-0.059684	-0.00123	0.025201	0.011853	0.00071	0.028922	0.013249
0.15	-0.001378	-0.380382	-0.063644	-0.001346	0.022613	0.011994	0.00053	0.025346	0.013599
0.16	-0.000582	-0.377459	-0.065949	-0.001417	0.020648	0.011903	0.000333	0.022042	0.013542
0.17	0.000208	-0.371299	-0.067499	-0.001694	0.019005	0.011638	0.000093	0.018396	0.013231
0.18	0.000872	-0.362222	-0.068412	-0.001657	0.016999	0.011702	-0.000168	0.014393	0.012805
0.19	0.001199	-0.351384	-0.069197	-0.001806	0.01565	0.011583	-0.000242	0.009607	0.0125
0.2	0.001431	-0.339975	-0.069768	-0.001754	0.014247	0.011454	-0.000416	0.005123	0.011979
0.22	0.001586	-0.327838	-0.070464	-0.00206	0.011892	0.01143	-0.000495	0.00108	0.01135
0.24	0.002105	-0.315717	-0.070923	-0.002182	0.010088	0.011109	-0.000594	-0.003132	0.010895
0.26	0.002804	-0.304897	-0.070892	-0.002165	0.007987	0.010586	-0.000717	-0.006867	0.010164
0.28	0.004145	-0.294767	-0.070115	-0.002006	0.00537	0.010175	-0.000927	-0.010194	0.009226
0.3	0.005664	-0.28422	-0.069107	-0.002022	0.002101	0.009863	-0.001149	-0.013484	0.008246
0.32	0.007143	-0.274344	-0.067769	-0.002065	-0.000089	0.009195	-0.001371	-0.016854	0.007402
0.34	0.008218	-0.265698	-0.066471	-0.002112	-0.002194	0.008566	-0.00148	-0.020294	0.00667

Table 6. 1. Cont'd

Per (s)	$c_{1,1}$	$c_{1,2}$	$c_{1,3}$	$c_{2,1}$	$c_{2,2}$	$c_{2,3}$	$c_{3,1}$	$c_{3,2}$	$c_{3,3}$
0.36	0.008927	-0.257991	-0.065481	-0.002071	-0.004226	0.008125	-0.001632	-0.023387	0.006179
0.38	0.009063	-0.251513	-0.064781	-0.002241	-0.005805	0.00746	-0.001694	-0.025139	0.005755
0.4	0.008775	-0.246997	-0.064325	-0.002033	-0.00671	0.006677	-0.001582	-0.025941	0.005468
0.42	0.008114	-0.243799	-0.064284	-0.001581	-0.007706	0.005991	-0.001307	-0.026552	0.005421
0.44	0.007134	-0.242254	-0.064324	-0.001433	-0.009329	0.005305	-0.000976	-0.026644	0.00544
0.46	0.006106	-0.240629	-0.064575	-0.001698	-0.011437	0.004457	-0.000753	-0.026202	0.005319
0.48	0.005699	-0.237598	-0.064764	-0.001869	-0.015801	0.003976	-0.0007	-0.026696	0.005412
0.5	0.005547	-0.233937	-0.064478	-0.002086	-0.018917	0.003051	-0.000799	-0.027922	0.005283
0.55	0.005902	-0.227787	-0.063816	-0.002023	-0.021514	0.00219	-0.000951	-0.029563	0.004973
0.6	0.006719	-0.21918	-0.062587	-0.001754	-0.023454	0.001243	-0.001203	-0.030602	0.004248
0.65	0.007664	-0.209426	-0.060909	-0.001134	-0.024118	-0.000032	-0.001237	-0.033047	0.003778
0.7	0.008197	-0.200941	-0.058852	-0.000893	-0.023582	-0.00131	-0.001233	-0.034908	0.003176
0.75	0.008193	-0.192299	-0.057169	-0.000946	-0.024425	-0.002061	-0.001218	-0.035802	0.002565
0.8	0.007737	-0.187147	-0.05501	-0.000803	-0.025553	-0.002822	-0.001235	-0.036442	0.00201
0.85	0.006921	-0.183878	-0.052973	-0.000748	-0.026675	-0.00361	-0.00091	-0.037481	0.001639
0.9	0.005683	-0.181413	-0.0512	-0.000797	-0.02836	-0.004125	-0.000811	-0.036848	0.000834
0.95	0.004432	-0.178706	-0.049728	-0.000661	-0.029596	-0.004948	-0.000657	-0.036489	-0.000088
1	0.00392	-0.176007	-0.048407	-0.000524	-0.030917	-0.005808	-0.0003	-0.037328	-0.000605
1.1	0.00354	-0.172026	-0.047984	-0.000475	-0.03233	-0.006967	-0.000181	-0.038261	-0.001109
1.2	0.003273	-0.168642	-0.047953	-0.000105	-0.034299	-0.008004	-0.000478	-0.039206	-0.001467
1.3	0.004041	-0.165618	-0.048207	-0.000114	-0.036783	-0.009048	-0.000307	-0.039997	-0.001539
1.4	0.004582	-0.163247	-0.048883	0.000208	-0.039958	-0.009621	-0.000272	-0.040345	-0.001507
1.5	0.004771	-0.162211	-0.04924	0.000871	-0.042245	-0.010325	-0.000369	-0.040711	-0.001462
1.6	0.005402	-0.159827	-0.049653	0.000671	-0.044556	-0.010893	-0.00045	-0.041551	-0.001238

Table 6. 1. Cont'd

Per (s)	$c_{1,1}$	$c_{1,2}$	$c_{1,3}$	$c_{2,1}$	$c_{2,2}$	$c_{2,3}$	$c_{3,1}$	$c_{3,2}$	$c_{3,3}$
1.7	0.006214	-0.15545	-0.050615	0.000453	-0.046388	-0.011147	-0.000422	-0.042106	-0.001265
1.8	0.006326	-0.150839	-0.051626	0.000749	-0.047341	-0.011352	-0.00071	-0.043461	-0.001195
1.9	0.006887	-0.145962	-0.051752	0.000907	-0.048125	-0.01187	-0.000888	-0.044858	-0.000985
2	0.007292	-0.139795	-0.052117	0.000892	-0.048915	-0.012606	-0.000913	-0.044916	-0.001084
2.2	0.007093	-0.134524	-0.052229	0.001483	-0.049503	-0.012962	-0.000991	-0.044289	-0.001453
2.4	0.00669	-0.130639	-0.05158	0.001621	-0.050316	-0.013436	-0.000938	-0.044246	-0.001558
2.6	0.006486	-0.125641	-0.050505	0.001606	-0.052324	-0.013918	-0.000807	-0.044382	-0.001794
2.8	0.005973	-0.121139	-0.049817	0.001536	-0.054696	-0.014115	-0.00059	-0.044748	-0.002101
3	0.005723	-0.117845	-0.049298	0.001401	-0.056772	-0.01428	-0.000611	-0.045178	-0.002463
3.2	0.00592	-0.114804	-0.04842	0.001165	-0.059332	-0.01454	-0.000507	-0.045084	-0.002638
3.4	0.006374	-0.112346	-0.047738	0.001233	-0.061839	-0.014872	-0.000532	-0.043907	-0.002856
3.6	0.007404	-0.110524	-0.047141	0.001582	-0.06282	-0.014968	-0.000838	-0.043355	-0.00299
3.8	0.008642	-0.108912	-0.046305	0.001913	-0.063498	-0.01532	-0.001223	-0.041707	-0.003019
4	0.011176	-0.105342	-0.045614	0.002951	-0.062127	-0.015186	-0.00186	-0.04301	-0.003083

Table 6. 2. DSF regression coefficients for horizontal spectral ordinates (index i 4:6)

Per (s)	$c_{4,1}$	$c_{4,2}$	$c_{4,3}$	$c_{5,1}$	$c_{5,2}$	$c_{5,3}$	$c_{6,1}$	$c_{6,2}$	$c_{6,3}$
0.01	-0.000104	0.001432	-0.001113	0.002946	-0.000801	0.002973	0.001733	-0.001036	0.001661
0.02	0.000387	-0.000458	-0.000593	0.009187	-0.002223	0.008102	0.002404	-0.000878	0.002426
0.03	0.000664	-0.010015	-0.000465	0.017113	-0.004702	0.016379	0.005133	-0.000508	0.00511
0.04	0.00105	-0.027819	0.000878	0.025923	-0.003586	0.022437	0.011986	-0.002245	0.010168
0.05	0.001386	-0.036499	-0.000082	0.034072	-0.002199	0.029385	0.013388	0.002185	0.013223
0.075	0.00189	-0.045716	-0.002116	0.049981	0.000757	0.041528	0.015192	0.003326	0.018309
0.1	0.001147	-0.071687	-0.003927	0.049716	0.002192	0.042586	0.018613	0.008826	0.020338
0.11	-0.000077	-0.070355	-0.007067	0.050906	0.003474	0.044142	0.016939	0.010836	0.018608
0.12	-0.000623	-0.069421	-0.008688	0.048794	0.005917	0.043688	0.015758	0.008756	0.01874
0.13	-0.000855	-0.066276	-0.010321	0.049482	0.005854	0.045078	0.01795	0.010481	0.018213
0.14	-0.000791	-0.063357	-0.010801	0.05029	0.006878	0.046018	0.015987	0.009588	0.016133
0.15	-0.000528	-0.059211	-0.011039	0.051899	0.007075	0.047045	0.013493	0.007444	0.015328
0.16	0.000303	-0.054272	-0.011062	0.051283	0.008596	0.045616	0.011828	0.004895	0.016461
0.17	0.00084	-0.048431	-0.011556	0.052515	0.008689	0.045543	0.010311	0.006781	0.015174
0.18	0.001049	-0.044683	-0.011715	0.052594	0.007462	0.045576	0.005307	0.014053	0.01158
0.19	0.001627	-0.040771	-0.011925	0.050862	0.008244	0.043968	0.007603	0.012962	0.012704
0.2	0.002233	-0.03628	-0.01206	0.04933	0.00793	0.043589	0.009903	0.01014	0.012507
0.22	0.001274	-0.030985	-0.012603	0.049599	0.00744	0.042197	0.006776	0.008648	0.012006
0.24	0.00083	-0.027351	-0.012505	0.049097	0.007933	0.041106	0.004006	0.007526	0.010042
0.26	0.000798	-0.02259	-0.012683	0.049156	0.006887	0.041119	0.00532	0.011031	0.008372
0.28	0.000417	-0.018338	-0.012925	0.046797	0.00886	0.039296	0.004508	0.003049	0.011614
0.3	0.000096	-0.013848	-0.01315	0.048411	0.005822	0.040023	0.000065	0.000723	0.012317
0.32	0.001339	-0.011517	-0.012204	0.04582	0.007919	0.039044	0.005954	0.005774	0.010546
0.34	0.002267	-0.009002	-0.011066	.047598	0.008419	0.039091	0.009196	0.006515	0.010593

Table 6. 2. Cont'd

Per (s)	$c_{4,1}$	$c_{4,2}$	$c_{4,3}$	$c_{5,1}$	$c_{5,2}$	$c_{5,3}$	$c_{6,1}$	$c_{6,2}$	$c_{6,3}$
0.36	0.002373	-0.007028	-0.009964	0.047687	0.006261	0.039839	0.008373	0.005588	0.011275
0.38	0.002352	-0.005277	-0.00854	0.046685	0.00796	0.03897	0.007153	0.003844	0.010994
0.4	0.001794	-0.00354	-0.006996	0.047006	0.008451	0.038979	0.006417	0.001097	0.012472
0.42	0.000926	-0.000815	-0.005594	0.045956	0.008206	0.037955	0.00181	0.000578	0.011294
0.44	0.000011	0.00295	-0.004432	0.0466	0.006039	0.037918	-0.00139	0.001132	0.010798
0.46	-0.000395	0.006462	-0.002845	0.046847	0.004706	0.037878	0.001956	0.001277	0.01092
0.48	-0.000752	0.011666	-0.001748	0.046123	0.005021	0.037462	0.006552	-0.001379	0.012708
0.5	-0.000904	0.015135	-0.000429	0.046804	0.005188	0.037081	0.00964	0.001451	0.011667
0.55	-0.000879	0.01957	0.000476	0.047627	0.002717	0.037808	0.006807	0.00519	0.011518
0.6	-0.000482	0.02424	0.001618	0.047041	0.006283	0.037808	0.011625	0.001197	0.011602
0.65	-0.000168	0.030389	0.002232	0.047956	0.00651	0.038104	0.013703	-0.00078	0.013925
0.7	0.000281	0.034155	0.003588	0.048875	0.00664	0.038906	0.011243	0.003032	0.014126
0.75	0.000301	0.039576	0.004235	0.046953	0.007885	0.038768	0.012584	0.001159	0.015274
0.8	0.000418	0.043503	0.004967	0.046667	0.006235	0.039088	0.008753	0.000646	0.015595
0.85	0.000231	0.045371	0.005493	0.045597	0.00783	0.038788	0.008177	0.000865	0.014339
0.9	-0.000471	0.04504	0.006022	0.047716	0.007407	0.039241	0.007104	0.002238	0.013873
0.95	-0.000966	0.046288	0.005401	0.048955	0.007055	0.039282	0.006429	0.001391	0.014226
1	-0.001115	0.044602	0.00561	0.049176	0.006004	0.040136	0.00439	0.006055	0.012511
1.1	-0.001404	0.042764	0.005353	0.049056	0.004678	0.04034	0.004903	0.007611	0.011879
1.2	-0.001481	0.04259	0.004633	0.047208	0.007015	0.040184	0.0124	0.005686	0.013838
1.3	-0.001178	0.042173	0.004045	0.04738	0.009113	0.039909	0.012595	0.005246	0.015471
1.4	-0.000771	0.038944	0.004233	0.0471	0.008369	0.04128	0.013987	0.00519	0.016563
1.5	-0.000238	0.036168	0.003788	0.047777	0.009043	0.042481	0.013316	0.006169	0.016945
1.6	-0.000359	0.031741	0.003688	0.047799	0.009581	0.042335	0.01432	0.005323	0.017025

Table 6. 2. Cont'd

Per (s)	$c_{4,1}$	$c_{4,2}$	$c_{4,3}$	$c_{5,1}$	$c_{5,2}$	$c_{5,3}$	$c_{6,1}$	$c_{6,2}$	$c_{6,3}$
1.7	-0.000563	0.027164	0.003411	0.046691	0.009466	0.041679	0.014472	0.003951	0.016891
1.8	0.000015	0.023683	0.002946	0.045496	0.011368	0.040733	0.013386	0.006491	0.016092
1.9	-0.00011	0.020185	0.00218	0.046512	0.009785	0.041552	0.011168	0.005633	0.016314
2	-0.000172	0.016833	0.001299	0.046394	0.011464	0.040939	0.01072	0.006785	0.015758
2.2	-0.000274	0.013358	0.000202	0.046274	0.010269	0.039861	0.011042	0.006316	0.0177
2.4	-0.000368	0.00878	-0.000701	0.043038	0.010498	0.038232	0.013628	0.010247	0.018992
2.6	-0.000526	0.005266	-0.001427	0.04113	0.010412	0.038615	0.016391	0.013159	0.019994
2.8	-0.000077	0.004193	-0.002302	0.045557	0.013118	0.039377	0.013846	0.012847	0.020176
3	-0.000176	0.004307	-0.002825	0.043665	0.010874	0.038291	0.014682	0.013664	0.020779
3.2	0.000714	0.006845	-0.002443	0.042241	0.011226	0.038653	0.015725	0.01524	0.022079
3.4	0.001252	0.009296	-0.001812	0.040201	0.013265	0.037647	0.013352	0.017222	0.020598
3.6	0.001469	0.010984	-0.000968	0.037598	0.01244	0.037877	0.014243	0.019259	0.020701
3.8	0.001828	0.01259	0.00057	0.038742	0.013908	0.037337	0.017206	0.017087	0.02149
4	0.002149	0.01449	0.000704	0.040025	0.014647	0.036967	0.017957	0.015872	0.02218

Table 6. 3. DSF regression coefficients for vertical spectral ordinates (index i 1:3)

Per (s)	$c_{1,1}$	$c_{1,2}$	$c_{1,3}$	$c_{2,1}$	$c_{2,2}$	$c_{2,3}$	$c_{3,1}$	$c_{3,2}$	$c_{3,3}$
0.01	0.002398	-0.00464	-0.002329	0.000134	0.000824	0.000178	-0.000542	0.001026	0.000096
0.02	0.005533	-0.063643	-0.002893	-0.000427	0.000809	-0.000312	-0.001106	0.012461	0.000398
0.03	0.010098	-0.217022	0.006742	0.000278	0.002155	0.001846	-0.001597	0.041863	-0.000766
0.04	0.005007	-0.34911	-0.000082	0.000571	0.008769	0.002005	-0.000976	0.06518	0.00136
0.05	-0.005796	-0.437401	-0.009405	-0.000859	0.006867	0.002161	0.001963	0.075147	0.005143
0.075	-0.002768	-0.48161	-0.038472	0.000331	0.009436	0.008139	0.001848	0.063017	0.012584
0.1	-0.005456	-0.5014	-0.055652	-0.000244	0.005231	0.008305	0.001058	0.054456	0.013547
0.11	-0.005321	-0.487036	-0.061233	0.000133	0.005868	0.008617	0.001598	0.046579	0.014917
0.12	-0.004554	-0.474134	-0.063871	-0.000922	0.004987	0.008774	0.000962	0.041097	0.01499
0.13	-0.003618	-0.460266	-0.066451	-0.001412	0.004785	0.009595	0.000829	0.034783	0.01547
0.14	-0.003118	-0.445742	-0.068239	-0.001994	0.005221	0.010448	-0.000151	0.029322	0.015305
0.15	-0.002316	-0.431245	-0.06884	-0.002297	0.004934	0.011808	-0.000398	0.025253	0.014911
0.16	-0.001357	-0.416486	-0.069049	-0.0023	0.005763	0.013051	-0.000287	0.019842	0.015042
0.17	-0.001318	-0.402139	-0.069206	-0.002426	0.007292	0.013729	-0.000516	0.015634	0.014835
0.18	-0.001545	-0.388019	-0.069163	-0.002199	0.008689	0.014121	-0.000834	0.012086	0.014492
0.19	-0.000934	-0.376866	-0.068061	-0.001818	0.010312	0.013874	-0.000708	0.009533	0.013911
0.2	0.000263	-0.364613	-0.067487	-0.002131	0.011499	0.013214	-0.000654	0.006098	0.013541
0.22	0.000892	-0.354758	-0.066988	-0.001935	0.010562	0.013083	-0.00109	0.00417	0.012585
0.24	0.002223	-0.346716	-0.066477	-0.001348	0.009223	0.012916	-0.001175	0.001226	0.011875
0.26	0.003516	-0.340325	-0.065948	-0.001482	0.006536	0.012157	-0.001447	-0.000335	0.01078
0.28	0.003844	-0.33478	-0.065578	-0.001819	0.002092	0.011594	-0.001734	-0.002994	0.010115
0.3	0.003355	-0.330408	-0.065185	-0.001649	-0.000782	0.010869	-0.001561	-0.005242	0.009268
0.32	0.003127	-0.325206	-0.064505	-0.002231	-0.002902	0.009834	-0.001013	-0.006598	0.008191
0.34	0.002587	-0.318148	-0.063988	-0.002565	-0.003242	0.008364	-0.000919	-0.00842	0.007323

Table 6. 3. Cont'd

Per (s)	$c_{1,1}$	$c_{1,2}$	$c_{1,3}$	$c_{2,1}$	$c_{2,2}$	$c_{2,3}$	$c_{3,1}$	$c_{3,2}$	$c_{3,3}$
0.36	0.002635	-0.311328	-0.063276	-0.001992	-0.003533	0.007827	-0.000512	-0.011241	0.00695
0.38	0.003003	-0.302229	-0.063283	-0.001684	-0.00164	0.007089	-0.00015	-0.012996	0.006611
0.4	0.003602	-0.295165	-0.062644	-0.001086	-0.002172	0.007274	-0.000259	-0.013997	0.006229
0.42	0.003742	-0.289214	-0.062237	-0.000419	-0.002307	0.007333	-0.000281	-0.016076	0.006312
0.44	0.003663	-0.284528	-0.0617	-0.000272	-0.003928	0.007634	-0.000296	-0.017191	0.006256
0.46	0.003071	-0.27969	-0.061388	-0.000811	-0.005116	0.007125	-0.00059	-0.017439	0.005873
0.48	0.002673	-0.277195	-0.060256	-0.001952	-0.007886	0.006546	-0.000505	-0.019322	0.005918
0.5	0.00246	-0.274481	-0.059318	-0.002575	-0.00901	0.005028	-0.000643	-0.020396	0.0055
0.55	0.00226	-0.270912	-0.058583	-0.002412	-0.011116	0.00383	-0.000425	-0.020463	0.004906
0.6	0.002553	-0.268619	-0.057152	-0.001704	-0.01313	0.00245	-0.000136	-0.019455	0.004016
0.65	0.002352	-0.265989	-0.056048	-0.001244	-0.013523	0.000947	0.00028	-0.019759	0.003441
0.7	0.001766	-0.261392	-0.055765	0.000029	-0.012672	-0.000296	0.000475	-0.019565	0.002484
0.75	0.001086	-0.255241	-0.055569	0.000542	-0.013115	-0.001237	0.000952	-0.020973	0.002209
0.8	0.000546	-0.248719	-0.055317	0.000431	-0.01242	-0.002821	0.000722	-0.022983	0.001722
0.85	-0.000006	-0.242969	-0.055525	0.000102	-0.012571	-0.004134	0.000637	-0.025781	0.001442
0.9	-0.000074	-0.238624	-0.055811	0.000087	-0.015448	-0.004781	0.000413	-0.028597	0.001228
0.95	0.000436	-0.235569	-0.055962	-0.000473	-0.019932	-0.006161	0.000204	-0.029849	0.001027
1	0.001147	-0.234123	-0.056508	-0.000345	-0.024052	-0.00721	-0.000269	-0.029437	0.000776
1.1	0.002061	-0.233305	-0.057747	-0.000121	-0.027519	-0.007957	-0.000382	-0.029775	0.001095
1.2	0.002839	-0.231342	-0.058929	-0.000001	-0.030023	-0.008796	-0.000731	-0.030423	0.001555
1.3	0.003696	-0.226097	-0.060275	-0.000039	-0.031065	-0.010013	-0.00049	-0.029598	0.001647
1.4	0.004625	-0.219855	-0.061217	0.000686	-0.033173	-0.009714	-0.00061	-0.029653	0.001484
1.5	0.005222	-0.215143	-0.061177	0.00074	-0.033418	-0.010276	-0.000882	-0.03177	0.001425
1.6	0.005425	-0.210931	-0.060007	0.000846	-0.035041	-001062	-0.001196	-0.032543	0.001083

Table 6. 3. Cont'd

Per (s)	$c_{1,1}$	$c_{1,2}$	$c_{1,3}$	$c_{2,1}$	$c_{2,2}$	$c_{2,3}$	$c_{3,1}$	$c_{3,2}$	$c_{3,3}$
1.7	0.005197	-0.204898	-0.057848	0.000959	-0.042921	-0.009719	-0.000966	-0.032705	0.000312
1.8	0.003944	-0.205839	-0.057175	0.000911	-0.043165	-0.010245	-0.000818	-0.033562	0.000472
1.9	0.002785	-0.203641	-0.058086	0.001242	-0.044222	-0.010252	-0.000316	-0.032041	0.000413
2	0.002586	-0.200419	-0.060056	0.001381	-0.046168	-0.010115	-0.000022	-0.031397	0.000609
2.2	0.002809	-0.198664	-0.061972	0.001036	-0.046316	-0.01088	0.000036	-0.031227	0.000946
2.4	0.003506	-0.19657	-0.063649	0.00157	-0.04728	-0.011767	-0.000208	-0.031229	0.001362
2.6	0.00471	-0.195028	-0.06525	0.001866	-0.050844	-0.012131	-0.00046	-0.030049	0.0013
2.8	0.006202	-0.193888	-0.066752	0.001639	-0.055756	-0.012437	-0.000538	-0.030022	0.001253
3	0.007214	-0.193132	-0.067857	0.00192	-0.05844	-0.013605	-0.000484	-0.029197	0.001341
3.2	0.007918	-0.190657	-0.069582	0.002666	-0.060099	-0.014617	-0.000596	-0.02892	0.001585
3.4	0.008474	-0.184637	-0.072077	0.002605	-0.061309	-0.015424	-0.000849	-0.028894	0.001635
3.6	0.008474	-0.184637	-0.072077	0.002605	-0.061309	-0.015424	-0.000849	-0.028894	0.001635
3.8	0.009178	-0.177587	-0.0746	0.003055	-0.060945	-0.017035	-0.000924	-0.029093	0.002373
4	0.009549	-0.164839	-0.077598	0.001935	-0.060043	-0.017629	-0.001853	-0.031433	0.002593

Table 6. 4. DSF regression coefficients for vertical spectral ordinates (index i 4:6)

Per (s)	$c_{4,1}$	$c_{4,2}$	$c_{4,3}$	$c_{5,1}$	$c_{5,2}$	$c_{5,3}$	$c_{6,1}$	$c_{6,2}$	$c_{6,3}$
0.01	-0.00034	0.001767	-0.000415	0.005265	0.000924	0.005494	0.003564	-0.001349	0.002088
0.02	0.000423	-0.003151	-0.000152	0.014935	-0.004563	0.013462	0.005076	-0.002262	0.003633
0.03	0.000357	-0.017093	0.001313	0.035034	-0.007566	0.028221	0.008231	-0.000475	0.009057
0.04	-0.003918	-0.022082	0.000569	0.052255	-0.003483	0.039481	0.015437	-0.001977	0.01255
0.05	-0.001599	-0.022765	0.006149	0.058578	-0.004056	0.044772	0.010115	0.000274	0.013369
0.075	0.002601	-0.013952	0.000355	0.068836	0.000203	0.050315	0.011068	0.005923	0.016025
0.1	-0.004594	-0.015657	-0.005487	0.065102	0.001334	0.050329	0.015893	0.000911	0.018006
0.11	-0.00237	-0.015021	-0.004874	0.065388	0.005113	0.049697	0.012199	-0.001115	0.017943
0.12	-0.002124	-0.017066	-0.005098	0.062369	0.00345	0.048923	0.012079	0.009378	0.014058
0.13	-0.001467	-0.017985	-0.004575	0.063965	0.003345	0.049209	0.013143	0.002487	0.016381
0.14	-0.002168	-0.018375	-0.004317	0.06462	0.002566	0.049741	0.008376	0.006321	0.013896
0.15	-0.001455	-0.016471	-0.003839	0.062401	0.004246	0.049681	0.00669	0.004142	0.011661
0.16	-0.00162	-0.01284	-0.003721	0.062212	0.003591	0.050563	-0.000384	0.003411	0.008881
0.17	-0.001955	-0.010485	-0.003294	0.063568	0.004546	0.050406	0.000972	-0.002103	0.010614
0.18	-0.002101	-0.005612	-0.004145	0.063156	0.003768	0.049844	0.001774	-0.000267	0.009441
0.19	-0.002486	-0.00216	-0.005001	0.060692	0.003161	0.047906	0.007613	0.005473	0.008588
0.2	-0.002095	-0.001823	-0.004699	0.064469	0.004089	0.046537	0.006733	0.004407	0.011793
0.22	-0.002291	0.001452	-0.005859	0.063859	0.001044	0.046035	0.001468	0.004766	0.011344
0.24	-0.00201	0.002459	-0.006167	0.062011	0.006405	0.044901	0.008289	-0.000681	0.014418
0.26	-0.00181	0.002736	-0.006429	0.063701	0.002372	0.046284	0.001961	0.00689	0.012195
0.28	-0.001519	0.003179	-0.00726	0.061833	0.004709	0.0458	0.00439	0.005575	0.012368
0.3	-0.001185	0.003087	-0.008314	0.061431	0.004647	0.045281	0.008272	0.000026	0.012741
0.32	0.000444	0.001558	-0.008355	0.06281	0.001688	0.045761	-0.000874	0.0047	0.009664
0.34	0.00097	0.004247	-0.009892	0.063205	0.003423	0.045113	0.000119	-0.00208	0.010754

Table 6. 4. Cont'd

Per (s)	$c_{4,1}$	$c_{4,2}$	$c_{4,3}$	$c_{5,1}$	$c_{5,2}$	$c_{5,3}$	$c_{6,1}$	$c_{6,2}$	$c_{6,3}$
0.36	0.000682	0.004173	-0.010173	0.062157	0.002844	0.045202	0.009247	0.001978	0.010424
0.38	0.00122	0.00594	-0.009748	0.062162	0.00517	0.044573	0.008306	-0.001519	0.012657
0.4	0.001091	0.010125	-0.009797	0.062847	0.005084	0.044374	0.005145	0.000695	0.013102
0.42	0.00065	0.01409	-0.009597	0.061823	0.004932	0.044041	0.009231	0.004164	0.010869
0.44	0.000556	0.014618	-0.007867	0.060025	0.005299	0.044823	0.009011	-0.00034	0.01235
0.46	0.000685	0.018962	-0.007139	0.06147	0.004647	0.045031	0.004025	0.004381	0.013422
0.48	0.000582	0.020312	-0.005466	0.061463	0.003261	0.04485	0.005712	0.003043	0.015053
0.5	-0.000211	0.02152	-0.003585	0.058855	0.002856	0.044091	0.012835	0.002618	0.016743
0.55	0.000019	0.020927	-0.000557	0.06259	0.000701	0.043592	0.013275	0.007927	0.014642
0.6	-0.000122	0.024662	0.000744	0.062653	0.002335	0.044107	0.00936	0.007473	0.013238
0.65	0.000353	0.02648	0.00215	0.061933	0.003098	0.044236	0.007668	0.007747	0.013547
0.7	0.000848	0.030626	0.002224	0.064996	0.003305	0.044838	0.012634	-0.000478	0.017226
0.75	0.000718	0.031537	0.00227	0.064181	0.006075	0.044561	0.008911	-0.001321	0.013721
0.8	-0.00008	0.029522	0.002085	0.062139	0.004533	0.045227	0.011312	0.003193	0.010945
0.85	-0.001193	0.025184	0.002544	0.063628	0.004962	0.044928	0.017998	-0.003538	0.01466
0.9	-0.002068	0.019561	0.003963	0.060412	0.00556	0.045184	0.016523	0.009096	0.012247
0.95	-0.002713	0.018255	0.004831	0.062134	0.005231	0.045533	0.017885	0.002921	0.015468
1	-0.002562	0.017635	0.006128	0.063034	0.005479	0.045448	0.016261	0.001629	0.015567
1.1	-0.002163	0.022945	0.006041	0.062863	0.003001	0.046209	0.016341	0.002617	0.016774
1.2	-0.000947	0.02498	0.007309	0.060355	0.003395	0.045203	0.019745	0.007521	0.017371
1.3	-0.000483	0.027385	0.007075	0.062563	0.003429	0.045784	0.012593	0.007868	0.017438
1.4	-0.001223	0.025159	0.006963	0.062277	0.003299	0.046363	0.009416	0.013682	0.014901
1.5	-0.001717	0.02434	0.00653	0.06232	0.002838	0.04653	0.012108	0.009527	0.017909
1.6	-0.002143	0.021874	0.006875	0.060335	0.008063	0. 046194	0.011315	0.007898	0.018017

Table 6. 4. Cont'd

Per (s)	$c_{4,1}$	$c_{4,2}$	$c_{4,3}$	$c_{5,1}$	$c_{5,2}$	$c_{5,3}$	$c_{6,1}$	$c_{6,2}$	$c_{6,3}$
1.7	-0.002328	0.021344	0.006243	0.058562	0.010029	0.046553	0.009462	0.006933	0.017691
1.8	-0.002538	0.021828	0.005596	0.05856	0.007745	0.0485	0.011669	0.003045	0.016991
1.9	-0.001852	0.020015	0.005275	0.060049	0.009812	0.047146	0.0083	0.002958	0.01644
2	-0.001802	0.017399	0.003592	0.058796	0.008895	0.046878	0.008415	0.004801	0.01597
2.2	-0.001918	0.011741	0.002172	0.055582	0.01225	0.044625	0.013161	0.008576	0.017779
2.4	-0.00195	0.007394	0.000362	0.056639	0.013326	0.044615	0.013664	0.007564	0.018964
2.6	-0.001244	0.002093	-0.000681	0.057609	0.010431	0.047204	0.013016	0.009103	0.017472
2.8	-0.000963	-0.001297	-0.001874	0.055834	0.010866	0.045798	0.008765	0.009666	0.018857
3	0.000168	-0.004262	-0.00249	0.052093	0.011071	0.042998	0.01788	0.006693	0.022389
3.2	0.00075	-0.004724	-0.003189	0.052859	0.011876	0.041458	0.016052	0.013187	0.022183
3.4	0.000779	-0.004645	-0.003905	0.054074	0.010841	0.042883	0.013872	0.018451	0.020529
3.6	0.000372	-0.005678	-0.005073	0.054753	0.009288	0.04328	0.015853	0.017219	0.020888
3.8	-0.000109	-0.005442	-0.005668	0.050652	0.014105	0.042251	0.017265	0.015855	0.020985
4	-0.001065	-0.009397	-0.007537	0.047785	0.014943	0.041903	0.0197	0.015215	0.021287

$$\phi = b_{51} + b_{52} \ln(\beta / 5) + b_{53} \left[\ln(\beta / 5)\right]^2 \tag{6.4a}$$

$$\tau = b_{61} + b_{62} \ln(\beta / 5) + b_{63} \left[\ln(\beta / 5)\right]^2 \tag{6.4b}$$

$$\sigma = \sqrt{\phi^2 + \tau^2} \tag{6.4c}$$

Figure 6.2 shows the magnitude, distance and V_{S30} dependent variations of the proposed DSF model for horizontal (left column) and vertical (right column) PSA ordinates at T=0.1 s. The effect of damping is prominent at short spectral periods, which is the main reason for choosing T = 0.1 s in this illustrative case. The effect of magnitude scaling on DSF is presented on the 1st row for a stiff site (V_{S30} = 525 m/s) located at a distance of R_{JB} = 15 km from the causative fault. The magnitude influence is more visible on horizontal ground motions when β attains larger values. The variations in DSF for vertical spectral ordinates are less sensitive to magnitude. However, as in the case of horizontal DSF model, magnitude effect starts contributing to vertical DSF variations for heavily damped structural systems (i.e., β ≥ 20%). Distance-dependent scaling of DSF is plotted in the 2nd row on Figure 6.2 for M_w 6 and V_{S30} = 525 m/s. The effect of distance on DSF seems to be more apparent than the influence of magnitude. The decay due to geometrical spreading of DSF is faster at very low (β < 3%) and high (β > 15%) damping ratios. The 3rd row plots on Figure 6.2 shows the V_{S30} scaling of DSF for a scenario event of M_w 6 and R_{JB} = 15 km. The damping scaling of horizontal ground motions grows with increasing V_{S30} up to 1000 m/s and becomes stable after V_{S30} = 1000 m/s (imposed by the site model). This trend is more visible at lower and higher damping ratios. As in the case of magnitude, the damping scaling of vertical spectrum becomes sensitive to the changes in V_{S30} when β attains larger values (i.e., β ≥ 20%).

Figure 6.3 compares the horizontal (top row) and vertical (bottom row) DSF models with those of Rezaeian et al. (2012) and Eurocode 8. The Rezaeian et al. (2012) model is abbreviated as Retal12 on the plots. The comparisons are made for two different magnitudes: M_w 4.5 (left column) and M_w 7.5 (right column) that
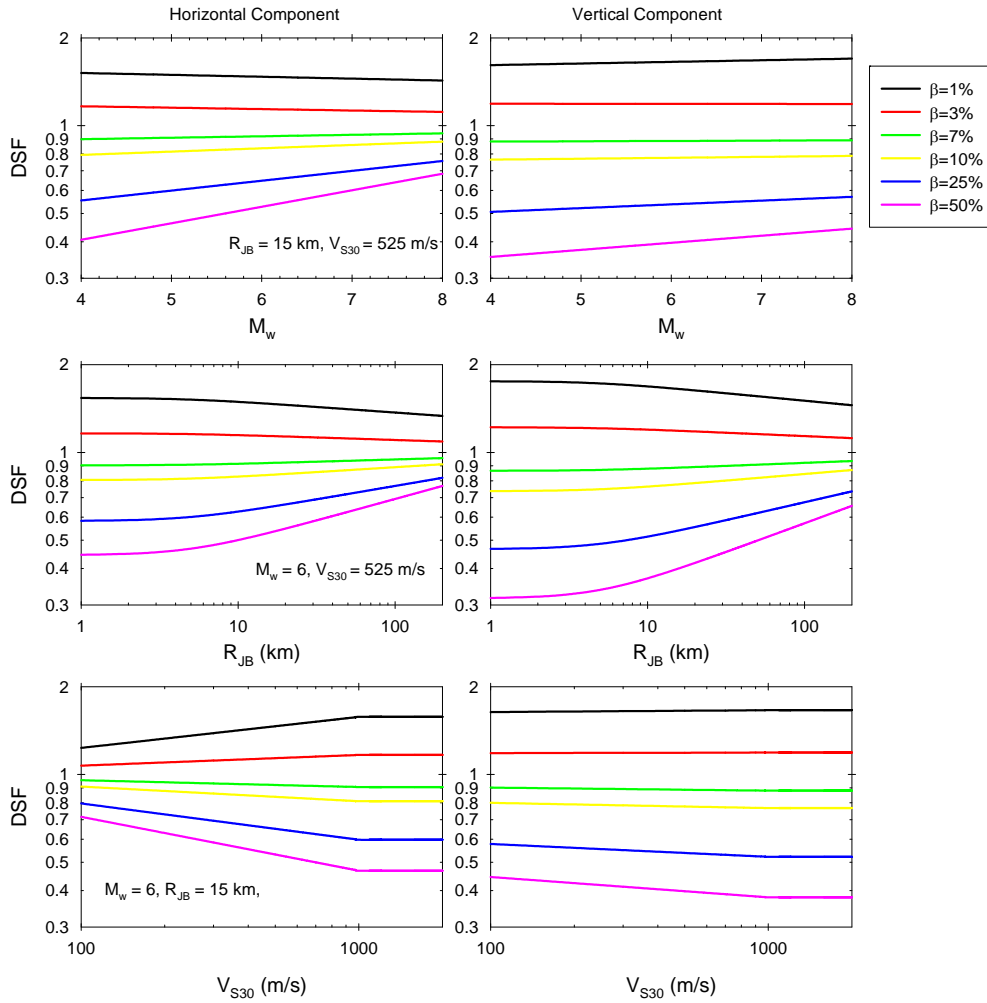
Figure 6. 2. Magnitude (first row), distance (second row) and V_{S30} (third row) dependent variation of horizontal (left panel) and vertical (right panel) DSF at T=0.1s

resemble low seismicity (Type II) and high seismicity (Type I) regions, respectively according to Eurocode 8. The fictitious site is selected as a generic rock site with V_{S30}=800 m/s. It is located at a distance of R_{JB} = 10 km from a 90 degrees dipping strike-slip fault. The top of the ruptured fault segment is assumed to be 5 km below the surface for both cases. Under this simple source geometry

the corresponding rupture distance (R_{rup}; the distance measure used in the Retal12) is computed as 11.2 km. The comparative plots indicate that DSF estimates of this study and Retal12 agree with each other fairly well. There are differences in the DSF values of Eurocode 8 and the other two GMPEs. The Eurocode 8 damping scaling is sensitive to period variation only in the very short spectral period range. The other two DSF models consider the period influence on damping for the entire period band. This conceptual difference between Eurocode
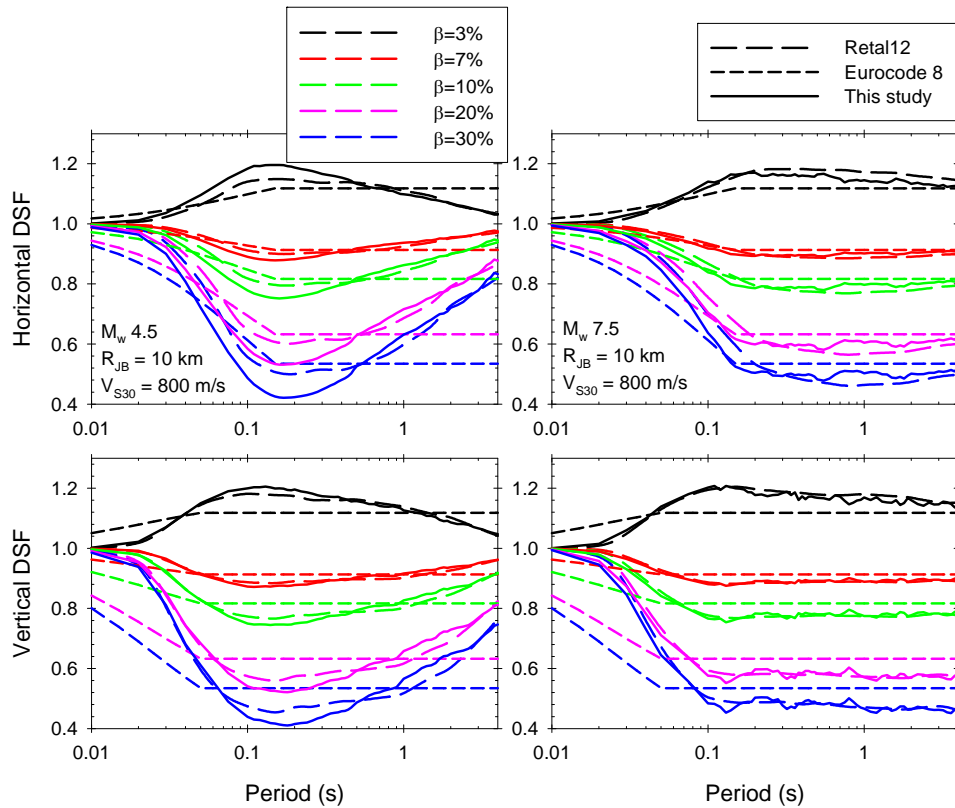
Figure 6. 3. Horizontal (top row) and vertical (bottom row) DSF values of the proposed model as well as those of Rezaeian et al (2012; Retal12) and Eurocode 8 for M_w 4.5 (left panel) and M_w 7.5 (right panel) at R_{JB}=10 km for a rock site of V_{S30}=800 m/s

8 and the other two DSF models show itself particularly in low seismicity regions (mimicked by M_w 4.5), towards longer periods (T > 1.0s) and when β attains large values. For short-period spectral regions the two DSF models tend to estimate larger spectral ordinates with respect to Eurocode 8. The less conservative short-period Eurocode 8 damping scaling is prominent in vertical spectral ordinates and at large damping values. These discussions advocate the reconsideration of damping scaling in the future modifications of Eurocode 8 ground-motion definition.

The last figure (Figure 6.4) in this section shows the significance of aleatory variability in DSF estimates. The left and right panels in this figure depict median and ± sigma horizontal and vertical DSF estimates of the proposed model for β = 1% and 10%. The chosen scenario event has a moment magnitude of M_w 7.0; however, it is noted that our sigma is independent of magnitude. The site resembles stiff soil conditions (V_{S30} = 400 m/s) and it is located R_{JB} = 10 km from a strike-slip fault. The comparative plots indicate that the aleatory variability is more significant in vertical DSF amplitudes.
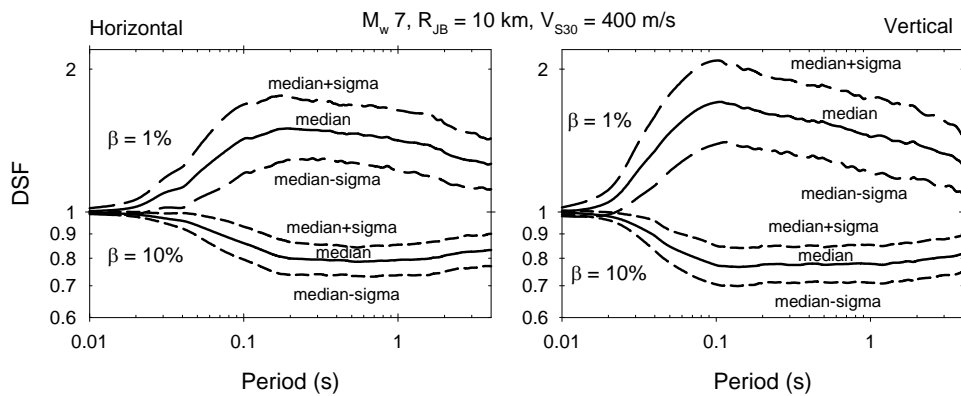
Figure 6. 4. Effect of aleatory variability on horizontal and vertical DSF models proposed in this study.

6.3 Vertical-to-Horizontal (V/H) Spectral Amplitude Ratio Predictive Model

The vertical-to-horizontal PSA GMPE presented in this section differs from the recently proposed vertical ground-motion models in Europe. This part of the study only discusses the most recent vertical ground-motion models in Europe. The reader is referred to Bommer et al. (2011) for a detailed literature review on the entire progress of pan-European vertical GMPEs. The proposed model is capable of estimating V/H ratios for all site conditions that makes it different from the V/H models of Edwards et al. (2011) and Poggi et al. (2012) that are valid for rock and soft sites, respectively. Although the empirical V/H model proposed in this study as well as the one proposed by Bommer et al. (2011) are based on European datasets, the GMPE of this study is developed on a more comprehensive and recently revised pan-European ground-motion database. The other major difference between the V/H model of this study and Bommer et al. (2011) is the consideration of site response function. The site term of our model is a continuous function of V_{S30} and considers soil nonlinearity whereas Bommer et al. (2011) use a set of dummy parameters to account for the site effects. Besides, the proposed V/H model is fully compatible with the pan-European 5%-damped horizontal GMPE because the database, thus all metadata and record processing, is common in both models. This property makes it more useful in probabilistic seismic hazard assessment of broader Europe region for computing consistent horizontal and vertical pseudo-acceleration spectral ordinates for scenario-specific engineering studies. The presented V/H GMPE is also different from the model proposed by (Ambraseys et al., 2005b) as the latter developed an independent GMPE for the estimation of vertical spectral ordinates. The approach in Ambraseys et al. (2005b) may produce vertical and horizontal spectral accelerations that are controlled by different earthquake scenarios. As discussed briefly in Introduction section, different controlling earthquake scenarios for horizontal and vertical ground motions may cause practical difficulties in seismic design and performance assessment procedures that utilize compatible horizontal and vertical spectral demands. This shortcoming is prevailed by using V/H models as

183

suggested in this paper. The particular features of the proposed V/H GMPE are described in the following paragraphs.

The proposed V/H model (Equations 6.5) uses a functional form similar to that of the horizontal GMPE for producing compatible vertical PSA as emphasized throughout the text.

$$\ln(V/H) = \begin{cases} a_1 + a_2(M_w - 6.75) + a_3(8.5 - M_w)^2 + [a_4 + a_5(M_W - 6.75)]\ln(\sqrt{R_{JB}^2 + a_6^2}) + \\ a_8 F_N + a_9 F_R + \ln(S) \qquad\qquad \text{for } M_w \leq 6.75 \\ a_1 + a_7(M_w - 6.75) + a_3(8.5 - M_w)^2 + [a_4 + a_5(M_W - 6.75)]\ln(\sqrt{R_{JB}^2 + a_6^2}) + \\ a_8 F_N + a_9 F_R + \ln(S) \qquad\qquad \text{for } M_w > 6.75 \end{cases}$$

(6.5a)

$$\ln(S) = \begin{cases} a_{10} \ln(\dfrac{V_{S30}}{V_{REF}}) - a_{11} \ln\left[\dfrac{PGA_{REF} + c(V_{S30}/V_{REF})^n}{(PGA_{REF} + c)(V_{S30}/V_{REF})^n} \right] & \text{for } V_{S30} \leq V_{REF} \\ a_{10} \ln\left[\dfrac{\min(V_{S30},1000)}{V_{REF}} \right] & \text{for } V_{S30} > V_{REF} \end{cases}$$

(6.5b)

$$\ln(PGA_{REF}) = \begin{cases} \text{for } M_w \leq 6.75 \quad 1.85329 + 0.0029(M_w - 6.75) - 0.02807(8.5 - M_w)^2 + \\ [-1.23452 + 0.2529(M_W - 6.75)]\ln(\sqrt{R_{JB}^2 + 7.5^2}) - 0.1091 F_N + 0.0937 F_R \\ \text{for } M_w > 6.75 \quad 1.85329 - 0.5096(M_w - 6.75) - 0.02807(8.5 - M_w)^2 + \\ [-1.23452 + 0.2529(M_W - 6.75)]\ln(\sqrt{R_{JB}^2 + 7.5^2}) - 0.1091 F_N + 0.0937 F_R \end{cases}$$

(6.5c)

The magnitude scaling consists of a quadratic magnitude term as well as a hinging magnitude (c_1) – this is different than the coefficient defined in the DSF models – to account for magnitude saturation effects. The model considers magnitude dependency in geometrical spreading and describes the soil effects with a nonlinear site function that is based on V_{S30} and PGA at the reference rock site

184

(V_{REF} = 750 m/s). The effect of faulting mechanism on V/H is addressed by dummy variables F_N and F_R that are unity for normal and reverse faults, respectively, and zero otherwise.

The regression coefficients a_1 to a_{10} are computed from mixed-effects regression algorithm of Abrahamson and Youngs (1992). The magnitude and source-to-site distance measures are moment magnitude (M_w) and Joyner-Boore distance (R_{JB}) that are now almost standard in most of the predictive models in Europe. The hinging magnitude is taken as 6.75 as in the case of the horizontal GMPE after making several observations on the empirical data trend. The fictitious depth and the coefficients of linear magnitude terms (a_2 and a_7) are held fixed for the entire period range for a smooth spectral shape. The site amplification function, designated by ln(S) in Eq. 6.5b, includes both linear and nonlinear soil amplification. The nonlinearity is considered by the reference horizontal peak ground acceleration (PGA_{REF}) that is computed for V_{S30}=750 m/s (see Eq. 6.5c). The unit of PGA_{REF} is in terms of gravitational acceleration, g. The V_{S30} value of 750 m/s defines reference rock conditions in the V/H nonlinear site model, which is also the case in the nonlinear site function of the horizontal GMPE. The regression coefficients c, n, and a_{11} are adopted from Chapter 3.

6.4 Evaluation of Proposed V/H GMPE with Emphasis on Nonlinear Soil Behavior

The nonlinear site behavior in the V/H model deserves some more discussion. The soil amplification of V/H inherently depends on the site behavior of vertical and horizontal acceleration components and it has yet to be better understood. In horizontal ground motions, the site-dependent amplification is represented by linear and nonlinear site terms. The latter term dominates at high ground-motion intensity levels and when V_{S30} attains low values (Choi and Stewart, 2005; Walling et al. 2008). On the other hand, there is no clear evidence on the nonlinear site behavior of vertical ground motions. To our knowledge, the

significance of nonlinearity in vertical ground motions has never been studied in detail from a GMPE perspective. Almost all independent vertical ground-motion GMPEs (e.g., Campbell and Bozorgnia, 2003; Ambraseys et al., 2005b; Cauzzi and Faccioli, 2008) consider linear site behavior. Of the recently developed V/H GMPEs, Gülerce and Abrahamson (2011) account for nonlinear soil behavior whereas Bommer et al. (2011) disregard nonlinear site effects in V/H estimates.

From a theoretical view point, modeling nonlinear site effect for horizontal and vertical ground motions is always possible provided that the strong-motion metadata contains sufficient and reliable information on the modeling parameters. Observations on the empirical data trend as well as the significance of nonlinear term after regressions would define their potential impact in vertical and horizontal ground-motion estimates. The common assumption of log-normal distribution in horizontal and vertical ground motions imposes the same probability distribution for their ratio, which constitutes the basis of our logarithmic V/H model as given in Eq. (6.5a). Since site effects of horizontal and vertical ground motions are additive in the logarithmic V/H model, the contributions of linear and nonlinear site terms should control the overall V/H behavior and this would be mapped on to the estimated vertical ground motions.

The above discussion is visually illustrated by Figures 6.5 and 6.6 that show the median + 1 sigma estimates of vertical PGA, and PSA at T = 0.05s, 0.1s and 0.2s. The vertical ground motions significantly affect the amplitudes of these high-frequency spectral ordinates as discussed in the previously cited references. The figures compare the median + 1 sigma vertical ground-motion estimates of three alternative predictive models. The first predictive model is the one proposed in this study (designated as "Nonlinear V/H" on the figures). The second model, "Linear V/H", constrains a_{11} to zero to disregard nonlinear site effects. The last GMPE directly estimates the vertical spectral ordinates and it is defined as "independent vertical" on the plots. All three models are derived from the database used in this study. The third GMPE (Independent Vertical) includes only

186
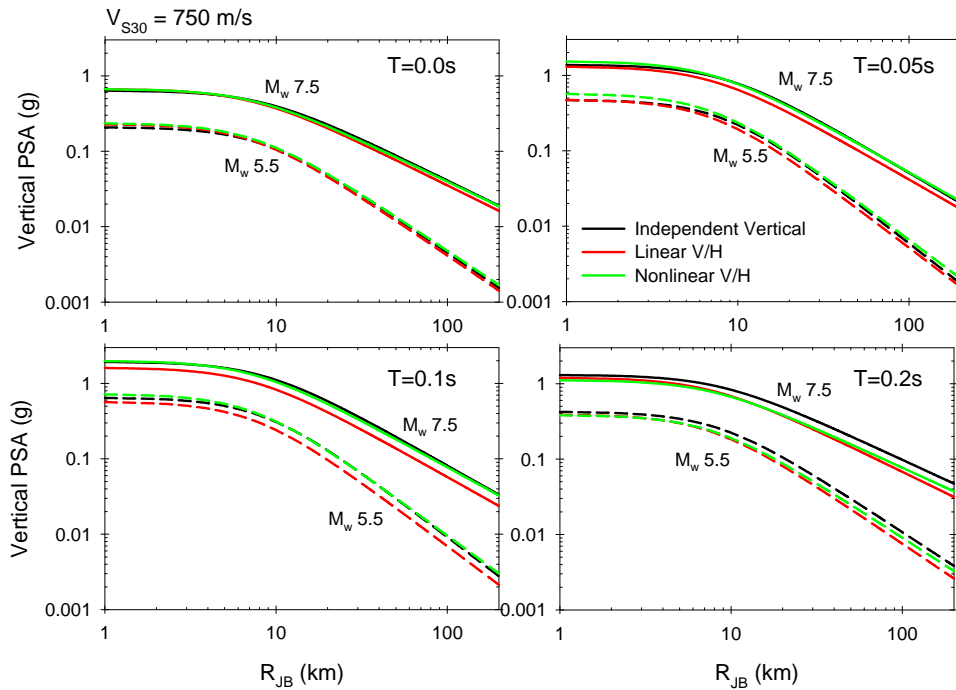
Figure 6. 5. Comparisons of vertical spectra computed from linear and nonlinear V/H models as well as an independent vertical ground-motion GMPE. The chosen site represents generic rock conditions (V_{S30} = 750 m/s). The comparisons are done for M_w 7.5 (solid lines) and M_w 5.5 (dashed lines) earthquakes generated by a strike-slip fault.

linear site effects as neither the regression analysis nor the empirical data trends supported the effects of nonlinear soil behavior on vertical ground motions. Figure 6.5 shows the distance-dependent variation of median + 1 sigma vertical ground-motion estimates from these alternative GMPEs for a generic rock site (V_{S30} = 750 m/s) for M_w 7.5 and M_w 5.5. The style-of-faulting is chosen as strike-slip for the scenario earthquakes. Figure 6.6 displays the same plots for a soft site represented by V_{S30} = 250 m/s. The median + 1 sigma spectral ordinates of the proposed horizontal GMPE are modified by the median linear and nonlinear V/H estimates to obtain the corresponding vertical spectra.
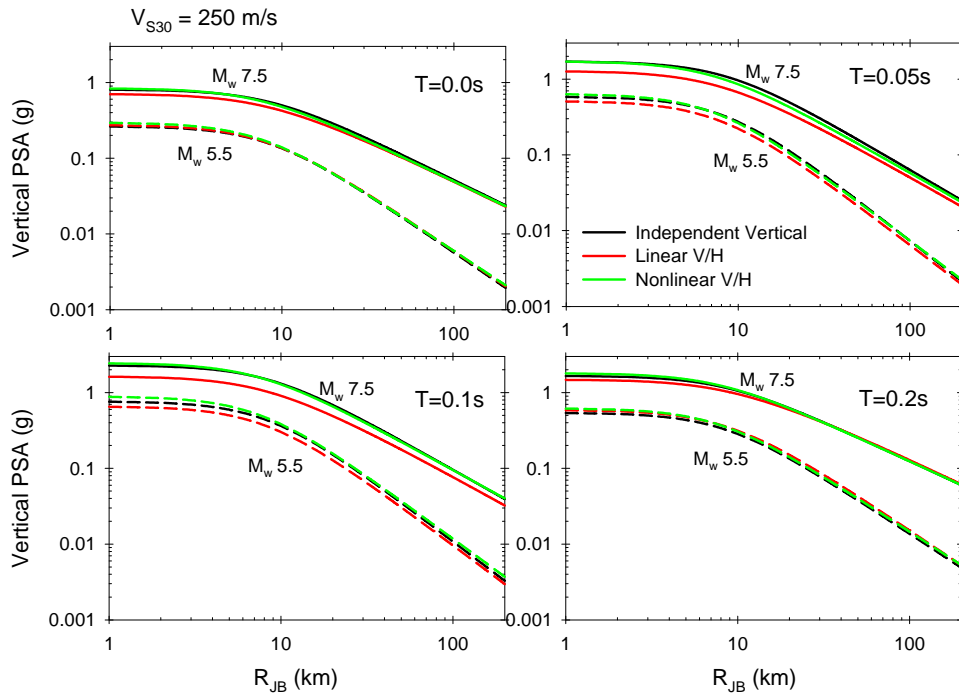
Figure 6. 6. Comparisons of vertical spectra computed from linear and nonlinear V/H models as well as an independent vertical ground-motion GMPE. The chosen site represents soft soil conditions (V_{S30} = 250 m/s). The comparisons are done for M_w 7.5 (solid lines) and M_w 5.5 (dashed lines) earthquakes generated by a strike-slip fault.

The comparative plots in Figure 6.5 indicate that all three GMPEs yield very similar vertical ground motions regardless of the variations in magnitude. The vertical ground-motion estimates from linear V/H model are slightly smaller with respect to the predictions of the other two GMPEs in many cases. The plots in Figure 6.6 depict very similar vertical ground-motion estimates for nonlinear V/H and independent vertical GMPEs. The plots almost overlap with each other for these models. The observed differences in linear V/H become more visible in Figure 6.6. The observations from Figures 6.5 and 6.6 suggest that the nonlinear site effects are not prominent in vertical ground motions regardless of the

variations in magnitude and distance. Thus, independent vertical GMPEs may overlook nonlinear soil behavior. However, consideration of soil nonlinearity in V/H models provides a control over the nonlinear soil effects of horizontal ground motions. This approach results in mimicking the genuine variations in the vertical ground-motion demands when V/H ratios are implemented together with the horizontal GMPEs. Under the light of these discussions and because we prefer providing a V/H model instead of an independent vertical GMPE for consistency between horizontal and vertical earthquake scenarios, the site amplification function given in Eq. (5b) considers the soil nonlinearity.

The proposed model is also evaluated in terms of classical residual analysis. Figure 6.7 shows the within-event and between-event residuals for $T = 0.2$s. The within-event residuals (left panel) are plotted in terms of V_{S30} whereas between-event residuals (right panel) are plotted for moment magnitude, M_w. The plots also show the average residuals for a set of pre-determined V_{S30} and M_w intervals. The V_{S30} intervals have a uniform spacing of 180 m/s for $V_{S30} \leq 900$ m/s. A single average of between-event residuals is computed for $V_{S30} > 900$ m/s as the data are sparse after this V_{S30} value. The M_w intervals are incremented by 0.5 units between $4 \leq M_w \leq 7$. The between-event residuals are also represented by a single average after M_w 7.0 due to sparse data distribution. The residuals are randomly distributed over the magnitude and V_{S30} range considered in this study. Their averages for the pre-determined intervals fluctuate about zero. These observations suggest unbiased estimates of the proposed V/H GMPE. The random distribution of within-event residuals can be interpreted as the satisfactory performance of the preferred nonlinear site model. The similar residual plots for other spectral periods are produced and the trends discussed for $T = 0.2$s are also valid for these figures.

Figure 6.8 shows the influence of aleatory variability on V/H estimates of the proposed model. The plots in this figure are prepared for earthquake scenarios of M_w 5 (left panel) and M_w 7.5 (right panel). The chosen V_{S30} value assumes stiff site conditions ($V_{S30} = 400$ m/s). The fictitious site is at a distance of $R_{JB} = 15$ km

from the strike-slip fault. The median ± sigma curves indicate that the variations in vertical ground-motion amplitudes can be significant due to aleatory variability. This variation should be considered seriously in vector-valued probabilistic hazard studies. Table 6.5 lists the regression coefficients of the V/H GMPE.
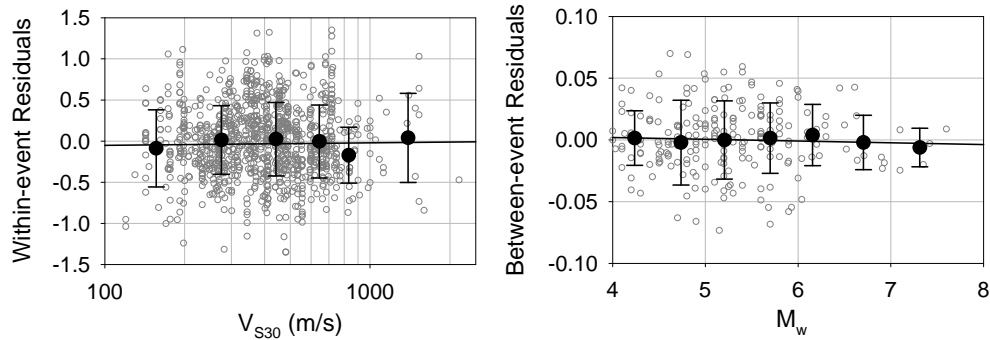
Figure 6. 7 Between- and within-event residual distributions for the V/H GMPE at T=0.2s. The between-event residuals are plotted in terms of M_w whereas within-event residuals are given as a function of V_{S30}.
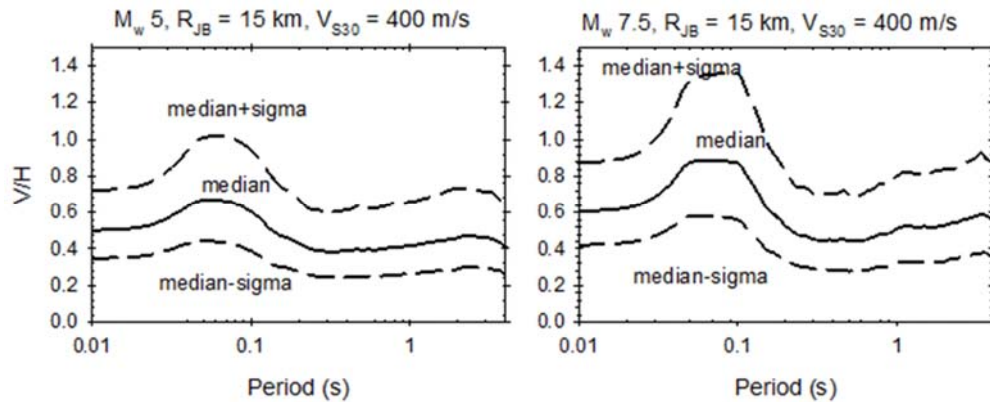
Figure 6. 8. Effect of aleatory variability in the proposed V/H GMPE

190

Table 6. 5. Period-dependent regression coefficients of the V/H ground-motion model for the selected periods. Period-independent coefficients are given in the footnote

Period	a_1	a_3	a_4	a_8	a_9	a_{10}	a_{11}	Φ^{**}	τ^{**}	σ^{**}
PGA	-0.55429	0.03124	-0.01172	0.04174	0.00483	0.2153	-0.28846	0.3578	0.0663	0.3639
PGV	-0.83717	0.0253	0.06389	0.10829	0.10998	0.36054	-0.19688	0.3655	0.0204	0.3661
0.01	-0.54467	0.03109	-0.01347	0.04465	0.00688	0.20949	-0.28685	0.3571	0.0747	0.3648
0.02	-0.46655	0.03099	-0.02821	0.04626	0.00711	0.21464	-0.28241	0.3558	0.0844	0.3657
0.03	-0.25416	0.03095	-0.07133	0.04137	-0.00933	0.20684	-0.26842	0.3613	0.0969	0.3741
0.04	-0.03087	0.02804	-0.10768	0.02432	-0.06283	0.17531	-0.24759	0.373	0.1161	0.3907
0.05	0.09261	0.02211	-0.12033	-0.01097	-0.0786	0.11306	-0.22385	0.3922	0.1259	0.4119
0.075	-0.02755	0.01822	-0.07373	0.00883	-0.09063	0.06983	-0.17525	0.405	0.1377	0.4278
0.1	-0.2157	0.01558	-0.02512	0.01238	-0.15905	0.0824	-0.29293	0.4103	0.1701	0.4442
0.11	-0.32916	0.01699	-0.00588	0.0125	-0.14341	0.08801	-0.31837	0.4196	0.1556	0.4475
0.12	-0.46642	0.01807	0.02141	0.01987	-0.1223	0.10167	-0.3386	0.4274	0.1473	0.4521
0.13	-0.58641	0.01944	0.04036	0.03518	-0.08773	0.12228	-0.36646	0.4418	0.133	0.4614
0.14	-0.69689	0.02211	0.05488	0.03488	-0.05192	0.13351	-0.38417	0.4481	0.112	0.4619
0.15	-0.79732	0.02578	0.06757	0.03577	-0.04592	0.15636	-0.39551	0.4455	0.1057	0.4579
0.16	-0.86803	0.02861	0.07634	0.03198	-0.03992	0.17327	-0.40869	0.4417	0.089	0.4506
0.17	-0.90007	0.03034	0.07831	0.02705	-0.03092	0.18018	-0.41528	0.436	0.0975	0.4468
0.18	-0.94543	0.03154	0.08296	0.03999	-0.02192	0.19604	-0.42717	0.4397	0.1014	0.4512
0.19	-0.97616	0.03311	0.08361	0.04976	-0.01292	0.21518	-0.4413	0.4377	0.0882	0.4465
0.2	-1.02981	0.03463	0.08653	0.05953	-0.00392	0.21837	-0.44644	0.4404	0.0816	0.4479

[*] $a_2 = 0.33$; $a_5 = -0.04$; $a_6 = 5$; $a_7 = 0.19$; $c_1 = 6.75$; $V_{REF} = 750$m/s, $c = 2.5$g; $n = 3.2$

** ϕ, τ and σ refer to within-event, between-event and total standard deviations, respectively.

Table 6.5. Cont'd

Period	a_1	a_3	a_4	a_8	a_9	a_{10}	a_{11}	Φ^{**}	τ^{**}	σ^{**}
0.22	-1.07671	0.0358	0.08945	0.0693	0.01901	0.24782	-0.44872	0.4368	0.0423	0.4388
0.24	-1.12512	0.03697	0.09237	0.07907	0.0447	0.26281	-0.46341	0.4393	0.0425	0.4414
0.26	-1.1253	0.0372	0.09305	0.08884	0.04903	0.29272	-0.48705	0.4459	0.0557	0.4494
0.28	-1.13542	0.03772	0.09373	0.09861	0.05336	0.30253	-0.47334	0.443	0.0554	0.4465
0.3	-1.14208	0.0382	0.09311	0.10302	0.05769	0.31643	-0.4573	0.4454	0.0249	0.4461
0.32	-1.13456	0.03889	0.09249	0.08986	0.06202	0.3336	-0.44267	0.4426	0.0655	0.4474
0.34	-1.12307	0.03912	0.09187	0.0767	0.06535	0.35046	-0.43888	0.4433	0.0894	0.4522
0.36	-1.11484	0.03935	0.09125	0.06354	0.06868	0.3631	-0.4382	0.4412	0.0986	0.4521
0.38	-1.09807	0.03905	0.09063	0.05038	0.07201	0.37453	-0.43678	0.4455	0.0863	0.4538
0.4	-1.09718	0.03975	0.09001	0.04878	0.07534	0.38181	-0.43008	0.4468	0.0828	0.4544
0.42	-1.08269	0.03955	0.08939	0.04718	0.07867	0.38909	-0.4219	0.4474	0.0902	0.4564
0.44	-1.06474	0.03945	0.08877	0.04558	0.082	0.39637	-0.40903	0.4499	0.1006	0.461
0.46	-1.04287	0.03939	0.08815	0.04458	0.08533	0.40365	-0.39442	0.453	0.0981	0.4635
0.48	-1.05469	0.0401	0.08753	0.05103	0.08866	0.40378	-0.38462	0.4592	0.0629	0.4635
0.5	-1.0642	0.0401	0.08691	0.06349	0.09199	0.40009	-0.37408	0.4557	0.0674	0.4607
0.55	-1.04314	0.04019	0.08346	0.07215	0.09532	0.40795	-0.35582	0.4424	0.0958	0.4527
0.6	-1.03283	0.03903	0.08162	0.08081	0.09865	0.40066	-0.34053	0.4433	0.1136	0.4576
0.65	-0.99033	0.0371	0.07978	0.07862	0.10198	0.39847	-0.30949	0.4494	0.1095	0.4625
0.7	-0.9426	0.0358	0.07794	0.08061	0.10331	0.41919	-0.28772	0.4519	0.0668	0.4568
0.75	-0.89263	0.0349	0.0751	0.07806	0.10535	0.44592	-0.28957	0.4584	0.0256	0.4591
0.8	-0.86344	0.03407	0.07226	0.0818	0.10739	0.45559	-0.28555	0.4601	0.0257	0.4608
0.85	-0.8344	0.03387	0.06942	0.08835	0.10943	0.48732	-0.28364	0.459	0.0257	0.4597

Table 6.5. Cont'd

Period	a_1	a_3	a_4	a_8	a_9	a_{10}	a_{11}	Φ^{**}	τ^{**}	σ^{**}
0.9	-0.78762	0.03283	0.06658	0.09074	0.11147	0.51765	-0.28037	0.4563	0.0255	0.457
0.95	-0.76116	0.03223	0.06374	0.09313	0.11351	0.523	-0.2839	0.4522	0.0253	0.4529
1	-0.73533	0.03063	0.0609	0.08829	0.11555	0.50958	-0.28702	0.4508	0.0252	0.4515
1.1	-0.71971	0.02874	0.05806	0.08105	0.11759	0.47333	-0.27669	0.4539	0.0254	0.4546
1.2	-0.71537	0.02973	0.05522	0.07564	0.11963	0.46148	-0.27538	0.4531	0.0358	0.4545
1.3	-0.71435	0.03098	0.05238	0.07362	0.12167	0.44972	-0.25008	0.4456	0.0705	0.4511
1.4	-0.71433	0.03175	0.04954	0.0716	0.12371	0.43796	-0.23508	0.4503	0.0712	0.4559
1.5	-0.70636	0.03203	0.0467	0.06958	0.12575	0.4262	-0.24695	0.4462	0.0864	0.4545
1.6	-0.71323	0.03279	0.044	0.06756	0.12779	0.41444	-0.2287	0.4542	0.088	0.4626
1.7	-0.69803	0.03323	0.0413	0.06554	0.12983	0.41244	-0.21655	0.4615	0.0774	0.4679
1.8	-0.67663	0.03315	0.0386	0.06352	0.13187	0.41444	-0.20302	0.4641	0.0686	0.4691
1.9	-0.65827	0.03301	0.0359	0.0615	0.13391	0.41448	-0.18228	0.4635	0.0579	0.4671
2	-0.62766	0.03247	0.0332	0.06344	0.13595	0.42834	-0.17336	0.4632	0.0518	0.4661
2.2	-0.57933	0.03171	0.0305	0.06915	0.13622	0.44195	-0.15463	0.4428	0.0606	0.4469
2.4	-0.54072	0.03064	0.0278	0.07486	0.13649	0.46382	-0.13181	0.4351	0.0877	0.4439
2.6	-0.50617	0.02789	0.0251	0.08635	0.13676	0.46709	-0.14066	0.433	0.0906	0.4424
2.8	-0.47909	0.02556	0.0224	0.09171	0.13703	0.47826	-0.13882	0.44	0.0696	0.4455
3	-0.42904	0.02433	0.0197	0.0934	0.14271	0.51101	-0.13336	0.4337	0.0686	0.4391
3.2	-0.39207	0.02196	0.017	0.10253	0.14187	0.53391	-0.1377	0.4446	0.0556	0.4481
3.4	-0.35245	0.01938	0.0143	0.1147	0.14455	0.5631	-0.15337	0.4464	0.0611	0.4506
3.6	-0.34017	0.01705	0.01439	0.13859	0.14723	0.56909	-0.10884	0.4301	0.0538	0.4335
3.8	-0.35356	0.01565	0.01115	0.18354	0.15273	0.55762	-0.08884	0.4353	0.0644	0.44
4	-0.35034	0.01392	0.00738	0.19948	0.15823	0.54615	-0.07749	0.4427	0.0821	0.4502

6.5 Details of the Proposed V/H GMPE and Its Comparisons with the Previous pan-European Model

The proposed V/H model is studied further to have better insight about its behavior. Figure 6.9 shows the median V/H estimates for T = 0.1s under the variation of fundamental estimator parameters (i.e., M_w, R_{JB} and V_{S30}). However, the discussions made here generally hold for the entire period range considered in this study. Figure 6.9.a displays the magnitude-dependent V/H variation for different RJB values. The assumed site condition is rock (V_{S30} = 750 m/s) and the chosen SoF is strike-slip in this case. The median V/H curves indicate that for magnitudes up to M_w 6 (acts like a node in this panel) one would expect larger V/H values with increasing distance. Thus, horizontal spectral ordinates tend to decay faster with respect to vertical spectral ordinates for small to moderate size events. This trend changes for M_w > 6 and increase in distance yields a decrease in V/H ratios that eventually indicates slower decay of horizontal spectral ordinates with respect to their vertical counterparts. Figure 6.9b that shows the distance-dependent behavior of V/H for a set of magnitude values supports the observations in Figure 6.9a. The increase in distance yields larger V/H for magnitudes up to M_w 6 that is reversed for M_w > 6. As pointed out in Figure 6.9b, the horizontal spectral ordinates of small to moderate size events (M_w < 6) attenuate faster with respect to their vertical counterparts and this trend reverses as magnitude becomes larger. The median V/H curve for M_w 6 is almost insensitive to variations in distance, which explains its "nodal" position in Figure 6.9b. Figure 6.9c that shows the particular influence of V_{S30} on V/H suggests that the vertical spectrum tends to attain larger values for soft to very soft sites (V_{S30} < 350 m/s) and large magnitudes (M_w > 7). As the site gets stiffer the variations in V/H are mild and stable.

The proposed model is also compared with the recent pan-European V/H GMPE that is developed by Bommer et al. (2011; BAK11). The magnitude scaling is linear and geometrical spreading does not consider a magnitude dependent slope
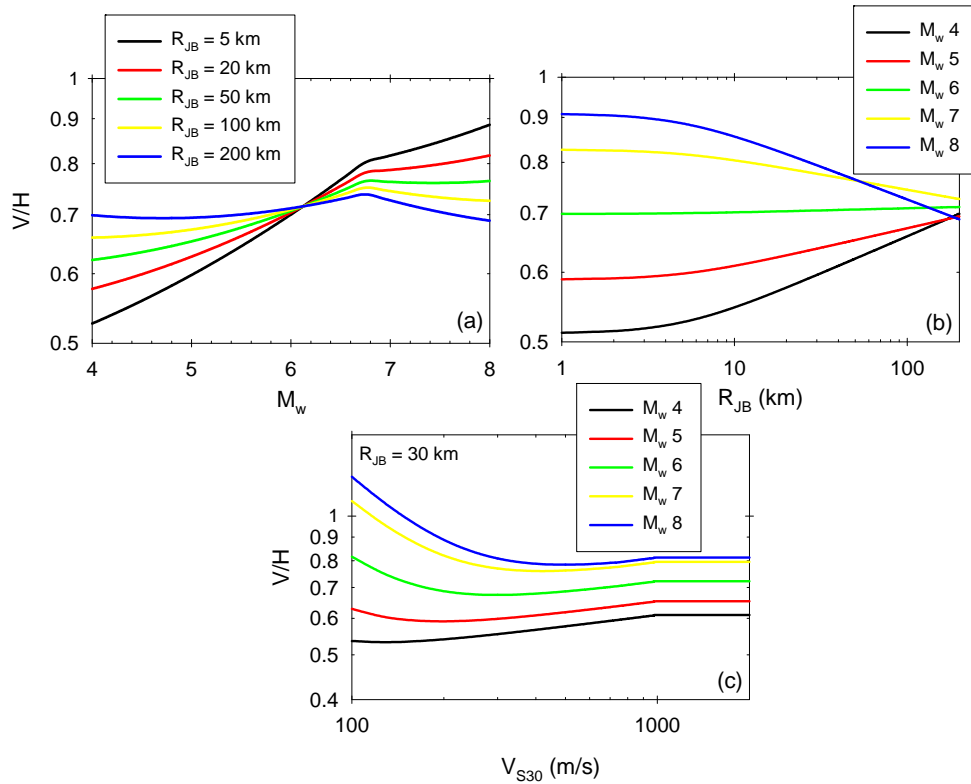
Figure 6. 9 Median V/H variations of the proposed model in terms major
estimator parameters for T = 0.1s.

in BAK11. It disregards the soil nonlinearity in V/H estimates. Figure 6.10 compares the median V/H estimates of these two models. The comparisons are made for median V/H trends as this spectral quantity is used while constructing the horizontal spectrum compatible vertical spectral ordinates for scenario-specific PSHA. The details of this procedure are described in the subsequent sections. The spectral comparisons in Figure 6.10 are done for R_{JB} = 10 km for M_w 5 and M_w 7.5 (left and right columns, respectively). A strike-slip fault is used in the scenario earthquakes as in the case of previous examples. The top row panels compare the median V/H estimates for V_{S30}=800m/s (generic rock site) whereas the bottom row comparisons are plotted for V_{S30}=255m/s (soft soil). The
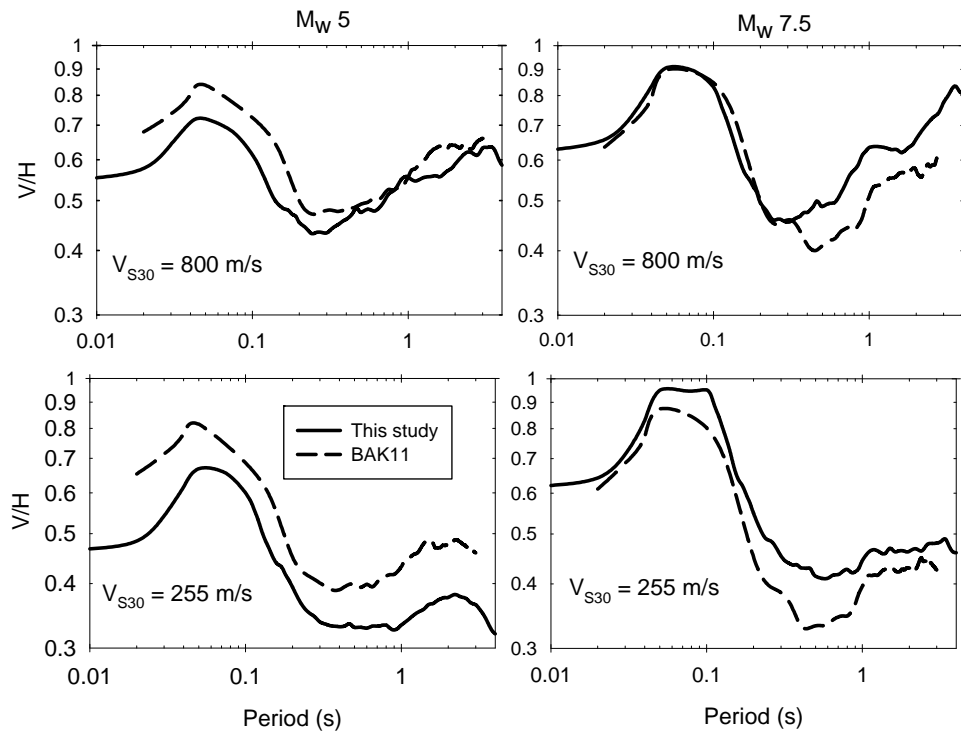
Figure 6. 10. Comparison of the proposed equation with Bommer et al. (2011; BAK11) V/H model for different magnitudes and site conditions at R_{JB}=10km

median V/H estimates of the proposed model depict differences with respect to BAK11. However, the differences are not substantial. Our model tends to estimate larger V/H ratios towards longer periods for larger magnitudes. The opposite holds for small magnitudes and BAK11 yields larger V/H estimates particularly for softer sites. The discrepancies between the median V/H estimates of BAK11 and the proposed model can be the attributes of different functional forms as well as the size and resolution of databases although they are originated from the same region . This study uses a more complicated functional form that considers magnitude-dependent geometrical spreading as well as linear and nonlinear soil behavior as a function of continuous V_{S30}. These features are not included in BAK11 due to insufficient metadata features in their database. Although BAK11

and this study use strong-motion data collected from broader Europe, the pan-European database used in this study is recently updated and expanded in terms of waveform quality and metadata information.

6.6. Comparison of the Models Different Distance Metrics

The proposed DSF and V/H GMPEs use R_{JB} as the source-to-site distance metric. This section provides information on the applicability of these models for point source distance measures (epicentral distance -R_{epi}- and hypocentral distance -R_{hyp}-) as horizontal GMPEs are developed for estimating horizontal ground motions in R_{epi}, R_{hyp} and R_{JB}. Figure 6.11 shows median horizontal DSF estimates computed for R_{JB}, R_{epi} and R_{hyp} for a stiff site of V_{S30} = 400 m/s. The availability all three distance measures in our strong-motion database enabled us to develop DSF predictive GMPEs for the latter two distance measures. The same functional form as of R_{JB}-based DSF predictive model was used in these GMPEs and same steps were followed in the regressions. The distance range considered in comparisons is up to 200 km. Each raw in Figure 6.11 compares the median horizontal DSF estimates of R_{JB}, R_{epi} and R_{hyp} for a specific period. The selected spectral periods for comparisons are T = 0.1s, T = 0.5s, T = 1.0s, T = 2.0s and T = 4.0s. They represent the overall spectral period interval of concern in the paper.

Each column in Figure 6.11 shows a specific magnitude taking values between M_w 4 and M_w 8 with unit increments. The comparisons are shown for 2% and 10% damping ratios in order not to crowd the panels. The other damping ratios yield similar results to those given in Figure 6.11. Figure 6.12 makes the same comparisons for vertical DSF estimates. The display format in this figure is the same as in Figure 6.11. The comparative plots indicate that median horizontal and vertical DSF estimates are practically independent of distance definition. For lightly damped systems (represented by 2% critical damping in Figures 6.11 and 6.12) and towards large magnitudes, the variations in R_{JB}-based DSF model are slightly different than the median DSF trends of the point-source distance metrics.

However, the observed discrepancies are not more than 5% for the entire distance range. The observations highlighted by these plots are valid for the whole magnitude, period and damping ratios covered in this study. Thus, the overall discussions from Figures 6.11 and 6.12 suggest the general applicability of R_{JB}-based horizontal and vertical DSF GMPEs for the modification of 5%-damped horizontal GMPE without making any adjustments for R_{epi} and R_{hyp}.
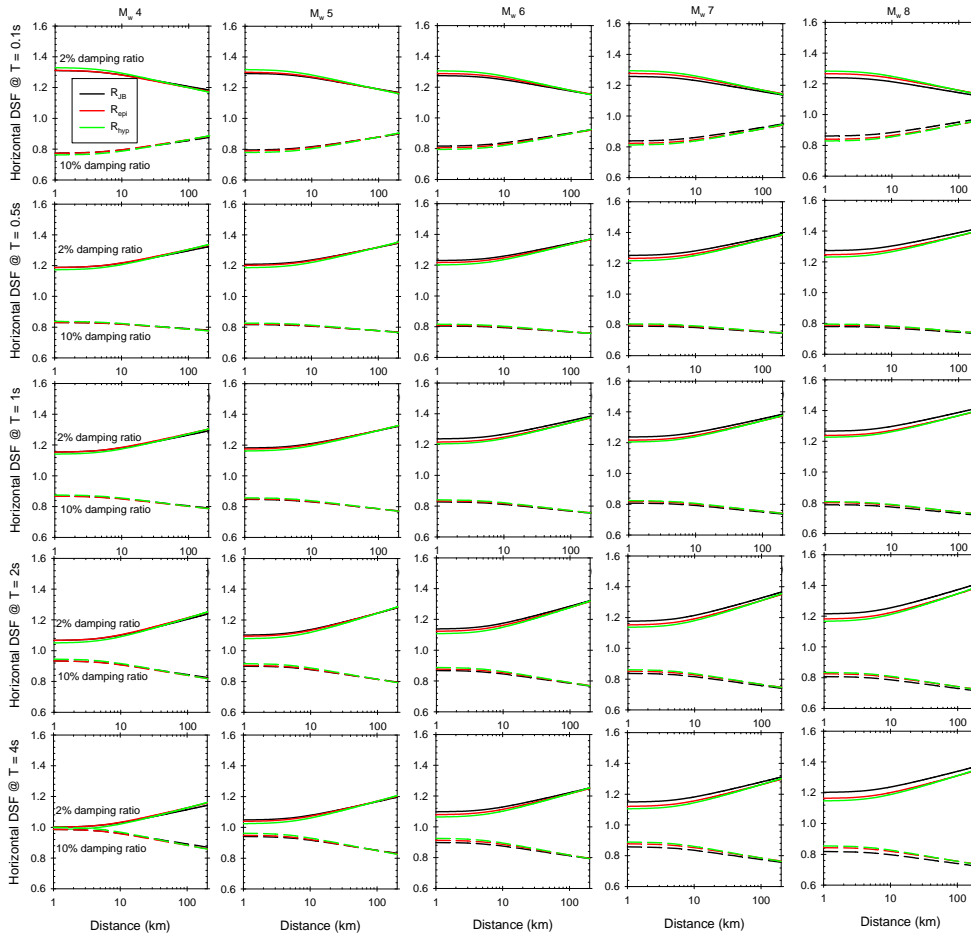
Figure 6. 11. Comparisons of median horizontal DSF estimates from R_{JB}-, R_{epi}- and R_{hyp}-based GMPEs that are derived from the same strong-motion database. The functional forms of all three GMPEs are the same. The solid and dashed lines show the comparisons for 2% and 10% damping, respectively.
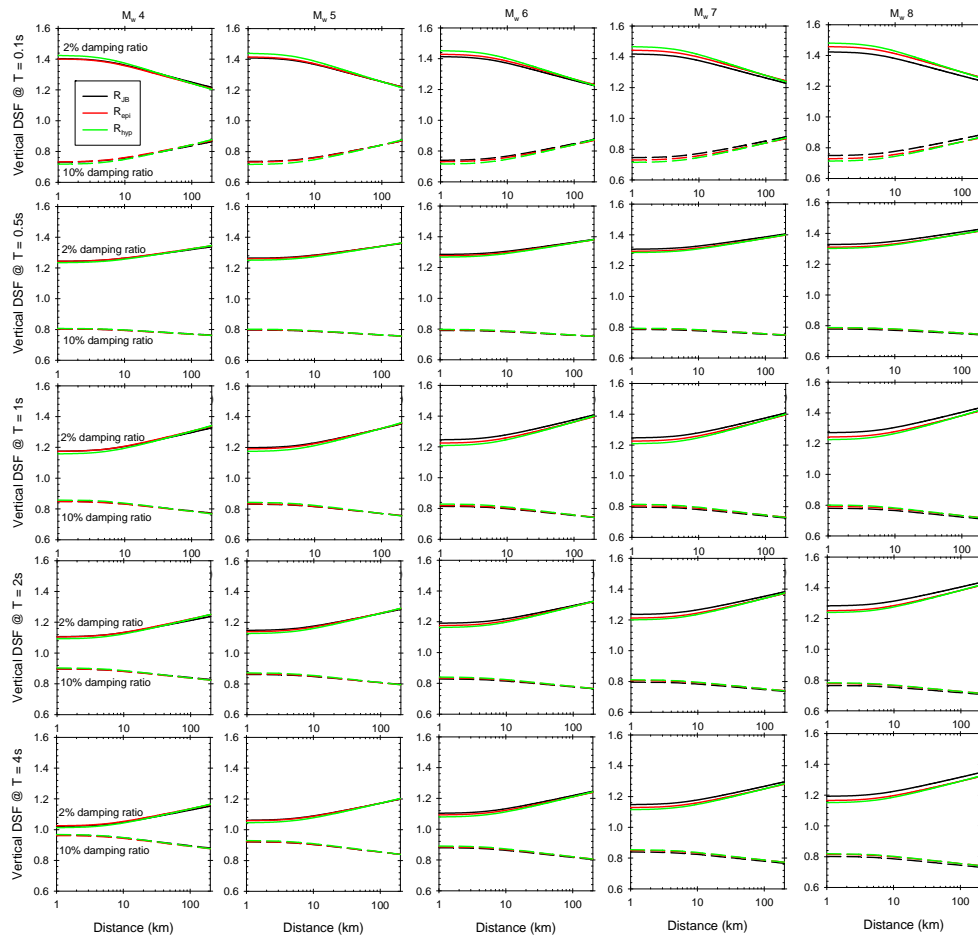
Figure 6. 12. Comparisons of median horizontal DSF estimates from R_{JB}-, R_{epi}- and R_{hyp}-based GMPEs that are derived from the same strong-motion database. The functional forms of all three GMPEs are the same. The solid and dashed lines show the comparisons for 2% and 10% damping, respectively.

Similar comparisons are repeated for the median V/H estimates. Figure 6.13 shows the median V/H estimates of R_{JB}, R_{epi} and R_{hyp} predictive models. The GMPEs for R_{epi} and R_{hyp} are developed by following the methodology described in the DSF comparisons: same functional forms as of R_{JB}-based GMPE and the same type of regression analysis by utilizing the strong-motion database used for
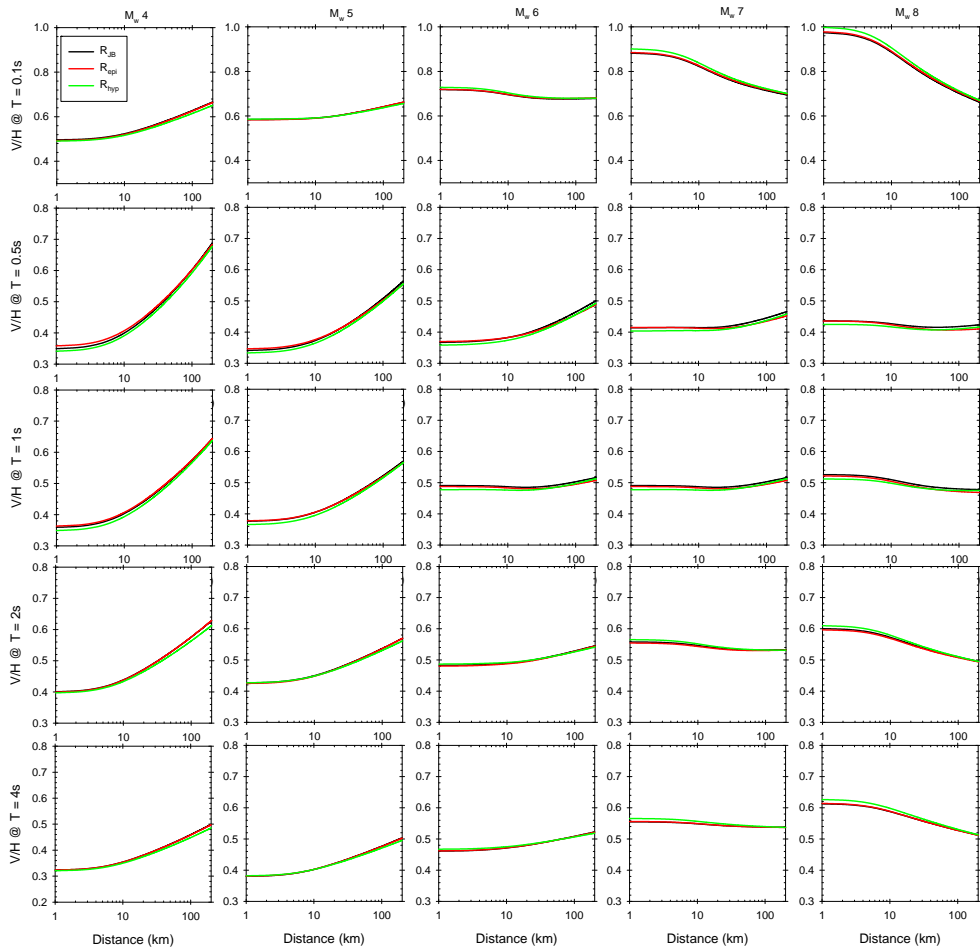
Figure 6. 13. Comparisons of median V/H estimates from R_{JB}-, R_{epi}- and R_{hyp}-based GMPEs that are developed from the same database. The functional forms of the predictive models are the same.

developing R_{JB}-based GMPE. The plots in Figure 6.13 compare median V/H estimates for the above three distance measures by using the period and magnitude combinations given in Figures 6.11 and 6.12. The comparisons in Figure 6.13 display very similar patterns between the median V/H estimates of R_{epi}, R_{hyp} and R_{JB} GMPE. Although some minor discrepancies in V/H trends do exist between R_{hyp} and the other two distance metrics, we believe that these

differences can be neglected for all practical purposes. Thus, one can use the R_{JB}-based V/H model in confidence with the horizontal GMPEs with all three distance measures of concern to generate fully consistent vertical ground-motion estimates.

The conclusions derived from the median DSF and V/H comparisons are further investigated by studying the total standard deviations of the DSF and V/H GMPEs that are developed separately for each source-to-site distance metric. The comparative results are shown in Figure 6.14. The left and right panels in the first row of Figure 6.14 show the period-dependent variation of total sigma for horizontal and vertical DSF GMPEs. The panel in the second row displays same type of comparisons for V/H model. The information inferred from Figure 6.14 once again justifies that any existing difference among the three considered distance measures becomes immaterial for DSF and V/H ratio estimates.

6.7 Conclusions

This chapter presents ground-motion models to estimate damping scaling factors and vertical-to-horizontal pseudo-acceleration spectral ratios. The spectral period range of the predictive equations is between 0.01s and 4.0s. The vertical-to-horizontal ratio GMPE additionally estimates horizontal-to-vertical ratio at PGA and PGV. The proposed models use the same subset of the recent pan-European databank as of the 5%-damped horizontal PSA does. Thus, the ground-motion prediction equations presented in here complement the horizontal predictive model for its modification for consistent vertical design spectrum as well as horizontal and vertical spectral ordinates of damping ratios other than 5%. Although both DSF and V/H GMPEs are derived for R_{JB}, the verifications showed that these models are equally applicable to horizontal and vertical ground-motion estimates that are based on R_{epi} and R_{hyp}. The horizontal and vertical damping scaling models use M_w, R_{JB} and V_{S30} as independent parameters and can modify 5%-damped spectral ordinates for damping levels ranging between 1% and 50%. They are applicable of moment magnitudes between 4 and 8 and for distances up

to 200 km. These models can also serve for the future updates of damping scaling factors in Eurocode 8 as the comparisons given in the paper indicate biased spectrum estimates of Eurocode 8 for very short periods and high damping ratios. The proposed V/H GMPE considers M_w, R_{JB}, SoF and V_{S30}-based nonlinear site function. The recommended magnitude and distance ranges of the predictive model are the same as those of damping scaling GMPEs. The nonlinear site model has an applicability range of 150 m/s $\leq V_{S30} \leq$ 1200 m/s. The presented models as well as the horizontal GMPE, when used together, can serve for consistent vector-based PSHA studies in the broader Europe region. They can be also used for future updates of vertical seismic demands in Eurocode 8 (CEN 2004).
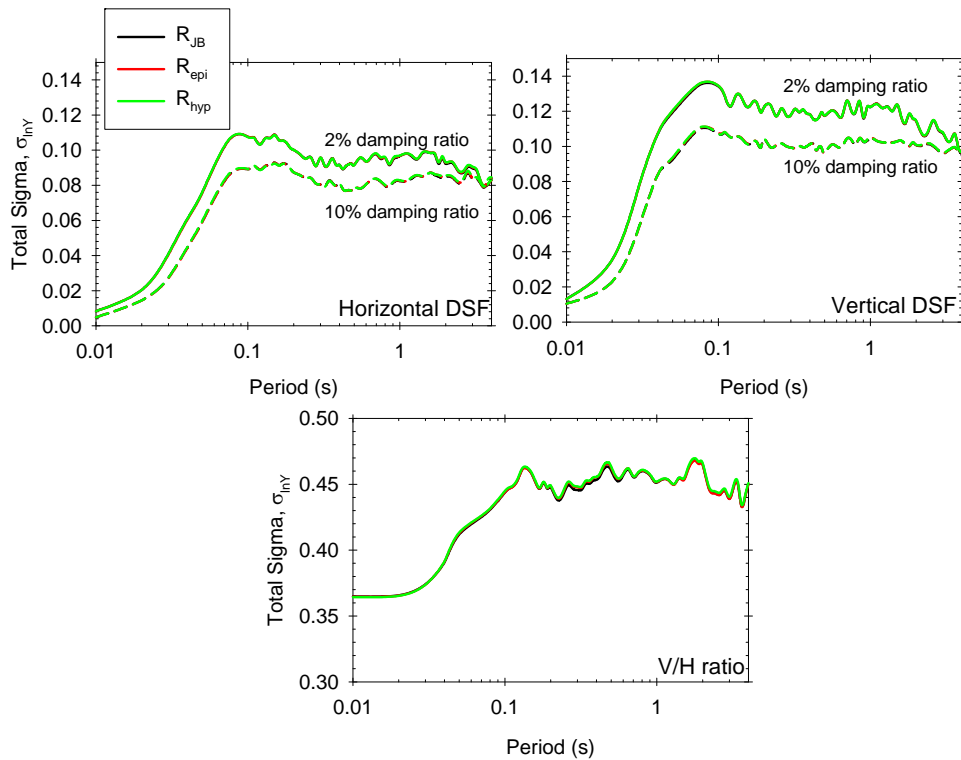
Figure 6. 14. Comparison of total standard deviations of DSF (top row) and V/H (bottom row) GMPEs developed for different distance measures.

CHAPTER 7

CONCLUSIONS

7.1 Summary

This dissertation presents the recent pan-European strong-motion databank (RESORCE) (Akkar et al., 2014a) that is compiled within the SIGMA project. Another development undertaken in this study is the proposal of the first nonlinear site amplification model (Sandikkaya et al., 2013) for the pan-European region. The proposed model is used both in the derivation of new GMPEs and evaluation of current site factors in seismic design codes. The evaluation of site factors has led to a new procedure for the computation of these parameters that are fully compatible with regional and site-specific PSHA (Sandikkaya et al, 2014). The nonlinear site model is essentially used to develop a set of pan-European GMPEs for estimating horizontal and vertical accelerograms at multiple damping levels (Akkar et al., 2014b; Akkar et al., 2014c).

The dissertation starts with introducing the compilation procedure of RESORCE. The main source of RESORCE is ISESD (Ambraseys et al, 2004a), which is updated and expanded with the contributions of Turkish, Swiss, Italian, French and Greek accelerometric databases. The successor of ISESD (i.e. the update of ISESD) not only increases the number of events and accelerograms but also improves the data quality in terms of earthquake, site metadata and record processing scheme. It is believed that RESORCE, as a high-quality strong-motion databank, will be an important tool for hazard and risk studies in and around Europe.

More than 1000 three-component recordings from RESORCE and roughly 4500 accelerograms from Japan, Western US and Taiwan that are extracted from SHARE strong-motion databank (Yenier et al., 2010) are used in the derivation of nonlinear site model. The empirical site amplification model is used in GMPEs derived for shallow active crustal regions. The functional form is capable of addressing linear and nonlinear soil behavior. The proposed site model carries features similar to the one in Walling et al. (2008) that is entirely based on stochastic simulations. The agreement between these two models as well as its similar trends with the site models of recent global prediction equations advocates the reliability and robustness of the site model.

The discussions on the site amplification model continued with the evaluation of the current site factors of EC8 and NEHRP through an alternative procedure that was devised for the estimation of site- and region-specific soil amplification. The analysis made use of the next generation GMPE for pan-European region and the proposed nonlinear site model. The first set of comparison uses single earthquake scenarios with observing lack of magnitude and distance effects on spectral shape. In order to remove this deficiency, multiple earthquake scenarios are then used. The results of this procedure indicated the significance of soil nonlinearity that is disregarded in the EC8. The fairly good comparisons between the NEHRP site factors motivated us to develop the new procedure to compute site factors.

The proposed procedure uses probabilistic rock hazard together with a deterministic site amplification model. It accounts for the level of seismicity and influence of mean annual exceedance rate of rock ground-motion intensities that dominate the shape of design spectrum envelope and amplitude of site factors for different soil conditions. The main input to the nonlinear site model is the reference PGA_{rock} and it is proposed to use the conditional spectrum to describe PGA_{rock} from the pseudo-acceleration spectral ordinates.

The dissertation concludes with the proposal of a set of pan-European horizontal and vertical ground-motion prediction equations for different damping values. These equations supersede the Akkar and Bommer (2007), Akkar and Bommer (2010) and Bommer et al. (2012) GMPEs derived for estimating the horizontal and vertical ground motions in Europe and the Middle East, respectively. The formulation of the new equations covers broader ranges of response period, earthquake magnitude and distance. Dummy site classification is replaced by a continuous, V_{S30}-dependent site amplification function. The inclusion of the nonlinear site response is another improvement achieved by this study. These ground-motion equations are also capable of making estimations in terms of point- and extended-source distance metrics. The vertical-to-horizontal (V/H) spectral ratio GMPE is complementary to the horizontal ground-motion GMPE and it is fully compatible with the latter one as both of these models use the same ground-motion dataset in their development. This is not the case for Akkar and Bommer (2010) and Bommer et al. (2012) GMPEs because they are based on different ground-motion datasets. The most important improvement in the V/H GMPE is the site amplification model that considers linear and nonlinear site effects together. The last predictive models developed in this study are the damping scaling factors for estimating spectral ordinates at damping levels other than 5% for horizontal and vertical ground-motion spectral ordinates.

When proposed horizontal, V/H and damping scaling GMPEs are used together, they can serve for consistent vector-based PSHA studies in the broader Europe region. These GMPEs consider M_w, R_{JB}, R_{epi}, R_{hyp}, SoF and a V_{S30}-based nonlinear site function that has an applicability range of 120 m/s $\leq V_{S30} \leq$ 1200 m/s. The predictive models are valid for $4 \leq M_w \leq 8$ and $R_{JB} \leq 200$ km. The damping scaling model can modify 5%-damped spectral ordinates for damping levels ranging between 1% and 50% for horizontal and vertical components.

7.2 Major Results

This dissertation has focused on three major research fields in strong ground-motion characterization in Europe: (a) compilation of the recent pan-European strong-motion databank, (b) development of an alternative nonlinear site model and (c) development of ground-motion predictive models for horizontal and vertical spectra at different damping values. The major outcomes of the studies conducted within the context of these fields are outlined below for each topic separately.

7.2.1 Pan-European Strong-Motion Databank

- When compared to ISESD, the former pan-European strong-motion databank, the event and record size is increased by 2.5 times in RESORCE (5882 multi-component accelerograms from 1814 events) through additional data from recent Turkish, Italian, Swiss, French and Greek events and corresponding recordings.

- RESORCE improves the event information (e.g., M_w and focal mechanism) with respect to ISESD

  1. The reported M_w and focal mechanism information is compiled from recent literature as well as local and international seismological agencies. When moment magnitude information is unavailable, local magnitude conversion relations are used.

  2. The style-of-faulting for each earthquake is either reassessed or newly determined from plunge-angle definitions that are believed to be more robust when compared to the fault classification based on rake-angle definitions. The SoF classification that is based on plunge angles does not require the correct fault information from double-couple fault-plane solutions that are missing for most of the European earthquakes.

- RESORCE improves the information on source-to-site distance measures due to increased knowledge on double-couple solutions of earthquakes from regional seismological agencies)

- RESORCE uses the most updated site classification for the strong-motion station inventory. The updated site classification is mostly based on the shear-wave velocity profiles obtained from in-situ measurements that are conducted by recent national strong-motion projects in Turkey, Italy and Greece.

- Strong-motion data processing in RESORCE results in an increase in the usable period range of elastic spectrum as each individual accelerogram is band-pass filtered by inspecting its frequency content.

- The resulting databank is particularly useful for developing and testing ground-motion prediction equations for seismic hazard assessment studies in and around Europe. It is also useful for other studies of engineering interest such as performance verification of existing structural systems through nonlinear response history analysis.

7.2.2 Nonlinear Site Model

- The first nonlinear site model for the pan-European region is produced. A functional form that is based on stochastic simulations (Walling et al., 2008) is regressed with empirical data. The model by Walling et al. (2008) and this study make similar soil amplification estimates indicating that the proposed model validates the outcomes of stochastic simulations used in the Walling et al. (2008) site model.

- The soil amplification estimates of proposed model are also comparable with the previously developed site models in NGA project. For V_{S30} > 1000 m/s, the site amplification is considered as constant due to database limitations. The linear behavior of the proposed model is similar to other compared models (Abrahamson and Silva, 2008; Boore and Atkinson,

2008); however, higher nonlinear behavior is observed for the proposed model for lower to mild ground-motion levels at low V_{S30} values.

- The site factors in seismic design codes are compared with single and multiple earthquake scenarios. In the former approach it is observed that the use of a single earthquake scenario does not reflect the magnitude-distance effect of the strong-motion characteristics on soil behavior. The second approach (named as triplet approach in this study) estimates the site factors more realistically. For regions that lack probabilistic seismic hazard analysis, the triplet approach can be used to define site factors.

- An alternative procedure rather than conventional site factor studies (e.g., Borcherdt, 1994; Rey et al., 2002) is devised to determine the site coefficients used in design codes. This method uses the rock hazard results together with different site amplification models to map the epistemic uncertainty. The comparison of site factors computed from the proposed model with alternative site factors provided by design codes lead to the following results:

  1. Soil amplifications are period-dependent and they also vary with changes in PGA_{rock} level.

  2. The short-period (T < 0.5 s) and long-period (T > 1 s) amplifications are very different from one another and this difference becomes more prominent for soft sites.

  3. The soil behavior factors in EC8 are insufficient to simulate the genuine soil behavior at high levels of ground amplitudes.

  4. The comparisons between the triplet approach and NEHRP site factors yield fairly similar values except for a few cases for very soft soil conditions (NEHRP E site class) at short periods, where higher non-linear effects are predicted by the NEHRP site factors.

  5. The site amplifications computed from different design spectrum formats are very close to each other. Return period and seismicity of the region play an important role in site amplification; however, these effects can be modeled via PGA_{rock} or PSA_{rock}.

7.2.3 A Set of New GMPEs for Broader Europe

- A set of predictive models for horizontal and vertical ground-motions at multiple damping levels are published for the pan-European region. All proposed equations are compatible and consistent with each other.

- The ground-motion estimates of the new GMPEs are believed to be better constrained with respect to the former pan-European GMPEs because of the increased number of ground-motions with higher metadata quality of the ground-motion datasets used in their development.

- The proposed GMPEs are applicable to both point- and extended-source distance metrics.

- The anelastic term in the horizontal predictive model can still be not constrained with the current features of pan-European accelerograms. The effect of magnitude-dependent fictitious depth on median ground-motion estimates is found to be negligible after the studies conducted while developing the horizontal GMPE.

- The effect of magnitude on standard deviation cannot be verified for the proposed GMPEs since large magnitude events are still not uniformly distributed in the pan-European ground-motion datasets.

- A break in the linear term of quadratic magnitude scaling is included in the base functional form of the proposed horizontal and vertical GMPEs, leading to more stable estimates at large magnitudes.

- The soil nonlinearity is incorporated to the horizontal and vertical GMPEs. Although vertical spectrum seems to be independent of nonlinear soil effect, its consideration in the V/H GMPE results in more realistic estimates of vertical spectrum from horizontal spectral ordinates.

- Although the DSF and V/H models are developed for R_{JB} distance metrics, the analysis made on point-source distance metrics shows that, the proposed R_{JB} based equations are applicable to R_{epi} and R_{hyp}.

- The additional discussions made on depth dependence show the performance of the equations could be increased by constraining depth with magnitude and style-of-faulting.
- The long-distant recordings have significant impact on long-period within-event standard deviation (phi).

7.3 Concluding Remarks

The quality and content of RESORCE provides high standard accelerograms for earthquake engineering community in Europe and world-wide. This accelerometric databank is comparable with the NGA-West1 strong-motion databank (Power et al., 2008); however, more efforts should be put forward to complete the missing event and station metadata information from earthquake-specific studies, fast moment tensor solutions of local seismological agencies and in-situ site measurements. The continuous growth of the pan-European strong-motion data archive should be encouraged particularly for seismically very active regions in Europe such as Greece, Italy and Turkey. The future studies should also consider the inclusion of Iranian strong-motion database with special emphasis on site metadata. The subset of RESORCE that is used to develop pan-European GMPEs is mainly composed of accelerograms from Turkey (55% of the accelerograms) that is followed by Italian and Greek recordings. The contribution of Iranian database is negligibly small. The low level contributions of such highly seismic regions to pan-European databases are mostly due to the unavailable in-situ site measurements for shear-wave velocity profiles. Upon the recovery of such insufficient information, more coverage of the highly seismic regions in the broader Europe will be accomplished for the prediction of ground motions for hazard and risk studies. Moreover, these improvements will lead to advanced studies such as the investigation of regional effects on ground motions. More accelerometric data from moderate-to-low seismicity regions in Europe should also be included in the future versions of RESORCE to increase the databank's area coverage. A more comprehensible strong-motion databank will definitely

create numerous research opportunities in the fields of earthquake engineering and engineering seismology in Europe.

The assumptions made in some of the extended-source distance computations from double-couple solutions should also be reduced in the updated future versions of RESORCE by identifying the ruptured fault segments. It is a fact that precise identification of actual faults for low magnitude events (i.e., $M_w < 6$) is quite difficult and it requires comprehensive studies to propose an approach to calculate distance metrics for low magnitude events. The missing moment magnitude information of small earthquakes can be recovered by investigating the fast moment tensor solutions of regional seismological agencies. In the meantime, while such improvements are being planned as future actions, researchers should work on the adverse effects of such these metadata weaknesses on GMPEs in order to improve the reliability of ground-motion estimates.

The linear and nonlinear regression coefficients of the site model are directly used while developing the GMPEs proposed in this dissertation. This approach is previously followed by Boore and Atkinson (2008) and Akkar and Çağnan (2010) and should be questioned by future studies. To this end, a major research topic should be the effects of site model variability on the reliability of GMPE estimates. The end results of such a study would better correlate the soil nonlinearity and standard deviation for future updates of the proposed GMPEs. The magnitude dependency of standard deviation that is associated with the proposed GMPEs should also be investigated upon the growth and improvements of future RESORCE versions.

The proposed site model can be improved by considering stochastic simulations to increase its applicability range towards higher PGA_{REF} and lower V_{S30} where the nonlinear soil effects would be more prominent. Besides, additional estimator parameters such as kappa, κ, (Anderson and Hough, 1984) or fundamental site frequency, f_0 (Cadet et al., 2010) or depth-to-rock (e.g., Abrahamson and Silva,

2008) can be considered either in the site model or in the proposed GMPEs to capture the real site response and to improve the reliability of ground-motion estimates.

As for the last remarks, the findings of this study should be considered for the development of new site factors that utilize V_{S30} and PGA_{REF} as the main proxies. This study has focused on the site amplification based on these two parameters. With the recent advances in site response studies, the site classification schemes should also be revised by using the site information given in RESORCE.

REFERENCES

Abercrombie RE, Main IG, Douglas A, Burton PW (1995) The nucleation and rupture process of the 1981 Gulf of Corinth earthquakes from deconvolved broad-band data. *Geophys. J. Int.* **120**:393-405.

Abrahamson NA, Silva W (2008) Summary of the Abrahamson & Silva NGA ground-motion relations. *Earthq. Spectra* **24**: 67-97.

Abrahamson NA, Silva WJ (1996) *Empirical Ground Motion Models*. Report to Brookhaven National Laboratory.

Abrahamson NA, Silva WJ (1997) Empirical response spectral attenuation relations for shallow crustal earthquakes. *Seismol. Res. Lett.* **68**: 94-127.

Abrahamson NA, Youngs RR (1992) A stable algorithm for regression analyses using the random effects model. *Bull. Seism. Soc. Am.* **82**: 505–510.

Akkar S, Bommer JJ (2006) Influence of long-period filter cut-off on elastic spectral displacements. *Earthq. Engrg. Struct. Dyn.* **35**:1145-1165.

Akkar S, Bommer JJ (2007a) Empirical prediction equations for peak ground velocity derived from strong-motions records from Europe and the Middle East. *Bull. Seism. Soc. Am.* **97**: 511-530.

Akkar S, Bommer JJ (2007b) Prediction of elastic displacement response spectra at multiple damping levels in Europe and the Middle East. *Earthq. Engrg. Struct. Dyn.* **36:**1275-1301.

Akkar S, Bommer JJ (2010) Empirical equations for the prediction of PGA, PGV and spectral accelerations in Europe, the Mediterranean and the Middle East. *Seismol. Res. Lett.* **81:**195-206.

Akkar S, Çağnan Z (2010) A local ground-motion predictive model for Turkey, and its comparison with other regional and global ground-motion. *Bull. Seism. Soc. Am.* **100**:2978–2995.

Akkar S, Çağnan Z, Yenier E, Erdogan Ö, Sandıkkaya MA, Gülkan P (2010) The recently compiled Turkish strong-motion database: preliminary investigation for seismological parameters. *J. of Seismol.* **14**: 457-479.

Akkar S, Kale Ö, Yenier E, Bommer JJ (2011) The high-frequency limit of usable response spectral ordinates from filtered analogue and digital strong-motion accelerograms. *Earthq. Engrg. Struct. Dyn.* **40**:1387-1401.

Akkar S, Sandıkkaya MA, Ay BÖ (2014c) Predictive models for horizontal and vertical conditional mean response spectra at multiple damping levels derived for Europe and the Middle East. *B. Earthq. Eng.* **12**:517–547.

Akkar S, Sandıkkaya MA, Bommer JJ (2014b) Empirical Ground-Motion Models for Point- and Extended-Source Crustal Earthquake Scenarios in Europe and the Middle East. *B. Earthq. Eng.*, **12**:359–387.

Akkar S, Sandıkkaya MA, Şenyurt M, Azari Sisi A, Ay BÖ, Treversa P, Douglas J, Cotton F, Luzi L, Hernandez B, Godey S (2014a). Reference Database for Seismic Ground-Motion in Europe (RESORCE). *B. Earthq. Eng.* **12**:311–339.

Al Atik L, Abrahamson NA, Bommer JJ, Scherbaum F, Cotton F, Kuehn N (2010) The variability of ground-motion prediction models and its components. *Seismol. Res. Lett.* **81:**783-793.

Ambraseys N, Smit P, Berardi R, Rinaldis D, Cotton F, Berge-Thierry C (2000) Dissemination of European Strong-Motion Data. CD-ROM collection. European Commission, Directorate General XII, Science, Research and Development, Environment and Climate Programme, Bruxelles.

Ambraseys NN (1978) Preliminary analysis of European strong-motion data 1965-1978. *Bull. Eur. Assoc. Earthq. Engrg*. **4**:17-37.

Ambraseys NN (1990) Uniform magnitude re-evaluation of European earthquake associated with strong-motion records. *Earthq. Engrg. Struct. Dyn.* **19**:1-20.

Ambraseys NN and Bommer JJ (1991) Database of European strong-motion records. *Eur. Earthq. Engrg.* **5**:18-37.

Ambraseys NN, Douglas J, Sarma SK, Smit PM (2005a) Equations for the estimation of strong ground motion from shallow crustal earthquakes using data from Europe and the Middle East: horizontal peak ground acceleration and spectral acceleration. *B. Earthq. Eng.* **3**:1-53.

Ambraseys NN, Douglas J, Sarma SK, Smit PM (2005b) Equations for the Estimation of Strong Ground Motions from Shallow Crustal Earthquakes Using Data from Europe and the Middle East: Vertical Peak Ground Acceleration and Spectral. *B. Earthq. Eng.* **3**:54-73.

Ambraseys NN, Douglas J, Sigbjörnsson R, Berge-Thierry C, Suhadolc P, Costa G, Smit PM (2004b) Dissemination of European Strong-Motion Data, Volume 2. Proceedings of the 13th World Conference on Earthquake Engineering, Vancouver, British Columbia, Canada.

Ambraseys NN, Simpson KA (1996) The prediction of vertical response spectra in Europe. *Earthq. Eng. Struct. Dyn.* **25**:401–412.

Ambraseys NN, Simpson KA, Bommer JJ (1996) The prediction of horizontal response spectra in Europe. *Earthq. Eng. Struct. Dyn.* **25**:371-400.

Ambraseys NN, Smit P, Douglas J, Margaris B, Sigbjörnsson R, Olafsson S, Suhadolc P, and Costa G (2004a) Internet site for European strong-motion data. *B. Geofis. Teor. Appl.* **45**: 113-129.

Amorese D, Grasso JR, Plotnikova LM, Nurtaev BS, Bossu R (1995) Rupture kinematics of the three Gazli major earthquakes from vertical and horizontal displacement data. *Bull. Seism. Soc. Am.* **85**:552-559.

Anderson H, Jackson J (1987) Active tectonics of the Adriatic region. *Geophysical J. of the Royal Astronomical Society* **91**:937-983

Anderson JG, Hough SE (1984) A model for the shape of the Fourier amplitude spectrum of acceleration at high frequencies. *Bull. Seism. Soc. Am.* **74**:1969-1993.

Anderson JG, Zeng Y, Sucuoglu H (2001) Analysis of accelerations from the 1 October 1995 Dinar, Turkey, earthquake. *Bull. Seism. Soc. Am.* **91**:1433-1445.

Arvidsson R, Ekström G (1998) Global CMT analysis of moderate earthquakes, Mw4.5, using intermediate-period surface waves. *Bull. Seism. Soc. Am.* **88**:1003–1013.

Ashour SA (1987) Elastic Seismic Response of Buildings with Supplemental Damping. Ph.D. Dissertation, Department of Civil Engineering, University of Michigan, Ann Arbor, MI.

ATC, Applied Technology Council (2010) Modeling and acceptance criteria for seismic design and analysis of tall buildings. *ATC72-1*, Redwood City, CA.

Atkinson GM, Morrison M (2009) Observations on regional variability in ground-motion amplitude for small-to-moderate magnitude earthquakes in North America. *Bull. Seism. Soc. Am.* **99**:2393-2409.

Atkinson GM, Pierre JR (2004) Ground-motion response spectra in eastern North America for different critical damping values. *Seismo. Res. Lett.* **75**:541-545.

Bajc J, Aoudia A, Sarao A, Suhadolc P (2001) The 1998 Bovec-Krn mountain (Slovenia) earthquake sequence. *Geophys. J. Int.* **28**:1839-1842.

Baker JW (2011) Conditional mean spectrum: Tool for ground motion selection. *J. Struct. Eng.* **137**:322–331.

Bazzurro P, Cornell CA (1999) Disaggregation of seismic hazard. *Bull. Seismol. Soc. Am.* **89**: 501–520.

Bazzurro P, Cornell CA (2004a) Ground-Motion Amplification in Nonlinear Soil Sites with Uncertain Properties. *Bull. Seismol. Soc. Am.* **94**:2090–2109.

Bazzurro P, Cornell CA (2004b) Nonlinear soil-site effects in probabilistic seismic-hazard analysis. *Bull. Seismol. Soc. Am.* **94**:2110–2123.

Benetatos C, Dreger D, Kiratzi A (2007) Complex and Segmented Rupture Associated with the 14 August 2003 Mw 6.2 Lefkada, Ionian Islands, Earthquake. *Bull. Seism. Soc. Am.* **97**:35–51.

Benetatos C, Kiratzi A (2006) Finite-fault slip models for the 15 April 1979 (Mw 7.1) Montenegro earthquake and its strongest aftershock of 24 May 1979 (Mw 6.2). *Tectonophysics* **421**:129–143.

Berberian M, Qorashi M, Jackson JA, Priestley K, Wallace T (1992) The Rudbar-Tarom earthquake of 20 June 1990 in N.W. Persia: Preliminary field and seismological observations and its tectonic significance. *Bull. Seism. Soc. Am.* **82**:1726-1755.

Berge-Thierry C, Cotton C, Scotti O, Griot-Pommera D-A, Fukushima Y (2003) New empirical attenuation laws for moderate European earthquakes. *J. Earthq. Eng.* **7**:193-222.

Bernard P, Gariel JC, Dorbath L (1997) Fault location and rupture kinematics of the magnitude 6.8, 1992 Erzincan earthquake, Turkey, from strong ground motion and regional records. *Bull. Seism. Soc. Am.* **87**:1230-1243.

Bindi D, Luzi L, Massa M, Pacor F (2010) Horizontal and vertical ground motion prediction equations derived from the Italian Accelerometric Archive (ITACA). *B. Earthq. Eng.* **8**:1209-1230.

Bommer J, Elnashai AS, Chlimintzas GO, Lee D (1998) Review and development of response spectra for displacement-based design. ESEE Research Report No. 98-3, Imperial College London.

Bommer J, Mendis R (2005) Scaling of spectral displacement ordinates with damping ratios. *Earthq. Engrg. Struct. Dyn.* **34**:145–165.

Bommer JJ, Akkar S (2012) Consistent source-to-site distance metrics in ground-motion prediction equations and seismic source models for PSHA. *Earthq. Spectra* **28**:1-15.

Bommer JJ, Akkar S, Drouet S (2012) Extending ground-motion prediction equations for spectral ordinates to higher response frequencies. *B. Earthq. Eng.* **10**:379–399.

Bommer JJ, Akkar S, Kale Ö (2011) A model for vertical-to-horizontal response spectral ratios for Europe and the Middle East. *Bull. Seism. Soc. Am.***101**:1783-1806.

Bommer JJ, Alarcón JE (2006) The prediction and use of peak ground velocity. *J. Earthq. Eng.* **10**:1-31.

Bommer JJ, Ambraseys NN (1992) An earthquake strong-motion databank and database. Proc. of Tenth World Conference on Earthquake Engineering, A.A. Balkema. Rotterdam, The Netherlands. vol. 1, pp. 207-210.

Bommer JJ, Douglas D (2004) Processing of European strong-motion records at Imperial College London. Proceedings of the COSMOS Workshop on Record Processing Guidelines, Richmond, California.

Bommer JJ, Douglas J, Scherbaum F, Cotton F, Bungum H, Fäh D (2010b) On the selection of ground-motion prediction equations for seismic hazard analysis. *Seismol. Res. Lett.* **81**:783-793

Bommer JJ, Douglas J, Strasser FO (2003) Style-of-faulting in ground motion prediction equations. *B. Earthq. Eng.* **1**:171-203.

Bommer JJ, Pinho R (2006) Adapting earthquake actions in Eurocode 8 for performance-based seismic design. *Earthq. Engng Struct. Dyn.* **35**:39-55.

Bommer JJ, Scherbaum F (2008) The use and misuse of logic-trees in PSHA. *Earthq. Spectra* **24**:997-1009.

Bommer JJ, Scherbaum F, Bungum H, Cotton F, Sabetta F, Abrahamson NA (2005) On the use of logic trees for ground-motion prediction equations in seismic hazard assessment. *Bull. Seism. Soc. Am.* **95**:377-389.

Bommer JJ, Stafford PJ, Akkar S (2010a) Current empirical ground-motion prediction equations for Europe and their application to Eurocode 8. *B. Earthq. Eng.* **8**:5-26.

Bommer JJ, Stafford PJ, Alarcón JE, Akkar S (2007) The influence of magnitude range on empirical ground-motion prediction. *Bull. Seism. Soc. Am.* **97**:2152-2170.

Boore DM (2004) Estimating Vs(30) (or NEHRP Site Classes) from shallow velocity models (depths < 30 m). *Bull. Seism. Soc. Am.* **94**: 591–597.

Boore DM (2005) SMSIM--Fortran Programs for Simulating Ground Motions from Earthquakes: Version 2.3--A Revision of OFR 96-80-A. U.S. Geological Survey Open-File Report (A modified version of OFR 00--509, describing the program as of 15 August, 2005), Menlo Park, California.

Boore DM, Atkinson GM (2007) Boore-Atkinson NGA Ground Motion Relations for the Geometric Mean Horizontal Component of Peak and Spectral Ground Motion Parameters. PEER 2007/01, Pacific Earthquake Engineering Research Center, University of California, Berkeley, California.

Boore DM, Atkinson GM (2008) Ground-motion prediction equations for the average horizontal component of PGA, PGV, and 5%-damped PSA at spectral periods between 0.1s and 10.0s. *Earthq. Spectra* **24**:99-138.

Boore DM, Azari AS, Akkar S (2012) Using Pad-Stripped Acausally Filtered Strong-Motion Data. *Bull. Seism. Soc. Am.* **102**: 751-760.

Boore DM, Bommer JJ (2005) Processing of strong-motion accelerograms?: needs , options and consequences. *Soil Dyn. Earthq. Engrg.* **25**:93-115.

Boore DM, Joyner WB (1997) Site Amplifications for Generic Rock Sites. *Bull. Seism. Soc. Am.* **87**: 327-341.

Boore DM, Joyner WB, Fumal TE (1993) Estimation of response spectra and peak accelerations from western North American earthquakes: an interim report. Open-File Report 93-509, U.S. Geological Survey, California.

Boore DM, Joyner WB, Fumal TE (1997) Equations for estimating horizontal response spectra and peak acceleration from western North American earthquakes: a summary of recent work. *Seismol. Res. Lett.* **68**: 128-153.

Boore DM, Skarlatoudis AA, Margaris BN, Papazachos CB, Ventouzi C (2009) Along-Arc and Back-Arc Attenuation, Site Response, and Source Spectrum for the Intermediate-Depth 8 January 2006 M 6.7 Kythera, Greece, Earthquake. *Bull. Seism. Soc. Am.* **99**:2410–2434.

Borcherdt RD (1970) Effects of local geology on ground motion near San Francisco Bay. *Bull. Seism. Soc. Am.* **60**: 29-61.

Borcherdt RD (1994) Estimates of Site Dependent Response spectra for Design (Methodology and Justification). *Earthq. Spectra* **10**: 617-653.

Borcherdt RD (2002a) Empirical evidence for acceleration-dependent amplification factors. *Bull. Seism. Soc. Am.* **92**: 761-782.

Borcherdt RD (2002b) Empirical evidence for site coefficients in building-code provisions. *Earthq. Spectra* **18**: 189-218.

Bozorgnia Y, Abrahamson NA, Campbell KW, Rowshandel B, Shantz T (2012) NGAWest2: A comprehensive research program to update ground motion prediction equations for shallow crustal earthquakes in active tectonic regions. *Proceedings of 15th World Conference on Earthquake Engineering* Paper Number 2572, Lisbon, Portugal.

Bozorgnia Y, Campbell KW (2004) The vertical-to-horizontal spectral ratio and tentative procedures for developing simplified V/H and vertical design spectra. *J. Earthq. Eng.* **4**:539–561.

BSSC, Building Seismic Safety Council (2009) 2009 NEHRP Recommended Seismic Provisions For New Buildings and Other Structures: Part 1, Provisions. Federal Emergency Management Agency (P-750), Washington DC.

Burks LS, Baker JW (2012) Occurrence of negative epsilon in seismic hazard analysis deaggregation, and its impact on target spectra computation. *Earthq. Engng. Struct. Dyn.* **41**:1241–1256

Cadet H, Bard P-Y, Duval A-M, Bertrand E (2012b) Site effect assessment using KiK-net data - Part 2 - Site Amplification Prediction Equation (SAPE) based on f0 and Vsz. *Bull. Earthq. Engineering* **10**:451-489.

Cadet H, Bard P-Y, R-Marek A (2012a) Site effect assessment using KiK-net data - Part 1 - A simple correction procedure for surface/downhole spectral ratios. *Bull. Earthq. Engineering* **10**:421-448.

Cadet H, Bard P-Y, Rodriguez-Marek A (2010) Defining a Standard Rock Site: Propositions Based on the KiK-net Database. *Bull. Seism. Soc. Am.* **100**: 172-195.

Cameron WI, Green I (2007) Damping correction factors for horizontal ground-motion response spectra. *Bull. Seismo. Soc. Am.* **97**:934–960.

Campbell KW, Bozorgnia Y (2003) Updated near-source ground motion (attenuation) relations for the horizontal and vertical components of peak ground acceleration and acceleration response spectra. *Bull. Seismol. Soc. Am.* **93**:314–331.

Campbell KW, Bozorgnia Y (2008) NGA ground motion model for the geometric mean horizontal component of PGA, PGV, PGD and 5%-damped linear elastic response spectra at periods ranging from 0.1 s to 10.0 s. *Earthq. Spectra* **24**:139-171.

Castello B, Olivieri M, Selvaggi G (2007) Local and Duration Magnitude Determination for the Italian Earthquake Catalog, 1981-2002. *Bull. Seism. Soc. Am.* **97**:128-139.

Cauzzi C, Faccioli E (2008) Broadband (0.05 to 20 s) prediction of displacement response spectra based on worldwide digital records. *J. Seismol.* **12**:453–475.

CEN, Comité Européen de Normalisation (2004) Eurocode 8: Design of structures for earthquake resistance - Part 1: General rules, seismic actions and rules for buildings. European Committee for Standardization, Brussels.

Chiou B, Darragh R, Gregor N, Silva W (2008) NGA Project Strong-Motion Database. *Earthq. Spectra* **24**: 23-44.

Chiou B, Youngs R, Abrahamson N, Addo K (2010) Ground-motion attenuation model for small-to-moderate shallow crustal earthquakes in California and its implications on regionalization of ground-motion prediction models. *Earthq. Spectra* **26**:907-926.

Chiou BS-J, Youngs RR (2008) An NGA model for the average horizontal component of peak ground motion and response spectra. *Earthq. Spectra* **24**:173-215.

Chiou BS-J, Youngs RR (2013) Update of the Chiou and Youngs NGA Ground Motion Model for Average Horizontal Component of Peak Ground Motion and Response Spectra. PEER 2013/07, Pacific Earthquake Engineering Research Center, University of California, Berkeley, California.

Choi Y, Stewart JP (2005) Nonlinear site amplification as function of 30m shear wave velocity. *Earthq. Spectra* **21**:1-30.

Chouliaras G, Stavrakakis GN (1997) Seismic source parameters from a new dial-up network in Greece. *Pure Appl. Geophys.* **150**:91–111.

Cramer, CH (2003) Site specific seismic hazard analysis that is completely probabilistic, Bull. Seismol. Soc. Am. 93, 1841–1846.

Crouse CB, McGuire JW (1996) Site response studies for purpose of revising NEHRP seismic provisions. *Earthq. Spectra* **12**: 407-439.

Danciu L, Tselentis G-A (2007) Engineering ground-motion parameters attenuation relationships for Greece. *Bull. Seism. Soc. Am.***97**: 162-183.

Decriem J, Árnadóttir T, Hooper A, Geirsson H, Sigmundsson F, Keiding M, Ófeigsson BG, Hreinsdóttir S, Einarsson P, LaFemina P, Bennett RA (2010)

The 2008 May 29 earthquake doublet in SW Iceland. *Geophys. J. Int.* **181**:1128–1146.

Delouis B, Giardini D, Lundgren P, Salichon J (2002) Joint Inversion of InSAR, GPS, Teleseismic, and Strong-Motion Data for the Spatial and Temporal Distribution of Earthquake Slip: Application to the 1999 Izmit Mainshock. *Bull. Seism. Soc. Am.* **92**:278–299.

Derras B, Bard P-Y, Cotton F, Bekkouche A (2012) Adapting the neural network approach to PGA prediction: an example based on the KiK-net data. *Bull. Seismol. Soc. Am.* **102**: 1446-1461.

Dobry R, Borcherdt RD, Crouse CB, Idriss IM, Joyner WB, Martin GR, Power MS, Rinne EE, Seed RB (2000) New site coefficients and site classification system used in recent building seismic code provisions. *Earthq. Spectra* **16**: 41-67.

Douglas J (2003a) What is a poor quality strong-motion record? *B. Earthq. Eng.* **1**:141-156.

Douglas J (2003b) Earthquake ground motion estimation using strong-motion records: a review of equations for the estimation of peak ground acceleration and response spectral ordinates. *Earth-Sci. Rev.* **61**:43-140.

Douglas J (2011) Ground-motion prediction equations 1964-2010. *Final Report BRGM/RP-59356-FR*.

Douglas J, Boore DM (2011) High-frequency filtering of strong-motion records. *B. Earthq. Eng.* **9**:395-409.

Douglas J, Halldórsson B (2010) On the use of aftershocks when deriving ground-motion prediction equations. *Proceedings of the 9th U.S. National and 10th Canadian Conference on Earthquake Engineering.* Paper no. 220.

Douglas J, Jousset P (2011) Modeling the difference in ground-motion magnitude-scaling in small and large earthquakes. *Seismol. Res. Lett.* **82**: 504-508.

Edwards B, Poggi V, Fäh D (2011) A Predictive Equation for the Vertical-to-Horizontal Ratio of Ground Motion at Rock Sites Based on Shear-Wave Velocity Profiles from Japan and Switzerland. *Bull. Seism. Soc. Am.* **101**:2998–3019.

Elnashai AS, Papazoglu AJ (1997) Procedure and spectra for analysis of RC structures subjected to vertical earthquake loads. *J. Earthq. Eng.* **1**:121–155.

EPRI, Electric Power Research Institute (2004) CEUS Ground Motion Project: Final Report. EPRI Report 1009684 Palo Alto, California.

Erdik M (1984) Report on the Turkish earthquake of October 30, 1983. *Earthq. Spectra* **1**:151-172.

Faccioli E, Paolucci R, Rey J (2004) Displacement spectra for long periods. *Earthq. Spectra* **20**:347–376.

Field EH (2000) A Modified Ground-Motion Attenuation Relationship for Southern California that Accounts for Detailed Site Classification and a Basin-Depth Effect. *Bull. Seism. Soc. Am.* **90**: S209-S221.

Frohlich C, Apperson KD (1992) Earthquake focal mechanisms, moment tensors, and the consistency of seismic activity near plate boundaries. *Tectonics* **11**:279-296.

Fukushima Y, Berge-Thierry C, Volant P, Griot-Pommera D-A, Cotton F (2003) Attenuation relation for West Eurasia determined with recent near-fault records from California, Japan and Turkey. *J. Earthq. Eng.* **7**:573-598.

Giardini D, Woessner J, Danciu L, Crowley H, Cotton F, Gruenthal G, Pinho R, Valensise G, Akkar S, Arvidsson R, Basili R, Cameelbeck T, Campos-Costa A, Douglas J, Demircioglu MB, Erdik M, Fonseca J, Glavatovic B, Lindholm C, Makropoulos K, Meletti F, Musson R, Pitilakis K, Sesetyan K, Stromeyer D, Stucchi M, Rovida A (2013) Seismic Hazard Harmonization in Europe (SHARE): Online Data Resource. Doi:10.12686/SED-00000001-SHARE.

Goulet CA, Stewart JP (2009) Pitfalls of Deterministic Application of Nonlinear Site Factors in Probabilistic Assessment of Ground Motions. *Earthq. Spectra* **25:**541-555.

Gülerce Z, Abrahamson NA (2011) Site-specific spectra for vertical ground motion. *Earthq. Spectra* **27**:1023–1047.

Haessler H, Gaulon R, Rivera L, Console R, Frogneux M, Gasparini G, Martel L, Patau G, Siciliano M, Cisternas A (1988) The Perugia (Italy) earthquake of 29, April, 1984: A microearthquake survey. *Bull. Seism. Soc. Am.* **78**:1948-1964.

Harmsen S (2001) Mean and Modal ϵ in the Deaggregation of Probabilistic Ground Motion *Bull. Seismol. Soc. Am.* **91**:1537-1552.

Hatzfeld D, Karakostas V, Ziazia M, Selvaggi G, Leborgne S, Berge C, Guiguet R, Paul A, Voidomatis P, Diagourtas D, Kassaras I, Koutsikos I, Makropoulus K, Azzara R, Di Mona M, Baccheschi S, Bernard P, Papaioannou (1997) The Kozani-Grevena (Greece) earthquake of 13 May 1995 revisited from a detailed seismological study. *Bull. Seism. Soc. Am.* **87**:463-473.

Hatzigeorgiou GD (2010) Damping modification factors for SDOF systems subjected to near-fault, far-fault and artificial earthquakes. *Earthq. Engrg. Struct. Dyn.* **39**:1239-1258.

Huang Y-N, Whittaker AS, Luco N (2010) NEHRP Site Amplification Factors and the NGA Relationships. *Earthq. Spectra*, **26**:583–593.

Idriss IM (1990) Response of soft soil sites during earthquakes, Proc. H. Bolton Seed Memorial Symposium, J. M. Duncan (ed.), Vol. 2, pp. 273–90.

Idriss IM (1993) Procedures for selecting earthquake ground motions at rock sites. Report NIST GCR 93–625, National Institute of Standards and Technology, Washington DC.

Jackson J, Bouchon M, Fielding E, Funning G, Ghorashi M, Hatzfeld D, Nazari H, Parsons B, Priestley K, Talebian M, Tatar M, Walker R, Wright T (2006)

225

Seismotectonic, rupture process, and earthquake-hazard aspects of the 2003 December 26 Bam, Iran, earthquake. *Geophys. J. Int.* **166**:1270–1292.

Joyner WB, Boore DM (1981) Peak horizontal acceleration and velocity from strong-motion records including records from the 1979 Imperial Valley, California, earthquake. *Bull. Seism. Soc. Am.* **71**:2011-2038.

Joyner WB, Boore DM (1993) Methods for regression analysis of strong-motion data. *Bull. Seism. Soc. Am.* **83**: 469-487.

Kagawa T, Irikura K, Somerville PG (2004) Differences in ground motion and fault rupture process between the surface and buried rupture earthquakes. *Earth Planets Space* **56**:3-14.

Kaklamanos J, Baise LG, Boore DM (2011) Estimating unknown input parameters when implementing the NGA ground-motion prediction equations in engineering practice. *Earthq. Spectra* **27:**1219-1235.

Kunnath SK, Erduran E, Chai YH, Yashinsky M (2008) Effect of near-fault vertical ground motions on seismic response of highway overcrossings. *J. Bridge Eng.* **13**:282–290.

Lee Y, Anderson JG (2000) Potential for Improving Ground-Motion Relations in Southern California by Incorporating Various Site Parameters. *Bull. Seism. Soc. Am.* **90**: S170-S186.

Leonard M (2010) Earthquake fault scaling: self-consistent relating of rupture length, width, average displacement, and moment release *Bull. Seism. Soc. Am.* **100**:1971-1988.

Lin T, Harmsen SC, Baker JW, Luco N (2013) Conditional Spectrum Computation Incorporating Multiple Causal Earthquakes and Ground Motion Prediction Models. *Bull. Seism. Soc. Am.* **103**:1103-1116.

Lin YY, Chang KC (2003) Study on damping reduction factor for buildings under earthquake ground motions. *J. Struct. Engrg.* **129**:206–214.

Lin YY, Chang KC (2004) Effects of site classes on damping reduction factors. *J. Struct. Engrg.* **130**:1667–1675.

Lin YY, Miranda E, Chang KC (2005) Evaluation of damping reduction factors for estimating elastic response of structures with high damping. *Earthq. Engrg. Struct. Dyn.* **34**:1427–1443.

Louvari E, Kiratzi AA, Papazacchos BC (2004) The Cephalonia Transform Fault and its extension to western Lefkada Island (Greece). *Tectonophysics* **308**:223–236.

Luzi L, Hailemikael S, Bindi D, Pacor F, Mele F, Sabetta F (2008) ITACA (ITalian ACcelerometric Archive): A web portal for the dissemination of the Italian strong motion data. *Seismol. Res. Lett.* **79**:716-722.

Lyon-Caen H, Armijo R, Drakopoulos J, Baskoutass J, Delibassis N, Gaulon R, Kouskouna V, Latoussakis J, Makropoulos K, Papadimitriou P, Papanastassiou D, Pedotti G (1988) The 1986 Kalamata (south Peloponnesus) earthquake: Detailed study of a normal fault, evidences for east-west extension in the Hellenic arc. *J. Geophys. Res.* **93**-B12:14967-15000.

Mai MP, Spudich P, Boatwright J (2005) Hypcenter locations in finite-source rupture models. *Bull. Seism. Soc. Am.* **95**:965-980.

Makaris DI, Theodulidis NP, Stavrakakis GN (2000) Estimation of strong ground motion due to hypothetical fault ruptures and comparison with recorded values: The Zakynthos, Western Greece Earthquake of 18 November 1997. *Nat. Hazards* **21**:297-315.

Malhotra PK (2006) Smooth spectra of horizontal and vertical ground motions. *Bull. Seism. Soc. Am.* **96**:506-518.

Manighetti I, Campillo M, Sammis C, Mai PM, King G (2005) Evidence for self-similar, triangular slip distributions on earthquakes: implications for earthquake and fault mechanics. *J. Geophys. Res.* **110**: B05302, doi:10.1029/2004JB003174.

Moss RES (2009) Reduced uncertainty of ground motion prediction equations through Bayesian variance analysis. *Report No: 2009/105*, Pacific Earthquake Engineering Research Center, University of California, Berkeley, California.

Naeim F, Kircher CA (2001) On the damping adjustment factors for earthquake response spectra. *Struct. Des. Tall. Spec.* **10**:361-369.

Newmark NM, Hall WJ (1982) Earthquake Spectra and Design. Earthquake Engineering Research Institute, Berkeley, CA.

Ni S-D, Anderson JG, Zeng Y, Siddharthan RV (2000) Expected Signature of Nonlinearity on Regression for StrongGround-Motion Parameters. *Bull. Seism. Soc. Am.* **90:** S53-S64.

Oncescu LC, Bonjer KP (1997) A note on the depth recurrence and strain release of large Vrancea earthquake. *Tectonophysics* **272**:291-302.

Pace B, Boncio P, Lavecchia G (2002) The 1984 Abruzzo earthquake (Italy): an example of seismogenic process controlled by interaction between differently oriented synkinematic faults. *Tectonophysics* **350**:237-254.

Papaspiliou M, Kontoe S, Bommer JJ (2012a) An exploration of incorporating site response into PSHA—Part I: Issues related to site response analysis methods. *Soil Dyn. Earthq. Eng.* **42**:302-315.

Papaspiliou M, Kontoe S, Bommer JJ. (2012b) An exploration of incorporating site response into PSHA-part II: Sensitivity of hazard estimates to site response approaches. *Soil Dyn. Earthq. Eng.* **42**:316-330.

Papazachos BC, Karakostas VG, Kiratzi AA, Margaris BN, Papazachos CB, Scordilis EM (2002) Uncertainties in the estimation of earthquake magnitudes in Greece. *J. of Seismol.* **6**: 557–570.

Pedersen R, Jónsson S, Árnadóttir T, Sigmundsson F, Feigl KL (2003) Fault slip distribution of two June 2000 M_w6.5 earthquakes in South Iceland estimated from joint inversion of InSAR and GPS measurements. *Earth and Planetary Science Letters* **213**:487-502.

Perniola B, Bressan G, Pondrelli S (2004) Changes in failure stress and stress transfer during the 1976–77 Friuli earthquake sequence. *Geophys. J. Int.* **156**:297-306.

Petersen MD, Frankel AD, Harmsen SC, Mueller CS, Haller KM, Wheeler RL, Wesson RL, Zeng Y, Boyd OS, Perkins DM, Luco N, Field EH, Wills CJ, Rukstales KS (2008) Documentation for the 2008 update of the United States national seismic hazard maps. *USGS Open-File Report 2008-1128, US Geological Survey*, Reston, Virginia.

Pitilakis K, Riga E, Anastasiadis A (2012) Design spectra and amplification factors for Eurocode 8. *B Earthq Eng.* **10**: 1377-1400.

Pitilakis K, Riga E, Anastasiadis A (2013) New code site classification, amplification factors and normalized response spectra based on a worldwide ground-motion database. *B. Earthq. Eng.* DOI 10.1007/s10518-013-9429-4.

Poggi V, Edwards B, Fäh D (2012) Characterizing the vertical-to-horizontal ratio of ground motion at softsediment sites. *Bull Seismol. Soc. Am.* **102**:2741–2756.

Pousse G, Thierry CB, Bard PY (2005) Eurocode 8 design response spectra evaluation using the K-NET Japanese database. *J. Earthq. Eng.* **9**: 547–574.

Power M, Chiou B, Abrahamson N, Bozorgnia Y, Shantz T, Roblee C (2008) An overview of the NGA project. *Earthq. Spectra* **24**:3-21.

Priestly MJN (2003) Myths and Fallacies in Earthquake Engineering, Revisited. The Mallet Milne Lecture, IUSS Press, Istituto Universitario di Studi Superiori di Pavia, Pavia, Italy.

Ramirez OM, Constantinou MC, Kircher CA, Whittaker AS, Johnson MW, Gomez JD, Chrysostomou CZ (2000) Development and evaluation of simplified procedures for analysis and design of buildings with passive energy dissipation systems. Report No: MCEER-00-0010, Multidisciplinary Center for Earthquake Engineering Research, University of New York, Buffalo, NY.

Ramirez OM, Constantinou MC, Whittaker AS, Kircher CA, Chrysostomou CZ (2002) Elastic and inelastic seismic response of buildings with damping systems. *Earthq. Spectra* **18**:531–547.

Rey J, Faccioli E, Bommer J (2002) Derivation of design soil coefficient (S) and response spectral shapes for Eurocode 8 using the European Strong-Motion Database. *J. of Seismol.* **6**:547-555.

Rezaeian S, Bozorgnia Y, Idriss IM, Campbell K, Abrahamson N, Silva W (2012) Spectral Damping Scaling Factors for Shallow Crustal Earthquakes in Active Tectonic Regions. PEER 2012/01, Pacific Earthquake Engineering Research Center, University of California, Berkeley, California.

Rodriguez-Marek A, Bray JD, Abrahamson NA (2001) An empirical geotechnical seismic site response procedure. *Earthq. Spectra* **17**: 65-87.

Rosenblad BL, Rathje EM, Stokoe KH (2002) Shear wave velocity profiling by SASW method at selected strong-Motion stations in Turkey. Lifelines Projects Topic 2 – Site Response Report No. 2A02a, Pacific Earthquake Engineering Research Center, University of California, Berkeley, California.

Roumelioti Z, Kiratzi A (2002) Stochastic simulation of strong-motion records from the 15 April 1979 (M 7.1) Montenegro earthquake. *Bull. Seism. Soc. Am.* **92**:1095-1101.

Sadigh K, Chang CY, Egan JA, Makdisi F, Youngs RR (1997) Attenuation relationships for shallow crustal earthquakes based on California strong motion data. *Seismol. Res. Lett.* **68**: 180-189.

Salvi S, Stramondo S, Cocco M, Tesauro M, Hunstad I, Anzidei M, Briole P, Baldi P, Sansosti E, Fornaro G, Lanari R, Doumaz F, Pesci A, Galvani A (2000) Modeling coseismic displacements resulting from SAR inferferometry and GPS measurements during the 1997 Umbria-Marche seismic sequence. *J. of Seismol.* **4**:479-499.

Sandıkkaya M.A., S. Akkar, P.-Y. Bard (2014). A Proposal to Describe Site Amplification Factors for Seismic Design Codes. *Earthquake Spectra*, (submitted).

Sandıkkaya MA, Akkar S (2012) How style-of-faulting ratios change with database features. *Seismol. Res. Lett.* **83**:123-124.

Sandıkkaya MA, Akkar S, Bard P-Y (2013) A nonlinear site amplification model for the new pan-European ground-motion prediction equations. *Bull. Seism. Soc. Am.* **103**: 19-32.

Sandıkkaya MA, Yılmaz MT, Bakır BS, Yılmaz Ö (2010) Site classification of Turkish national strong-motion stations. *J. of Seismol.* **14**:543-563.

Scasserra G, Stewart JP, Bazzurro P, Lanzo G, Mollaioli F (2009) A comparison of NGA ground-motion prediction equations to Italian data. *Bull. Seism. Soc. Am.* **99**:2961-2978.

Scherbaum F, Cotton F, Staedtke H (2006) The estimation of minimum-misfit stochastic models from empirical ground-motion prediction equations. *Bull. Seism. Soc. Am.* **96**:427-445.

Scherbaum F, Schemedes J, Cotton F (2004) On the Conversion of Source-to-Site Distance Measures for Extended Earthquake Source Models. *Bull. Seism. Soc. Am.* **94**:1053-1069.

Scordilis EM (2006) Empirical global relations converting M_s and m_b to moment magnitude. *J. of Seismol.* **10**: 225-236.

Seed HB, Ugas C, Lysmer J (1976) Site-dependent spectra for earthquake-resistant desing. *Bull Seismol Soc Am.* **66**:221–244.

Snoke JA (2003) FOCMEC: Focal Mechanism Determinations. International Handbook of Earthquake and Engineering Seismology 81B:1629-1632. Academic Press, UK.

Sokolov VY (1997) Empirical models for estimating Fourier-amplitude spectra of ground acceleration in the northern Caucasus (Racha seismogenic zone). *Bull. Seism. Soc. Am.* **87**: 1401-1412.

Sokolov VY (2000) Hazard-Consistent Ground Motions: Generation on the Basis of Uniform Hazard Fourier Spectra. *Bull. Seism. Soc. Am.* **90**: 1010-1027.

Soufleris C, Jackson JA, King GCP, Spencer CP, Scholz CH (1982) The 1978 earthquake sequence near Thessaloniki (northern Greece). *Geophys. J. R. Astr. Soc.* **68**:429-458.

Spudich P, Joyner WB, Lindh AG, Boore DM, Margaris BM, Fletcher JB (1999) SEA99: A revised ground motion prediction relation for use in extensional tectonic regimes. *Bull. Seism. Soc. Am.* **89**:1156-1170.

Stafford PJ, Mendis R, Bommer, JJ (2008b) Dependence of damping correction factors for response spectra on duration and numbers of cycles. *J. Struct. Engrg.* **134**:1364–1373.

Stafford PJ, Strasser FO, Bommer JJ (2008a) An evaluation of the applicability of the NGA models to ground-motion prediction in the Euro-Mediterranean region. *B. Earthq. Eng.* **6**:149-177.

Steidl JH (2000) Site Response in Southern California for Probabilistic Seismic Hazard Analysis. *Bull. Seism. Soc. Am.* **90**: S149-S169.

Stewart JP, Liu AH, Choi Y (2003) Amplification Factors for Spectral Acceleration in Tectonically Active Regions. *Bull. Seism. Soc. Am.* **93**: 332-352.

Strasser FO, Abrahamson NA, Bommer JJ (2009) Sigma: Issues, insights, and challenges. *Seismol. Res. Lett.* **80:**40-56.

Talebian M, Biggs J, Bolourchi M, Copley A, Ghassemi A, Ghorashi M, Hollingsworth J, Jackson J, Nissen E, Oveisi B, Parsons B, Priestley K, Saiidi A (2006) The Dahuiyeh (Zarand) earthquake of 2005 February 22 in central

Iran: reactivation of an intramountain reverse fault. *Geophys. J. Int.* **164**:137–148.

Tan O, Pabuçcu Z, Tapırdamaz MC, İnan S, Ergintav S, Eyidogan H, Aksoy E, Kuluöztürk F (2011) Aftershock study and seismotectonic implications of the 8 March 2010 Kovancılar (Elazıg, Turkey) earthquake (Mw = 6.1). *Geophys. Res. Lett.* **38**-L11304, doi:10.1029/2011GL047702.

Tatar M, Jackson J, Hatzfeld D, Bergman E (2007) The 2004 May 28 Baladeh earthquake (M_w 6.2) in the Alborz, Iran: overthrusting the South Caspian Basin margin, partitioning of oblique convergence and the seismic hazard of Tehran. *Geophys. J. Int.* **170**:249–261.

Theodulidis N, Kalogeras I, Papazachos C, Karastathis V, Margaris B, Papaioannou Ch, Skarlatoudis A (2004) HEAD 1. O: A Unified HEllenic Accelerogram Database. *Seismol Res Lett.* **75**:36-45.

Thompson EM, Baise LG, Kayen RE, Morgan EC, Kaklamanos J (2011) Multiscale Site Response Mapping: A case study of Parkfield, California. *Bull. Seism. Soc. Am.* **101**: 1081-1100.

Tolis SV, Faccioli E (1999) Displacement design spectra. *J. Earthq. Engrg.* **3**:107-125.

Triep EG, Abers GA, Lerner-Lam AL (1995) Active thrust front of the greater Caucasus: The April 29, 1991, Racha earthquake sequence and its tectonic implications. *J. Geoph. Res.* **100**-B3:4011-4033.

Trifunac MD, Lee VW (1989) Empirical models for scaling pseudo relative velocity spectra of strong earthquake accelerations in terms of magnitude, distance, site intensity and recording site conditions. *Soil Dyn. Earthq. Engrg.* **8**:126-144.

Trifunac MD, Todorovska MI (2001) A note on the usable dynamic range of accelerographs recording translation. *Soil Dynamics and Earthquake Engineering*, **21**:275-286

Tsai C-C P (2000) Probabilistic seismic hazard analysis considering nonlinear site effects. *Bull. Seismol. Soc. Am.* **90**:1–7.

Tselentis GA, Melis NS, Sokos E, Papatsimpa K (1996) The Egion June 15, 1995 (6.2ML) earthquake, western Greece. *Pure Appl. Geophys.* **147**:83-98.

Tselentis GA, Zahradnik J (2000) Aftershock Monitoring of the Athens Earthquake of 7 September 1999. *Seismol. Res. Lett.* **71**:330-337.

Umutlu N, Koketsu K, Milkerit C (2004) The rupture process during the 1999 Düzce, Turkey earthquake from joint inversion of teleseismic and strong motion data. *Tectonophysics* **391**:315-324.

Walker R, Jackson J, Baker C (2003) Surface expression of thrust faulting in eastern Iran: source parameters and surface deformation on the 1978 Tabas and 1968 Ferdows earthquake sequences. *Geophys. J. Int.* **152**:729-765.

Walker RT, Bergman E, Jackson J, Ghorashi M, Talebian M (2005) The 2002 June 22 Changureh (Avaj) earthquake in Qazvin province, northwest Iran: epicentral relocation, source parameters, surface deformation and geomorphology. *Geophys. J. Int.* **160**:707-720.

Walling M, Silva W, Abrahamson NA (2008) Nonlinear Site Amplification Factors for Constraining the NGA Models. *Earthq. Spectra* **24**:243-255.

Wells DL, Coppersmith KJ (1994) New empirical relationships among magnitude, rupture length, rupture width, rupture area, and surface displacement. *Bull. Seism. Soc. Am.* **84**:974-1002.

Westaway R, Smith RB (1989) Strong ground motion from normal-faulting earthquakes. *Geophys. J. Int.* **96**:529-559.

Wu J, Hanson RD (1989) Study of inelastic spectra with high damping. *J Struct. Engrg.* **115**:1412-1431.

Yenier E, Sandıkkaya MA, Akkar S (2010). Report on the fundamental features of the extended strong motion databank prepared for the SHARE project, pp. 44.

Deliverable 4.1 of Seventh Framework Programme Project Seismic Hazard Harmonization in Europe (SHARE), 34 pages, Ankara.

Zhao JX, Zhang J, Asano A, Ohno Y, Oouchi T, Takahashi T, Ogawa H, Irikura K, Thio HK, Somerville PG, Fukushima Y (2006) Attenuation relations of strong ground motion in Japan using site classifications based on predominant period. *Bull. Seism. Soc. Am.* **96**:898-913.

Zoback ML (1992) First- and second-order patterns of stress in the lithosphere: The World Stress Map Project. *J. Geophys. Res.* **97**:11703–11728.

CURRICULUM VITAE

M. Abdullah SANDIKKAYA

Address   : Bülbülderesi Cad. 41/7 Küçükesat, Çankaya, Ankara, Turkey
Mobile Phone : +90 533 730 9044
Skype Name   : asandikkaya
E-mail   : asandikkaya@gmail.com
LinkedIn Name: Abdullah Sandikkaya

EDUCATION

Ph.D. (2014; exp.)	Civil Engineering, Middle East Technical University, Ankara, Turkey Institut des Sciences de la Terre, Université Joseph Fourier, Grenoble, France
M.Sc. (2008)	Civil Engineering, Middle East Technical University, Ankara, Turkey
B.Sc. (2005)	Civil Engineering, Middle East Technical University, Ankara, Turkey

PROFESSIONAL EXPERIENCE

Nov. 2013-…	Science Programming Expert The Scientific and Technological Research Council of Turkey
Sep. 2012- …	Independent Researcher
Nov. 2006- Sep. 2012	Research Assistant at Middle East Technical University, Faculty of Engineering, Department of Civil Engineering, Division of Geotechnical Engineering, Ankara, Turkey
July 2005- Oct. 2005	Site Engineer at Upeks Highway Materials Company, Ankara, Turkey

TEACHING EXPERIENCE

Soil Mechanics, Foundation Engineering, Introduction to Soil Dynamics, Seismic Hazard Assessment (descriptions of the courses are available at **www.ce.metu.edu.tr**).

PROJECTS INVOLVED

Sep. 2013	SWUS GMC SSHAC Level 3 Project.
Jan. 2011- Dec. 2014	SIGMA Project. Compilation of the strong ground motion database. Funded by the EDF, France and other collaborators
June 2009- June 2012	Strong ground motion modeling, site amplification factors (Task 4) in the "*Seismic Hazard Harmonization in Europe (SHARE)*." Funded by the European Community FP7.
Jan. 2008- July 2009	Compilation of strong motion and seismic hazard data for Mediterranean countries (in particular Italy and Turkey) for infrastructural works (existing or under design) (Task 1) in the "*Assessment and Reduction of Seismic Risk to Large Infrastructural Systems (FIRB)*." Funded by the Italian Ministry for Research and Higher Education.
Nov. 2005- Oct. 2009	Compilation of National Strong Ground Motion Database in Accordance with International Standards. Funded by the Scientific Research and Technical Council of Turkey.

LANGUAGES

Turkish: Native language
English: Advanced level
French : Beginner level

COMPUTER SKILLS

Various soft-wares related to earthquake engineering and engineering seismology (seismic hazard analysis, ground-motion simulation and manipulation, site response analysis, etc.) as well as computer programming in Matlab and scripting in Visual Basic.

MEMBERSHIPS

2014 – Present	Earthquake Engineering Research Institute, Student Member
2011 – Present	Seismological Society of America, Student Member
2009 – Present	Earthquake Engineering Association of Turkey, Student Member
2008 – Present	American Society Civil Engineers, Student Member
2003 – Present	Turkish Chamber of Civil Engineers, Member

AWARDS AND HONORS

Feb 2013 - Aug 2013	Doctorate Scholarship provided by the Scientific Research and Technical Council of Turkey.
April 2012 & 2013	Student travel grant provided by Seismological Society of America.
Nov. 2005 - Oct. 2009	Scholarship provided by the Scientific Research and Technical Council of Turkey, Under the project of 'Compilation of National Strong Ground Motion Database in Accordance with International Standards'.

PERSONAL INFORMATION

Date of birth   : 10 February, 1981, Malatya, Turkey
Gender   : Male
Marital status : Married
Nationality   : Republic of Turkey
Military service: Done
Driving license: Class B

THESIS AND DISSERTATION

Sandıkkaya, M.A. (2014). Next Generation Pan-European Ground-Motion Prediction Equations for Engineering Parameters. (Supervisors: Dr. Sinan Akkar, Middle East Technical University, Ankara, Turkey and Dr. Pierre-Yves Bard, Universite Joseph Fourier, Grenoble, France)

Sandıkkaya, M.A. (2008). Site classifications of Turkish national strong-motion stations. M.Sc. thesis, Department of Civil Engineering, Middle East Technical University, Ankara, Turkey, 94 pages. (Supervisors: Dr. B. Sadık Bakır and Dr. M.Tolga Yılmaz

TECHNICAL MANUSCRIPTS

Sandıkkaya, M.A., S. Akkar and P.-Y. Bard (2014). A Proposal to Describe Site Amplification Factors for Seismic Design Codes, *Earthquake Spectra*, (submitted).

Akkar S.,, **M.A. Sandıkkaya** and B.Ö. Ay (2014). Ground-motion prediction equations on damping scaling factors and vertical-to-horizontal spectral amplitude ratios for their implementation in the broader Europe region, *Bulletin of Earthquake Engineering*, **12**:517-547.

Akkar, S., **M.A. Sandıkkaya** and J.J. Bommer (2014). Empirical ground-motion models for point- and extended-source crustal earthquake scenarios in Europe and the Middle East, *Bulletin of Earthquake Engineering*, **12**: 359-387.

Douglas J., S. Akkar, G. Ameri, P-Y. Bard, D. Bindi, J.J. Bommer, S.S. Bora, F. Cotton, B. Derras, M. Hermkes, N.M. Kuehn, L. Luzi, M. Massa, F. Pacor, C. Riggelsen, **M.A. Sandıkkaya**, F. Scherbaum, P.J. Stafford and P. Treversa (2014). Comparisons between the five ground-motion models developed using RESORCE for the prediction of earthquake ground motions in Europe and the Middle East, *Bulletin of Earthquake Engineering*, **12**: 341-358.

Akkar, S., **M.A. Sandıkkaya,** M. Şenyurt, A. Sisi Azari, B.Ö. Ay, P. Traversa, J. Douglas, F. Cotton, L. Luzi, B. Hernandez, S. Godey (2014). Reference Database for Seismic Ground-Motion in Europe (RESORCE), *Bulletin of Earthquake Engineering*, **12**: 311-339.

Sandıkkaya, M.A., S. Akkar and P.-Y. Bard (2013). A nonlinear site amplification model for the next pan-European ground-motion prediction equations, *Bulletin of Seismological Society of America*, **103**:19-32.

Delavaud, E., F. Cotton, S. Akkar, F. Scherbaum, L. Danciu, C. Beauval, S. Drouet, J. Douglas, R. Basili, **M.A. Sandıkkaya**, M. Segou, E. Faccioli and N. Theodoulidis (2012). Toward a Ground-Motion Logic Tree for Probabilistic Seismic Hazard Assessment in Europe, *Journal of Seismology*, **16**: 451-473.

Akkar, S., A. Aldemir, A. Askan, S. Bakır, E. Canbay, I.O. Demirel, M.A. Erberik, Z. Gülerce, P. Gülkan, E. Kalkan, S. Prakash, **M.A. Sandıkkaya**, V. Sevilgen, B. Ugurhan and E. Yenier (2011). 8 March 2010 Elazığ-Kovancılar (Turkey) Earthquake: Observations on ground motions and building damage, *Seismological Research Letters*, **82:**42-58.

Sandıkkaya, M.A., M.T. Yılmaz, S.B. Bakır and Ö. Yılmaz (2010). Site classification of Turkish national strong-motion stations, *Journal of Seismology*, **14**: 543-563.

Akkar S., Z. Çağnan, E. Yenier, Ö. Erdoğan, **M.A. Sandıkkaya** and P. Gülkan (2010). The Recently Compiled Turkish Strong-Motion Database: Preliminary Investigation for Seismological Parameters, *Journal of Seismology*, **14**: 457-479.

INTERNATIONAL AND NATIONAL CONFERENCE PROCEEDINGS

Sandıkkaya, M.A., PY Bard, S. Akkar (2014). Effect of site models on standard deviation of GMPEs and fundamental site frequency as a new complementary site parameter. SSA 2014 Annual, Alaska.

Sandıkkaya, M.A. and S. Akkar (2013). Avrupa ve Ortadoğu için hesaplanan yer hareketi tahmin denklemlerinin Türkiye ile uyumluluğunun irdelenmesi, 2. Türkiye Deprem Mühendisliği ve Sismoloji Konferansı, 25-27 Eylül 2013, Hatay (in Turkish).

Sandıkkaya, M.A., S. Akkar and P-Y. Bard (2013). Evaluation of the Eurocode 8 and the NEHRP Site Amplification Factors, SSA 2013 Annual Meeting, Salt Lake City.

Sandıkkaya, M.A., P-Y. Bard and S. Akkar (2013). New site amplification factors for Eurocode 8, EGU 2013 Annual Meeting, Vienna.

Gülerce, Z., K.Ö. Çetin, M.T. Yılmaz, N.H., Y.S. Ünsever, S. Ünsal, **A. Sandıkkaya** and M. Türkoğlu (2012). 23 October 2011 Van-Tabanlı

Earthquake (Mw=7.1) Geotechnical Field Observations, 10th International Congress on Advances in Civil Engineering, October 2012, Ankara.

Sandıkkaya, M.A. and S. Akkar (2012). Applicability of the NGA Ground-Motion Prediction Equations for Europe, SSA 2012 Annual Meeting, San Diego.

Sandıkkaya, M.A. and S. Akkar (2012). How Style-of-Faulting Ratios Change with Database Feature, SSA 2012 Annual Meeting, San Diego.

Gülerce, Z., K.Ö. Çetin, M.T. Yılmaz, N.H. Sarıhan, Y.S. Ünsever, S. Ünsal, S. Sağlam and **M.A. Sandıkkaya** (2012). Geotechnical Field Observations from 23 October 2011 Van Earthquake (Mw=7.1), SSA 2012 Annual Meeting, April 2012, San Diego.

Yenier, E., **M.A. Sandıkkaya** and S. Akkar (2010). Report on the fundamental features of the extended strong motion databank prepared for the SHARE project, pp. 44. Deliverable 4.1 of Seventh Framework Programme Project Seismic Hazard Harmonization in Europe (SHARE), 34 pages, Ankara.

Sandıkkaya, M.A., M.T. Yılmaz and B.S. Bakır (2008). Ulusal Kuvvetli yer hareketi kayıt istasyonlarının TDY-2007 ve Eurocode-8'e göre zemin sınıflandırması, *Zemin Mekaniği ve Temel Mühendisliği Onikinci Ulusal Kongresi*, Turkey (in Turkish).

Yılmaz, Ö., M. Eser, **A. Sandıkkaya,** S. Akkar, S. Bakır and M.T. Yılmaz (2008). Comparison of Shear-Wave Velocity-Depth Profiles from Downhole and Surface Seismic Experiments, 14th World Conference on Earthquake Engineering, Beijing, China, Paper No. 03-03-0014.

Sandıkkaya, M.A., M.T. Yılmaz, B.S. Bakır and S. Akkar (2008). An Evaluation of Site Classification for National Strong-Motion Recording Stations in Turkey, *Proceedings of Geotechnical Earthquake Engineering and Soil Dynamics IV*, A.S.C.E.